GRI 86/0102.2

TA7
.C6
CER-84/85-50b
copy 2

GUIDELINE FOR FLUID MODELING

OF

LIQUEFIED NATURAL GAS CLOUD DISPERSION
Volume II: Technical Support Document

FINAL REPORT

(August 1984 - October 1985)

Gas Research Institute
8600 West Bryn Mawr Avenue
Chicago, Illinois 60631

CER84-85RNM 50b

GRI 86/0102.2

GUIDELINE FOR FLUID MODELING OF LIQUEFIED NATURAL GAS CLOUD DISPERSION

Volume II: Technical Support Document

FINAL REPORT
(August 1984 - October 1985)

by

Robert N. Meroney*

Fluid Mechanics and Wind Engineering Program
Civil Engineering Department
Colorado State University
Fort Collins, CO 80523

for

GAS RESEARCH INSTITUTE

Contract No. 5083-252-0962

GRI Project Manager
Kiran M. Kothari
Environment and Safety Research

May, 1986

* Professor, Colorado State University

GRI DISCLAIMER

LEGAL NOTICE this report was prepared by Colorado State University as an account of work sponsored by the Gas Research Institute (GRI). Neither GRI, members of GRI, nor any person acting behalf of either:

a. Makes any warranty of representation, expressed or implied with respect to the accuracy, completeness, or usefulness of the information contained in this report, or that the use of any information, apparatus, method or process disclosed in this report may not infringe privately owned rights; or

b. Assumes any liability with respect to the use of, or for damages resulting from the use of, any information, apparatus, method, or process disclosed in this report.

272-101

REPORT DOCUMENTATION PAGE

1. REPORT NO.	2.	3. Recipient's Accession No.
GRI 85/0102.2		

Title and Subtitle

Guideline for Fluid Modeling of Liquefied Natural Gas Cloud Dispersion
Volume II: Technical Support Document

5. Report Date
May, 1986

6.

Author(s)
Robert N. Meroney

8. Performing Organization Rept. No.
CER84-85RNM-50B

Performing Organization Name and Address
Fluid Mechanics and Wind Engineering Program
Civil Engineering Department
Colorado State University
Fort Collins, Colorado 80523

10. Project/Task/Work Unit No.
5083-252-0962

11. Contract(C) or Grant(G) No.
(C)
(G)

12. Sponsoring Organization Name and Address
Gas Research Institute
8600 West Bryn Mawr Avenue
Chicago, Illinois 60613

13. Type of Report & Period Covered
Final (August 1984 - July 1985)

14.

15. Supplementary Notes

16. Abstract (Limit: 200 words)

Measurements of the behavior of simulated liquefied natural gas clouds dispersing over small-scale models placed in meteorological wind tunnels provide an opportunity to evaluate the fluid physics of dense cloud movement and dispersion in a controlled environment. The data also provide guidance for health and safety engineers during plant design and an opportunity to confirm mitigation procedures. The capabilities and limitations of fluid modeling for dense gas cloud behavior are summarized and standards to be followed during such studies recommended.

The primary intent of this support is to provide a technical support document which reviews the capabilities and limitations of physical modeling techniques and supports the recommendations made in Volume I: Instruction Guide for the fluid model prediction of liquefied natural gas (LNG) storage and transportation hazards.

17. Document Analysis a. Descriptors

b. Identifiers/Open-Ended Terms

c. COSATI Field/Group

18. Availability Statement:	19. Security Class (This Report)	21. No. of Pages
Distribution unlimited	Unclassified	
	20. Security Class (This Page) Unclassified	22. Price

(See ANSI-Z39.18) See Instructions on Reverse

OPTIONAL FORM 272 (4-77)
(Formerly NTIS-35)
Department of Commerce

RESEARCH SUMMARY

Title	Guideline for Fluid Modeling of Liquefied Natural Gas Cloud Dispersion, Volume II: Technical Support Document
	Accession Code: GRI-86/0102.2
Contractor	Colorado State University Fort Collins, Colorado 80523
Principal Investigator	Robert N. Meroney
Report Period	August 1984 - October 1985, Final Report
Objective	The primary intent of this report is to provide a technical support document which reviews the capabilities and limitations of physical modeling techniques and supports the recommendations made in Volume I: Instruction Guide for the fluid model prediction of liquefied natural gas (LNG) storage and transportation hazards.
Technical Perspective	Measurements of the behavior of simulated liquefied natural gas clouds dispersing over small-scale models placed in meteorological wind tunnels permits evaluation of the fluid physics of dense cloud movement and dispersion in a controlled environment. Wind-tunnel data also provide guidance for health and safety engineers during plant design and an opportunity to confirm mitigation procedures. The capabilities and limitations of fluid modeling for dense gas cloud behavior are summarized, and standards to be followed during such studies are recommended.
Results	Data from twenty six dense gas field experiments are compared with physical model simulations. In general the model clouds are very similar in appearance, they spread and travel at correct rates, measured concentrations compare very well, and peak concentrations are often predicted to within a factor of two or better. Model simulations where specific gravity, volume flux ratio and Froude number equality are maintained produce the most successful predictions of field concentrations. When only volume flux ratio and flux Froude number equality are stipulated, peak concentration isopleths are preserved, but the time of arrival and departure of the dense clouds are distorted. The value and limitations of specifying equality in gas cloud simulation parameters such as

specific gravity ratio; volume, mass and momentum source ratios; flux Froude number; Reynolds numbers; Peclet/ Richardson number ratios; specific heat capacity ratios; humidity; and terrain slope are examined. Ranges over which these parameters must be maintained or ignored are specified.

Technical Approach

The open literature on the topics of wind tunnel simulation and dense gas dispersion were reviewed and critiqued for pertinent information relating to fluid modeling of LNG cloud dispersion. Additional model tests of the Burro 8, China Lake test, were completed to verify some conclusions concerning the simulation of releases at small model scales under conditions of low level speed prototype conditions.

Project Implications

This volume provides technical support for the Instruction Guide (Volume I) of the Guideline for Fluid Modeling of Liquefied Natural Gas Cloud Dispersion.

GRI Project Manager
Kiran M. Kothari
Environment and Safety Research

ACKNOWLEDGMENTS

During the preparation of this report I have had the benefit of many technical discussions with colleagues and friends working in this field of research. I have attempted to extract the essence from their reports and papers and our discussions. Their imagination and ingenuity in extending this body of endeavor is impressive, and any loss or misrepresentation of point of view during the effort to summarize is the unintentional fault of the author. The information which is included in this guideline is not claimed to be encyclopedic, but it includes those features which seem to me to be most significant in the fluid model description and estimation of the diffusion of liquefied natural gas released in the atmosphere.

Many persons have contributed either directly or indirectly to this review; I should like to mention some of them by name:

Dr. William Snyder, Environmental Protection Agency, whose own guideline for fluid modeling of diffusion set a standard to approach.

Drs. J. Puttock and G. Colenbrander, Shell Research, who shared insights gained during their own comparisons between fluid modeling and the Maplin Sands experiments.

Dr. James McQuaid, Health and Safety Executive, U.K., who graciously provided advice and information over a wide range of topics.

Mr. David Neff, Colorado State University, whose idealism concerning our profession and his own high standards of laboratory metrology provided a backdrop upon which to prepare this guideline.

Drs. J. Havens, R. Hosker, J. Rottman, and D. Wilson provided careful reviews of the text materials and many helpful suggestions for improving the report.

I would also like to acknowledge the financial support and management guidance provided by the Gas Research Institute. Drs. S. Wiersma and K. Kothari were ever helpful in maintaining perspective and balance concerning the needs of the public and the gas industry.

TABLE OF CONTENTS

LIST OF TABLES

LIST OF FIGURES

LIST OF SYMBOLS

Symbol	Description
a	Constant, Equation (4.3)
A	Constant, Equation (3.3) or (3.28)
A	Source exhaust area, boiloff area
A	Gas cloud surface contact area
B	Constant, Equation (3.3), or Bowen Ratio, Equation (3.26)
Br	Brinkman number
BR	Blockage ratio
C_c	Calculated or measured concentration
C_D	Drag coefficient
CF	Correction factor for spatial resolution
C_o	Observed concentration
Cp	Specific heat capacity
d	Zero plane displacement
D	Source diameter
DU_{mx}	Maximum mean velocity deficit
e	Voltage
Ec	Eckert number
Eu	Euler number
f	Reduced frequency
f_c	Coriolis parameter
f_m	Peak reduced frequency
f_N	Surface pattern fraction factor
f_t, f_b	Top and bottom friction coefficients
$F_L(n)$	Lagrangian spectrum function
Fr_a	Froude number, ambient reference density
Fr_f	Flux Froude number
Fr_s	Froude number, source reference density
g	Gravitational acceleration
g(x)	Eddy spatial correlation
G	Gradient wind velocity
Gr	Grashof number
h	Obstacle height
h_s	Surface heat transfer coefficient
H	Cloud height
H(f)	Heavyside operator
k	von Karman constant
k	Conductivity
k	Constant Equation (3.4)
K	Dimensionless concentration coefficient
l_b	Buoyancy length scale
L	Length scale
L_{mo}	Monin-Obukhov stability length
Lu_i	Integral time scale

M	Molecular weight
M	Mass flux ratio
n	Cyclic frequency
n	Moles
p,P	Pressure
p	Power law coefficient
Pe	Peclet number
Pr	Prandtl number
Q	Source flow rate
r	Radius
R	Gas constant, correlation coefficient
Ra	Rayleigh number
Re	Reynolds number
Re_{Da}	Source Reynolds number, ambient reference
Re_{Ds}	Source Reynolds number, source reference
Ri	Richardson number
Ri_b	Bulk Richardson number
Ri_*	Richardson number, friction velocity
Ri_f	Flux Richardson number
R_{ij}	Correlation coefficient
s	Distance downwind of an obstacle
$S_u(n)$	Longitudinal power spectral density
Sc	Schmidt number
SG,sg	Specific gravity
St	Stanton number
t,T	Time
t_v	Time scale before viscous influence
T^v	Temperature
u,U	Velocity
u,v,w	Velocity components
u_*	Friction velocity
V	Volume flux ratio
V	Gas volume
V_f	Frontal velocity
W	Source gas exhaust velocity
x,y,z	Cartesian coordinates
z_i	Mixed layer height
z_o	Roughness length
z_T	Tropopause height

Greek symbols

α	Thermal diffusivity
γ	Specific heat capacity ratio

Γ	Temperature lapse rate
δ	Boundary layer depth
δ_{ij}	Kronecker delta
ε_{ijk}	Alternating tensor
η	Kolmogoroff microscale
Θ	Potential temperature
Θ_*	Friction temperature
β	Terrain slope
λ	Microscale
λ_T	Taylor microscale
λ	Integral lenght scale
μ	Dynamic viscosity
μ	Ekman stability parameter
ν	Kinematic viscosity
π	Pi (3.141)
ρ	Density
σ	Variance
τ	Time increment
ϕ_h	Nondimensional heat flux
Φ_m	Nondimensional momentum flux
$\Phi_{T'w}$	Constant Equation (3.15)
χ	Concentration
Ω	Earth rotation rate

Superscript symbols

$\overline{\quad}$	Overbar denotes average
*	Molar value
'	Fluctuating component

Subscript symbols

a	Ambient atmospheric conditions
g,o	Source gas
i,j,k	Summation coefficients
m	Model
p	Prototype
R	Reference

1.0 INTRODUCTION

This document provides technical support and background information for the recommendations found in Volume 1: Instruction Guide, Guideline for Fluid Modeling of Liquefied Natural Gas Cloud Dispersion. The guidance is intended for use by industries and their consultants during the design and safety review of liquefield natural gas installations and by regulatory agencies.

1.1 Background

Natural gas is a highly desirable form of energy, since it is convenient to transport. Sophisticated distribution network already service industrialized countries. Recent efforts to expand this gas supply and its availability include the transport of natural gas in a liquefied state from distant gas fields and the storage of emergency supplies in "peak-shaving" facilities. Liquefied natural gas (LNG) is cooled to a temperature of $-162^{\circ}C$ for transportion and storage. If a storage tank or a pipe were to rupture and the contents spill out onto the earth's surface, rapid boiling of the LNG would ensue, and a flammable vapor cloud would result. Past studies have demonstrated that the cold LNG vapor plume will remain negatively buoyant for most of its flammable lifetime. The vapor cloud hazard will persist until the atmosphere has diluted the LNG vapor below the lower flammability limit (LFL; the maximum local concentration below which the gas is not flammable; 5 percent by volume for methane). The location of the LFL region in space and time determines regulatory and response strategies.

It is important that accurate predictive models for LNG vapor cloud physics be developed, so that the associated hazards of

transportation and storage may be realistically assessed. Industrial and Government agencies have sponsored a combination of field measurements and analytical, numerical, and physical modeling studies to analyze such problems. Analytical and numerical solutions are valuable because of the phenomenological insight they provide, and the now general availability of computer facilities. But the more complex the boundary conditions, the less rewarding a theoretical or numerical solution becomes because of its lack of general validity, and the higher effort required to obtain the solution. Physical modeling permits a comparatively simple analog solution to a complex situation. The analog consists of the use of fluid models, in which the boundary conditions are simulated through a geometrical scale model, and the atmosphere is simulated by flowing of water or air in a laboratory apparatus. The primary intent of this report is to review the capabilities and limitations of physical modeling techniques for the prediction of LNG storage and transportation hazards.

Thermal effects, topography, the presence of obstacles and spray curtain mitigation devices can affect the dispersion of dense gas clouds. Fluid modeling studies are desirable mostly because such variables can be controlled at will, with great savings in time and expense over full-scale tests. The physical model inherently includes fluid physics for which only limited understanding can presently be incorporated in numerical models.

1.2 Summary of Support Document Contents

This technical support document discusses constraints which exist on a physical model's ability to predict large scale atmospheric plume behavior. These constraints are due to the limited range of transport properties of air and water, the inherent characteristics of fluid turbulence, and the size range of available fluid modeling facilities. Section 2 considers the general similarity requirements associated with the governing equations of motion, thermodynamic state, and energy. A discussion is also provided of the relative merits of the concepts of model verification, validation, and calibration. Section 3 reviews the ability of fluid modeling facilities to reproduce the significant characteristics of the atmospheric surface layer. Modeling limitations specifically associated with dense cloud behavior are discussed in Section 4. Verification of various modeling rules are examined in Section 5, through comparisons between field and laboratory measurements.

2.0 GENERAL SIMILARITY REQUIREMENTS

The concept of similitude is basically simple. Two systems at different geometric scales will exhibit similitude if a one to one correspondence exists in space and time between fluid particle kinematics (locations, velocities, accelerations and rotations) caused by fluid particle dynamics (pressures, gravity, Coriolis forces, viscous forces, etc.), when properly scaled by characteristic scales of fluid properties, force, length and time. To achieve this similarity, however, is not trivial. The specification of dimensionless parameters which guarantee similarity has historically been the subject of much discussion and debate.

In the nineteenth century a number of workers (most notably Lord Rayleigh) commonly solved problems by direct use of the similarity principle with the intuitive identification of relevant force ratios. During the early twentieth century, the force ratio methods lost favor and were replaced almost entirely by dimensional analysis, as represented by the Buckingham Pi theorem. The most systematic and reliable method currently used to identify relevant scaling parameters is the "normalization" of the governing partial differential equations of motion. Normalization makes the equations and boundary conditions nondimensional in terms of scaling variables of standard magnitude. In the following sections the primary similitude parameters are identified by applying this technique. The chapter ends with a review of methods necessary to verify that similitude has indeed been achieved.

2.1 The Equations of Motion

The equations of motion are the starting point for the

normalization procedure. Given a reference frame fixed to the surface of the Earth which is rotating at an angular velocity j, then for an incompressible atmosphere one can generate the following equations:

Conservation of Mass

$$\frac{\partial U_i}{\partial x_i} = 0 \tag{2.1}$$

Conservation of Momentum

$$\frac{\partial U_i}{\partial t} + \frac{U_j \partial U_i}{\partial x_j} + 2\varepsilon_{ijk} U_k \Omega_j = -\frac{1}{\rho}\frac{\partial P}{\partial x_i} + \frac{g}{T_o}\delta T \delta_{3i} + \frac{\nu \partial^2 U_i}{\partial x_k \partial x_k} \tag{2.2}$$

Conservation of Energy

$$\frac{\partial T}{\partial t} + \frac{\partial T}{\partial x_i} U_i = \kappa \frac{\partial^2 T}{\partial x_i \partial x_i} + \frac{Ui}{\rho}\frac{\partial P}{\partial x_i} \tag{2.3}$$

Conservation of Species

$$\frac{\partial \chi}{\partial t} + U_i \frac{\partial \chi}{\partial x_i} = \alpha \frac{\partial^2 \chi}{\partial x_i \partial x_i} \tag{2.4}$$

Equation of State

$$P/\rho = RT/M \tag{2.5}$$

The Cartesian index convention has been used, where the x_3 axis is taken vertically upward, U_i is a component of the instantaneous velocity, ε_{ijk} is the alternating tensor (if any two of the indices i, j, or k are equal, the component is zero; if i, j, and k are all

unequal and in cyclic order, the component is +1; but if not in cyclic order, the component is -1), δ_{ij} is the Kronecker delta (equal to 1 if the two indices are equal and 0 if unequal), and the summation convention is followed (whenever a suffix is repeated in a term it is to be given all possible values and the terms are to be added).

The next step is to identify characteristic scales through which the equations will be normalized. Reference quantities are usually identified through specified boundary conditions. Choosen are L, length; U_R, velocity; ρ_R, density; Ω_R, rotational speed; T_R, absolute temperature; ΔT_R, temperature deviation; g, gravitational constant; P_R, reference pressure; and μ_R, k_R, D_R, Cp_R, which are the reference viscosity, conductivity, diffusivity and specific heat capacity respectively. The dimensionless variables are:

$$x_i' = \frac{x_i}{L} \qquad U_i' = \frac{U_i}{U_R} \qquad P' = \frac{P}{\rho_R U_R^2} \qquad T' = \frac{T}{\delta T_R}$$

$$t' = \frac{U_R}{L} t \qquad \rho' = \frac{\rho_o}{\rho_R} \qquad \Omega_j' = \frac{\Omega_j}{\Omega_R}$$

Introducing these dimensionless variables in Equations 2.1 to 2.5 yields:

$$\frac{\partial U_i'}{\partial x_i'} = 0 \tag{2.1a}$$

$$\frac{\partial U_i'}{\partial t'} + U_j' \frac{\partial U_i'}{\partial x_j'} + \frac{2}{R_o} \varepsilon_{ijk} U_k' \Omega_j' = - \frac{Eu}{\rho'} \frac{\partial P'}{\partial x_i'} + Ri \quad \delta T' \delta_{3i} + \frac{1}{Re} \frac{\partial^2 U_i'}{\partial x_j' \partial x_j'} \tag{2.2a}$$

$$\frac{\partial T'}{\partial t'} + U_i' \frac{\partial T'}{\partial x_i'} = \frac{1}{Pe} \frac{\partial^2 T'}{\partial x_i' \partial x_i'} + EuEc \frac{U_i'}{\rho'} \frac{\partial P'}{\partial x_i'} \tag{2.3a}$$

$$\frac{\partial \chi'}{\partial t'} + U_i' \frac{\partial \chi'}{\partial x_i'} = \frac{1}{ReSc} \frac{\partial^2 \chi'}{\partial x_i' \partial x_i'} \tag{2.4a}$$

(2.5a)

$$P'/(\rho'T') = \rho_R U_R^2 R \delta T_R / M_o = 1/Eu$$

where $Ro = U_R/L\Omega_R$ is the Rossby number,

$Eu = P_R/(\rho_R U_R^2)$ is the Euler number,

$Re = \rho_R U_R L/\mu_R$ is the Reynolds number,

$Ri = g_R \Delta T_R L/(T_R U_R^2)$ is the Richardson number,

$Pe = \rho_R Cp_R U_R L/k_R$ is the Peclet number,

$Pr = \mu_R Cp_R/k_R$ is the Prandtl number,

$Sc = \mu_R/(\rho_R D_R)$ is the Schmidt number, and

$Ec = U_R^2/(Cp_R \Delta T_R)$ is the Eckert number.

The physical significance of these parameters will be discussed at some length in later paragraphs.

"Exact" similarity requires equality of the nondimensional coefficients listed above for the physical model and the prototype situation. If separate length scales are chosen for the different coordinate directions additional parameters are generated; however, current wisdom is that distorted geometric scaling is not justified.

Furthermore boundary conditions governing the flow domain of interest must also be similar for the model and prototype. Surface boundary conditions would require similarity of the following features:

1) Topographical relief,

2) Surface roughness distribution,

3) Surface temperature distribution, and

4) Reproduction of associated obstacles, buildings, fences, source areas, etc.

Similarity of the approach-flow characteristics requires similarity of the following flow features:

1) Distributions of mean and turbulent velocities,

2) Distributions of mean and fluctuating temperatures and humidities, and

3) Distributions of turbulent scales and energies.

Similarity of the boundary conditions aloft would require similarity of the following features:

1) The upper stream line should follow a similar trajectory with respect to the ground surface, and

2) The longitudinal pressure gradient should be nearly zero.

These seven equations and associated boundary conditions contain seven unknowns, U_1, U_2, U_3, T, p, ρ, and χ, so that (in principle) their solutions can be determined. Any prototype and model flow which is constrained by the same scaled initial and boundary conditions, and for which all the dimensionless coefficients identified above are invariant, must have a unique solution in terms of the dimensionless variables. The non-dimensional equations apply to both laminar and turbulent flows; hence it is not necessary to know a priori whether the flow is laminar or turbulent.

It is not necessary to actually solve the differential equations if one uses a laboratory facility as an analog computer. If all the foregoing requirements could be met simultaneously, all scales of motion ranging from micro to mesoscale, ie. 10^{-3} to 10^{3} m, could be

simulated within the modeled flow field.

Unfortunately, all similarity requirements cannot be satisfied simultaneously and modelers must use partial or approximate similitude. Hence, model conditions must be chosen which are designed to simulate most accurately those scales of motion which are of greatest significance for the application (Cermak, 1975).

2.2 The Dimensionless Parameters

Kline (1965) observed that, in engineering work, it is often not feasible to mathematically model all aspects of the behavior of the prototype. Rather, it becomes necessary to determine under what conditions some parameters can be neglected. For example, this approach is the essence of perturbation analysis used for inner and outer expansions in boundary layer theory. In both mathematical analysis and physical modeling it is helpful to use order-of-magnitude analysis of the individual terms in the equations of motion to eliminate insignificant terms. Since the dimensionless variables have been scaled to be of order one, O(1), the relative importance of each term lies in the magnitude of the associated dimensionless coefficients.

It is generally impossible to simultaneously match all of the dimensionless parameters when the ratio of the prototype and model length scales is greater than about 10. Consider the behavior of the Reynolds and Richardson numbers:

$$Re = \rho_R U_R L/\mu_R \qquad \text{and} \quad Ri = g\,\Delta T_R L/(T_R U_R^2)$$

If one models an LNG spill in a wind tunnel, the property values of ρ, μ and g are identical, and T_R is roughly the same. Equality of Reynolds numbers between model and prototype then requires an increase of 10 fold in the flow velocity. But to match the Richardson number

criterion if L is decreased by 10 and U_R is increased by 10, ΔT_R must be increased by 1000! Such an increase in temperature difference (or density difference) is obviously impractical.

Because of the difference in kinematic viscosity between air and water, a factor of about 15 in Reynolds number may be gained by modeling an atmospheric phenomenon in a water facility, but then the Peclet number and Reynolds number criteria can not be met simultaneously. Also the Prandtl number in air is of order one, whereas its value in water is about 10.

Consider the roles played by each dimensionless parameter in some detail. Barnett (1964) summarizes the majority of the relevant dimensionless parameters used by fluid mechanists and meteorologists. Only those parameters identified during the normalization of the equations of motion in section 2.1 are considered.

Rossby Number: $[U_R/(L\Omega_R)]$

The Rossby number is a measure of the relative magnitudes of the advective or local accelerations as compared to Coriolis accelerations. Local accelerations result from unsteadiness or divergence in the flow field. Coriolis accelerations result from the fact that we all live on a non-inertial reference system (the surface of the Earth). Since the Earth's Coriolis accelerations (or forces) are relatively small, they only become important when motions persist over distances long enough for the associated spatial deviations to become significant. If the Rossby number is large, Coriolis accelerations are small. A nearly infinite model Rossby number exists in most laboratory wind tunnels and water channels.

Euler Number: $[P_R/(\rho_R U_R^2)]$

The Euler number compares the relative magnitude of pressure

fluctuations and inertial accelerations. Since P_R is usually of order $\rho_R U_R^2$, this parameter is of order one and is automatically simulated in air.

Reynolds Number: $[\rho_R U_R L/\mu_R]$

The magnitude of the Reynolds number indicates the relative importance of inertial forces and viscous or frictional forces. It imposes very strong limitations on rigorous simulation, since scale reductions of 1:100 to 1:1000 commonly result in model Reynolds numbers two to three orders of magnitude smaller than those found in the atmosphere. Thus the viscous forces are relatively more important in the model than in the prototype. If strict Reynolds number equality is required, no atmospheric phenomena could be modeled. Various arguments have been proposed to justify the use of smaller Reynolds numbers in model studies. Snyder (1972) reviews suggested concepts of the laminar flow analogy, dissipation scaling, and Reynolds number independence. He concludes that only Reynolds number independence is a viable possibility. This concept will be discussed further in sections 3.3.2 and 4.2.

Richardson Number: $[g \Delta T_R L/(T_R U_R^2)]$

A large value of the Richardson number implies that buoyancy forces are very large compared to inertial forces. Thermal effects or density differences become less important as the Richardson number decreases toward unity. The Richardson number can also be considered as the inverse square of a densimetric Froude number, $Fr = U_R/[g(\Delta T_R/T_R)L]^{0.5}$. Alternatively $Ri = Gr/Re^2 = Ra/(Re^2 Pr) = Ra/(RePe)$. In this case, Gr and Ra are known as the Grashof numbers and Rayleigh numbers, respectively. The Grashof number is important when flow motions are driven by free convection. The Rayleigh number

The Rayleigh number is often used to typify the onset of cellular convections driven by temperature differences.

The Richardson number is not necessarily a difficult parameter to duplicate in a fluid model. Unfortunately, to match model and prototype Richardson numbers for typical scale reductions of 1:100 to 1:1000 using reasonable temperature or density differences, it is necessary to decrease the mean flow speeds substantially. Yet to match the Reynolds number requires that the flow speed in the model be increased; hence, a conflict arises. Specific problems related to simulations of atmospheric flows and dense gases will be discussed in sections 3.3.3 and 4.2.1, respectively.

Peclet Number: $[\rho_R Cp_R U_R L/k_R]$ or $[U_R L/D_R]$

The Peclet number can also be expressed as the product of a Reynolds number and the Prandtl number or the Schmidt number, ie., RePr or ReSc. The parameter is a measure of the ability of the fluid to advect heat or mass compared with its ability to disperse heat or mass by molecular transport. The Peclet number often becomes important when Reynolds number independence does not exist. In such cases the relative ability of the fluid to transport heat or mass by molecular collision and the rate of transport provided by turbulent motions become comparable. Such a situation can produce incorrectly simulated plume entrainment and transport rates.

Prandtl Number: $[\mu_R Cp_R/k_R]$

The Prandtl number is the ratio of the momentum diffusivity to the thermal diffusivity. It indicates the relative ability of the fluid to transport momentum as compared to heat via molecular processes. If air is used to simulate the atmosphere, this parameter is automatically satisfied. The Prandtl number is a weak function of

air temperature. In water the Prandtl number is about 10 times larger than it is in air, and varies with temperature. This parameter always appears multiplied by the Reynolds number. The product or thermal Peclet number is, thus, the governing parameter.

Schmidt Number: $[\mu_R/(\rho_R D_R)]$

The Schmidt number is the ratio of momentum diffusivity to mass diffusivity. It also indicates the relative ability of the fluid to transport momentum versus mass species by molecular processes. If air is used to simulate the atmosphere, then the magnitude of the Schmidt number will be dependent on the model tracer gas chosen; however, it will usually be close to a value of one. However, the Schmidt number for typical tracers such as sodium chloride or alcohol dispersing in water is nearly 800; hence, Schmidt number equality is unlikely in water facilities. This parameter always appears multiplied by the Reynolds number. The product or mass Peclet number is, thus, the governing parameter.

Eckert Number: $[U_R^2/(Cp_R \Delta T_R)]$

The Eckert number indicates the ratio of kinetic to excess internal energy. Eckert numbers are not normally equal when equal Richardson numbers are achieved. This compromise with exact similarity has not been found to have significant effect on the similarity of wind characteristics. The Eckert number is also equal to a Mach number squared, and this is generally small compared to unity for both laboratory and atmospheric flows. Its small value in the energy equation (2.3a) suggests that viscous dissipation or compression do not affect temperature distributions significantly. In some texts the Eckert number is expressed as (Br/Pr), where $Br = [\mu_R U_R^2/(k_R \Delta T_R)]$ is the Brinkman number. The Brinkman number

relates the rate of viscous dissipation to conductive heat transfer which will occur over the reference temperature difference.

2.3 Verification

The intent of verification is to determine the performance of a model (analytical, numerical or physical) in the context of a particular application (Knox, 1984). Within the process one attempts to learn the range of conditions of reliable model application, to identify conditions of failure, and to determine the level of confidence that can be placed in the model solutions. Usually models are constructed and used in response to specific technical questions or regulatory requirements. In one situation ensemble average behavior may be needed; in another situation exact replication is necessary. Often a solution is sought which provides upper bounds on all potentially undesirable consequence. The same model may not perform all jobs; hence, the desired model result should be specified before evaluation begins.

The American Meteorological Society and the Electric Power Research Institute sponsored workshops which recommended that a rigorous research effort be made to evaluate the ability of numerical models to predict ambient air pollution (Egan et al., 1981; Hilst, 1978; and Fox, 1981). Subsequently the air pollution research community established rigorous protocols prior to evaluation, a potpourri of tests for statistical evaluation of residuals, and rules to evaluate models in the context of very specific regulatory uses. Both EPA and EPRI sponsored operational validation projects for large buoyant plumes from tall stacks (Hilst, 1978; Londergan et al., 1982).

The AMS Woods Hole conference recommended basing performance

evaluation on the magnitude of differences between observed and predicted concentrations. The recommended performance measures were the bias (average), the variance (noise), and the gross variability (gross error) of the differences. Correlation measures in space and time were also considered helpful. Londergan et al., (1980) produced a extensive set of statistics based on the Woods Hole recommendations as part of the AMS review process. Reviewers concluded that most calculations were actually uninformative or redundant (A. M. S.,1983). Alternatively, Rao and Visalli (1981) emphasized the importance of extreme value theory to qualitatively and quantitatively evaluate the performance of models. Some Woods Hole participants felt strongly that scientific judgment (ie. scientific performance -- or recognition of cause-and-effect relationships) might prove to be the only effective method to distinguish among model approaches. Wheatley and Webber (1984) followed such an approach when they reviewed some 45 numerical models designed to predict denser-than-air vapor dispersion. They chose to differentiate among models based on whether the numerical models included correct and consistent fluid physics for all physical effects of importance within the range of scales being considered. All too often they found important features missing or misrepresented.

Despite the variety of emphasis within the recent literature it is clear that the engineering and scientific consensus recommends a balanced approach that includes both scientific as well as "operational" criteria.

One of the principal findings of the EPRI validation project is that "existing (numerical) plume models are unable to predict air quality impacts for a specific event; uncertainties associated with the magnitude and location of plume impacts are as large as the

predicted or observed ground level concentrations" (Bowne et al., 1981, 1983, 1985). The concepts of "limits to predictability" and "inherent uncertainty of the turbulent atmosphere" have emerged in connection with the expectations of model performance. These concepts suggest that, even under apparently identical conditions in the atmosphere, the inherent uncertainties act as a barrier to the repeatability of experiments. For example, for air quality numerical models it is apparently unrealistic to predict hourly average ground level concentrations within a factor of two more than about 80% of the time (Bowne et al., 1985). Few investigations have reported numerical model success close to this level and, for shorter time periods, numerical model performance reported departs dramatically from this ideal.

The data bases developed, the testing procedures evaluated, and the findings have been invaluable for the air pollution research community. However, one consequence of the exercise is that the search for the "perfect modeling technique" has been abandoned, and model validation is now considered a part of the learning process.

Physical modeling operates under similar constraints. A physical model cannot possibly reproduce prototype LNG spill behavior better than the average of multiple replications of field experiments under apparently identical conditions. Meroney (1980, 1981) and Meroney et al. (1980) compared multiple field measurements of wind fields over complex terrain to fluid model experiments. The laboratory reproduced field behavior to within its own variability, but no better. Turbulence induces its own scale of variability. Meroney and Lohmeyer (1983) found that multiple replications of a laboratory release of dense gas in a simulated atmospheric boundary layer showed significant

variations in time of cloud arrival, time of arrival of maximum concentration, time of departure of cloud, plume dimensions, and maximum concentrations. Multiple replications of fluid model studies of the Burro 8 China Lake LNG spill produced concentration variations about the mean concentration of the same magnitude as the mean. This point is especially significant since, to date, only individual field experiments have been performed; hence, it will be considered further in Sections 4 and 5.

3.0 PHYSICAL MODELING OF THE ATMOSPHERIC BOUNDARY LAYER

During early (1920-1955) wind tunnel studies of wind engineering problems researchers mistakenly presumed that the uniform-flow low-turbulence conditions known to be suitable for aerodynamic tests of flight vehicles would also be suitable for simulation of atmospheric flows. Comparison of model and prototype data revealed such wide discrepancies that many engineers concluded simulation of atmospheric phenomena was impossible. However, in the mid 1950s, several scientists realized that the shear layers and turbulence variations found in the atmospheric boundary layer played a critical role in the kinematics and dynamics of atmospheric transport phenomena (Jensen, 1958; Strom et al., 1957; Cermak, 1958). Jensen tested simple shelter belts, model buildings, and plumes from smoke stacks in both uniform and shear flows produced by roughening the lower boundary. Comparable measurements were made at full scale in the atmosphere. In each case the deviations of uniform flow model results from the field cases were considerable. Figure 3-1 displays Jensen's shelter belt results, and Figure 3-2 corresponds to his building pressure measurements. As noted, the uniform flow approximation considerably overpredicts the reduction of wind speeds for the fence study, and it also overpredicts pressure coefficient magnitudes on the windward and leeward sides of the model house.

As time progressed, wind engineers learned that it was not sufficient to just simulate mean velocity and longitudinal turbulent intensity profile shapes. The scale and distribution of turbulent energy among eddy sizes plays an important role in plume spread or entrainment rates as well as the fluctuating forces on buildings. In order to accomplish model similitude to the atmosphere, it is

necessary to reproduce the important features of the atmospheric surface layer. The following sections review the relevant characteristics of the atmosphere (Sections 3.1 and 3.2), discuss methods to reproduce these characteristics at model scales (3.3, 3.4, and 3.5), and attempt to establish guidelines for modeling of the atmospheric surface layer (3.6).

3.1 Mean Flow Characteristics of the Atmospheric Boundary Layer

The atmospheric boundary layer (ABL) is that portion of the atmosphere where surface drag due to the motion of the air relative to the ground modifies synoptic-scale motions caused by horizontal pressure gradients, Coriolis forces, and buoyancy. The following sections review some pertinent facts about the boundary layer; for more detailed information, one should consult meterological text books (e.g., Panofsky and Dutton, 1984) or review papers (e.g., Nieuwstadt and van Dop, 1982).

3.1.1 Depth of the Atmospheric Boundary Layer

The depth of the boundary layer is highly variable (50 to 2000 m), but it generally increases with proximity to the equator, with wind speed, and as the earth surface roughens, but decreases at night, and is strongly modified by thermal winds, inversions, and stratification. Even selecting a depth for adiabatic (neutrally stable) conditions is difficult. Counihan (1975) reviewed all adiabatic atmospheric boundary layer data between 1880 to 1972. For high wind speeds (U_{10} > 5-7 m/s) Counihan recommended 600 m as a reasonable average boundary layer depths for both rural and urban cases independent of wind speed and roughness. Since it represents an

average of actual measurements, a value of 600 m is recommended for neutrally stable conditions.

Boundary layer depth is highly dependent upon atmospheric stratification. At night, radiational ground cooling stabilizes the lower atmosphere, and effectively decouples the winds aloft from the effects of the earth's surface. The boundary layer may then be very shallow, perhaps as low as a few tens of meters (Wolfe, 1985). When the sun rises, convection begins and the thermally mixed layer deepens until mid-afternoon. The upper limit to the layer depth depends on the initial lapse rate strength of the elevated inversion, the wind speed, and the available insolation. Between noon (1300 CDT) and near-sunset the depth is nearly constant, even after surface heat fluxes become negative. Late afternoon depths values between 600 and 2000 m are possible. A simple algorithm for boundary layer depth is:

$$\delta = a\,(L_{mo} u_* / f_c)^{1/2} \qquad (3.1)$$

where $0.4 \leq a < 1.0$, L_{mo} is the Monin Obuknov similarity length $[L_{mo} = -T(u_*)^3/(kgt\ \overline{w'})]$, and f_c is the Coriolis parameter $2\ \sin(\phi)\,\Omega$ and u_* is the friction velocity. An alternative formula (Deardorff, 1972) yields lower heights during convective conditions:

$$\delta = [\ (1/(30L_{mo}) + f_c/(0.25u_*) + 1/z_T\ ]^{-1} \qquad (3.2)$$

where z_T is the height of the tropopause. Note that $\delta = 0.25\ u_*/f_c$ under neutral conditions, and $\delta = 30L_{mo}$ under very stable conditions.

It is customary to use a geostrophic drag law to calculate the friction velocity u_*:

(3.3)

$$\ln[G/(f_c z_o)] = A + \ln[G/u_*] + [k^2G^2/u_*^2 - B^2]^{1/2}$$

where G is the geostrophic wind speed, k is the von Karman constant (0.4) z_o is the surfaces aerodynamic roughness, and A and B are constants dependent upon stability. In a critical review, Arya (1977) suggested values for different stability conditions:

For neutral situations: A = 1.7 and B = 4.7.

For stable atmospheres:

$$A = \ln(\delta/L_{mo}) - 0.96(\delta/L_{mo}) + 2.5$$

$$B = 1.15(\delta/L_{mo}) + 1.1$$

For unstable atmospheres:

$$A = \ln(-\delta/L_{mo}) + \ln(f_c\delta/u_*) + 1.5$$

$$B = k(f_c\delta/u_*)^{-1} + 1.8(f_c\delta/u_*)\exp(0.2\delta/L_{mo})$$

Figure 3-3 shows boundary layer depths predicted from Equations 3.1 and 3.2 using the associated values of friction velocity shown in Figure 3-4. Figure 3-5 displays the variation of the adiabatic boundary layer depth with roughness and gradient wind speed. An iteration procedure is used since Equations 3.1 to 3.3 all involve u_*.

Unstable boundary layer depth varys diurnally, as the mixed layer penetrates capping inversions from sunrise until about 1300 when the solar heat flux reaches its maximum. As the heat flux levels off during the afternoon the mixed layer penetration height, z_i, levels off to a maximum between 1000 and 2000 meters. Wolfe (1985) reported early morning mixing layer depths (Figure 3-6) from measurements at the Boulder Atmospheric Observatory tower near Boulder, Colorado. Maximum mixing layer depth may be estimated as:

(3.4)

$$z_i = \left\{ [2.8/\Gamma] \int_o^t A \sin(wt)\, dt \right\}^{1/2}$$

where Γ is initial lapse rate, and A is the maximum surface heat flux.

3.1.2 Logarithmic Velocity Profiles in the Surface Layer

The lowest 10% of the ABL is called the surface layer. It is characterized by the sharpest variations of wind speed, temperature, humidity, and turbulence characteristics with height. Counihan (1975) concluded the surface (or constant flux layer) could be assumed to be about 100 m deep during adiabatic conditions. In diabatic (stratified) situations one might assume that the surface layer depth is about equal to the absolute value of the Monin Obukhov length.

Within the surface layer the mean wind-speed profile is commonly described by logarithmic expressions. An expression which has been repeatedly found to represent neutral flows in wind and water tunnels and in atmospheric profile measurements is:

(3.5)

$$u/u_* = (1/k) \ln [(z - d)/z_o]$$

where d is the zero plane displacement thickness and z_o is a roughness length. The displacement thickness, d, is important for tall roughness elements such as agricultural crops, forests, and cities. When the roughness elements are short, such that $z_o < 0.2$ m, one can set d = 0 (Snyder, 1981). The roughness length can be determined from representative field measurements; however, repeated experiments have produced the surface classifications noted in Table 3.1 (from Simiu and Scanlan, 1978).

In a diabatic boundary layer during reasonably stationary time

periods, it is possible to define nondimensional vertical gradients of wind speed and temperature; i.e.,

$$\phi_m = (kz/u_*)(du/dz); \quad \phi_h = (z/\theta_*)(d\theta/dz) \tag{3.6}$$

where $u_* = (\overline{u'w'})_o$ and $\phi_* = (\overline{w'T'})_o/u_*$. According to Monin Obukhov similarity theory these non-dimensional gradients should only be a function of the parameter z/L_{mo}. Thus, he formulated that for,

unstable air:

$$\phi_m = (1 - 15\ z/L_{mo})^{-1/4} \quad , \text{ and}$$

unstable air:

$$\phi_m = 1 + 5\ z/L_{mo}.$$

These expressions can be integrated to obtain expressions for the mean velocity profiles:

unstable air:

$$u/u_* = (1/k)\{\ln[z/z_o] - 2\ln[(1+1/\phi_m)/2] - \ln[(1+1/\phi_m^2)/2] + 2\tan^{-1}[1/\phi_m] - \pi/2\}. \tag{3.7}$$

stable air:

$$u/u_* = (1/k)\{\ln[z/z_o] + 5\ z/L_{mo}\}. \tag{3.8}$$

Note, under neutral conditions where $L_{mo} = \infty$, $\phi_m = 1$, and the

equations reduce to the familiar log-law, Equation (3.5). In a similar manner forms for nondimensional temperature flux, $\emptyset_h$, and temperature profiles are for:

unstable air:

$$\emptyset_h = (1 - 15\ z/L_{mo})^{-1/5} \quad , \text{ and}$$

stable air:

$$\emptyset_h = 1 + 5\ z/L_{mo}.$$

Hence, in unstable air:

(3.9)

$$(\theta - \theta_o)/\theta_* = \ln[z/z_o] - 2\ \ln[(1+1/\emptyset_h)/2], \text{ for } z/L_{mo} < 0$$

and in stable air:

(3.10)

$$(\theta - \theta_o)/\theta_* = \ln[z/z_o] + 5\ z/L_{mo}, \text{ for } z/L_{mo} > 0,$$

where θ is the potential temperature, and θ_o is the extrapolated temperature for $z = z_o$ (See Figures 3-7 and 3-8).

3.1.3 Power-law representation of the mean velocity profiles

The mean velocity profile throughout the entire depth of the neutral boundary layer may also be represented by a power law with only small errors associated with wind veering with height; i.e.,

(3.11)

$$(u/u_R) = (z/z_R)^p; \quad \text{or } (u/G) = (z/\delta)^p$$

In unstable situations the power law may work well up into the "tower layer" ($z < 150$ m) identified by Panofsky (1974), but for stable conditions one should limit expressions to the surface layer alone. The exponent, p, in the power-law description and the aerodynamic

roughness length, z_o, in the log description are functions of the surface roughness. Rougher boundary conditions (z_o and p larger) increase the momentum deficit in the mean shear flow. Although comprehensive data has been obtained in the atmosphere for a variety of different conditions, most correlations over this data base emphasize strong winds. The flow characteristics at lower wind speeds generally display a much greater variability. Unstable stratification reduces the effective power-law exponent, whereas stable stratification increases the value. Panofsky et al. (1960), Irwin (1979), and Huang (1979) have established theoretical relationships between p, z_o, and L_{mo}. Huang's results are shown in Figure 3-9 and Irwin's results are shown in Figure 3-10. Also shown in Figure 3-11 is the expression recommended by Counihan (1975) based on his extensive review of high wind data:

$$p = 0.24 + 0.096 \log_{10} z_o + 0.016(\log_{10} z_o)^2 \qquad (3.12)$$

where z_o is specified in meters.

3.2 Turbulence Characteristics of the Atmospheric Boundary Layer

The mean velocities in the surface layer determine the rate at which the center of gravity of a plume is transported over the ground. Vertical and lateral shear and wind veering with height work together to spread plume products over horizontal layers. The volume a plume occupies only increases as turbulence mixing tears the original plume volume into eddies and streamers which move across mean streamlines. Dilution finally occurs at small scales of order 1 mm as microscopic transport processes actually mix air and plume molecules. The effective rate of final plume entrainment depends upon the scales and

intensities of atmospheric turbulence. Statistically the turbulent state of the atmosphere is described in terms of moments of velocity fluctuations, characteristic length and time scales, or energy spectra.

3.2.1 Turbulence intensity profiles

The turbulent intensity of a boundary layer is defined as the rms of the fluctuating component of the velocity, σ_u, divided by the local mean velocity, u. By correlating strong wind atmospheric data over a large variety of different roughness conditions ESDU (1974) concluded that the variation of longitudinal turbulent intensity with height up to 100 meters is:

(3.13)

$$\sigma_u/u = \frac{\{0.867 + 0.556\ \log_{10}[z] - 0.246\ (\log_{10}[z])^2\}\ B}{\log_e[z/z_o]}$$

where $B = 1.0$ for $z_o \leq .02$ m,

$B = 0.76/z_o^{0.07}$ for $0.02 < z_o < 1.0$ m, and

$B = 0.76$ for $z_o > 1.0$ m.

Near a smooth surface this may be approximated as $\sigma_u/u = 1/\ln(z/z_o)$.

Alternatively Snyder (1981) suggests a formula which extrapolates Counihan's data at 30 meters to other heights, ie.:

(3.14)

$$\sigma_u/u = p(\ln(30/z_o))/\ln(z/z_o)$$

where p is determined from Equation 3.12. Equations 3.13 and 3.14 are compared in Figure 3-12 and Figure 3-13. Meterological measurements for neutral flow in the lower surface layer suggest that $\sigma_u/u_* = 1.5\text{-}3.0$, $\sigma_w/u_* = 1.2\text{-}1.3$, and $\sigma_w/\sigma_u = 0.3\text{-}0.4$ (Haugen, 1973,

p. 49, 50, 114, 165-166). A turbulent boundary layer developing over a smooth surface may also be compared to the classical results of Klebanoff, as given by Hinze (1975), who quotes values of $\sigma_u/u = 0.22$ at $z/\delta = 0.010$.

The standard deviations of the vertical velocity, σ_w, and temperature, σ_T, follow Monin-Obukhov similarity scaling, so that:

(3.15)

$$\sigma_w/u_* = \phi_w(z/L_{mo}), \text{ and}$$
$$\sigma_T/i_* = \phi^{(z/L_{mo})},$$

where
$$\phi_w = 1.25 \qquad \text{for } z/L_{mo} > 0.0,$$
$$= 1.25\ (1-3z/L_{mo})^{1/3} \qquad \text{for } z/L_{mo} < 0.0,$$
$$\phi_T = 1.8 \qquad \text{for } z/L_{mo} > 0.0,$$
$$= 5.0\ (1-16z/L_{mo})^{-1/2} \qquad \text{for } -1 < z/L_{mo} < 0.0, \text{ and}$$
$$\phi_T = 0.95\ (-z/L_{mo})^{-1/3} \qquad \text{for } z/L_{mo} < -1.$$

Unfortunately, the horizontal velocity components σ_u and σ_v do not appear to obey Monin-Obukhov similarity scaling, and the data scatter widely. Nonetheless, some authors have persisted in presuming such similarity exists (Binkowski, 1979--See Figures 3-14 and 3-15).

Convective boundary layers or mixed layers located above the surface layer ($z > -L_{mo}$) show similar behavior when scaled by the mixed layer depth, z_i, and a convective velocity, $w_* = (gz_i\ w'T'/T)^{1/3}$. Willis and Deardorff (1974) demonstrated such similarity in a laboratory water tank. Poreh and Cermak (1984) produced equivalent behavior in a meteorological wind tunnel, and Briggs (1984) measured convective boundary layer turbulence on the Boulder Atmospheric Observatory tower. Figure 3-16 compares water

tank, wind tunnel and field behavior.

3.2.2 Shear stresses in the atmospheric surface layer

In the near-adiabatic "constant flux" surface layer the correlations $\overline{u'v'}$, $\overline{w'T'}$, or $\overline{w'q'}$ do not vary significantly. However, one does expect magnitudes to decrease from surface values to near zero as height increase above 0.1k. Hence, convenient forms for the flux variations are:

$$-\overline{u'w'}/u_*^2 = \overline{w'T'}/(u_*\theta_*) = (1 - z/\delta) \tag{3.16}$$

where one might use the expression recommended by Counihan (1975) for adiabatic boundary layers:

$$u_*^2/U_{30}^2 = 0.00275 + 0.0006(\log_{10}(z_o)) \tag{3.17}$$

Shear stresses in near neutral and stable boundary layers appear to obey Monin-Obukhov similarity, unstable layers scale with mixed layer parameters, ie. layer height and convective velocity.

3.2.3 Turbulence length and time scales in the surface layer.

Frequently the size and distribution of turbulent eddies are characterized by time and length scales associated with mechanisms of their production or dissipation. For example the shape of correlations of turbulence fluctuations in space or time can be characterized by such parameters. Consider the correlation of components of velocity fluctuations separated by varying increments in time and space,

$$R_{ij}(x,y,z;\lambda) = \overline{u'_i(X,Y,Z;t)u'_j(X+x,Y+y,Z+z;t+\lambda)} / \sqrt{\overline{u'_i{}^2}}\sqrt{\overline{u'_j{}^2}} \qquad (3.18)$$

where x, y, z, and g are increments of separation. When x = y = z = 0 the product is termed a turbulence autocorrelation, when x, y, or z are finite the product is called a space-time correlation. Typically the correlation is assumed to decay in an exponential manner as the increment increases. The rate of decay at small increments is characteristic of small eddy sizes; whereas the overall gross area of the correlation is associated with larger or "energy containing" eddies; hence, integral time scales may be defined as:

$$Lu_x = \int R_x(\lambda)d\lambda \quad , \quad Lu_y = \int R_y(\lambda)d\lambda \quad , \quad Lu_z = \int R_z(\lambda)d\lambda \qquad (3.19)$$

Counihan (1975) concluded that the longitudinal integral scale Lu_x decreased with increase of surface roughness and increased with height up to 200-300m. Above this level, he thought Lu_x was independent of surface roughness and decreased with height. A summary of his results showing the variation of Lu_x with elevation and roughness length is given in Figure 3-17. In addition, Counihan concluded other integral scales varied as:

$$\begin{aligned} &Lu_y = 0.3 \text{ to } 0.4\ Lu_x \\ &Lu_z = 0.5 \text{ to } 0.6\ Lu_x \end{aligned} \qquad \text{for } 10 < z < 240 \text{ m}, \qquad (3.20)$$

$$Lu_y = Lu_z = (Lu_x)/2 \qquad \text{for } 240 < z < 600 \text{ m, and}$$

$$Lw_z = 0.4\ z \qquad \text{for } z < 100 \text{ m.}$$

The space or time scales associated with small eddies are called microscales. The Kolmogorov microscale depends only on dissipation, ε, and molecular viscosity, ν and is defined by $\underline{\eta} = (\nu^3/\varepsilon)^{1/4}$. For

typical values of viscosity and dissipation in the surface layer, the Kolmogorov microscale is about a millimeter. It is at this scale that turbulent motions are finally dissipated into heat by molecular motions. The Taylor microscale is related to the radius of curvature of a correlation, R, at zero increment. One may say that it is a measure of the average dimension of the eddies that are mainly responsible for dissipation. Since the Kolmogoroft microscale depends primarily on fluid properties, their magnitudes do not change significantly between atmospheric and laboratory flows. Thus, there can not be similarity between turbulent flows at different geometric sizes with respect to the complete range of turbulent eddies present. Fortunately, single particle dispersion is dominated by the larger eddy sizes for most flows of interest; hence, the critical questions are: "Is the correct mix of large size eddies present?", and "Is the ratio of large (integral) to small (microscales) in a laboratory flow sufficiently large?"

Stratification is expected to have a strong influence on the distribution of turbulent intensity among the various eddies sizes; hence, it is also expected to influence the integral scales. Stable stratification decreases the size of the integral scale; whereas unstable stratification increases that size. Most measurements of scale size in stratified flow are estimated from the peak of spectral distributions as discussed in the following section.

Integral space and time scales are normally related through Taylor's frozen flow hypothessis, that is $Lu_x = U*T$. There is no guarantee that this is correct, especially in shear flows, but it is frequently applied.

3.2.4 Power spectrum of turbulent velocity fluctuations.

A measure of the turbulent kinetic energy associated with the fluctuating velocity compoent, u' is $\overline{u'^2}$. The random variation of this energy measure can be harmonically decomposed into the sum of cosine and sine waves of varying amplitudes and frequencies through the technique of Fourier integral transformations. It is convenient to present this energy measure at the cyclic frequency n (Hz) as the integral of power over an incrementally small frequency range, dn. Mathematically, $S_u(n) = \overline{du'^2}(n)/dn$ where $S_u(n)$ is the longitudinal power spectral density, and $\overline{u'^2}(n)$ is the energy density at frequency n. Integrating $S_u(n)$ over all frequencies yields the total mean square velocity fluctuations, $\sigma_u^2 = \overline{u'^2}$. The characteristics of the rms velocity fluctuation, σ_u, were discussed in the previous Section 3.2.1.

Spectral data is presented in a normalized form, such that equal areas on a graph represent equal fractional energies. In a presentation of $nS_u(n)/\overline{u'^2}$ versus n/u on log-log paper, the magnitude of the function is the ratio of the turbulent energy at a specific wave number (or wavelength characteristic of a turbulent eddy) to the total turbulent energy of the flow. The wave length, λ_m, characteristic of the eddies of largest energy will be at the peak of the curve.

Empirical expressions have been proposed to correlate atmospheric spectral data. Several predictions of the spectral distribution of turbulent energy in a strong-wind, neutrally-stable atmosphere at a ten meter height are presented in Figure 3-18. There is a fairly large scatter among these spectral curves, as well as in the original data base. The Harris, Davenport, and Kaimal curves do not predict

any variation in the spectral distributions with changing surface roughness, but the ESDU curves do predict variation with changing z_o. Kaimal reported that atmospheric spectra rapidly change character with the slightest onset of unstable density gradients. He proposed a neutral expression as the limit to stable distributions, and he included the shaded area shown in Figure 3-18 as a highly variable range of spectral distributions for neutral or undetectable unstable conditions. All the expressions predict the -2/3 decay characteristic of an "inertial subrange". The inertial subrange is the turbulence size range where no production or dissipation occurs, but convective stretching progressively distributes energies from larger eddies into smaller ones, until the energy is finally dissipated at very small scales by viscosity.

The large variability found for the peak wavelength is due to the fairly flat variation of spectral energies at peak wavelengths and the large variations in predicted atmospheric spectral behavior. The flatness of the spectral distribution suggests there should be some flexibility in choosing representative model length scale ratios based on peak values. The large variation in atmospheric spectral behavior is undoubtedly due to the grouping together of measurements taken at many different sites.

Empirical expressions suggested by Kaimal et al. (1972) for the behavior of adiabatic boundary layer spectra over homogeneous terrain are:

(3.21)

$$nS_u(n)/u_*^2 = 105f/(1+33f)^{5/3}$$

$$nS_v(n)/u_*^2 = 17f/(1+9.5)^{5/3}$$

$$nS_w(n)/u_*^2 = 2f/(1+5.3f^{5/3}), \text{ and}$$

$$-nC_{uw}(n)/u_*^2 = 14f/(1+9.6f)^{2.4},$$

where $f = nz/u$ is a nondimensional reduced frequency.

Velocity spectra in stable and unstable air may be estimated from expressions suggested by Kaimal (1973) and Hojstrup (1981) respectively. These expressions are found to be driven by the parameters $n = fz/U$, $n_i = fz_i/U$, and z_i/L_{mo} where i is the Cartesian vector index. Figures 3-19 and 3-20 display spectral variations suggested for stable and unstable spectra respectively.

Dutton et al. (1980) have suggested that the peak reduced frequency, n_m, can be well approximated for vertical spectra by

(3.22)

$$f_m = 0.183 \qquad \text{for } z/L_{mo} < -.7,$$

$$f_m = 0.482 + 0.437z/L_{mo} \qquad \text{for } -.7 < z/L_{mo} < 0, \text{ and}$$

$$f_m = 0.482 + 0.87z/L_{mo} \qquad \text{for } z/L_{mo} > 0.$$

as shown in Figure 3-21 extracted from Kaimal, et al. (1972). The wavelength corresponding to the peak in the logarithmic spectrum nS(n) can be related to n or f by $\lambda_m = U/n_m = z/f_m$, where n_m and f_m are the cyclic and reduced freqencies at the spectral peak. The spectral peak may be related to the earlier discussion of the integral scales by,

(3.23)

$$L_x = 0.16z/f_m = \lambda_m/2$$

Although Counihan identified apparent variations in L_x with roughness,

there is no systematic evidence of dependence of f_m or λ_m on roughness.

3.3 Partial Simulation of the Atmospheric Boundary Layer

Rigorous similarity requires that the eight nondimensional parameters identified in Section 2.2 plus a set of nondimensional boundary conditions must be matched in both model and prototype. For interactions between a heavy plume released at or near ground level and the atmospheric boundary layer several of the aforementioned parameters are unnecessarily restrictive and may be relaxed without causing a significant effect on the resultant concentration field (measurements retain value if they are known to be inherently conservative from a safety standpoint, or if they permit calibration of modules in an analytic or numerical model.) The following section reflect on the rationale for partial simulation of the various dynamic parameters.

3.3.1 The Rossby Number

For a large-scale flow like a midlatitude cyclone ($u \simeq 10$ m/s, $f \simeq 10^{-4}$ s^{-1}, and $L \simeq 10^3$ km; thus, $Ro \simeq 0.1$), advective accelerations and viscous forces are negligible compared to Coriolis force. But for atmospheric turbulence ($u \simeq$ 1-10 m/s, $f \simeq 10^{-4}$ s^{-1}, and $L \simeq$ .001-1000 m; thus, $Ro \simeq 10$ to 10^4), Coriolis forces play an insignificant role. Hence, we can assume the effect of rotation on turbulence can be neglected, even though we know the effect on large-scale mean flow dynamics should be retained.

The Rossby number magnitude controls the extent to which the mean wind direction changes with height. However, little deviation occur

in the surface layer, only a few degrees of rotation occurs in the mixed layers of unstable flow, and no systematic variation in wind direction with height below 200 m appears during neutral stability (high wind speed) flow over flat terrain. Significant wind veering may occur above the stable stratification surface layer, especially during the night, when upper level flows may become uncoupled from the surface flow.

Any veering of the wind with height will cause a gradual turning of the mean path of the center of a diffusion cloud. In addition, there is an associated effect of the vertical gradients in velocity and turbulence, which accelerates the dilution of the cloud. Indeed, since the lateral spread due to turbulence alone will grow as $t^{1/2}$, while the growth due to a uniform shear flow varies as $t^{3/2}$, it is clear that the shear effect will eventually dominate the dispersion process. Snyder (1972, 1981) reviewed various analytical, numerical, and experimental studies on shear flow dispersion phenomena, and he concluded that effects of the Rossby number are important for passive plumes when transport distances exceed 5 km.

The heights of ground level dense plumes ($\simeq$ 1 to 10 m) are usually two orders of magnitude smaller than the neutral or unstable atmospheric boundary layer depth (600-2000m). However, the surface layer may only be 10 to 20 m deep under stable stratification conditions. Thus, shear-induced diffusion may be important during stable situations even if transport distances are less than 5 km. Nonetheless, laboratory estimates of distances to the lower flammability limit for dense plumes should be conservative in the absence of rotation effects.

3.3.2 The Reynolds Number

The Reynolds number is said by Snyder (1981) to be "the most abused criterion in models of atmospheric flows." Scale reductions commonly result in model values three to four orders of magnitude smaller than their field counterpart values. As a consequence, viscous forces must be relatively more important in a laboratory physical model study than they are in the atmosphere. There can be no doubt that Reynolds number inequality results in differences between the model and prototype flows. The critical questions must be "What are the differences?" and "Are they significant?"

Fortunately, it is possible to circumvent the effect of Reynolds number in many cases. Townsend (1956) suggested that, for a flow system in which thermal and Coriolis effects were absent and whose boundary conditions were similar when normalized by the appropriate characteristic length L and velocity U_R, the turbulent flow structure would be similar at all sufficiently high Reynolds numbers. Townsend called this hypothesis of Reynolds number independence "Reynolds number similarity". Exceptions must be (a) the very small scale turbulent structures involved in the dissipation of turbulence into heat and (b) flow fields very close to boundary surfaces where the no-slip boundary condition results in locally very small Reynolds numbers. Consequently, viscosity has very little effect on the bulk of the fluid motions.

The neutrally stratified atmospheric boundary layer is generally accepted to be a constant thickness layer in which Coriolis force and pressure gradient maintain profiles of velocity and shear stress. A wind tunnel or water channel boundary layer obtains its energy input from the external flow above the boundary layer; hence, the depths

must increase and the profiles must adjust accordingly. However, the lower part of the laboratory boundary layer presents an exact analog of the lower part of the atmospheric boundary layer. To what height this correspondance is maintained depends on the nature of the lower surface and the stratification of the flow. Within the atmospheric surface layer the flow scales with friction velocity, u_*, roughness length, z_o, and Monin-Obukhov length, L_{mo}. Measurements by many experimentalists reveal the same behavior is true in the laboratory. Figure 3-22 displays mean velocity and temperature profiles from a meteorological wind tunnel and the atmosphere log-linear profiles. Experimentalists have successfully reproduced atmospheric mean profile behavior for neutral flows (Jensen, 1958; Counihan, 1969), stable flows (Chuang and Cermak, 1966; Arya and Plate, 1969), unstable flows (Arya, 1975; Mery, et al., 1974), suburban regions (Castro, et al., 1975), and even mixed layers (Poreh and Cermak, 1984).

How does such similarity come about in the face of such strong Reynolds number inequality? First, for simple flat plate and pipe flow situations it has long been observed that the surface drag coefficient becomes invariant with respect to Reynolds number when the surface is "sufficiently rough" and "sufficiently long". Cermak (1975) prepared Figure 3-23 to document that typical wind-tunnel conditions fall within the envelope where total surface drag becomes constant for a specified surface length roughness length ratio. Since the surface friction coefficient ($\sqrt{C_f} = u_*/U_k$) is invariant, then the normalized mean velocity profiles will also be invariant.

Secondly, the gross structure of the turbulence may also be similar over a very wide range of Reynolds numbers. The atmosphere contains time and space scales associated with mechanical and thermal

turbulence produced by roughness and differential heating, motions caused by frontal systems, the diurnal changes, seasonal variations, and annual changes. The smaller scale aerodynamic driven motions are called "turbulence", fronts are part of "weather", and seasonal and annual variations are classified as "climatological" information.

Van der Hoven (1957) examined spectra derived from measurements of horizontal wind components at various towers. He found in all cases that there is a small-scale maximum, between 10^{-2} and 10^{-3} Hz, and a large-scale maximum between 10^{-5} and 10^{-6} Hz, with a gap in between centered near frequencies of $3x10^{-4}$ Hz (or periods of about one hour) (see Figure 3-24). The large scale maximum is associated with weather and climatological variations, whereas the small scale maximum at higher frequencies is associated with roughness, terrain shape, and surface heating. Spectra of vertical motions contain a strong turbulent peak between 10^{-2} and 10^{-3} Hz but negligible energy at low frequencies.

It is the smaller scales of motion below the spectral gap region that are simulated in fluid modeling facilities. Motions associated with the larger scales are often called meandering, and dispersion associated with these movements is dealt with using separate statistics. As a consequence the equivalent upper limit for averaging time in laboratory facilities must be about 10 to 20 minutes. This is an averaging range similar to that used in most of the data which contributed to the famous Pasquill-Gifford dispersion curves.

Figure 3-25 shows that a reduced Reynolds number changes only the higher frequency portion of an Eulerian spectral energy distribution. The ratio of the integral scale to the microscale of turbulence is a measure of the width of the spectrum (or the range of eddy sizes in

the turbulence). Snyder (1981) argues that the Reynold number effect on the separation between energy-containing and dissipation scales may be represented by the formula:

(3-24)

$$\frac{(\Lambda / \eta)_m}{(\Lambda / \eta)_p} = \frac{Re_m^{3/4}}{Re_p} = \frac{L_m^{3/4}}{L_p}$$

assuming that the flow speed and viscosity are the same in field and model. Hence, at a scale of 1:100, a seven-decade-wide atmospheric spectrum is modeled by a 5 1/2-decade-wide laboratory spectrum. On the other hand, if the velocity is controlled by a Froude number criterion, then the velocity scales as $L^{1/2}$, and a seven-decade-wide atmospheric spectrum is modeled by only a 4 1/2-decade-wide laboratory spectrum.

To determine whether such deviation from field scale behavior is critical, one must consider the contribution of individual scales to dispersion. Consider the spectral form of the Taylor diffusion equation proposed by Batchelor (1949):

(3-25)

$$\overline{y'^2}(T) = \overline{v'^2}\, T^2 \int_0^\infty F_L(n) \{ \sin[\pi nT]/(\pi nT) \}^2 \, dn$$

where $\overline{y^2}(T)$ is mean-square particle displacement, $\overline{v'^2}$ is variance of particle velocities, T is travel time from source, n is frequency, and $F_L(n)$ is the Lagrangian spectrum function. The squared term under the integral is very small when $n > 1/T$ and is near unity when $n < 0.1/T$; consequently it behaves as a filter function as shown in Figure 3-26. Thus, at very small travel times all scales of turbulence contribute to the dispersion with the same weight, but for larger travel times the larger scales of turbulence progressively dominate the dispersion process. Thus, eddies with scales less than one-tenth of the plume

diameter or depth do not contribute significantly to the spread of the plume.

Unfortunately, there is no precise definition as to which portion of a spectrum is dominant in dispersing ground level dense plumes. When finite size clouds are under consideration, it is more likely that the smallest scales contribute less to the total dispersion. On the other hand, dense gas clouds, while often large horizontally, dimensions, may have rather small vertical dimensions. Thus, small eddies may still be important to vertical entrainment. Corrsin (1961) argued that during puff dispersion the principal contribution to dispersion comes from eddies of the same size as the particle pair separation; hence, puff diffusion in a model will depend somewhat more strongly upon the model Reynolds number.

The most convincing evidence for the presence of adequate Reynolds number magnitude is obtained when laboratory evidence over a range of Reynolds numbers show that no strong deviations in plume decay rate or plume growth occur. Hatcher and Meroney (1977) plotted curves for the growth and concentration decay of plumes released in stable, neutral, and unstable simulated atmospheric boundary layers. Chaudhry and Meroney (1973) compared the dispersion of elevated and ground level point source plumes in simulated neutral and stable flows against atmospheric data. Figure 3-27 indicates the tunnel results follow the Lagrangian similarity behavior also found by Horst (1979) in atmospheric flows. Yang and Meroney (1973) found that measurements of dispersing puffs in a simulated atmospheric boundary layer reproduced field scale decay rates when integrated over space and time. Neff and Meroney (1982) examined neutrally buoyant gas releases from a ground source area source over a threefold range of Reynolds

numbers that included wind-tunnel speeds varying from 21 to 63 cm/sec at a 2 cm reference height above the wind-tunnel floor. Figure 3-28 does not indicate any systematic deviations in decay rate at the lower velocities.

Li and Meroney (1984) measured Eulerian space-time correlations in a low-speed simulated atmospheric boundary layer in which they also measured plume dispersion. They found that neutral, stable and unstable shear flows reproduced the plume growth behavior found in the atmosphere by Draxler (1976). Earlier Panofsky (1982) had suggested that reproduction of such behavior in the laboratory would be a convincing argument that fluid model facilities could reproduce the essence of atmospheric dispersion. Figures 3-29 and 30 compare dispersion rates for both ground level and elevated releases, and in neutral and stratified environments.

A consequence of low model Reynolds numbers will be shear flows near the ground which are more laminar like in profile shape, and turbulence will not contain scaled eddys of the smaller sizes. These changes in the near flow field affect a gas plume in two ways:

a) the lower model velocities near the surface will not carry undiluted gases downward as fast as prototype velocities. This will tend to provide non-conservative estimates of LFL., but

b) the absence of smaller eddys in the model will slow two-particle dispersion resulting in higher instantaneous concentrations and narrower plumes.

Over some range of Reynolds numbers these two effects will compensate resulting in correct predictions of the LFL but narower plumes.

Since most experiments have not documented the model turbulence

fields at low tunnel speeds, it is not possible to assign magnitudes to the perturbations expected at low Reynolds numbers.

3.3.3 The Richardson Number

Although most wind tunnel investigations are conducted with neutrally stratified boundary layers, there are circumstances when the stratification of the atmosphere must be considered. In particular, air pollution and dispersion problems are often critical during stratified conditions. Unstable stratification may be expected to mitigate hazards by accelerating plume dilution, whereas stable stratification may permit high concentrations to persist. The stability state of the atmosphere is typically characterized by the Richardson number.

The atmospheric gradient Richardson number can be computed from averaged quantities through the equation

$$Ri = \frac{g}{T}\left(\Gamma_d - \Gamma\right)\left(1 + \frac{0.07}{B}\right) \Big/ \left[\left(\frac{\partial u}{\partial z}\right)^2 + \left(\frac{\partial v}{\partial z}\right)^2\right] \qquad (3\text{-}26)$$

where b and b_d are the actual and dry adiabatic potential temperature lapse rates, and $B = [c_p(T_2-T_1)]/[(z_2-z_1)(q_2-q_1)]$ is the Bowen ratio of sensible to latent heat flux at the surface. The Ri number can be taken to represent the ratio of the relative importance of convective and mechanical turbulence. Negative Ri numbers of large value indicate strong convection and weak mechanical turbulence; zero Ri numbers imply purely mechanical turbulence. Positive Ri numbers less than some critical value, $Ri_{critical}$, suggest the presence of mechanical turbulence damped by the density-induced buoyancy forces; for larger positive Ri numbers, turbulence essentially disappears, since the stratification overpowers production by wind shear. The

critical Richardson number has a value near 0.25.

Other stability parameters which are frequently used are the flux Richardson number, the bulk Richardson number, the Ekman stability parameter, or the Monin-Obukhov similarity length:

The flux Richardson Number: $$Ri_f = \frac{g\ w't'}{T\ u'w'\ (du/dz)}$$

The bulk Richardson Number: $$Ri_b = \frac{gz^2(dT/dz - \Gamma)}{T\ u^2}$$

The Ekman stability Parameter: $$f = \frac{ku_*}{f_c L_{mo}}$$

The Monin-Obukhov Length: $$L_{mo} = \frac{-T\ u_*^3}{k\ g\ w't'}$$

The Richardson Ri, number, is a local parameter rather than a global one, since it is based on local flow conditions, but it is inherently related to other parameters such as the Monin-Obukhov stability length. Table 3-2 displays typical values for the various stability parameters prepared by Snyder (1981). Golder (1972) considered the relationships among different stability parameters in the surface layer, and he produced Figure 3-31 to show the relationship between Ri, Ri_b and z/z_o. Note that Ri always approaches zero as z goes to zero at the surface, where mechanical turbulence production due to shear is a maximum. Since dense plumes hug the ground their dilution usually occurs in an environment governed by simple mechanical turbulence. Hence, in most cases, the effect of atmospheric Ri number on local mixing may be minimal. Indeed, the larger local stratification induced by the presence of the dense gas cloud itself may dominate any ambient stratification effects.

A few laboratory facilities exist which can control stratification. Wind tunnel temperatures are generally controlled

through upstream heat exchangers, injection of heated air, or the use of a thermal boundary layer permitted to grow over long segments of heated or cooled surfaces (Plate and Cermak, 1963; Teunissen, 1975; Ogawa et al., 1985; Schon and Mery, 1971). Water channels maintain stratification using either heat or, more frequently, layered salt water (Hunt et al., 1978; Snyder, et al., 1979).

Arya (1969, 1975) performed velocity, temperature, and turbulence measurements in the lowest 15% of a 70 cm deep boundary layer over a smooth surface, where conditions ranged from unstable to moderately stable ($-0.3 < z/L_{mo} < 0.3$). Free stream flow speeds varied from 3 to 9 m/s, and temperature differences were about 40°C across the boundary layer. Cermak, Shrivastava, and Poreh (1983) reported mean velocity and turbulence measurements made for a variety of simulated atmospheric boundary layers over different surface roughness. Free stream flow speeds varied from 2.4 to 3.0 m/s and temperature differences were from 150° to -80°C across the boundary layer. Poreh and Cermak (1984) reproduced unstable lapse conditions including mixed layers and elevated inversions. They reproduced the characteristics of convective boundary layer turbulence measured in the atmosphere (See Figures 3-10 and 3-33).

Diffusion studies made by Chaudhry and Meroney (1973) in stable boundary layers investigated previously by Arya have shown agreement of experimental results with Lagrangian similarity theory. Horst (1979) tested Lagrangian similarity predictions (See Figure 3-32) of crosswind-integrated ground concentration against the Prairie Grass diffusion experiment (Barad, 1958) and an experiment at Idaho Falls (Islitzer and Dumbauld, 1963). He reported good agreement for all stabilities at distances x/z_o out to 2×10^5. Poreh and Cermak (1984,

1985) released plumes in their modeled mixing layer (See Figure 3-33). Their plumes exhibited the plume lofting typical of ground sources and the descent typical of elevated sources, predicted from water tank experiments by Willis and Deardorff (1974, 1976, 1978) and numerically by Lamb (1982).

Staff at the Fluid Mechanics Laboratory at the Ecole Centrale de Lyon have studied unstable wind tunnel boundary layers and compared them with the atmospheric boundary layer (Schon and Mery, 1978). Flow speeds were typically 2 to 4 m/s and the floor temperature was maintained 50°C above ambient. Comparisons with the Kansas data (Haugen et al., 1971) were quite satisfactory, but longitudinal turbulence intensities exhibited a slight Reynolds number dependence, and spectral energy was too low in the high frequency portions of the spectra. The most unstable flow they studied had a Monin-Obukhov scale length of about -1 m at model scales, or -500 to -1000 when scaled to the atmosphere.

Failure to simulate approach flow Richardson numbers will result in model concentrations which overpredict LFL distances under stable field conditions, and underpredict LFL distances under stable field conditions. These effects are likely to be important only for flat homogeneous and unobstructed terrain spills where wake dilution by obstacles is unimportant.

3.4 Boundary and Initial Conditions

Normalization of the governing partial differential equations of fluid mechanics identified flow and property parameters which must be identical if particle kinematics and dynamics are to be similar between model and prototype flows. Fluid modelers have also found

that for the overall model and prototype flow field to be identical the non-dimensional boundary conditions must be identical. Batchelor (1953) comments that exact similitude in boundary conditions would certainly be sufficient to assure exact similarity for every possible fluid realization; however he suggests that in some circumstances this may well be over-sufficient. Since all the boundary conditions cannot be completely specified for atmospheric flows, scientists attempt to simulate boundary conditions during numerical or physical modeling over the ensemble average. It is not now possible, however, to specify anything but the first few moments of the ensemble. Snyder (1981) observes "It is not known if the specification of only the first few moments is sufficient; it is plausible, from physical experience, that such a specification is sufficient."

Armitt and Counihan (1968) have given qualitative arguments which conclude that, for the study of plume dispersal, the mean velocity flow field, the turbulent intensity, and the spectrum of energy for each velocity component at the lower frequencies must be reproduced in the upwind flow field.

The presence of fluid viscosity automatically assures that the mean velocity at all solid boundaries is zero (no-slip); hence, geometrical similarity between model and prototype is required. Yet what detail is necessary in the model to assure flow similarity? Must every door knob, leaf, and window fenester be included? Jensen (1958) suggested that, if the roughness length of the prototype can be estimated, then the model should be scaled such that:

(3-27)

$$(z_{om}/z_{op}) = (L_m/L_p)$$

where L_m/L_p is the model scale ratio. This equation implies that

details of the surface smaller than the irregularities required to produce z_o will have very little effect on the overall flow. Experiments performed in sand roughened pipes suggests that $z_o = k_s/30$, where k_s is mean diameter of uniformly distributed sand grains (Schlichting, 1968). If there were only one combination of roughness elements and their distribution which corresponded to each z_o value, then it would probably be impossible to model a rough earth surface. Fortunately, any required z_o can be obtained by a suitable arrangement of roughness elements and externally impressed disturbances -- such as by grids or fences at the inlet of the wind tunnel test section.

Another difficulty is that fluid flow close to a smooth boundary is not Reynolds number independent, since the no-slip condition at the surface is a viscous constraint. A viscous sublayer exists adjacent to the wall where turbulence diminishes to zero. In some cases scaled roughness elements, k_{sm}, would be buried within this sublayer. But atmospheric flows are almost always aerodynamically rough; thus, it is necessary that modeled roughness be large enough to extend beyond the viscous sublayer which would exist in the absence of the roughness. In other words, the model surface must also be aerodynamically rough. A criterion which insures that the flow is aerodynamically rough is $Re_* = u_* z_o / \nu > 2.5$.

At Re_* below 2.5 it is observed that the mean velocity profiles in turbulent pipe flow lose similarity in shape and deviate from the universal curve of a rough wall turbulent boundary layer. For Re_* above 2.5, it is observed that the surface drag coefficient (and thus the normalized velocity profile) is invariant with respect to increasing Re_*. For Re_* between 0.11 and 2.5, the velocity profiles

are more characteristic of smooth wall turbulent boundary layers, and for values below 0.11, the growth of a laminar sublayer on the wall is observed to increase with decreasing Re_*.

Extrapolation of these results from pipe flow measurements to a simulated atmospheric boundary layer may cause a slight shift in the magnitude of the minimum Re_* requirement. It is the distribution of turbulent velocities which has the greatest effect on dispersion. It si the mean wind shear, however, which generates the turbulent velocities. It is possible that the specification of a minimum Re_* of 2.5 is overly conservative for dispersion simulation. To define the lower limit of Re_* for which turbulent dispersion is invariant in a particular model setting, the investigator should perform several passive plume releases at decreasing wind speeds. Significant changes of concentrations or plume dimensions signal the lower limit for similar plumes.

The presence of a non-passive plume could significantly change the Re_* range over which dispersion invariance exists. Velocities within a heavy plume released at ground level have been observed to be significantly less than those in the approach flow. The laminarization of the velocity field within the dense plume under these circumstances is highly possible; hence, the effect of surface Re_* magnitude on plume dispersion similarity can only be evaluated by direct comparison to field results.

The smallest z_o which can be obtained in most wind tunnels is of the order of 0.001 cm. Measurements made by Neff and Meroney (1982) over a smooth floor wind tunnel at speeds between 0.20 to 1.0 m/s produced a roughness length near z_o = 0.01 cm and Re_* between 0.67 and 3.3. If length scaling were based upon z_o alone, a model scale of

1:250 would be representative of farmland, and a model scale of 1:1000 would be appropriate for a rural setting with a few trees. This correspondence between scale and terrain type suggests a definite limitation to the ability of a wind tunnel to model a large release of heavy gas over a smooth surface (ice, mud flats, calm open sea).

Failure to simulate z_o properly due to thick laminar sublayers would normally result in lower ambient turbulence intensities. Lower turbulence intensities would tend to diminish dispersion and increase model LFL values. Relamarization during dispersion of cold dense field plumes may produce the same effects. Hence, field and model values of LFL will not deviate significantly.

3.5 Simulation of Atmospheric Motions Perturbed by Buildings, Obstacles, and Terrain

Often atmospheric turbulence may cause only weak dispersive effects compared to the turbulence generated by buildings, obstacles, and terrain. Yet the magnitude of the perturbations depends upon the incident flow turbulence scale and intensity, details of the obstacle shape and surface roughness, and the size of the obstacle compared to the boundary layer depth. Geometrical scaling implies that the ratio of the building height to length scale must be matched and, of course, that all other building length scales be reduced to this same ratio.

Several questions should be considered when modeling flows which include surface obstacles:

a.) What size obstacles should be disregarded?
b.) What detail or roughness on a obstacle need be included?
c.) To what upwind distance should all obstacles be included?
d.) At what point does the size of a modeled obstacle become too big for the wind tunnel (i.e., blockage effects)?
e.) What is the effect on the flow field of mismatching obstacle and approach flow length scales?
f.) What is the minimum allowable model obstruction Reynolds

number?

Obstacle sizes to be disregarded:

Boundary layer studies of rough surfaces reveal that if protuberances are of a size k, such that $u_*k/\nu < 5$, they will have little effect on the flow in a turbulent boundary layer. Thus, assuming a laboratory wind speed of 1 m/s and a typical friction coefficient $C_f/2 = (u*/u)^2 = .0025$, obstacles of size less than 2 mm would go unnoticed.

Required obstacle surface detail or roughness:

Another question that always arises is "How much detail is required for the building or obstacle model?" The answer is, of course, dependent upon the size of the protuberance compared to the plume and the dominant eddies of mixing. If the obstruction is large enough to modify the separated wake over the main obstacle, then it must be included. Often an equivalent obstacle surface roughness suffices. Snyder (1981) concludes a generic surface roughness criterion might be $u_*k/\nu > 20$. For a 1 m/s laboratory flow this results in model roughness elements equal to about 6 mm. But since the exterior flow is usually highly turbulent, the body typically includes a highly unsteady wake, and the u_* value to be used should be that acting on the building surface, rather than that of the approach flow. Hence, even this roughness may be unnecessarily large. In the absence of field information, smoke visualization studies of the influence of various size perturbations on the obstacle wake behavior would be appropriate.

Upstream fetch to be modeled:

Suppose there is another building, tree line, fence, tank, or obstacle some distance, s, upstream of a potential LNG release

location; is it necessary to include this obstacle in the wind-tunnel model? Hunt (1974) showed that the velocity deficit in the wakes of cubes and cylinders is given approximately by:

$$DU_{mx}/U(h) = A\ (s/h)^{-3/2} \qquad (3\text{-}28)$$

downwind of the separation bubble, where DU_{mx} is the maximum mean velocity deficit created by the obstacle, h is the height of the obstacle, S is the distance downstream of the obstacle, and A is a constant dependent upon the obstacle shape, orientation, boundary layer thickness, etc. Typically, A = 2.5, but it may range from 1.5 to 5.0. If we desire that the velocity at the spill site be within 3% of its undisturbed value, Snyder (1981) recommends that any upstream obstacle as high as s/20 be included upstream in the model of the spill site. If the obstacle's width is much greater than its height (for example, a fence or ridge), one should include it in the physical model if its height is greater than s/100.

Blockage effects:

Because of the influence of wind tunnel walls on the behavior of the flow past models, it is desirable to use small models or big tunnels, or both. On the other hand, larger models are not only easier to work with, but they may be needed for similarity reasons to achieve large enough Reynolds numbers. It is possible to identify three different types of effects of wind tunnel constraints. The first is the simple "solid blockage" effect which arises because the fluid stream is unable to expand laterally as it normally would in unconfined flow. The second effect, called "wake blockage", results because the accelerated flow between an obstacle and the tunnel walls, continues to "pinch" the wake flow region and reduce its normal

lateral rate of growth. The third effect is produced by the growth of boundary layers on the tunnel walls which produce "wall boundary interference." Tunnel blockage can cause separation and reattachment locations to vary, produce higher velocities, larger wake turbulence, and modify the dispersion patterns in the vicinity of obstructions.

The ratio of the cross-sectional area of a model obstacle to that of the tunnel is called the "blockage ratio", BR. Mass continuity produces an average velocity speed-up of S = BR/(1-BR). Although wind tunnels with adjustable ceilings can compensate to some extent by raising the roof locally, this is not a perfect solution to the problem. Measurements on building and cooling tower models placed in different size wind tunnel test section reveal major changes in the character of pressure distributions, separation, and wake growth in the presence of flow restricted by wind-tunnel side walls (Farell et al., 1977). Figure 3-34 displays the variation of the base pressure coefficient, C_{pb}, for various wall mounted shapes with total blockage ratio, BR. Open-jet tunnels appear to avoid most of the wake blockage effect.

Blockage corrections, which are conventionally applied in aeronautical tunnels, can not usually be applied to the typical asymmetric model configuration placed against the wall of a meteorological wind tunnel (Ranga Raju and Singh, 1976). Conventional wisdom now suggests the "rule of thumb" that blockage ratios greater than 5% should be avoided.

Effect of scale mismatch on flow around obstaeles:

Some dense gas simulations require a model scale of small scale ratio, but the only available boundary layer turbulence environment is characterized by a larger scale ratio. Experimentalists have

generally accepted the mismatch, and rationalized that since the shear produced by the dense gravity current and nearby obstacles dominate the mixing process the exact state of the background approach flow is unimportant (Neff and Meroney, 1982; Kothari and Meroney, 1981 and 1982). Hunt (1981) examined the influence of boundary layer to obstacle scale mismatch on wind tunnel measurements of surface pressures on model buildings. He found that the effect of using a model twice the correct size is to underestimate the magnitude of all mean pressures, by i.) 5% on the front face, ii.) 20% on negative peaks, and iii.) 30% on base pressures. The effect of using a model half the correct size is to overestimate the magnitude of all mean pressures , by i.) 5% on the front face, ii.) 6% on negative peaks, and iii.) 30% on base pressures. These variations result because the character of separation and reattachment around an obstacle is very sensitive to the level of turbulence intensity and eddy size in the approach flow (See Figure 3-35). A relatively small model encounters eddies that are proportionally too large, which tends to broaden the spread of the shear layer which forms across the separation streamlines. This increased entrainment reduces the pressure immediately behind the body, causing the cavity length to shrink in size. This modifies the curvature of the streamlines, the location of reattachment points, and the width of the wake region.

Humphries and Vincent (1976) and Vincent (1977, 1978) reported experiments with disks and cubes using uniform smooth, uniform turbulent, and turbulent boundary layers as incident flows. The model height, or scale, was varied, and the variation in pressures, cavity size, and cavity pollution retention time was found to vary with a dimensionless turbulence parameter $\tau = (u_{rms}/U)(\Lambda_x/H)$, where Λ_x is the

integral length scale. As shown in Figure 3-36, when λ increases then cavity retention time decreases, cavity dimensions decrease and obstacle drag increases. The effect of turbulence intensity is well established (Bearman, 1978), but the effect of the independent variation of integral scale is less certain. Lee (1977) has reported data which show a 15% to 20% variation of drag coefficients with longitudinal turbulence scale of the approach flow, L_{ux}. Petty (1979) investigated the effects of the length scale of approaching turbulence on the base pressure of a square prism. He found these effects are probably small, although it seems that the larger the relative scale of the turbulence , the less effect it has.

One must conclude that mismatching the obstacle and flow scales may indeed influence plume dispersion, but it is not possible to specify an error magnitude for the practice. Hosker (1984) recommended that experiments should be performed which independently examine the effects of turbulence intensity, shear flow, and turbulence integral scales on the flow field about simple building shapes. Such experiments would be very valuable for the evaluation of physical models of LNG spills in the presence of surface obstacles.

Minimum Reynolds number criterion will be discussed separately in Sections 3.5.1 and 3.5.2 for sharp edged and rounded obstacles respectively.

3.5.1 Simulation of the flow over sharp-edged obstacles

A number of authors have discussed flow studies about simple cubical or rectangular sharp-edged obstacles. An extensive review about such flow fields and the subsequent character of diffusion near obstacles has been provided by Hosker (1984). Peterka, Meroney and

Kothari (1985) describe typical flow deviations which result from the presence of a sharp-edged building.

Figure 3-37 illustrates the main features of the flow around a sharp-edged building. Typically, when the approach flow is normal to the building face, the flow separates from the ground upwind of the building and produces a "horse-shoe"-shaped vortex which wraps around the base of the building. The surface streamline reattaches on the front of the building, and fluid parcels move up and down the building's forward face. An elevated streamline flows over the obstacle, dips down behind, and stagnates on the surface at the end of the recirculating cavity immediately downwind of the building. Sometimes separation streamlines from the forward building edges reattach to the same face, yet in other cases the streamlines enter the downwind cavity and mingle with the other recirculating fluid. Air which enters the cavity departs through turbulent mixing across the dividing streamlines, mingles with downwind-pointing vortices and is ejected laterally out of the cavity, or leaves suddenly during an exhalation when the entire cavity appears to collapse and then reform.

When the building is oriented obliquely to the wind, flow over the front side walls does not separate, but strong recirculation occurs on the downwind faces. Flow over the roof often produces counter-rotating "delta-wing" vortices which increase mixing over the top and in the wake of the building. These vortices can cause reattachment of the flow in the middle of the roof and serious plume downwash in the near wake. Other features of the flow near the building include vertical vortices produced by the vertical corners of the building.

The highly mixed region downwind of an obstacle can lead to rapid

mixing of an otherwise sluggishly dispersing dense gas plume. Such passive means of reducing concentrations may inadvertently or by design mitigate hazards from LNG spills (See Kothari and Meroney, 1981, 1982; McQuaid, 1985).

During laboratory tests of dense gas dispersion about model obstacles it is desirable that the flow structure and associated dispersion be Reynolds number independent. Only a few systematic studies have been made on Reynolds number independence relating to atmospheric modeling. Dagliesh (1975) compared wind tunnel and full-scale measurements of pressures on the Commerce Court Tower, Montreal, Canada (Figure 3-38). The wind tunnel values were provided at the design stage and are represented by open circles. The solid lines join average values of estimates derived from actual observations of pressure differences on the building; the shaded areas indicate the standard deviation of the full scale estimates. It is seen that the agreement between model and full-scale measurements of the mean pressures are very good. However, it appears that wind-tunnel data on local fluctuating pressures attributable to vortex shedding differ at some points significantly from the pressures on the prototype. In this study, the model Reynolds number was about $Re = 10^6$, whereas the prototype values were about three orders of magnitude larger. Tunnel velocities were of course much higher (U_m = 15.2 m/s) than those commonly used to model dense gas dispersion (U_m < 2 m/s).

Golden (1961) measured the concentration patterns above the roof of model cubes in a wind tunnel. Two sizes of cubes were used to vary the Reynolds number from 1000 to 94,000. The concentration isopleths in the fluid above the cube roof showed only slight variations over

the entire range of Reynolds numbers studied. The maximum concentration on the roof itself was found to vary strongly with Reynolds numbers less than 11,000, but to be invariant with Reynolds numbers between 11,000 and 94,000. Frequently modelers quote Golden's experiments as justification for presuming dispersion invariance when obstacle Reynolds numbers exceed 11,000. However, Golden's "11,000 rule" is limited to the measurement of concentrations at only one point on the roof of smooth-walled cubes placed in an uniform approach flow of very low turbulent intensity. It is probably quite conservative, because the shear and high turbulence in a simulated atmospheric boundary layer are likely to further reduce the critical Reynolds number. Indeed Halitsky (1968) observed that for dispersion in the wake region no change in isoconcentration isopleths from passive gas releases was found to occur for values of Reynolds number as low as 3300.

Fackrell and Pearce (1981) examined wind tunnel measurements of near-wake parameters for many different building shapes in a variety of boundary layer flows. Measurements of recirculation region (cavity) characteristics at Reynolds numbers of 5000 and upwards showed no significant differences in residence time or recirculation region length. They concluded their results were independent of Reynolds number.

Flow around sharp-edged obstacles will remain kinematically similar at very low Reynolds numbers. Wake width variation will be minimal, and obstacle generated turbulence scales and intensity will only vary slowly as Reynolds number decreases. Gas clouds dispersing in this environment will remain similar at very low model speeds.

3.5.2 Simulation of flow over rounded obstacles

Flow around a smooth cylinder is Reynolds number dependent. This dependence reflects changes in the nature of the boundary layer that forms over the cylinder and its behavior in the vicinity of the flow separation. At low Reynolds numbers, the boundary layer is laminar, and separation occurs easily under the influence of even modest positive pressure gradients. At higher Reynolds numbers, the boundary layer becomes turbulent and flow separation is delayed; i.e., the flow can move farther along a curved surface without separation. At prototype scales, obstacles are large enough that only turbulent separation occurs. However, model flows are usually at such low Reynolds numbers that the local boundary layer growing over a curved surface would be laminar. Most modelers attempt the reproduction of full-scale similarity around curved surfaces by artificially roughening the model surface to force transition to turbulence in these laminar boundary layers. This can be done by providing the surface with special (or artificial) roughness elements, for example, sandpaper, thin wires, or grooves. The height of the roughness, k, should be such that $Uk/\nu > 400$ and $k/R < 0.01$, where U is the mean wind speed at obstacle height and R is the characteristic obstacle radius of curvature. Szechenyi (1975) studied flows about rough circular cylinders and obtained the results in Fig. 3-39. As Reynolds number decreases, roughening the surface becomes less effective. Fage and Warsap (1929) prepared Fig. 3-40 which displays the effect of increasing the surface roughness of cylinders on their drag coefficient. As shown eventually, even ridiculously large roughness is ineffective.

But for dense gas dispersion studies most curved or cylindrical

obstacles of interest are not extremely long cylinders. Typically, such spills occur near storage tanks, ships, or tank cars. Flow studies by Roper (1967) and Symes and Meroney (1970) about truncated cylinders immersed in deep turbulent shear layers suggest that the approach flow turbulence, the shear flow, and wall-bound vortices are similar down to rather low Reynolds numbers (Re = 2.7 x 10^2 - 3.7 x 10^4). Hosker (1984) reviewed a number of studies which report flow measurements about ground-mounted obstacles -- cylinders, hemispheres, spheres, cones, and cone frustrums. He observed that all model studies report the presence of a horseshoe vortex on the ground, elevated vortex pairs due to the bending over at roof level of the spiral vortices generated behind the sides of the bodies, and other qualitative features seen in low speed flows which are similar to those observed in high speed turbulent flow. Hosker noted that for curved obstacles placed in turbulent shear layers only turbulence details of minor importance to the dispersing plume depended on on obstacle Reynolds number.

Niemann and Ruhwedel (1980) compared pressures and forces about a 1:333 scale model to a full scale hyperbolic cooling tower shell. They roughened their model with vertical ribs of height 0.09 mm and width 0.77 mm, producing a roughness coefficient of k/2R = .0006 and roughness Reynolds number, Re_k > 270. Fig. 3-41 compares measured meridion forces on the cooling tower model and prototype. Model Reynolds numbers were between 4.5 x 10^5 and 6.0 x 10^5, and this corresponding to U_m > 45 m/s. But again these speeds are much higher than is appropriate for dense gas experiments.

Halitsky et al.(1963) examined dispersion about a smooth-model nuclear-reactor containment building (a hemisphere fitted on a

vertical cylinder) and found a critical Reynolds number greater than 79,000. (Yet this critical Reynolds number was for flow very close to the vessel wall. The behavior of concentration isopleths further downwind are likely to be less Reynolds number dependent.)

As Snyder (1981) observed "the more streamlined is the object, the larger is the critical Reynolds number." In the extreme case of an airfoil the changes resulting from the movement of separation bubbles can be very dramatic indeed, as shown in Figure 3-42 from Mueller and Batill (1982).

Although the details of fluid motions around rounded obstacles vary significantly with Reynolds number, the gross features of the flow do not change. Even small models at low wind speeds will produce horse-shoe shaped ground vortexes, elevated pairs, and regular vortex shedding. If the internal boundary layer over the obstacle is laminar, then the wake region will be broader and less intense. Gas clouds dispersing in this environment will dilute slower and model LFL distances will be conservatively too large.

3.5.3 Terrain, slope and roughness effects

Model requirements for simulating neutral flow over hilly terrain are essentially the same as those for modeling that around buildings. Terrain, however, is generally much more irregular, roughness is distributed in random asymmetric patches, and stratification may play an important role. Terrain slope is very important during dense gas dispersion, because the fluid motions are strongly gravity driven, and the gases will tend to drift downhill and along contour lines constrained by terrain contours.

Since model velocities are normally quite low, it is necessary to

roughen the surface to assure turbulent separation. The same roughness criterion as for buildings should be applied, i.e., $Re_k = U_m k/\nu > 400$, or $Re_{k*} = u_* k/\nu > 20$. In this case, however, since the dense gas cloud tends to hug the surface, care must be taken that roughness elements are not large compared with the depth of the cloud itself! For this reason the common practice of constructing models from layers of plywood, expanded plastic foam, or cardboard must be considered carefully, or the model terrain steps will exceed the plume gravity head height.

Enough upwind terrain fetch must be included in the model that the boundary layer has reached an equilibrium condition. Two-dimensional ridges should be included if their height is greater than 1/100th their distance upwind from the spill location, while three-dimensional hills may be ignored if their height is less than 1/20th their upwind distance (Snyder, 1981). Note that the recommendations indicate the fetch required to include local anomalies introduced by the unique terrain features; they do not indicate the fetch required to establish an equilibrium boundary layer depth.

Since an LNG plume is buoyancy dominated, surface slope can act to either accelerate or decelerate a dense plume lying on that surface. Criteria used to decide if slope effects are significant are discussed below. For even modest slopes, downslope flow due to gravitational effects can be as rapid as the outflow due to gravity spreading. de Nevers (1984) showed that even a 1.15^{o} slope would produce velocities greater than the gravity head velocities for a hypothetical LPG spill of 20 kg/sec of propane (54 $m^3 s^{-1}$ and a specific gravity of 1.43) only 10 seconds after the start of the flow. A criterion for including slope, β, influence based on de Nevers

calculations is:

(3-29)

$$\frac{2 \sin \beta}{[(SG)(f_t + f_b) + (2H\ C_D)/(\ R\ )]} < 1$$

where f_t and f_b are the top and bottom friction coefficients respectively ($f \simeq 0.005$), C_D is the form drag coefficient ($C_D \simeq 1$), R is cloud radius, H is cloud height, and SG is the local dense gas specific gravity.

Fay and Ranck (1983) proposed a similar, but somewhat simpler criterion for releases of gas volumes driven by wind into adverse slopes. Their analysis suggested slope effects may be ignored if:

(3-30)

$$1/Ri_* = u_*^2/(g'H) >> \beta,$$

where H is local cloud depth and $g' = g\Delta\rho/\rho$.

Hall et al. (1974) measured the behavior of continuous releases of dense gas on up and down slopes of 1 in 12 ($\pm 4.76^o$), produced by adjusting the boards on the meteorological wind tunnel floor to which the surface roughness was attached. Because of blockage effects caused by the ramps , the flows were associated with accelerating and decelerating flows respectively. On the downhill slope, there was very little upstream movement of the gas and the plume was relatively narrow, while on the uphill slope, the plume was very wide, and upstream movement was considerable. A slight lateral slope of only 0.2^o was believed to cause a distinct asymmetry of the plume during the upstream slope condition.

Meroney et al. (1977) also performed continuous dense gas spills on 1 in 50 (1.15^o) up-sloping ramps. They included the presence of up

- and downwind model storage tanks in some tests. At low wind speeds enough dense gas eventually collected outside the ruptured model tank for the vapor to begin to travel continuously upwind. The storage tanks definitely sheltered a portion of the cloud, and enhanced the tendency of the gas to pool and then move upwind. The flow was very sensitive to start-up conditions, and random perturbations could cause the vapor motion to switch from upwind to a downwind character. Perturbations in source exhaust, perturbations in the approach wind field, or irregularities in the ramp construction sometimes caused a marked asymmetry in the vapor cloud.

Alessio et al. (1981) examined two models of a crater-shaped valley, 6 km in diameter, open on the West and East sides, close to Grosseto, Italy. The height of the valley walls was about 120 m. The hypothetical source was a geothermal well which vented large quantities of water vapor and carbon dioxide at high velocities from a 0.25-0.4 m diameter well hole. One model was at a scale of 1:4000 and the other was at a scale of 1:3000, reproducing an area of about 50 km^2 and 30 km^2, respectively. The authors permitted the source density ratio to vary, but specified emission Richardson numbers. The laboratory devices were a pair of large water tanks, and the source was a salt-water mixture emitted into clear water. The authors compared their average spread rates to algorithms suggested by Britter (1979), and felt their agreement was reasonable. See Fig. 3-43 which shows the initial formation of a toroidal annulus, followed by movement along terrain channels.

Surface slope must be included when modeling dense gas dispersion. Gravity flows generate most of the turbulence and motions which spread and dilute a dense gas cloud. Criterion described by

Equations (3-29) or (3-30) may be used to evaluate critical slope angles. Terrain slope may either accelerate or slow the dilution of a gas cloud. The slope may cause the cloud to pool or it may deflect the cloud laterally.

3.6 Summary and Recommendations

Similarity criteria for modeling atmospheric flows in air or water have been derived in Section 2.1 and described in Section 2.2. Rigorous similarity would require that the eight nondimensional parameters, plus a set of nondimensional boundary conditions, be matched in both model and prototype. In Sections 3.3 and 3.4 the arguments for partial simulation were presented. The following constraints were identified:

a.) Geometric similarity (i.e., undistorted models) is required to maintain similarity in particle kinematics, and the appropriate ratio between vertical and horizontal turbulence velocity scales.

b.) In the atmospheric boundary layer, the Rossby number governs the extent to which the mean wind direction changes with height. Coriolis effects are expected to have the largest effect above stable stratification surface layers at night. Coriolis effects on atmospheric turbulence near the ground, appears to be minimal. The presence of terrain, thermal winds, or surface obstacles will minimize the influence of the earth's rotation. Since dense gas plumes remain near the ground, neglected surface shear-induced diffusion may be compared with other effects. However, over smooth flat terrain (e.g., water surfaces), Coriolis forces should be considered in estimating plume dispersion beyond about 5 km.

c.) Reynolds number equality is not strictly possible between laboratory and prototype simulations of dense gas dispersion in an atmospheric surface layer. Heuristic arguments and experimental evidence indicate that it is not necessary to match Reynolds numbers if the model Reynolds number is "sufficiently" large. Modelers can not attempt to simulate all scales of atmospheric motion, but they should seek to match turbulent integral scale ratios, and maintain the integral-to-dissipation scale ratio as large as possible. Most validation work to date has emphasized the high wind speed boundary layer suitable for simulating building loading problems. Low model Reynolds numbers

result in shear flow mean and turbulent profile distortions. These distortions are likely to balance one another such that gas cloud growth remains the same to quite low Reynolds numbers. Most model experiments have been performed at tunnel speeds above 0.5 m/sec; hence, there is not enough experience with such plans to specify confidently the nature of model cloud behavior at lower shear layer speeds.

d.) A broad range of atmospheric stratification conditions can be simulated in special meteorological wind tunnels or water tunnels; hence, Richardson number equality is conceptually possible even if difficult. Unfortunately, equality of Richardson number usually imposes low fluid speeds, which reduce model Reynolds numbers. As noted in Section 3.3.3 failure to simulate the approach flow Richardson number will result in erroneous model values of gas cloud LFL. If the field flow is stabily stratified, model gas cloud LFL values may be too large.

e.) The mean velocity profile is logarithmic in the surface layer. Its depth is about 100 m under neutral conditions, and is proportional to the Monin-Obukhov similarity length, L_{mo}, under stratified conditions. Jensen's criterion that $(z_o/L)_m = (z_o/L)_p$ be satisfied is normally a necessary condition. Sometimes this would result in roughness immersed in a laminar sublayer. Maintaining an aerodynamically rough ground surface takes precedence over Jensen's criteria; hence, it is important that the roughness Reynolds number be kept as large as possible, (i.e., $Re_* = u_* k/\nu > 2.5$). Since the smallest z_o which can be obtained in most tunnels is 0.001 cm, it is not possible to simulate the large release of heavy gas over a smooth surface (e.g., ice, mud flats, open sea).

f.) Since dense gas dispersion occurs in only the lowest level of the atmospheric boundary layer, it may be satisfactory to simulate only the bottom 100 m of the flow field. In such a case, some of the larger eddy scales would be missing. The effect on the dispersion of dense gases is unknown, but it is likely that the critical vertical mass transport rate would only be slightly influenced.

g.) During neutral and unstable conditions, the surface layer properties extend to about 100 m depth, but during stable conditions the layer may only be 10 to 20 m in depth. During near-neutral situations, Monin-Obukhov similarity may be presumed to exist, and during lapse conditions convective scaling by convection velocity and mixing layer depth seems appropriate. Above the surface layer, wind veering with height is significant during neutral and stable flows. Incorporation of stratification during simulation of small dense gas spills may not be necessary, since the plume remains very near the ground where the local Richardson number is quite small. But for large dense gas releases, the mixing capacity of the diabatic atmosphere may be dominant once the initial mechanical mixing generated by the release conditions has decayed.

h.) When smooth-faced buildings, fences, or other sharp edged

obstructions are close to the release site, the obstacles should be modeled if their heights exceed s/100 or s/20 for two-dimensional or three-dimensional shapes, respectively. Yet for kinematic similarity, any wind-tunnel blockage should be limited to 5% (10% in a tunnel with an adjustable ceiling). If possible, the obstruction Reynolds number should be maintained above 10,000 if the source is on the obstacle and nearby concentrations are critical. If concentration isopleths some distance from the obstacle are more interesting, then the obstruction Reynolds number only needs to exceed 3000. These recommendations are based on passive plume behavior in a very few experiments.

i.) The surface of the obstacles should be covered with roughness, such that the roughness Reynolds number, $Re_* > 20\text{-}100$. In some cases, this results in an unacceptable surface roughness, ie. $k \simeq O(L_{obstacle})$.

j.) Simulation of flow over complex terrain requires the same modeling restrictions as flow over other obstacles. However, most terrain undulations would be considered curved; hence, the sharp-edged building minimum Reynolds number criteria may be too lenient. Roughness should obey Jensen's criterion and the minimum roughness Reynolds number constraint. Since this may result in rather large roughness elements, there is some conflict with the desire to simulate the low lying dense gas plume. Simulation of a large dense gas cloud flowing about rounded grassy hills may result in the model simulant moving in what appears to be a suburban housing district!

TABLE 3-1. VALUES OF SURFACE ROUGHNESS LENGTH FOR VARIOUS TYPES OF SURFACES[a]

Type of Surface	z_o (cm)
Sand	0.01 - 0.1
Sea Surface	0.0003[b] - 0.5[c]
Snow surface	0.1 - 0.6
Mown Grass (~0.01 m)	0.1 - 1
Low grass, steppe	1 - 4
Fallow field	2 - 3
High grass	4 - 10
Palmetto	10 - 30
Pine forest (Mean height of trees: 15 m; one tree per 10 m^2; $z_d \cong 12$ m)	90 - 100
Outskirts of towns, suburbs	20 - 40[d]
Centers of towns	35 - 45[d]
Centers of large cities	60 - 80[d]

(a) From Simiu and Scanlan (1978) and Snyder (1981).

(b) Wind speed at 10 m above surface = 1.5 m/sec.

(c) Wind speed at 10 m above surface > 15 m/sec.

(d) These values are exceptionally small; see text.

TABLE 3-2. TYPICAL VALUES FOR THE VARIOUS STABILITY PARAMETERS

Qualitative description	Pasquill-Gifford category	L,m	z/L	Ri_f	Ri	Ri_B[a]	Fr	μ	u_*,m/s[b]
Highly unstable	A	-5	-2	-5	-2	-0.03	-	-4000	0.3
Unstable	B	-10	-1	-2	-1	-0.02	-	-120	0.3
Slightly unstable	C	-20	-0.5	-1	-0.5	-0.01	-	-60	0.3
Neutral	D	∞	0	0	0	0	∞	0	0.3
Slightly stable	E	100	0.1	0.07	0.07	0.004	16	12	0.3
Stable	F	20	0.5	0.14	0.14	0.05	7	40	0.2
Highly stable	G	10	1	0.17	0.17	0.17	5	100	0.1

(a) The assumed height of the anemometer and upper thermometer was 10 m; the lower thermometer: 2 m. A roughness length of 0.01 m was also assumed in the calculations.

(b) The friction velocity listed is that value used in calculating μ.

(c) From Snyder (1981).

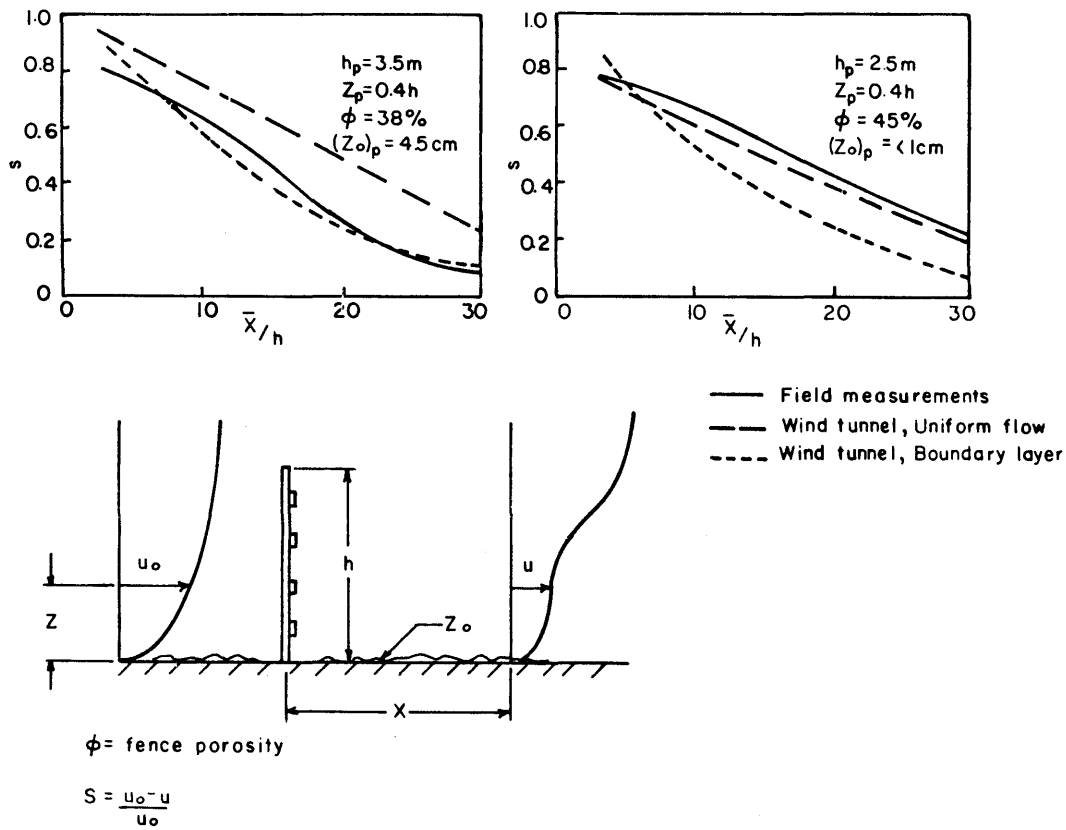

Figure 3-1. Comparison between shelter curves from measurements in nature. Shelter is a 3.5 m high screen and z_o = 4.5 cm, modeled by a 5 cm fence and a rough corrugated paper tunnel bottom. (Jensen, 1958).

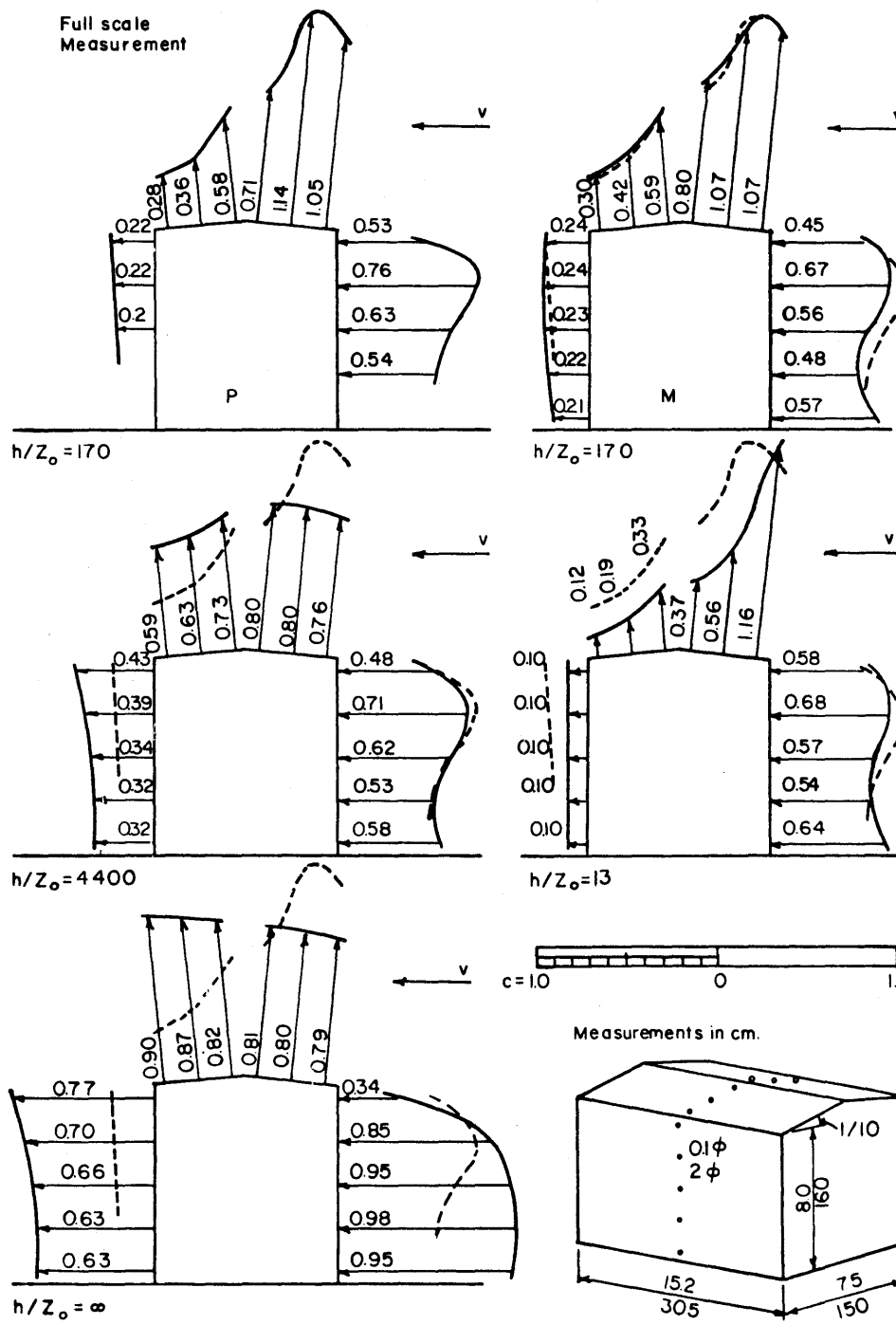

Figure 3-2. Wind load on a house in nature, and on a corresponding house in various tunnel tests. House height/roughness length in prototype was 170. (Jensen, 1958; Davenport, 1982).

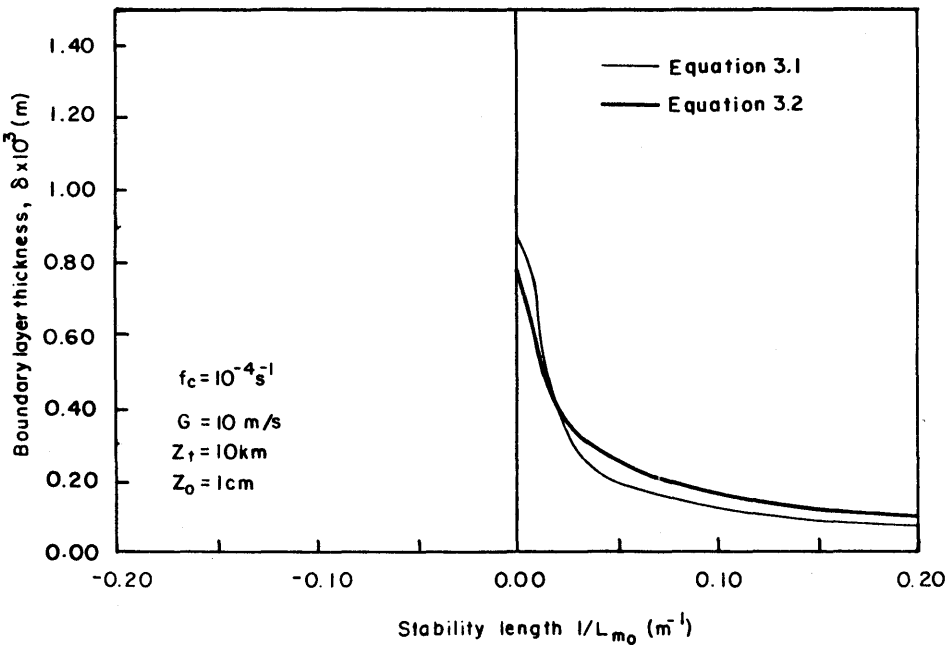

Figure 3-3. Typical nonadiabatic boundary layer depths calculated from the geostrophic drag relations (Equations 3.1 and 3.2), when G = 10 m/s, z_o = 0.01 m, z_T = 10 km, $f_c = 10^{-4}\ s^{-1}$, a = 1.

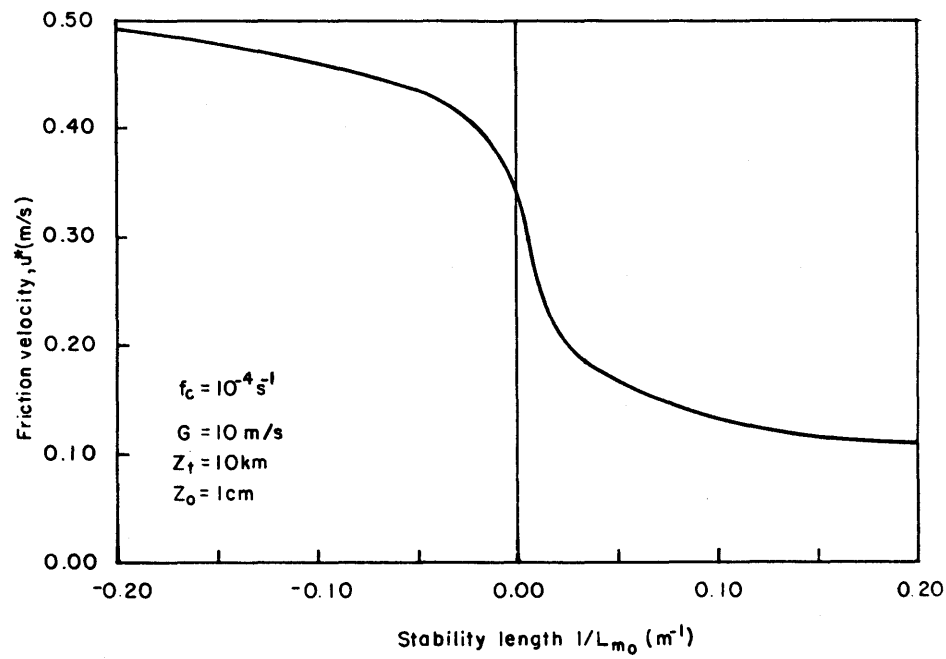

Figure 3-4. Variation of friction velocity, u_*, with stability parameter, $1/L_{mo}$, from Equations 3.3.

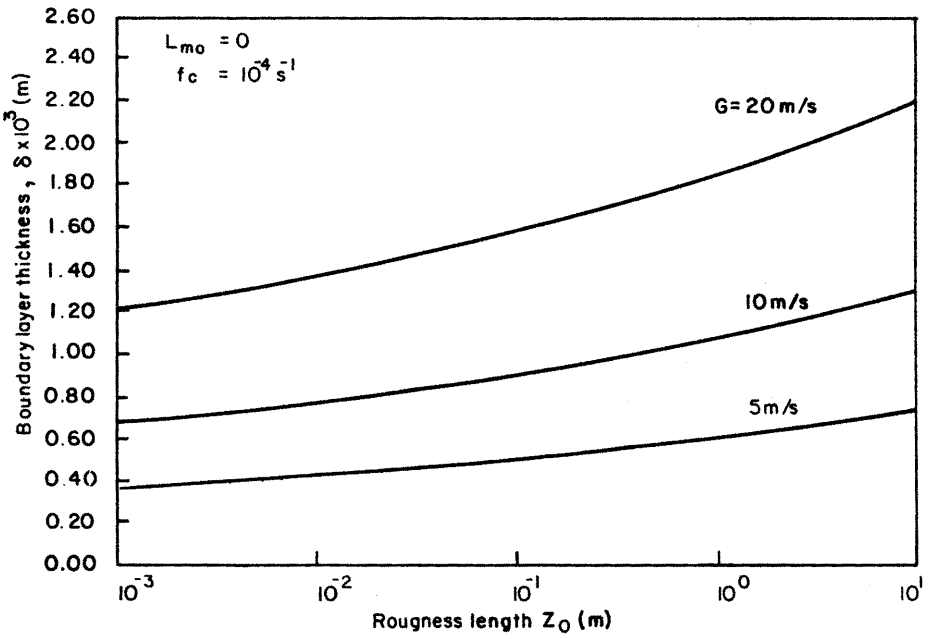

Figure 3-5. Comparison of various schemes to predict the depth of the adiabatic boundary layer according to the geostrophic drag law.

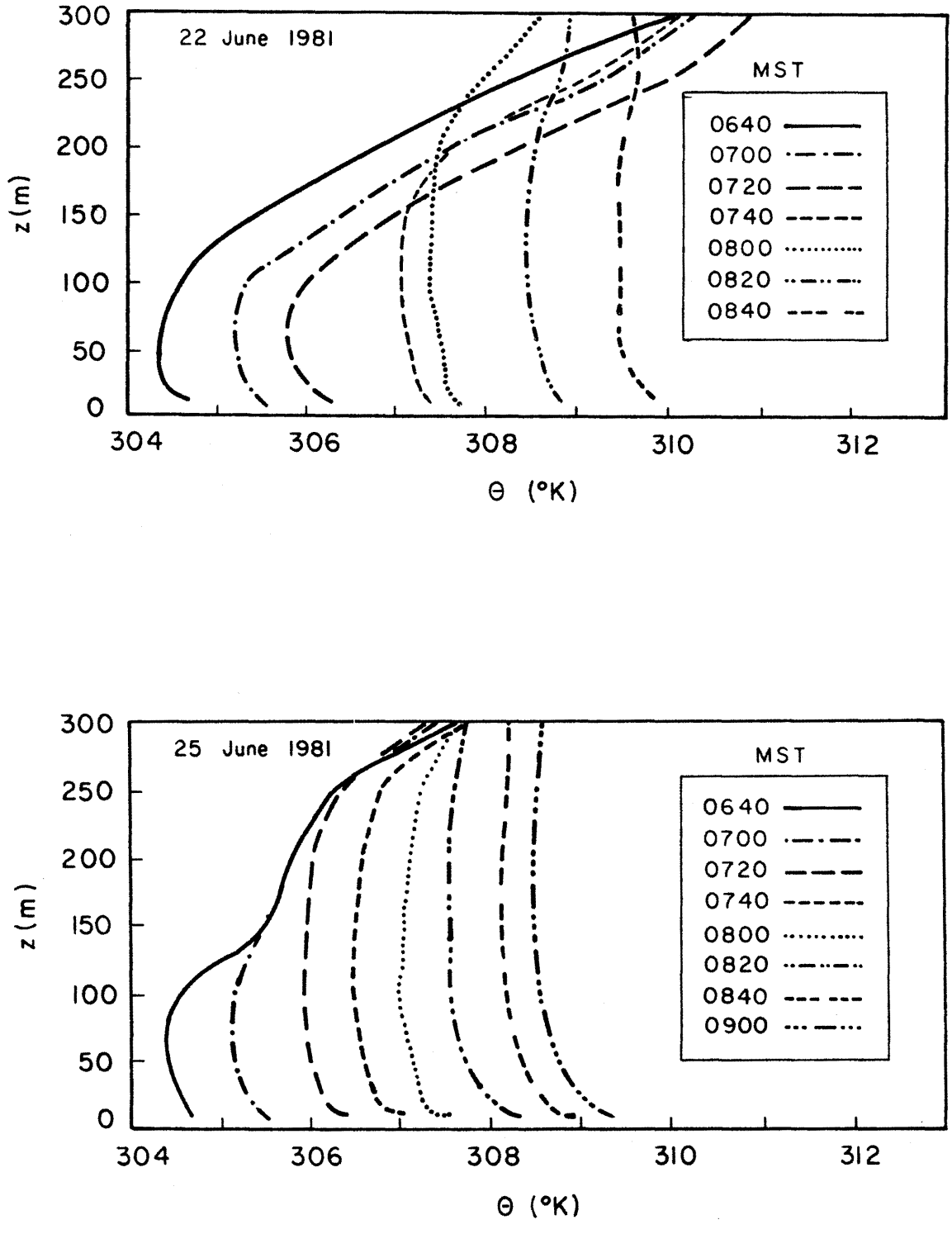

Figure 3-6. Early morning mixing layer depths, as measured on the Boulder Atmospheric Observatory tower, Boulder, CO (Wolfe, 1985).

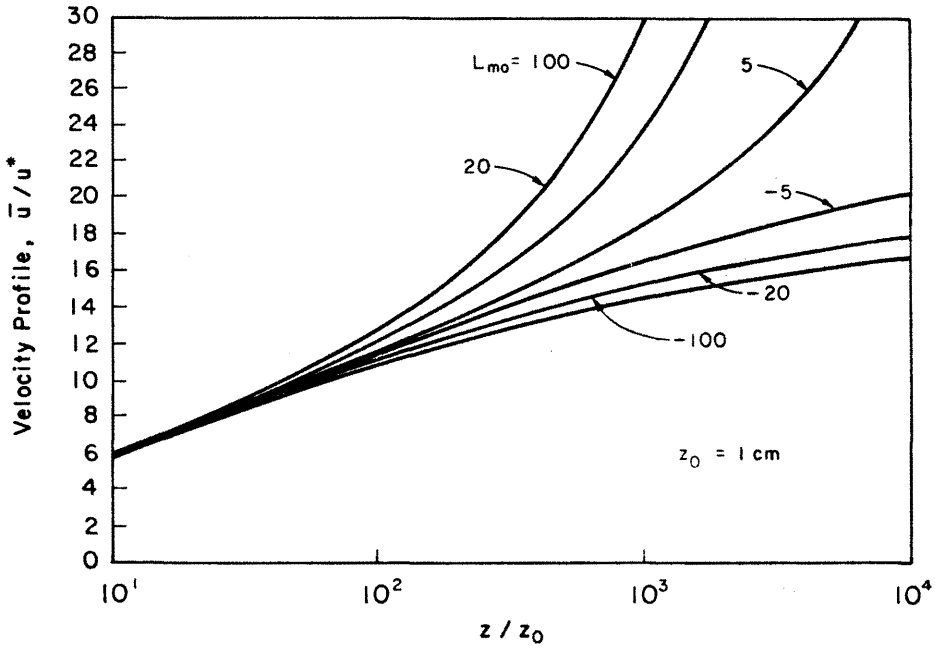

Figure 3-7. Surface layer velocity profiles under nonadiabatic conditions, calculated from Equations 3.7 and 3.8.

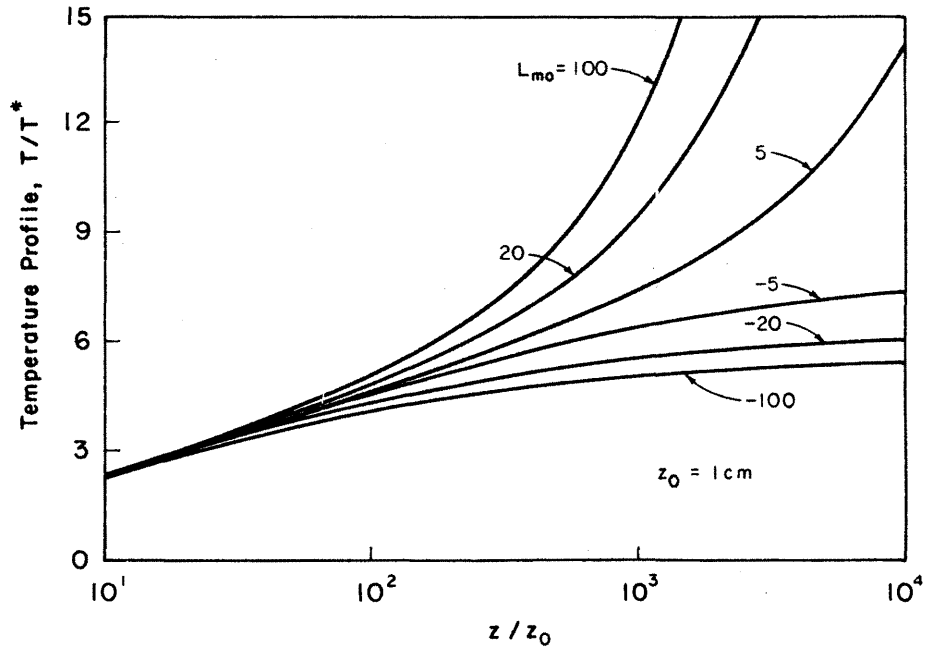

Figure 3-8. Surface layer temperature profiles under nonadiabatic conditions, calculated from Equations 3.9 and 3.10.

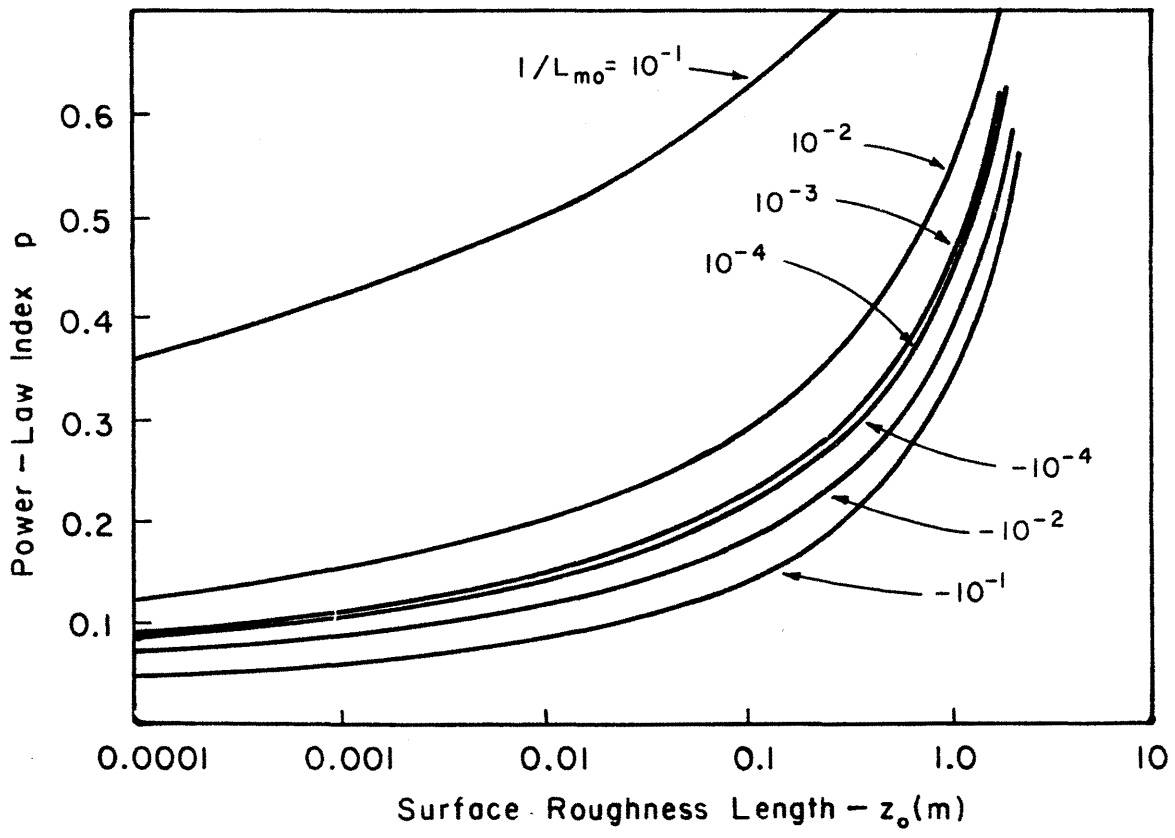

Figure 3-9. Power-law coefficient as a function of z_o and L_{mo} (Huang, 1981).

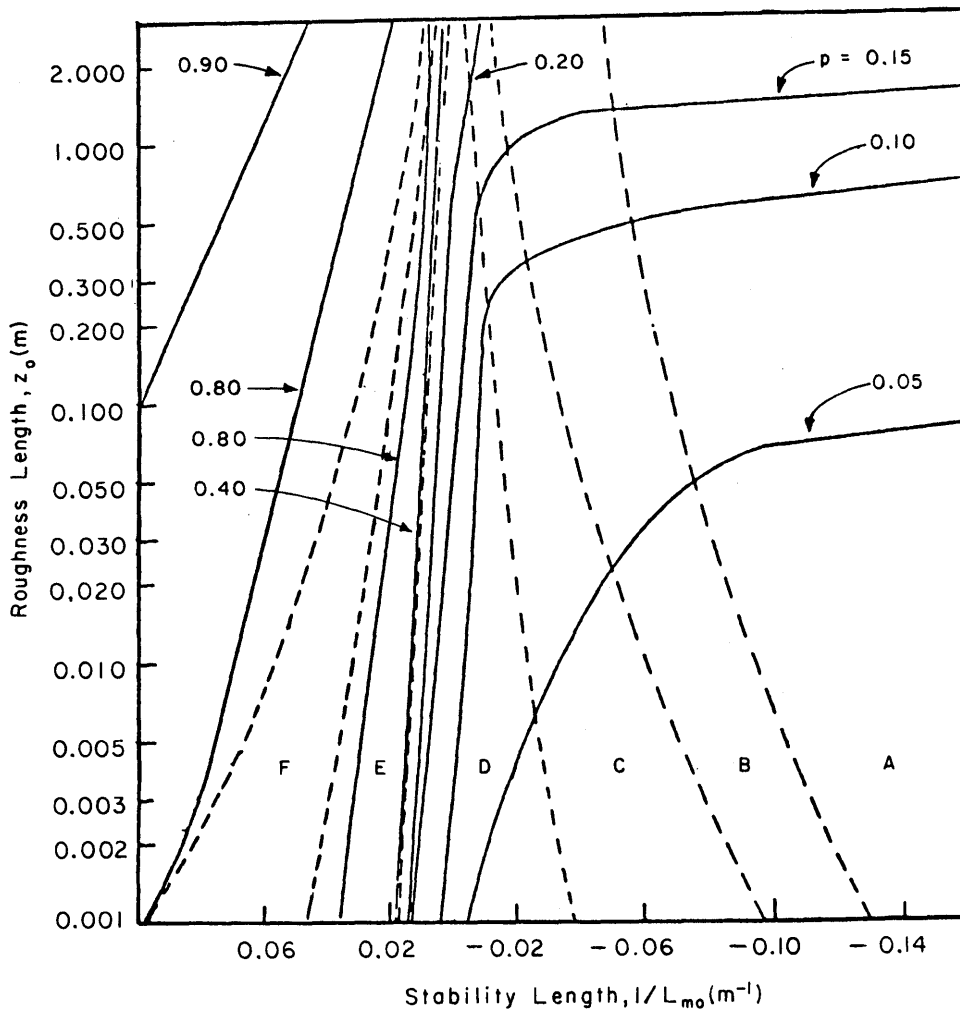

Figure 3-10. Variation of power-law coefficient as a function of z_o and L_{mo}, but overplotted with Pasquill stability classes (Irwin, 1978).

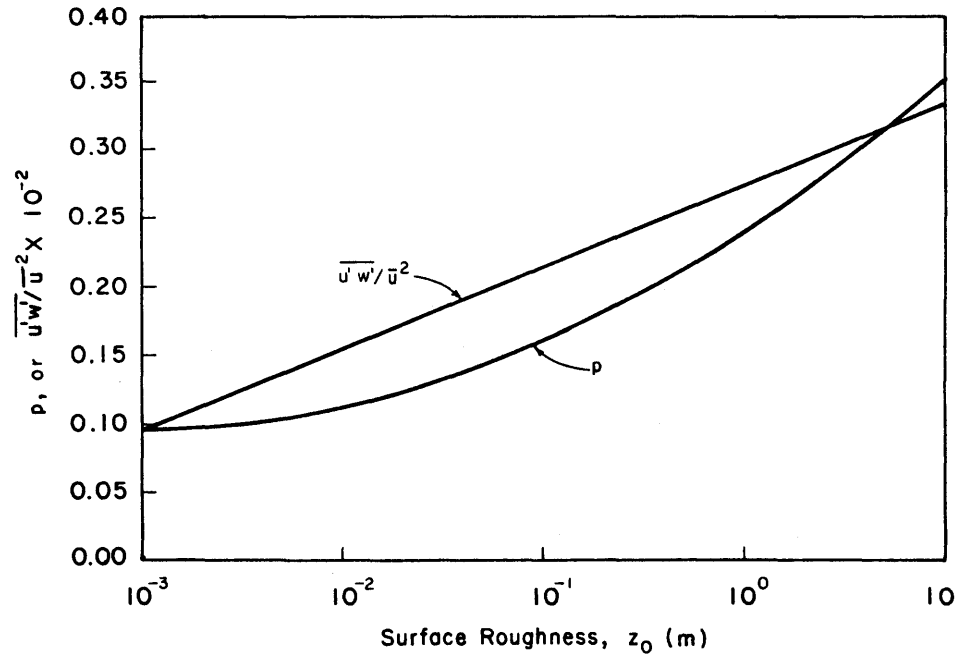

Figure 3-11. Power-law coefficient and shear stress (Counihan, 1975).

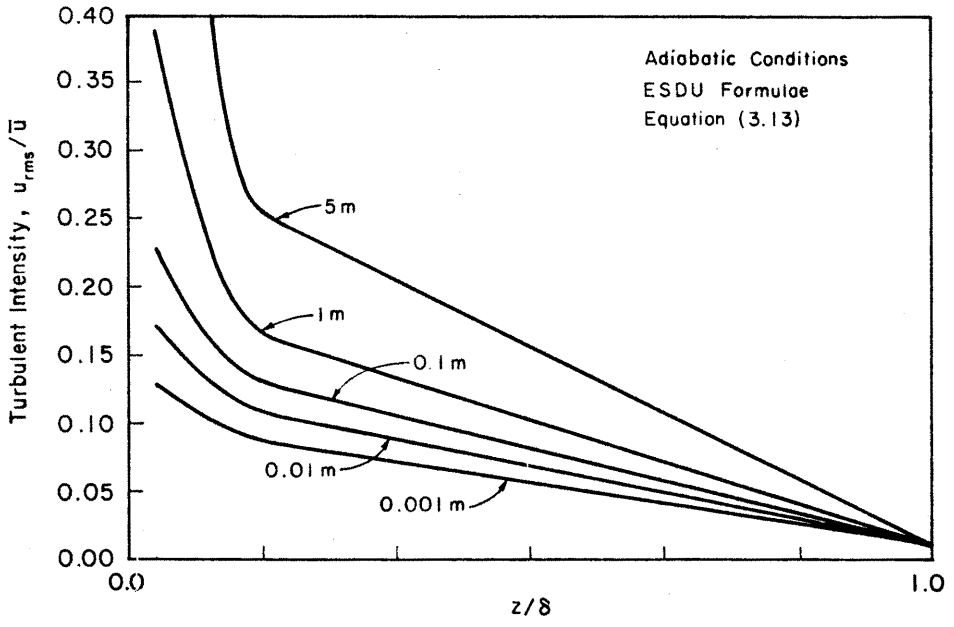

Figure 3-12. Variation of longitudinal intensity with height under adiabatic conditions. Calculated from Equations 3.13.

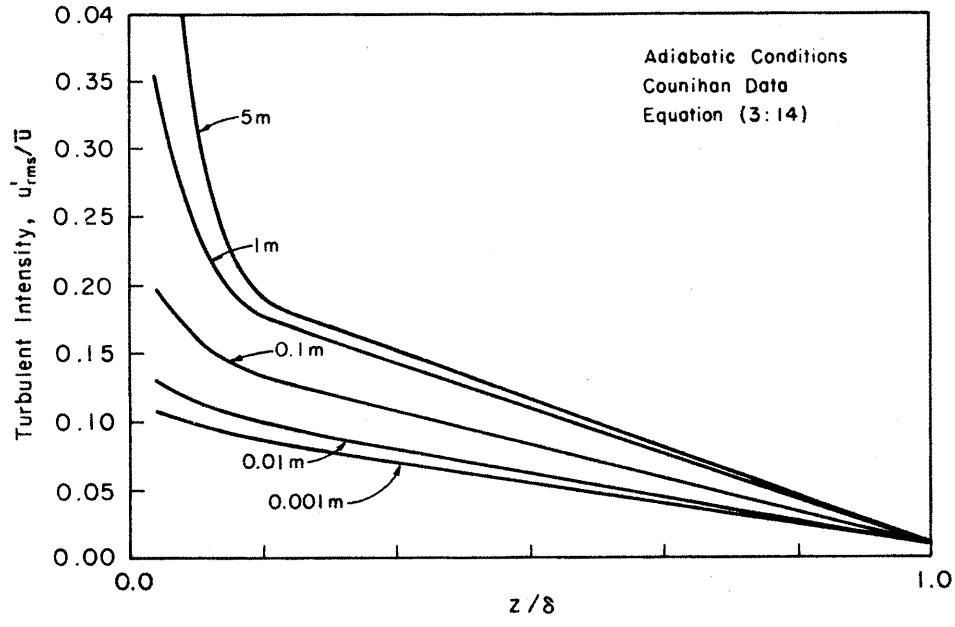

Figure 3-13. Variation of longitudinal intensity with height under adiabatic conditions. Calculated from Equations 3.14.

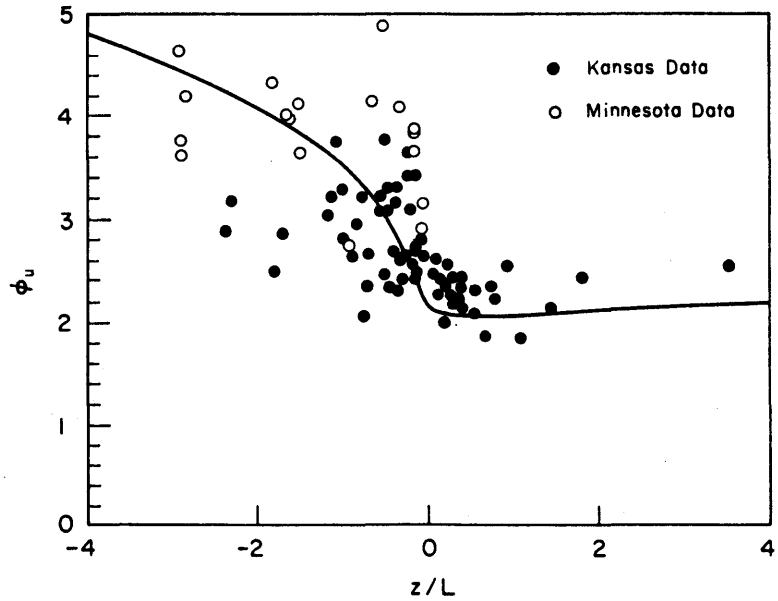

Figure 3-14. Variation of longitudinal turbulent intensities, when examined in similarity coordinates (Binkowski, 1979).

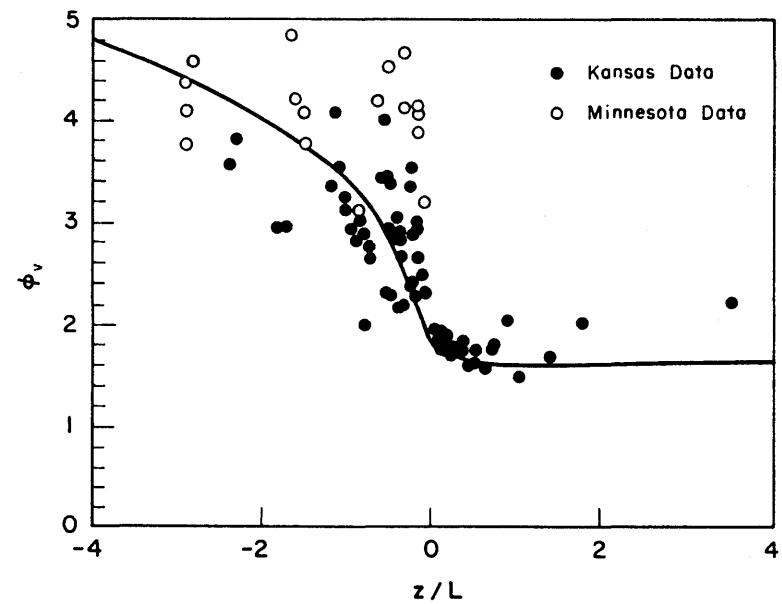

Figure 3-15. Variation of lateral turbulent intensities, when examined in similarity coordinates (Binkowski, 1979).

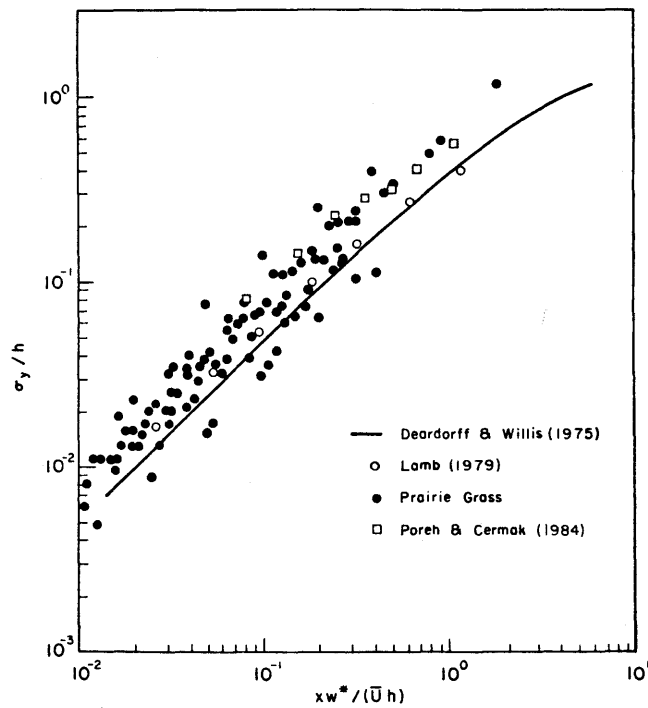

Figure 3-16. Turbulence from convective boundary layers compared via mixed layer similarity concepts (Poreh and Cermak, 1984).

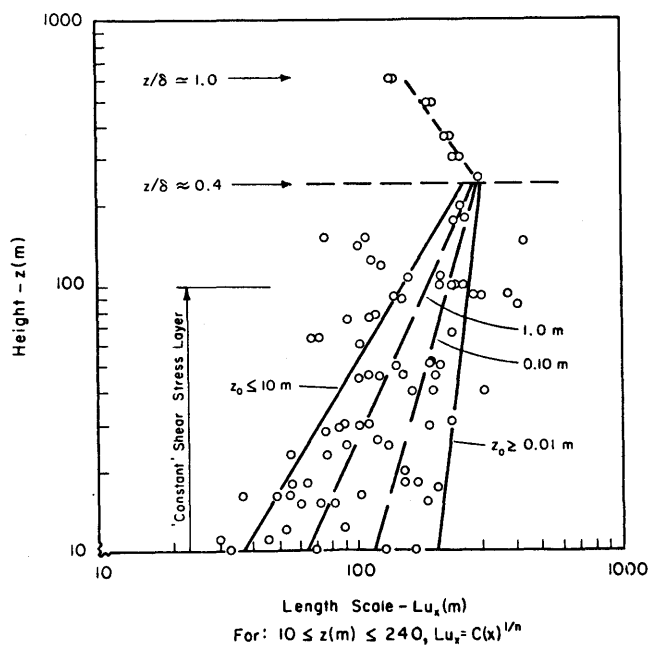

Figure 3-17. Variation of integral length scale with height and roughness length (Counihan, 1975).

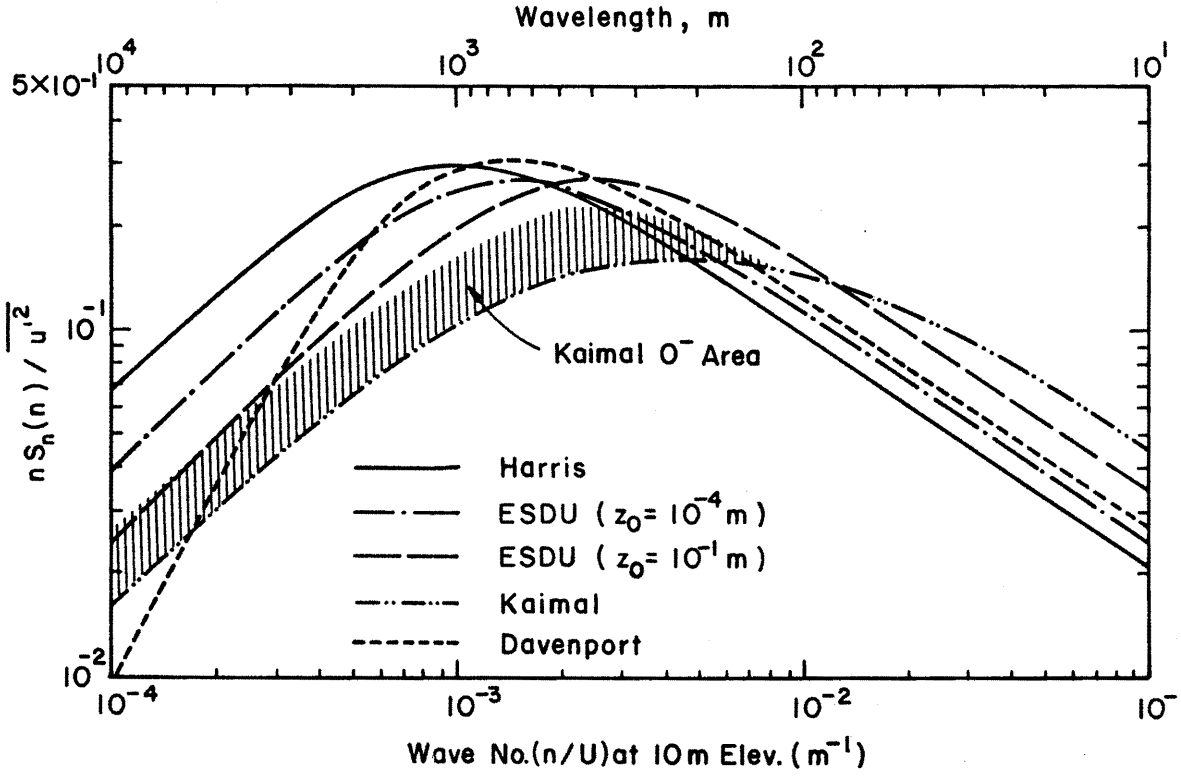

Figure 3-18. Different descriptions of the power spectrum of turbulent longitudinal velocity fluctuations for the atmospheric surface layer (Neff and Meroney, 1982).

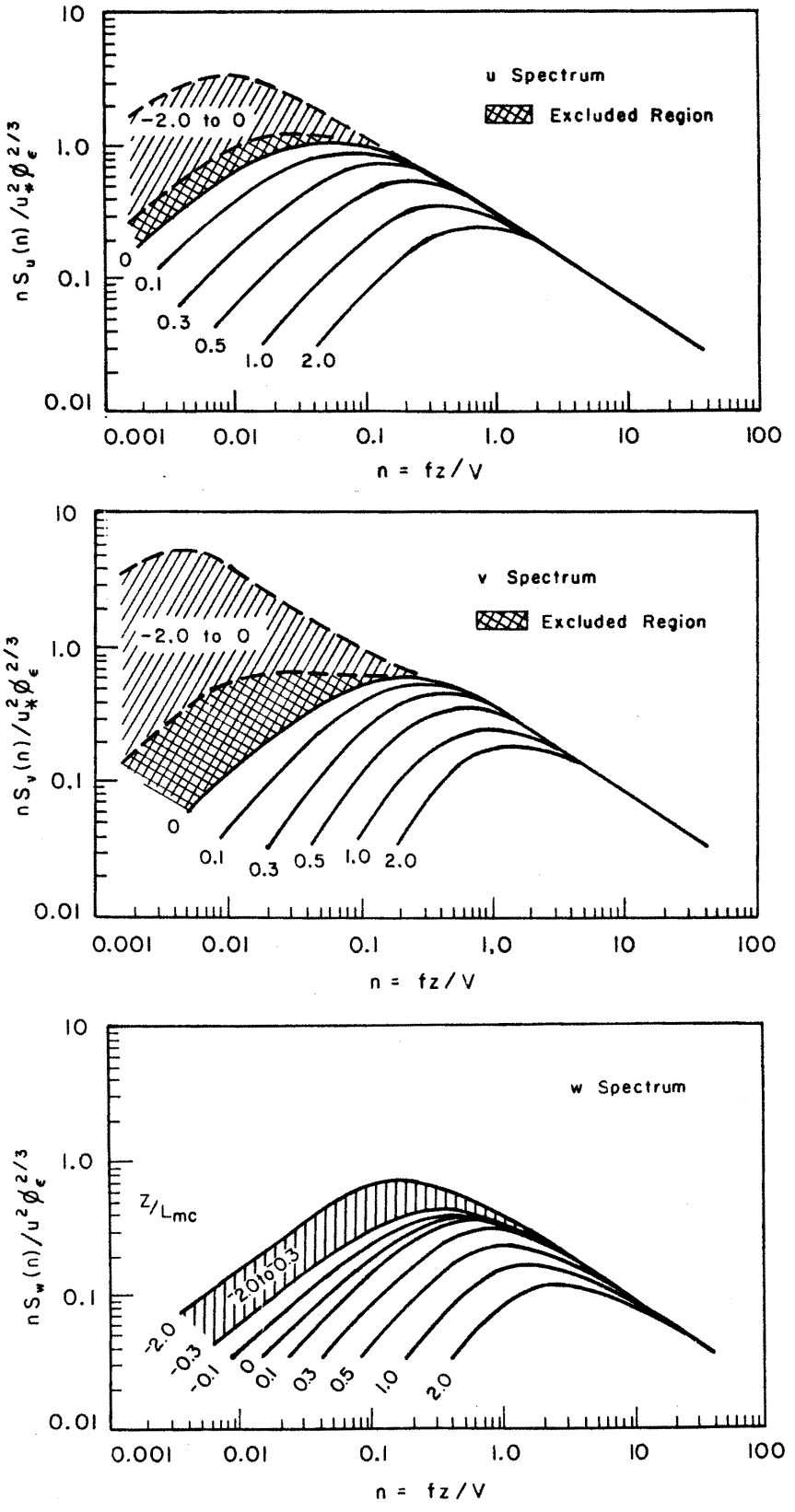

Figure 3-19. Normalized u, v, and w spectra for stably stratified flows, after Kaimal et al. (1972).

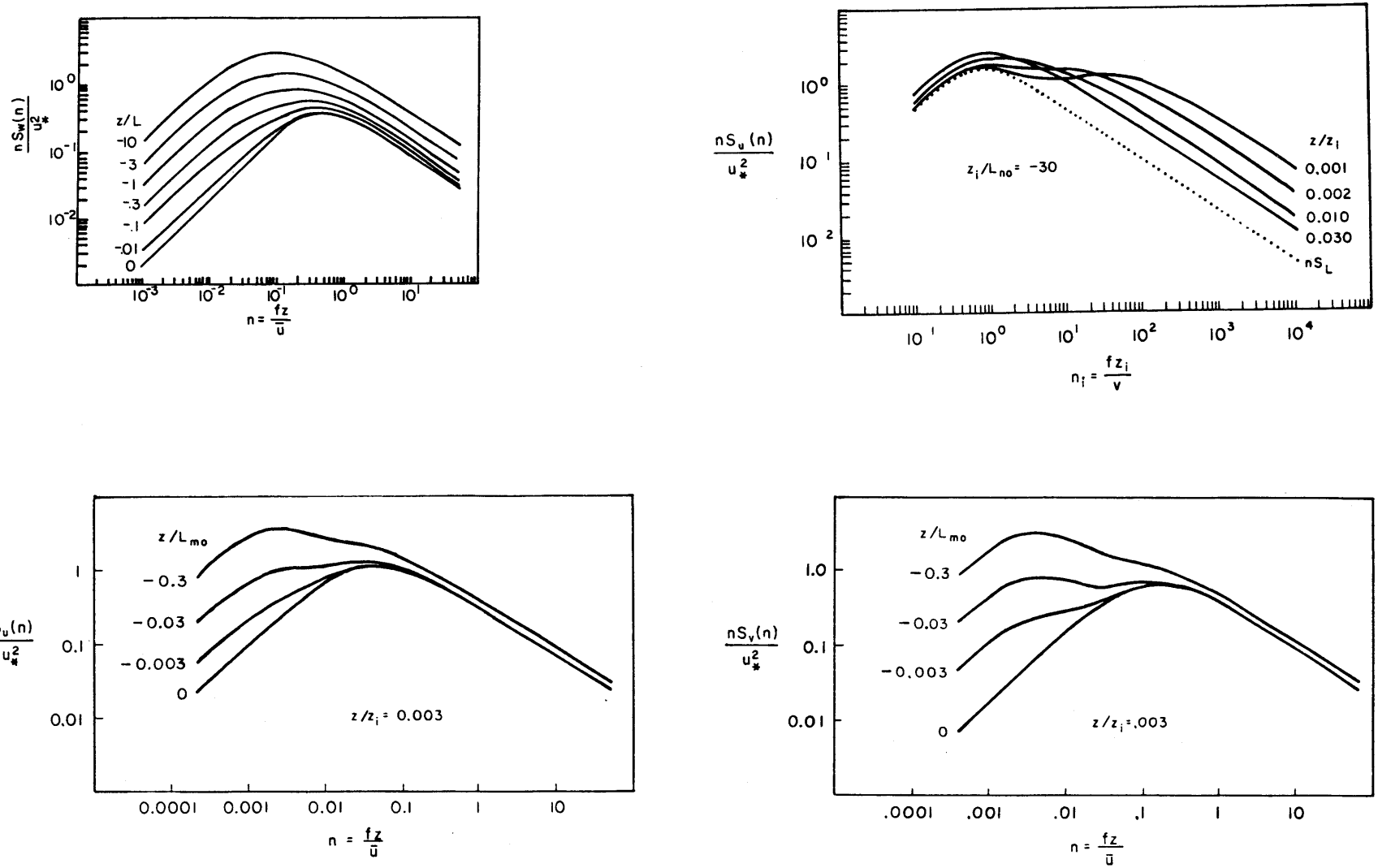

Figure 3-20. Normalized u, v, and w spectra for unstably stratified flows, after Hojstrup (1981).

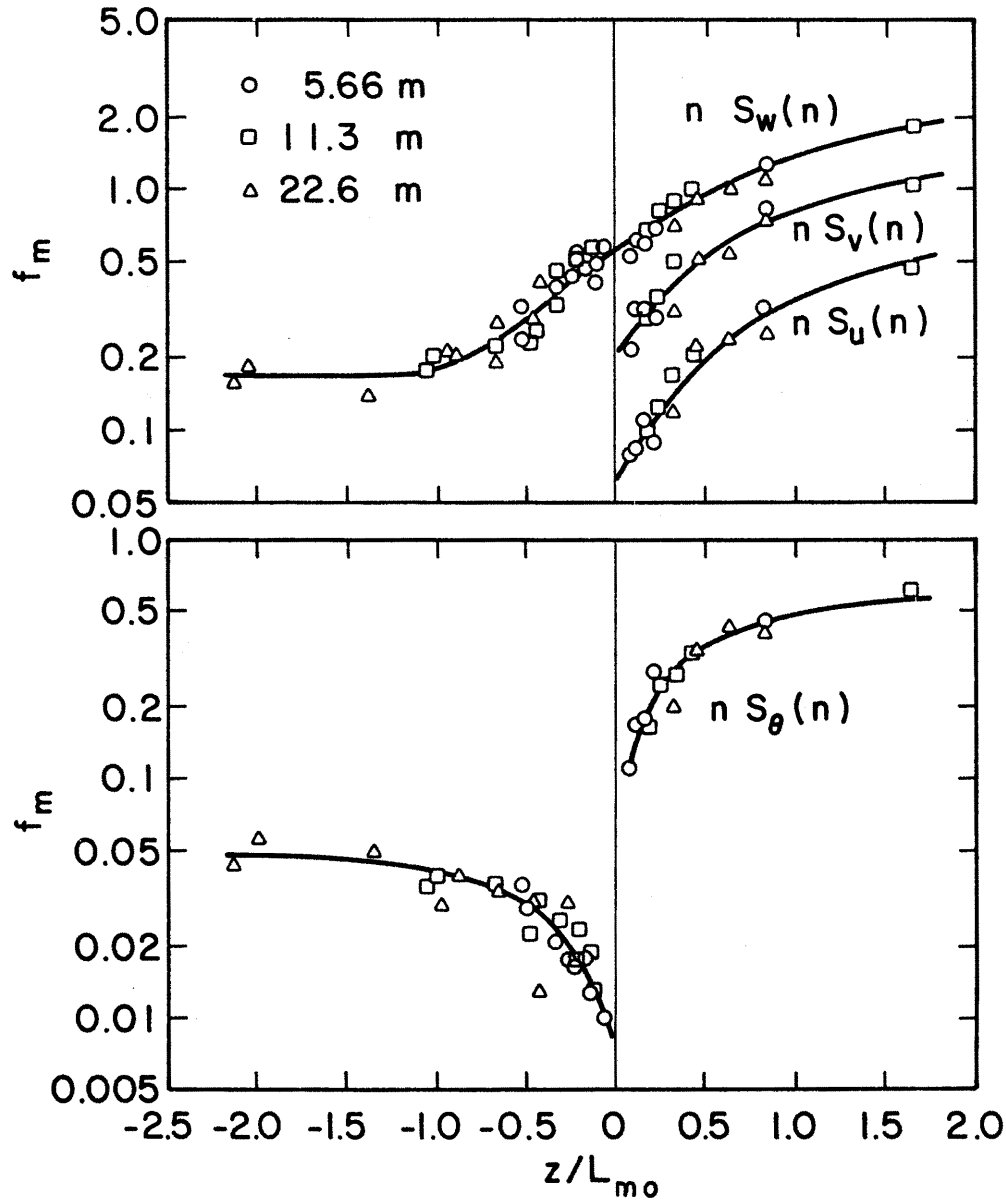

Figure 3-21. Location of spectral peak for u, v, w and i plotted against z/L. Curves shown are fitted by eye (from Kaimal et al., 1972).

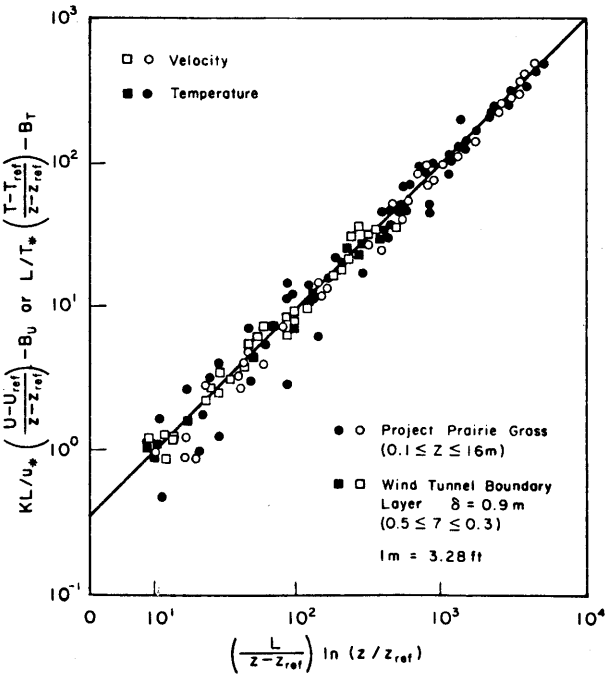

Figure 3-22. Mean velocity and temperature profiles from meteorological wind tunnel and atmosphere, compared to log-linear profile (Cermak, 1975).

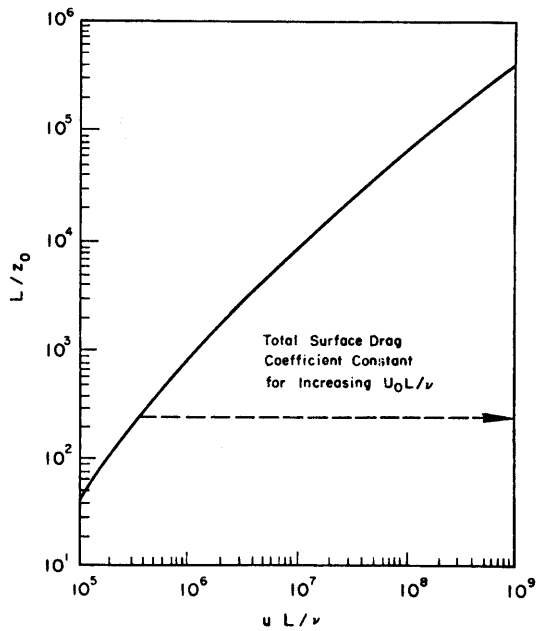

Figure 3-23. Wind-tunnel Reynolds number at which total surface drag coefficient becomes constant for a specified surface length-roughness length ratio (Cermak, 1975).

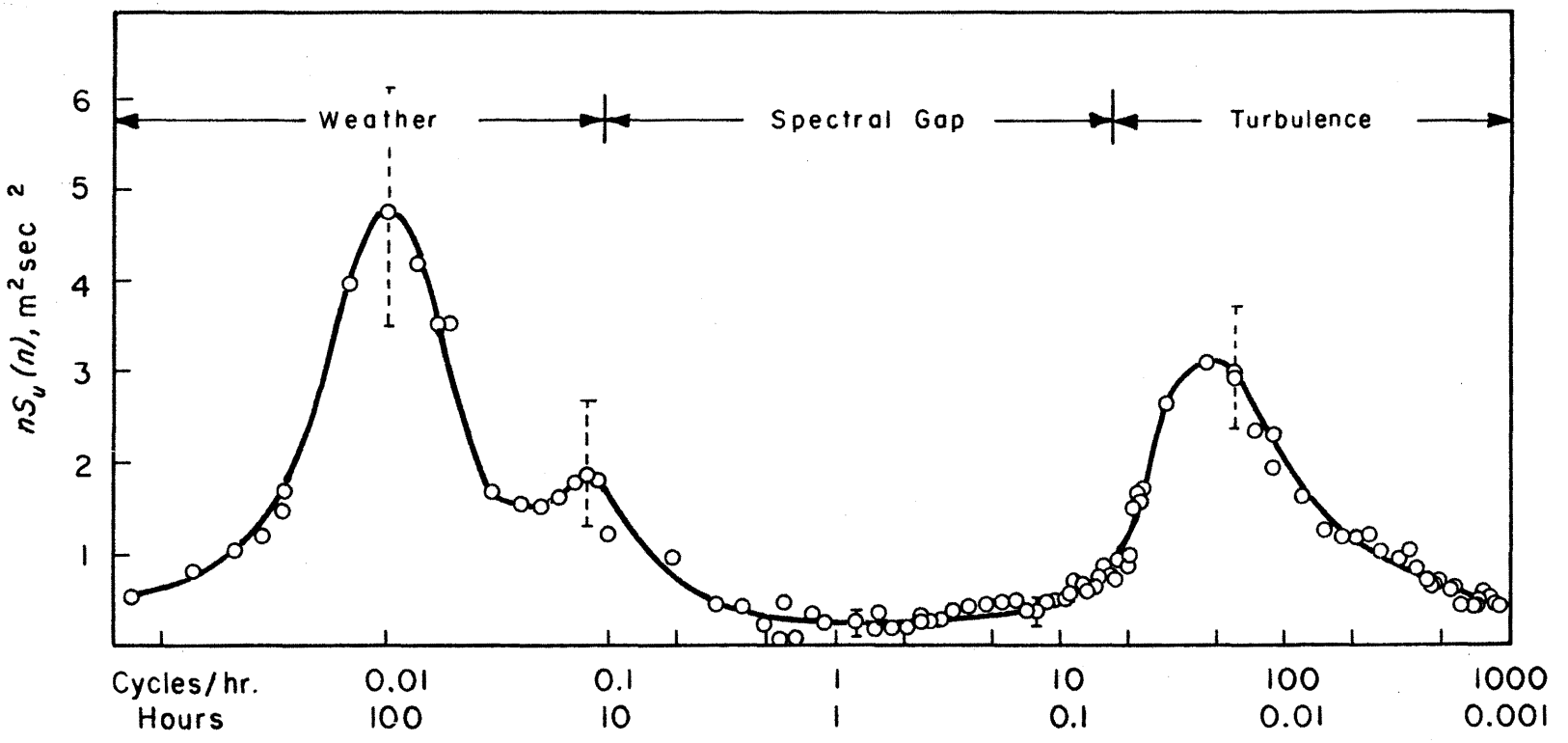

Figure 3-24. Spectrum of wind speed at 10 m (Van der Hoven, 1957).

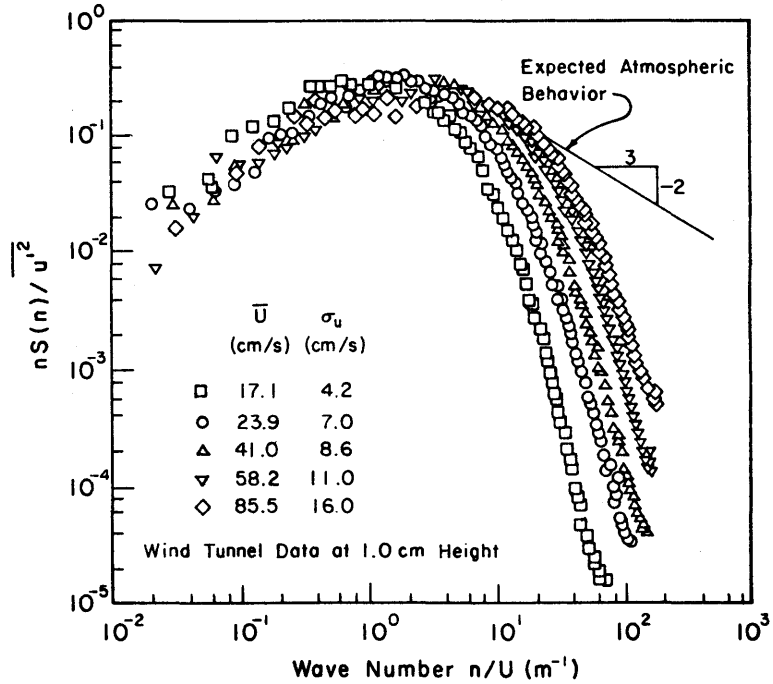

Figure 3-25. Power spectrum of turbulent longitudinal velocity fluctuations within model boundary layers at reduced Reynolds numbers (Neff and Meroney, 1982).

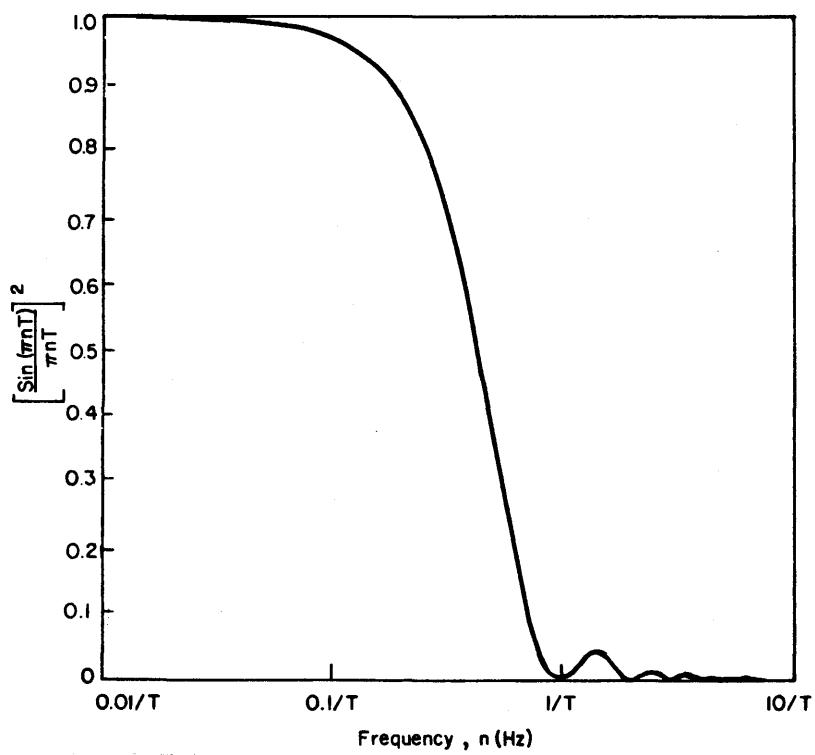

Figure 3-26. Filter function from Equation 3.25. Effect of averaging, over a time T, on the variance of a sinusoidal fluctuation of frequency n (Pasquill, 1962).

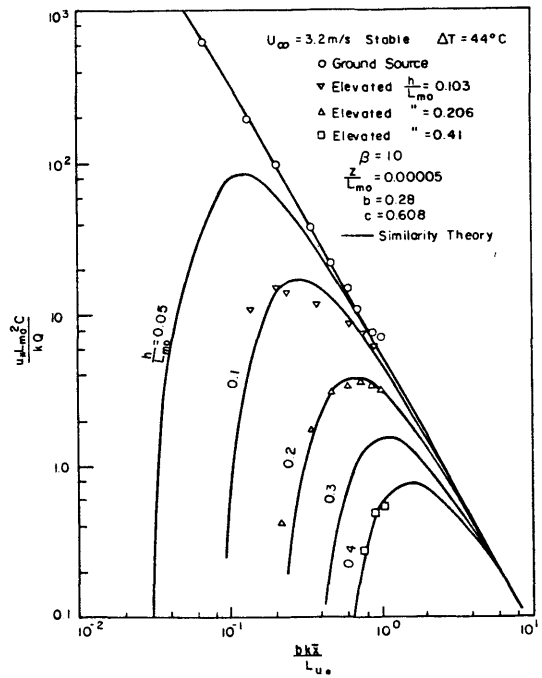

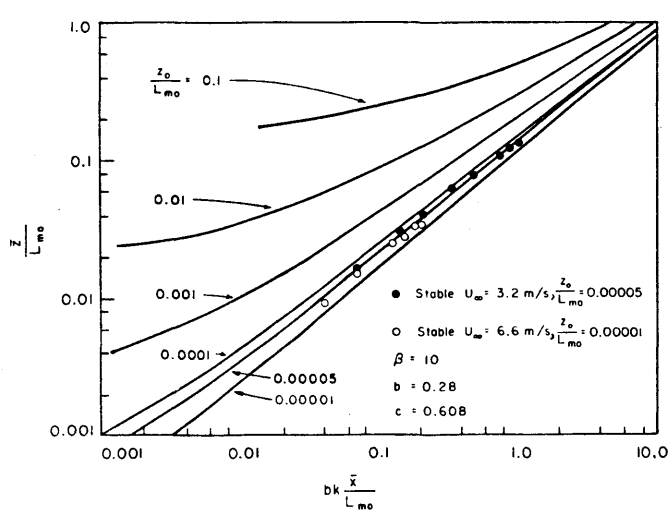

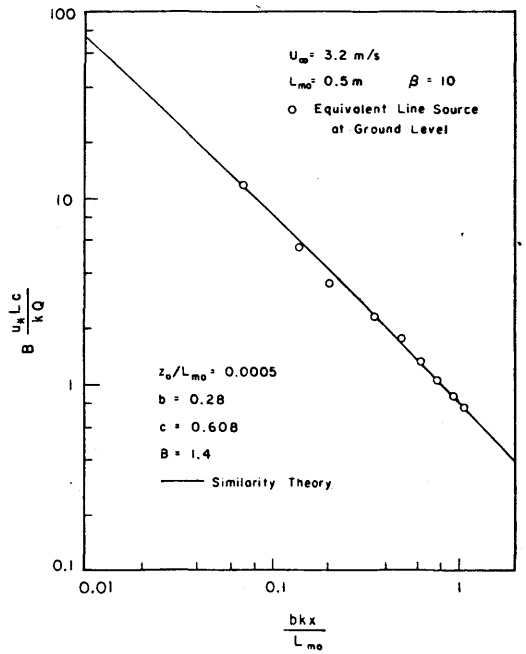

Figure 3-27. Measurements of plume center of gravity (or concentrations) compared to predictions from Lagrangian similarity theory (Chaudhry and Meroney, 1973).

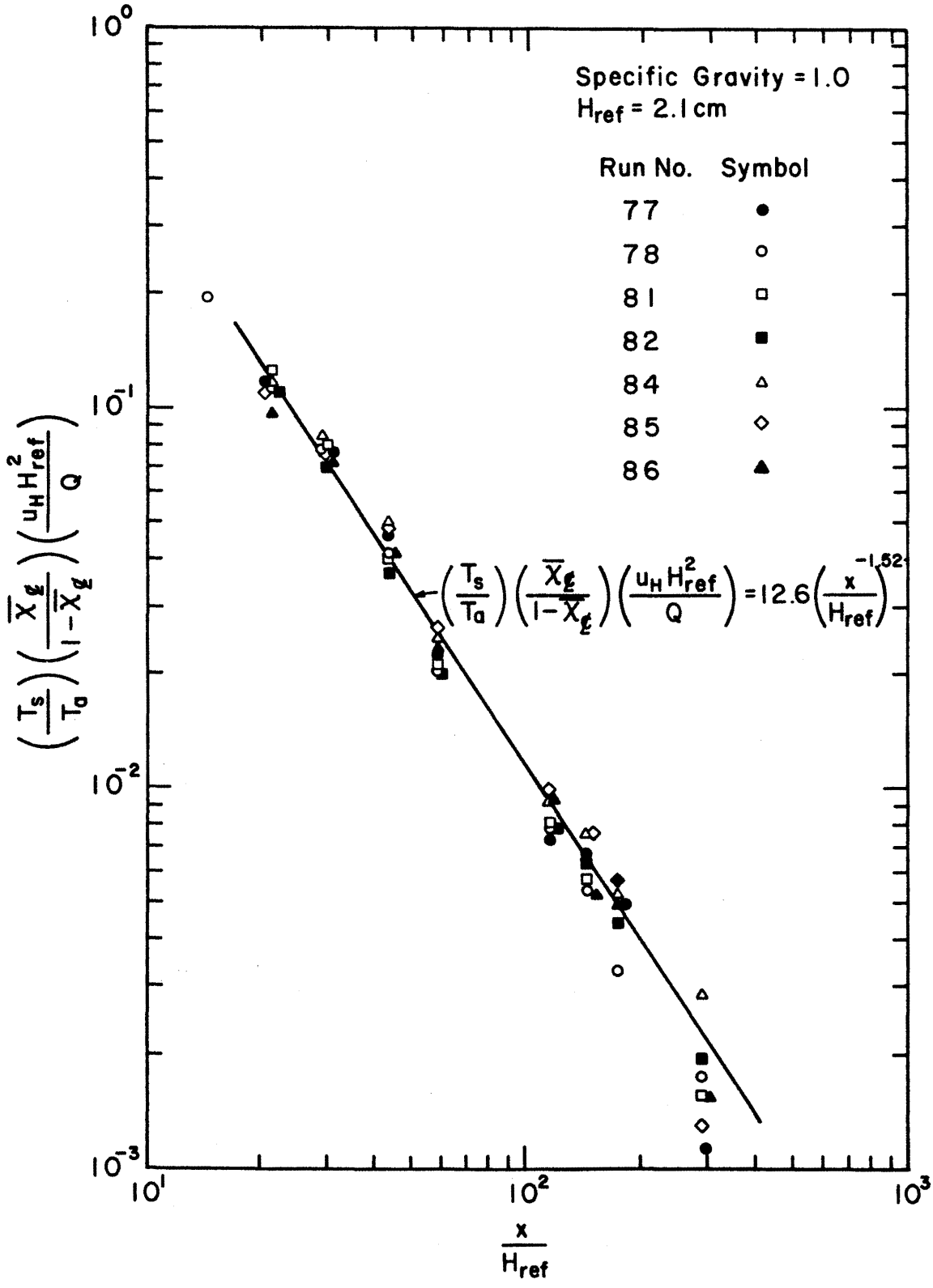

Figure 3-28. Normalized centerline concentration decay with downwind distance for passive dispersion of gases released from an area source at low Reynolds numbers (Neff and Meroney, 1982).

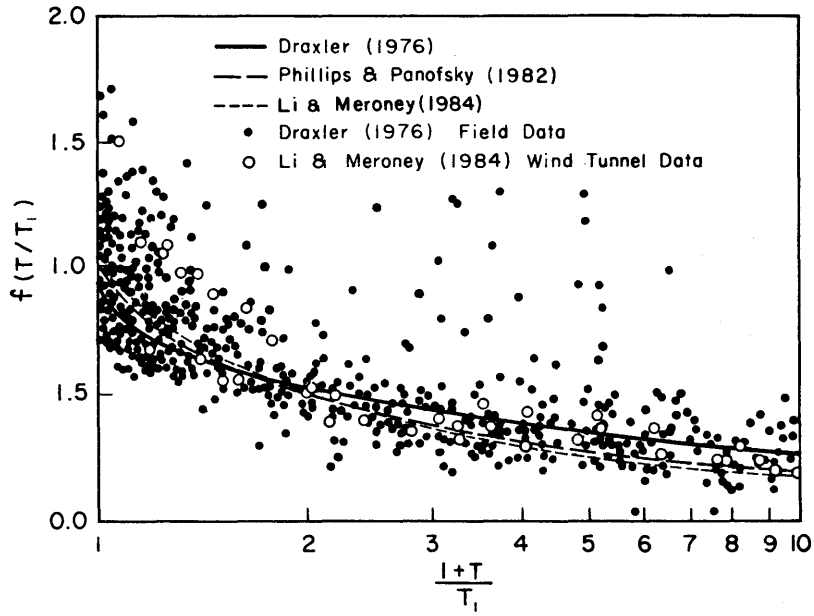

a) Neutral Data

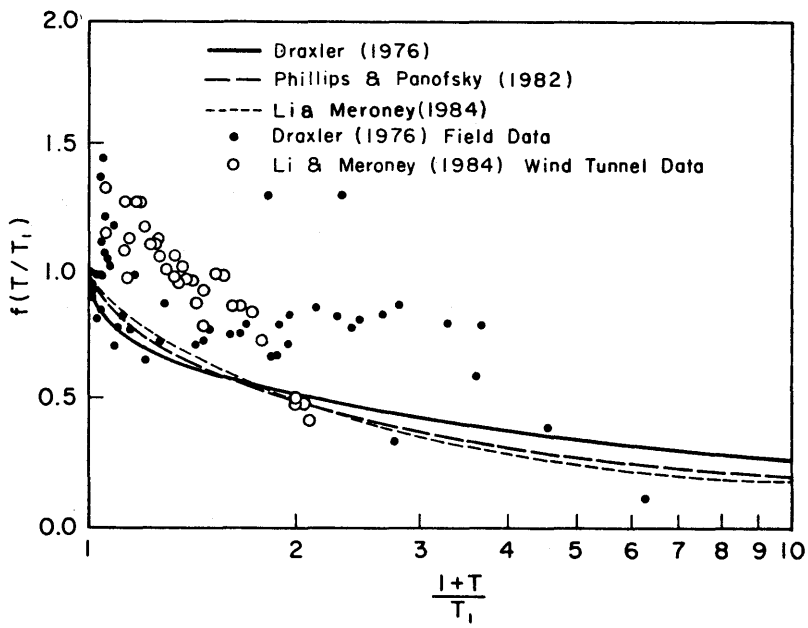

b) Stratified Data

Figure 3-29. Lateral plume dispersion from ground level point sources, scaled with Lagrangian time scales and variances suggested by Draxler (1975), from Li and Meroney (1984).

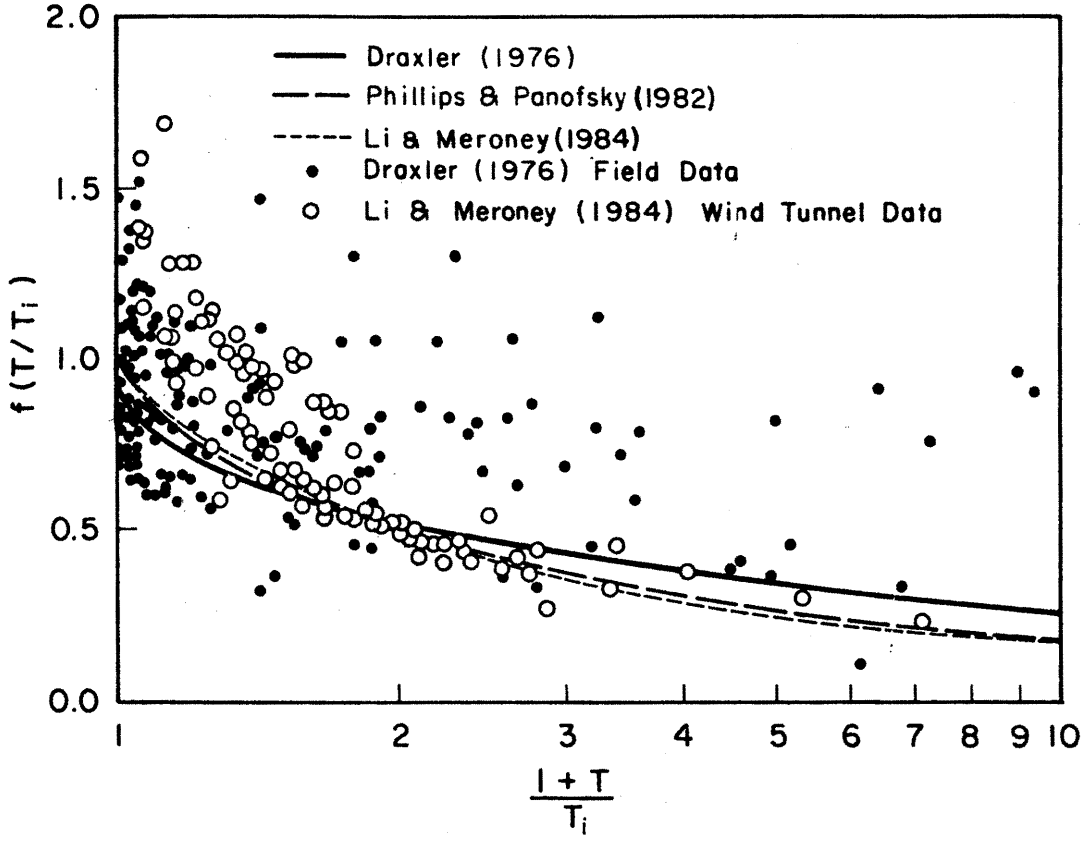

Figure 3-30. Lateral plume dispersion from elevated point sources, scaled with Lagrangian time scales and variances suggested by Draxler (1975), from Li and Meroney (1984).

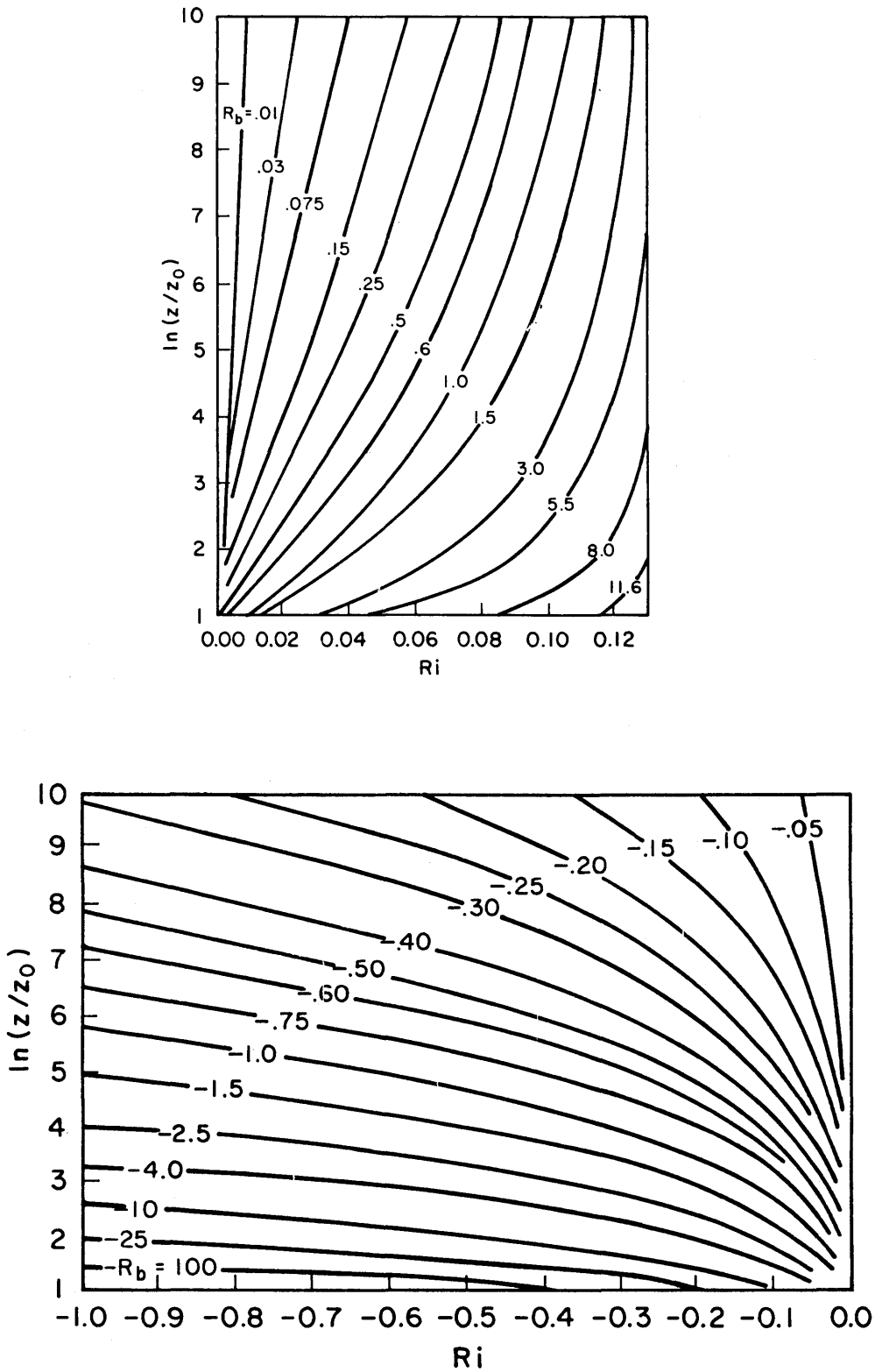

Figure 3-31. Variation of gradient Ri number with height, z/z_o, for various values of the bulk Richardson number, after Golder (1972).

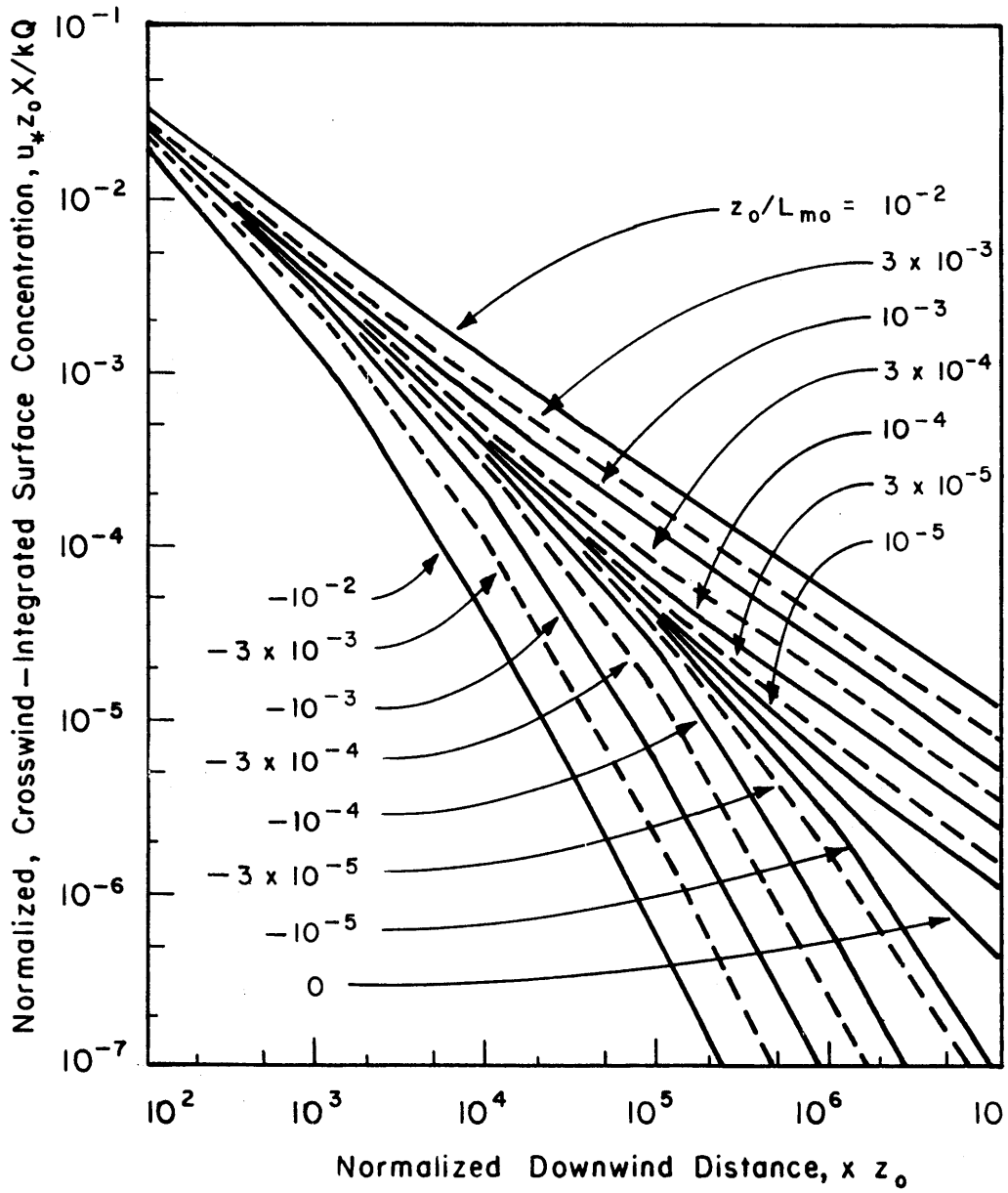

Figure 3-32. Comparison of Lagrangian similarity predictions of crosswind-integrated ground concentration against atmospheric data (Horst, 1979).

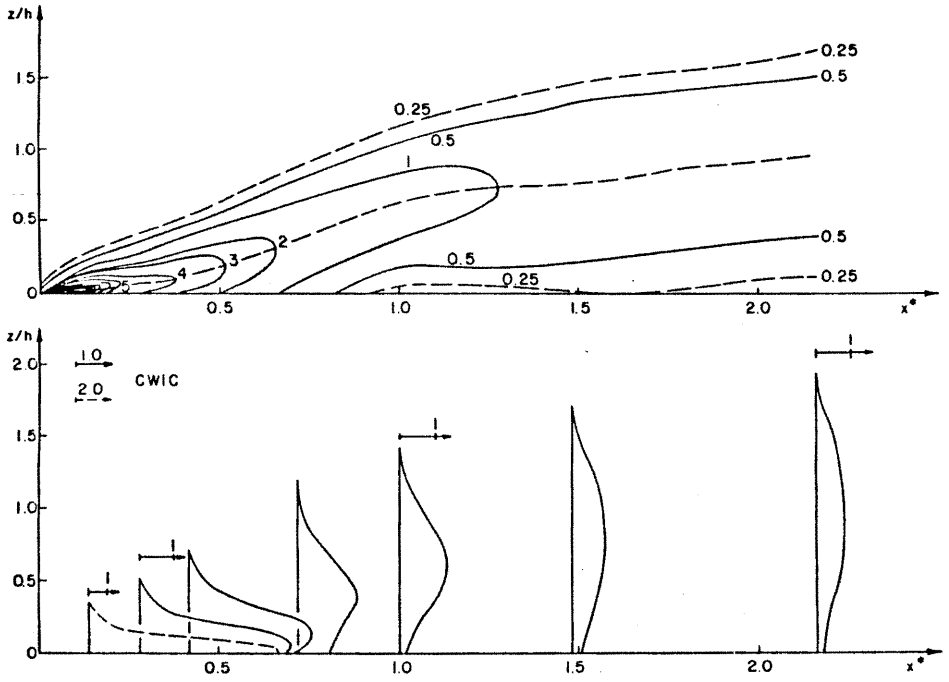

Measured dimensionless crosswind integrated mean concentrations for $z^s/h = 0.0175$.

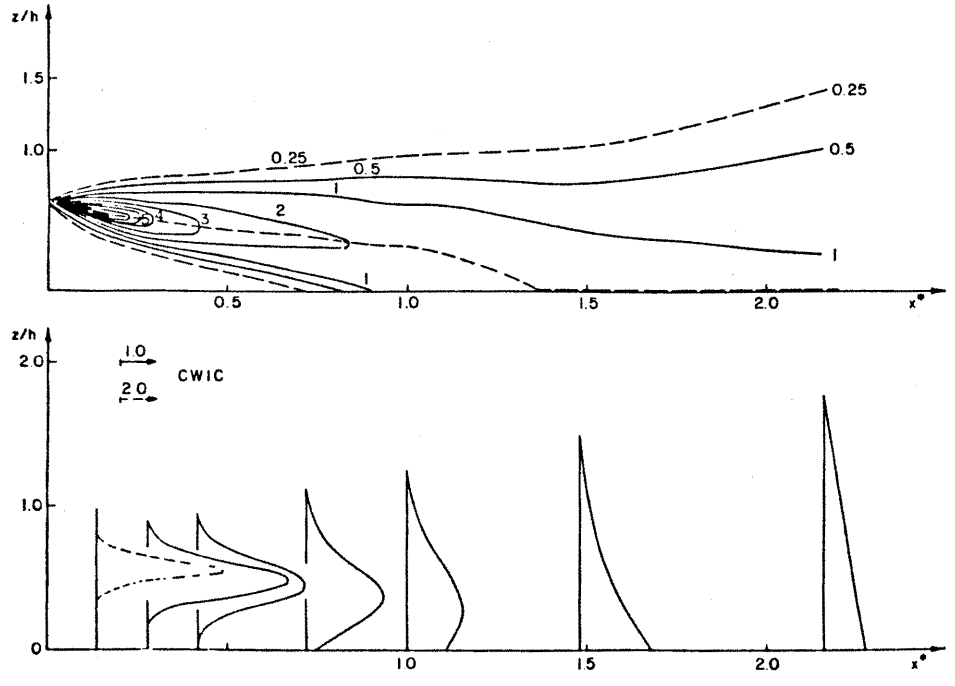

Measured dimensionless crosswind integrated mean concentrations for $z^s/h = 0.61$.

Figure 3-33. Plume movement within wind tunnel in convective boundary layers (Poreh and Cermak, 1984).

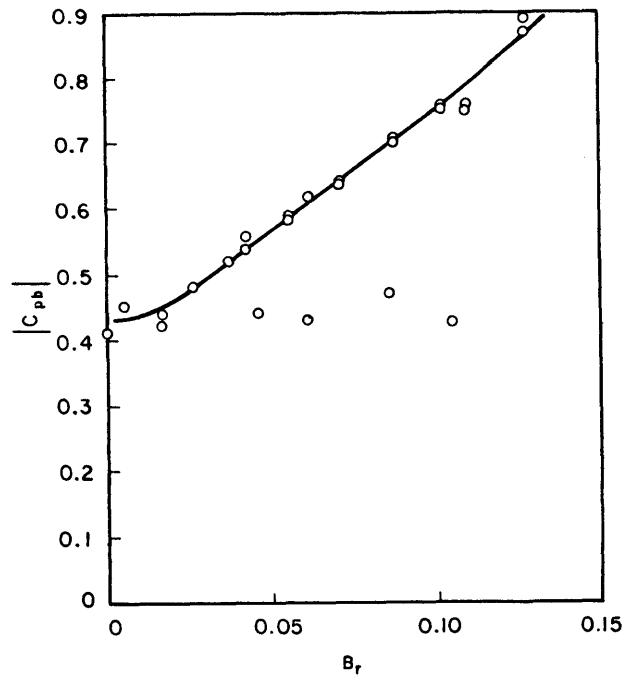

Figure 3-34. Variation of base pressure coefficient, C_{pb}, with blockage ratio, BR (Farrell et al., 1977).

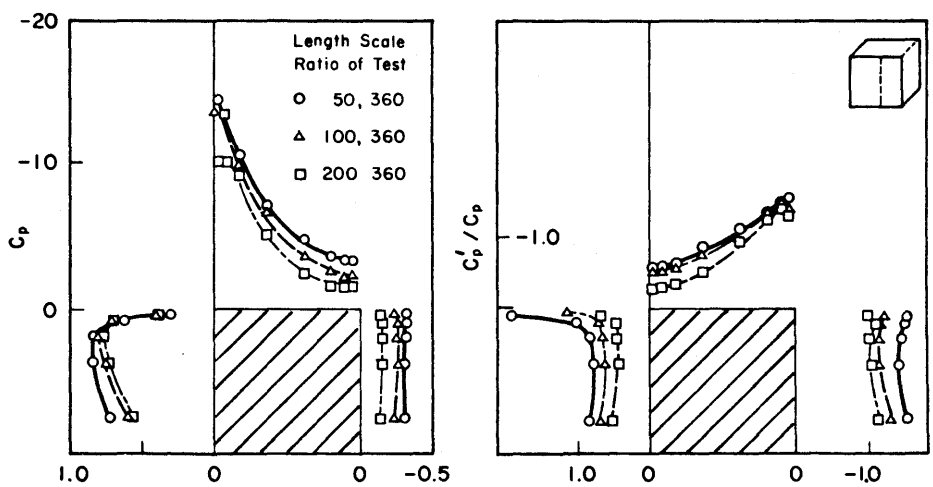

Figure 3-35. Pressure distributions about model cubes immersen in a 1:360 scale model atmospheric boundary layer (Hunt, 1981).

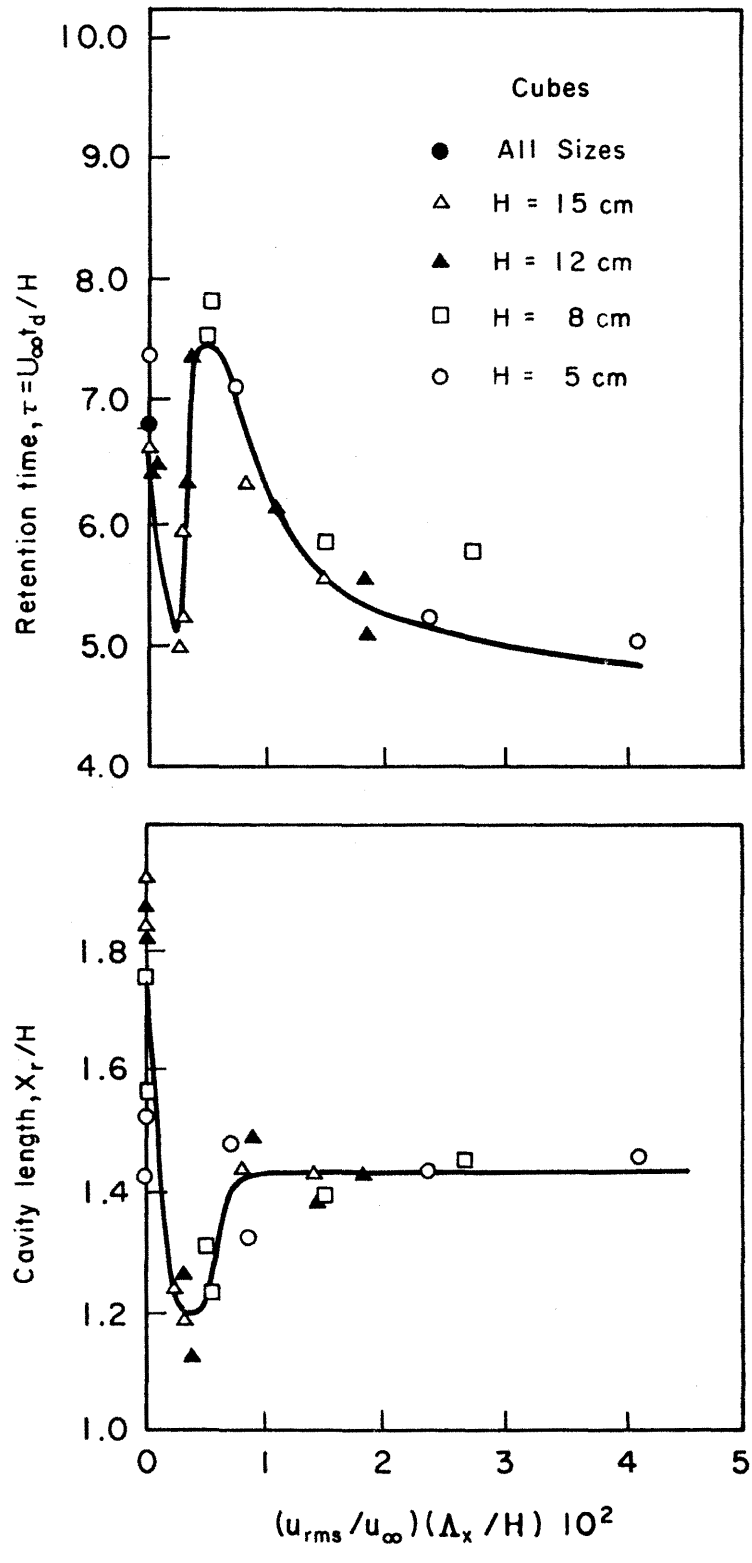

Figure 3-36. Dependence of wake cavity properties on approach turbulence scale and intensity (Vincent, 1977).

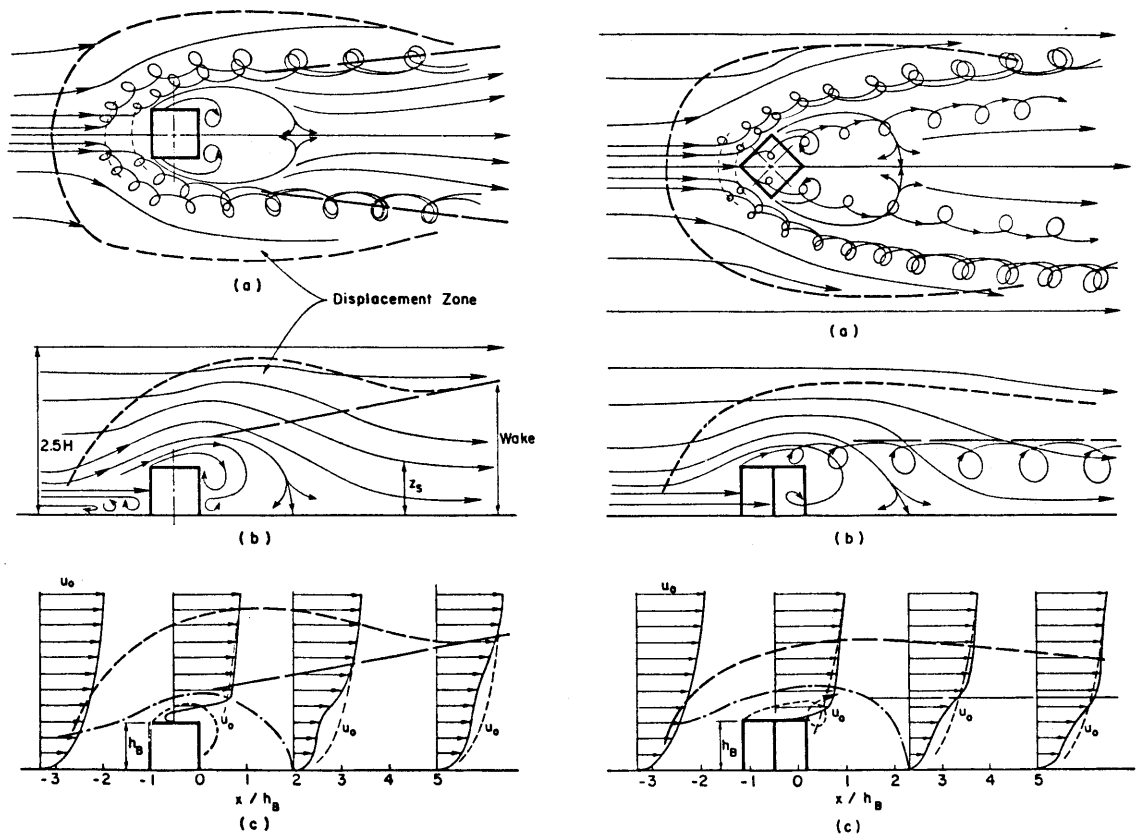

Figure 3-37. Fluid physics of a shear flow around a cubical building with wind normal to building face (Meroney, 1982).

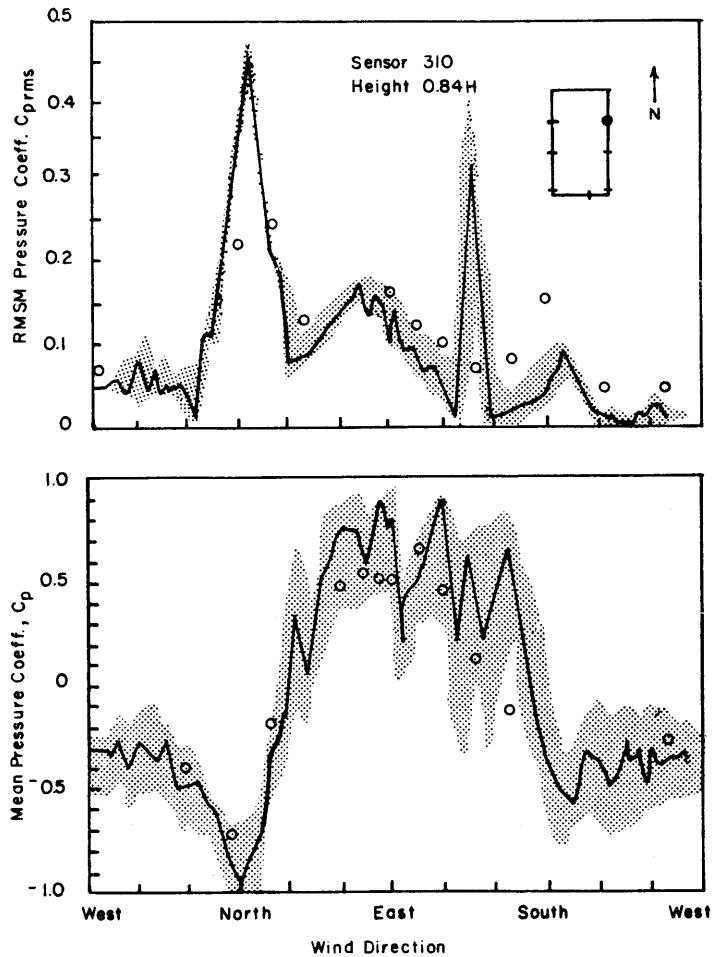

NE Corner

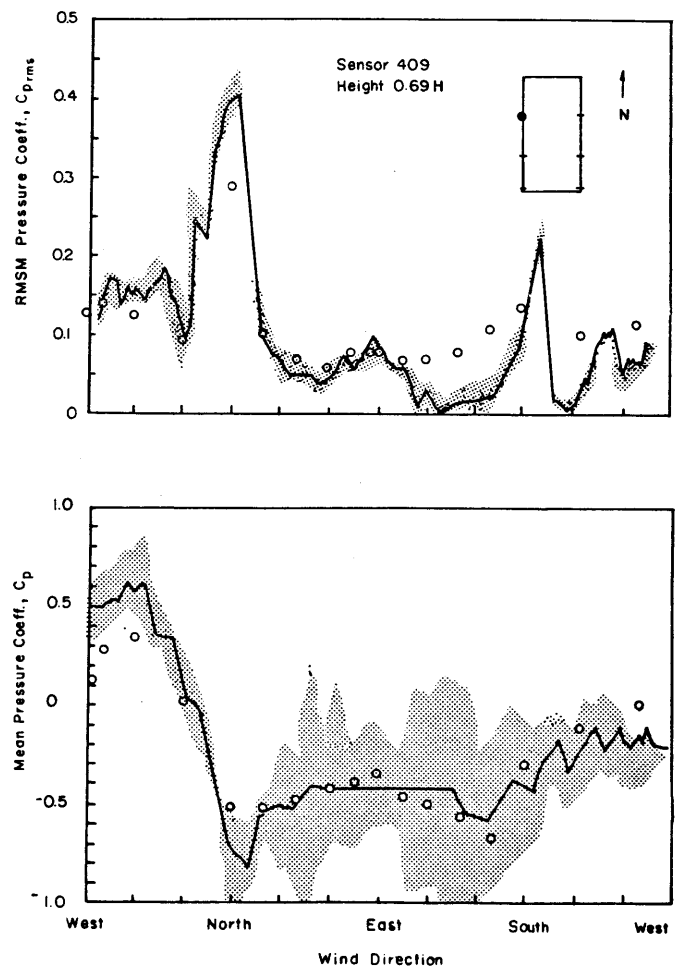

NW Corner

Figure 3-38. Pressures measured on west wall at 20.6 m from NW and NE corners, 41st floor, Commerce Court Tower (Dagliesh, 1975).

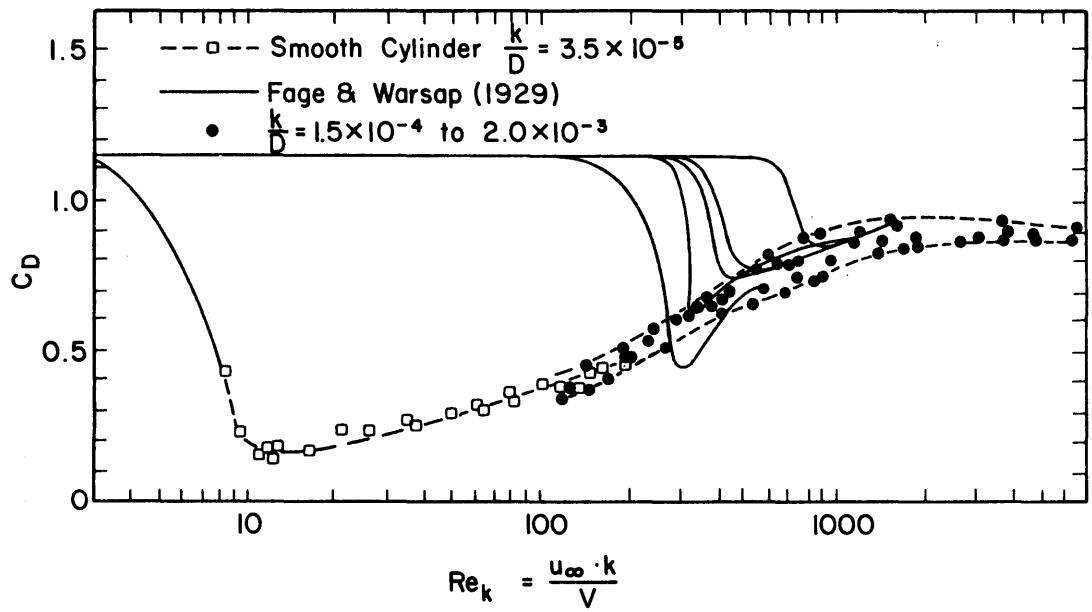

Figure 3-39. Dependence of the drag coefficient for circular cylinders on the roughness Reynolds number (Szechenyi, 1975).

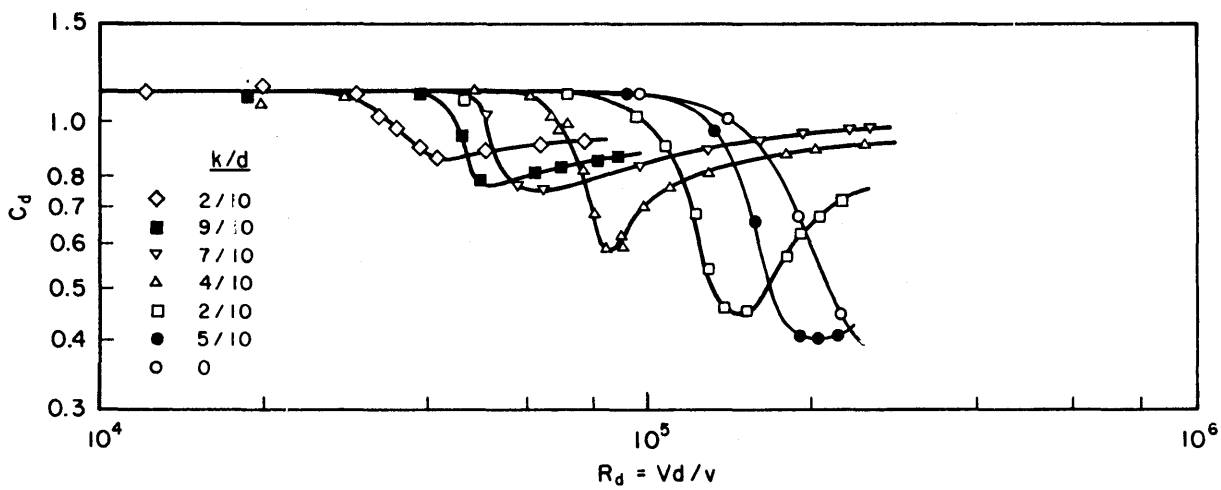

Figure 3-40. Variation of cylinder drag coefficient with Reynolds number for various surface roughness (Fage and Warsap, 1929).

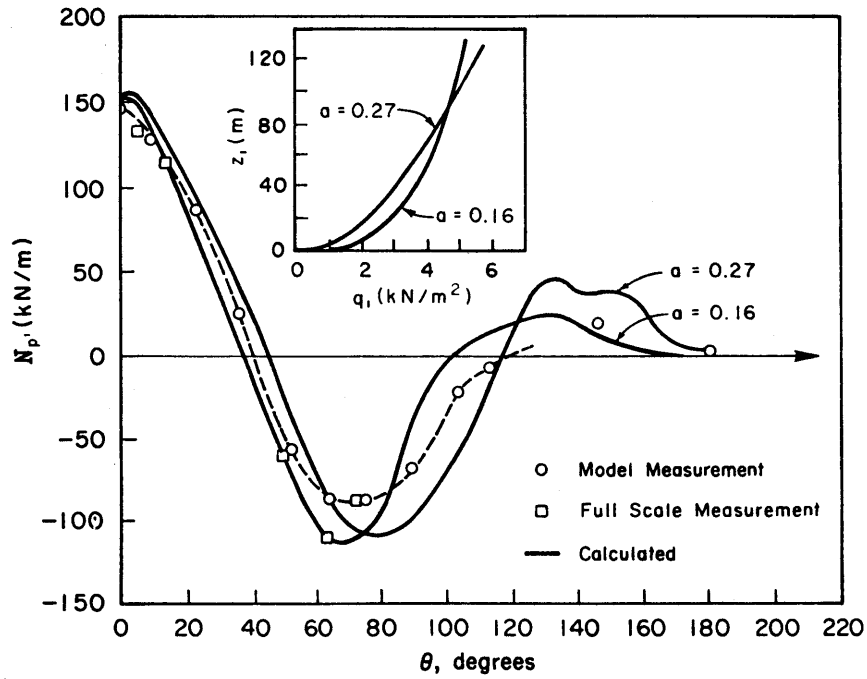

Figure 3-41. Measured and calculated meridional force (full-scale). z/H = 0.15; (o), model measurement; (x), full-scale measurement; (--), calculated. (Niemann and Ruhwedel, 1980).

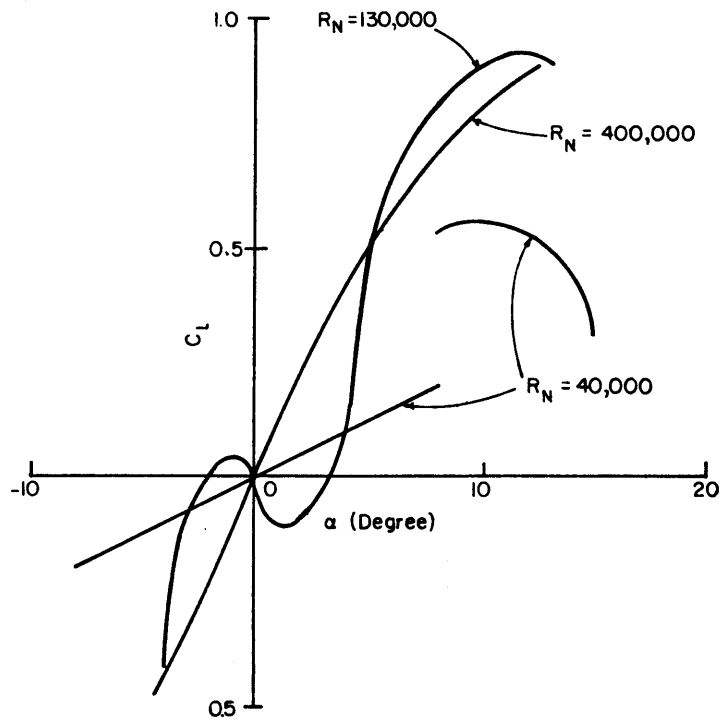

Figure 3-42. Lift curves for a smooth NACA 66_3-018 airfoil at three low Reynolds numbers (Mueller and Batill, 1982).

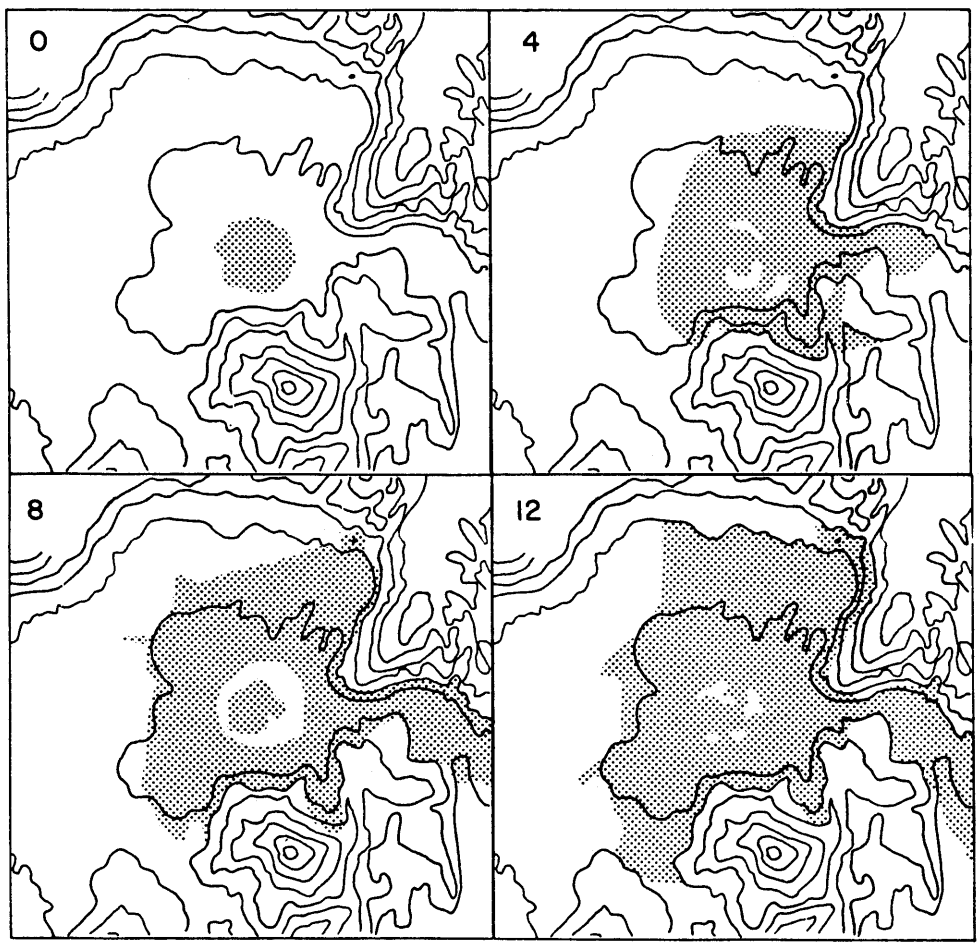

Figure 3-43. Water tunnel simulation of the spread of CO_2 from a well opening in a crater-shaped valley near Grosseto, Italy. Note initial toroidal annulus followed by terrain-channeled plume movement. These figures correspond to real times of t = 0.5, 1, 1,5 and 2 hrs. (Alessio et al., 1981).

4.0 PHYSICAL MODELING OF DENSE PLUME DISPERSION

Much of the present understanding of the dispersion of plumes, clouds, particles, and the mixing of fluid parcels results from laboratory experience. Turbulence measurements behind grids in wind tunnels established the foundation for statistical mixing theories; measurements downwind of jets and model chimneys guided the development of plume rise and trajectory algorithms; tracer studies in heated tanks have explained the confusing nature of ground and elevated plumes in convective boundary layers. Researchers have examined dispersion as influenced by:

- o point, line, area, and volume sources;
- o ground and elevated release locations;
- o passive, buoyant, and dense gases;
- o light and heavy particles;
- o particles which sublimate;
- o gases which chemically react;
- o terrain which is smooth, rough, undulating, or mountainous;
- o surfaces covered with vegetation, ice, snow, or sand;
- o neutral, stable and unstable stratification;
- o coastal boundary layers; convective boundary layers;
- o and even diffusion in anabatic and katabatic winds.

Experiments have considered the effect on dispersion of transportation vehicles (cars, trucks, trains, airplanes, ships, and even the space shuttle), buildings, building clusters (fossil fuel power plants, nuclear reactors, chemical processing facilities), cooling towers, fences, trees, forests, water and steam spray curtains, etc., etc..

Chapter 4.0 reviews the simulation criteria of the mean and

turbulent structure of the atmosphere. It is also necessary to properly scale the kinematics and dynamics of the source, and any additional dynamics introduced by the characteristics of the effluent itself. In Section 4.1 the method of similitude is used to identify pertinent property and flow parameters. Negative buoyancy and the thermal effects of heat transfer and latent heat release near cold plumes introduce interesting aspects to the model problem. Partial simulation of plume motions is considered in Section 4.2, where the implications of relaxing some requirements are discussed. In such cases concentration measurements must often be corrected before they can be applied to prototype situations as explained in Section 4.3.

4.1 Similitude of Plume Motions

A useful criterion for diffusion modeling is that all patterns of isoconcentration must be geometrically similar in model and prototype (Plate, 1982). Hence, the trajectory of the center of mass of a gas cloud must be geometrically similar, as well as the growth of the cloud dimensions about the center of mass in space and time.

The same equations of motion derived for the atmospheric boundary layer in Section 2.1 govern plume motion. Dispersion will be dominated in the near field by initial source conditions. It is convenient to use the approach of similitude (Kline, 1965). The method of similitude obtains scaling parameters by reasoning that the mass ratios, force ratios, energy ratios, and property ratios should be equal in both model and prototype. When one considers the dynamics of gaseous plume behavior, the following important parameters are identified:

Length Scale Ration = $[D/L]$

Specific Gravity Ratio = $[\rho_g / \rho_a]$

Volume Flux Ratio = $[W_g A_g/(U_a A_a)] = [Q/(U_a L^2)]$

Mass Flux Ratio = $[\rho_g W_g A_g/(\rho_a U_a A_a)] = [\rho_g Q/(\rho_a U_a L^2)]$

Momentum Flux Ratio = $[\rho_g W_g^2 A_g/(\rho_a U_a^2 A_a)] =$

$= [\rho_g Q^2/(\rho_a U_a^2 L^4)]$

Densimetric Froude No. relative to the inertia of air = $[\rho_a U_a^2/(g\{\rho_g - \rho_a\} L)]$

or,

Densimetric Froude No. relative to the inertia of the plume = $[\rho_g Q_a^2/(g\{\rho_g - \rho_a\} L^5)]$

or,

Flux Froude No. = $[\rho_a U_a^3 L/(g\{\rho_g - \rho_a\} Q)]$

Plume Reynolds No. = $[W_g D/\nu_g]$ or $[U D/\nu_a]$ or $[V_f H/\nu_a]$

Peclet No./Richardson No. Ratio = $[\rho_a U^3/(g\{\rho_g - \rho_a\} D)]$

Plume Stanton No. = $[h_s \Delta\theta R/(p\, Cp_g\, U\, M_g]$

Specific Heat Capacity ratio = $[Cp_o^*/Cp_a^*]$

Humidity = $[\rho_v/\rho_a]$

Terrain slope = $[\beta]$

Ideally these parameters must be equal at equivalent scaled locations and times over the entire lifetime of a dispersion episode. Usually it is argued that if the initial values of these parameters are equal, and if the surrounding flow fields are similar, then all subsequent plume motions and dilution must remain identical. This equality is restricted, of course, to the normal variance expectations that each atmospheric flow is a single realization from larger ensembles. The following sections consider the physical role played by each parameter.

4.1.1 Specific gravity ratio:

It is necessary to maintain equality of the plume specific gravity ratio, ρ_g/ρ_a, over the plume's entire lifetime, to obtain simultaneous simulation of all (4-1) parameters. Unfortunately the requirement for equality of the plume gas specific gravity ratio leads to several complications in practice. These are:

1. Equality of the source gas specific gravity between a model and its atmospheric equivalent leads to a wind speed scaling of $U_m = (L_m/L_p)^{1/2} U_p$. For a significant range of atmospheric wind speeds, this relationship leads to wind tunnel speeds at which there is a loss of Reynolds number invariance in the approach flow. To avoid this problem one could build a larger wind tunnel than those commonly in use today; thus, permitting scaling of the atmospheric flow at a larger length scale; or one could use a modified scaling scheme which relaxes equality of some of the previously mentioned plume parameters. Several alternative

scaling schemes are presented in Sections 4.2.1 to 4.2.4.

2. A hot or cold plume in the atmosphere is frequently simulated in the laboratory by an isothermal plume formed from a different gas of appropriate molecular weight. Unless the specific heat capacity of both the entrained air and the source gas in the actual situation are identical, this practice will lead to a nonsimilar variation of the local plume density ratio as the plume mixes with air. This behavior is discussed in Section 4.2.4.

4.1.2 Volume, mass and momentum source ratios

If the model and prototype specific gravity and volume ratios are equal, then all of these parameters are simulated. However, if the density ratio is exaggerated, a multitude of different recommendations for the priority of simulation of these ratios exists.

Elevated Source Release:

Table 4-1 from Snyder (1981) summarizes a list of these sets of parameters as used by nine modeling laboratories. Although various authors offer assurance that their methods have been proven or disproven by comparison with full scale conditions it is not always clear what criteria were used, or if minimum Re number requirements were met. Isyumov and Tanaka (1979) compare plume trajectories, maximum ground level concentrations, and entrainment behind model buildings using a variety of these approximation models. But Snyder (1981) concluded that none of the approximate techniques can be recommended for modeling the near-field rise of buoyant plumes. Poreh and Kacherginsky (1981) also reviewed a cross-section of ideas, and they concluded that only two critical parameters exist -- the dimensionless buoyancy flux, and the dimensionless momentum flux:

(4-2)

$$\text{Dimensionless Buoyancy Flux} = [\rho_a U_a^2/(\Delta\rho g L)](U_a/W_g)(L^2/D^2) \text{ and}$$

$$\text{Dimensionless Momentum Flux} = (\rho_g W_g^2)/(\rho_a U_a^2).$$

Poreh's approach seems to be similar to the buoyancy length scale method proposed by CALSPAN in Table 4-1. Distortions permitted under this approach are indicated in Figure 4-1. Poreh also commented that further systematic testing of approximate models is essential to determine their limitations.

Ground-level Source Release:

Most of the discussion concerning the significance of these specific gravity ratios revolves around the simulation of near- and far-field plume rise from chimneys. However, many dense gas release scenarios do not involve high speed release through a stack, pipe or chimney. Rather, they result from the boiloff from spills of cryogenic LNG on the ground or water. In such cases, the concern is not necessarily the matching of initial source momentum or mass flux, but the effect of increasing the density in the advective terms of the equations of motion during plume motions. In other words, plume inertia is increased, and the Bousinesqu approximation does not hold. The effect will be discussed further in Section 4.2.1. and 4.2.2.

4.1.3 Densimetric or flux Froude numbers

The effluent Froude number expresses the ratio of inertial to buoyancy forces in the effluent. Buoyancy forces play a major role in driving the initial fluid motions for dense gas plumes. Buoyancy forces tend to initiate the collapse and spreading of suddenly formed dense gas clouds, and they inhibit subsequent vertical mixing with the ambient air. There is some disagreement among investigators concerning the definition of the appropriate Froude number. Some prefer to define the Froude number using the effluent density as the reference density, Fr_s; others define it with the ambient density as

the reference density, Fr_a. The choice is not arbitrary unless density ratio equality is maintained. Numerical box or slab models must make the same choice with respect to specification of the gravity-driven frontal velocities; i.e., is $V_f \simeq [g(\Delta\rho/\rho_a)h]^{1/2}$, or is $V_f \simeq [g(\Delta\rho/\rho_g)h]^{1/2}$ (see Wheatley and Webber, 1984).

The Flux Froude number or the Buoyancy Length Scale Ratio are essentially identical, and are formed by combining the volume flux and Froude number parameters listed in Equation 4-1. The attraction of the flux Froude parameter is its similarity to the scaling procedure used by Briggs (1969), which was found to be so effective in correlating plume rise.

4.1.4 Plume Reynolds number

Two characteristic Reynolds numbers can be identified during dense gas cloud releases--a source Reynolds number, and a gravity-head Reynolds number.

Source Reynolds Number

The source Reynolds number characterizes the condition of the source gas flow during its exit from ruptured pipes, chimneys, stacks or vents. There are actually three possible source Reynolds numbers, corresponding to three different mechanisms which influence the near-source plume trajectory and entrainment: one for the flow inside the stack, $Re_{Ds} = W_o D/\nu_o$,; another for the interaction of the jet exiting the stack and the ambient wind at that point (also Re_{Ds}); and one for the ambient air interacting with the outside of the source, $Re_{Da} = UD/\nu_a$. When these Reynolds numbers exceed some critical values, i.e., $Re_D > Re_D$ minimum, the effects of the source Reynolds number, as well as the source Prandtl and Schmidt numbers, in both the

model and prototype, can normally be neglected.

To secure fully turbulent flow within the exhaust flue, a source Reynolds number of about 2000 is conventionally required. Roughening of the stack's interior walls, and/or insertion of screens, plugs, or orifices upstream of the exit, which enhance turbulence and make the velocity profile more uniform, allow a substantial reduction of the required Reynolds number down to about 300. Minor variations in velocity profile shape that occur over this Reynolds number range are not believed to be significant compared with other uncertainties.

Ricou and Spalding (1961) observed that entrainment into momentum-dominated jets emitted into calm surroundings increased substantially (by more than 20%) when Re_{Ds} fell below 15,000. Yet other authors such as Briggs and Snyder (1980) found that the critical Reynolds number for jets was approximately 2000, and for buoyant plumes it was as low as 200! (See Figure 4-2). As Snyder (1981) remarks, "it is difficult to reconcile the results of the various sets of experiments... It is evident that a basic systematic study needs to be undertaken to establish that Reynolds number (perhaps different ones for different sets of conditions) above which the rise and spread of model plumes is independent of Reynolds number." Dense gases exhausted vertically from stacks, vents, or relief valves lose vertical momentum and may actually descend to the ground (Hoot, Meroney, and Peterka, 1973). It is conceivable that critical Reynolds numbers for entrainment into dense plumes may be different than for neutral or positively buoyant gases.

The wake behind a stack or storage tank changes with exterior source Reynolds number, Re_{Da}. At moderate Reynolds numbers, $400 < Re_{Da} < 10^5$, a Karman vortex street (shedding vortices) is formed

downwind of the stack cylinder, but at larger Reynolds numbers, $Re_{Da} > 10^5$, transition to turbulence occurs earlier in the boundary layer; hence, the wake narrows and becomes more random in structure. Roughening the model stack or adding trip wires to the stack exterior may reduce the necessary Reynolds number by a factor of two. For a rectangular stack sharp corners force separation and the ranges are further decreased. However, the introduction of buoyancy makes these critical Reynolds number magnitudes very difficult to attain. Yet downwash of dense gas effluents will be influenced by the near-source flow around the stack, presenting a dilemna: simultaneous simulation of the dense plumes buoyancy dynamics and source flow structure is often difficult, if not impossible.

During the initial collapse of a volume of dense gas in the atmosphere, the cloud itself acts as an obstacle to the ambient flow. The interaction of the cloud and the wind results in acceleration of the bulk of the flow up to a speed near the characteristic speed of the approach flow and the wrapping-up of the windward edge of the cloud into a horse-shoe shaped pair of counter-rotating vortices. Rottman, Simpson, and Stansby (1984) performed a series of water channel releases, and found that the shape of released fluids were similar over a range of $500 < Re_{Da} < 2000$.

Gravity-head Reynolds Number

As a dense plume spreads at ground level it forms a gravity head vortex, which tends to move over the surface with a frontal velocity, V_f. This frontal velocity has been examined extensively in salt-water. To a first approximation, it has been found that $V_f = k(g(\Delta\rho / \rho_g)H)^{1/2}$ where H is the frontal cloud depth and k is a constant of order one. The gravity-head Reynolds number may be

defined as $Re_f = V_f H / \nu_a$. Above some critical value of Re_f, it is found that k remains constant, but below this value, k diminishes. (Note: in water channels, k will also be a function of the ratio of cloud depth to total fluid depth.) Thus, if the model Re_f value is too low, the dense cloud will not spread upwind or laterally at the rate observed in a prototype cloud.

Simpson and Britter (1979) suggested that for scale independent experiments, the local magnitude of Re_f must be greater than 1000. At small Re_f, the observed velocity of advance, the rate of mixing between the two fluids, the cloud front nose height relative to the head height, and the ratio of head height to the height of following fluid all become smaller (Figure 4-3). In the absence of entrainment, both frontal velocity and head height decay with time or distance for fixed volume releases; hence, Re_f must steadily decrease. The frontal velocity must eventually fall below the rate of lateral cloud growth associated with turbulent or molecular dispersion. If this occurs before the local Re_f falls below its critical value, then lateral cloud growth is essentially Reynolds number independent.

Hunt, Rottman, and Britter (1984) postulated the existence of four phases of dense gas dispersion.

- During the initial phase, (1) the inertia of the cloud and the mean atmospheric flow are the dominant forces.
- In the gravity-spreading phase (2), the cloud buoyancy forces and the pressure forces associated with the external mean flow are dominant.
- In the third nearly-passive phase (3), the external turbulence, external mean flow, and cloud buoyancy are important.
- Finally, during the passive phase (4), the dispersion is controlled entirely by atmospheric turbulence.

Depending on the atmospheric and source conditions, one or even

more of the phases may be bypassed as the cloud evolves. In addition, if Reynolds numbers are too small (i.e., viscous forces are relatively large enough), any phase may be cut short by the damping influence of viscosity. Britter (1979) prepared a table of similarity solutions for dense cloud behavior in plane and axisymmetric situations.

Britter suggested that viscous forces for axisymmetric point source dense gas plumes will be significant after $t_v = [Q/(g'_o \nu)]^{1/2}$ or $t^*_v = [Re]^{1/2}$. In a calm environment, for releases of constant volumes of dense gas, he discerned that both buoyancy and viscous forces are significant after $t_v = [V_o/(g'_o \nu)]^{1/3}$ or $t^*_v = Re^{1/3}$. Figure 4-4 plots the frontal position of constant-volume salt water releases into a fresh water-filled sector tank versus time, for different ratios of the initial intrusion depth to water depth. After an initial linear growth period, the cloud front grows as the square root of time (as predicted by Britter, 1979) until the cloud becomes so thin that viscous effects become important, causing the cloud to spread still more slowly. Figure 4-5 displays the change of temporal variation in a constant flux point source plume when viscous effects begin to dominate.

Fay and Zemba (1985) examined the area-source continuous-release plume spread results of Britter (1980) and Neff and Meroney (1982). They found that they could collapse all plume spread results on to one similarity curve when experiments were eliminated that fell below a critical Reynolds number. They also concluded that the reference velocity scale should be that value which occurs at the level of the plume rather than at an arbitrary height, but this value is constantly changing in a shear flow. They defined the Reynolds number as:

$$Re = Q^{5/3}L^{1/3}/[\,\nu(D + aL)^3(g'_o)^{1/3}] \qquad (4\text{-}3)$$

where $U = 2.5\ u_*\ \ln(H/z_o)$,

$L = g'_oQ/U^3$,

$H = [bQ^{2/3}L^{1/3}/[(D + aL)(g'_o)^{1/3}]\{1 + c/Re^{1/2}\}$

$a = 2.2$, $b = 1.17$, and $c = 0.034$, and

$g'_o = g\ (\rho g - a)/\rho a$

Obviously, these relations must be solved simultaneously for a given situation to determine magnitudes of the Reynolds number, Re, or the buoyancy length scale, L. When $Re > 0.01$, the ratio of the measured plume width and (D + aL) is close to one, as shown in Figure 4-6.

4.1.5 Peclet number/Richardson number ratio

Researchers at Shell Laboratory, Amsterdam, have concluded that molecular diffusion may play an important role in the laboratory when scaled turbulent diffusivity is very small (Colenbrander and Puttock, 1984; Puttock, 1985). They compared wind tunnel simulations of several of the Maplin Sands experiments to field data, as well as considering several experiments from the Neff and Meroney (1982) wind tunnel series. They discovered that when the parameter ratio of Peclet number to Richardson number is less than a critical value, simulations were inaccurate. Their parameter was based on the characteristic velocity and source scales, which gave:

$$Pe/Ri = U_R^3/(g'_oD), \qquad (4\text{-}4)$$

where D is a molecular diffusivity. This parameter measures the relative rates of turbulent entrainment and molecular diffusion. When this parameter is too small the scaled concentrations will be smaller

than field values. Table 4-2 and Figure 4-7 contain the comparisons considered by Shell Research. A critical value of Pe/Ri based on the approach wind speed at a 10 meter reference height is about 1500.

An alternative velocity scale is the friction velocity, u_*. In this form, the expression above represents the ratio between the turbulent entrainment velocity, $w_e \approx u_*/Ri_*$, and the effective molecular diffusion entrainment velocity, D/H. In the full scale prototype, the turbulent entrainment exceeds the effective molecular diffusion velocity by orders of magnitude; thus, molecular effects can be ignored. Figure 4-8 displays data from Neff and Meroney (1982) for which the Pe_*/Ri_* ratio varies from 0.05 to 0.5. Note that concentrations deviate noticeably from scatter associated with measurement error only when $Pe_*/Ri_* < 0.2$. Also plotted on this figures is the result of calculations with the depth-integrated model DENS20 (Meroney, 1984), when microscopic diffusion is added to the entrainment terms. The numerical model reproduces the decrease in concentration as the Pe_*/Ri_* parameter decreases.

Since the local density difference decreases as the cloud disperses, one expects molecular diffusion effects to decrease with time as the cloud moves downwind. Hence, the Pe*/Ri* < 0.2 criterion may be overly conservative in the presence of large initial mixing caused by collapse of a tall cloud or mixing caused by, fences, explosions, or water spray curtains.

Duijm et al. (1985) considered the effects of molecular diffusivity during model studies of the Thorney Island field experiments. They found their model measurements underestimated the field values by a factor of 2. While this may be a molecular diffusion effect, it seems more likely that low concentrations were

caused by non-isokinetic sampling during their measurements, which resulted in dilution at the sampling point. Wind tunnel speeds at instrument height were about 0.8 m/s, whereas aspiration velocities were near 2.8 m/s; hence, experiments of Duijm et al. should be disregarded. Indeed, Schatzman et al. (1985) reproduced the Thorney Island concentration magnitudes quite closely during similar wind-tunnel experiments. They report that maximum concentrations were essentially identical during simulations using various source gas density ratios, but at constant densimetric Froude number. This is not surprising since turbulence generated by cloud collapse dominates the early stages of entrainment. The collapse turbulence remains high even at low Pe_*/Ri_*.

Meroney (1984, 1985) reported the results of simulating the Burro No. 8 China Lake spill of 40 m^3 of LNG with distorted and undistorted density scaling. The undistorted density ratio case ($Pe_*/Ri_* = 0.05$) produced a laminar-like cloud with little evidence of turbulence. The concentrations and distances to the maximum average LFL (300 m) were less than the prototype case (400 m). The distorted density ratio case ($Pe_*/Ri_* = 0.60$) produced a puffy turbulent cloud similar to that observed during the field experiment. The cloud bifurcated over the terrain as in full scale and produced similar magnitude concentrations and distance to the maximum average LFL (350-400 m).

4.1.6 Plume Stanton number

Heat transfer across the boundaries of an LNG vapor plume will be governed by the modes of free, forced or mixed convection (Andriev, Neff, and Meroney, 1983). Consider the heat transfer from the ground surface into an idealized well-mixed cloud which is being convected over a plane surface (See Figure 4-9). A simple energy balance between the surface and the cloud volume requires:

(4-5)

$$\rho_g Cp_g \forall \, dT_g/dt = h_s A (T_w - T_g),$$

where h_s = Surface heat tranfer coefficient,
Cp_g = Specific heat capacity of dense gas mixture,
ρ_g = Plume density,
$\forall_g$ = Gas volume,
A = Surface contact area, and
T_g, T_w = Gas and wall temperatures respectively.

Using the ideal gas law and nondimensionalizing the equations by reference scales ρ_a, L, $\Delta T = (T_w - T_o)$, and T = L/U yields:

(4-6)

$$d(\rho^*)/dt^* = - [h_s \Delta T R/(p \, Cp_g \, U \, M_g] \rho^* \Delta T^*/H^*$$

where p = pressure,
H* = AL/V,
R = Universal gas constant, and
M_g = Molecular weight.

This equation shows that the bracketed term must be equal in model and prototype plumes in order to have the same specific gravity history. This term is a modified Stanton number. Alternatively, the bracketed expression may be written:

(4-7)

$$[h_s/(\rho_a Cp_a U)] [Cp_a/Cp_g] [M_a/M_g] [\Delta T/T_a],$$

where the first term is the classical Stanton number, St, the second and third terms are property ratios, and the third term is specified by the boundary conditions.

Assuming property ratios are equal, the expression implies that model (m) and prototype (p) temperature differences must be scaled as:

(4-8)

$$\Delta T_m = [(h_s)_m/(h_s)_p][U_m/U_p]\,\Delta T_p.$$

During forced convection of turbulent flow over a flat plate, the Stanton number is commonly found to equal the skin friction coefficient, $C_f/2$, which implies that the first bracket equals $[(C_f)_p/(C_f)_m)][U_p/U_m]$. Given a sufficiently rough surface $(C_f)_m = (C_f)_p$; thus, incorporating these relations into Equation (4-8) above shows that forced convection will be properly modeled when $\Delta T_m = \Delta T_p$.

Unfortunately, during free or mixed convection distorted temperature scaling would be required. For free convection from a horizontal plate, a common empirical relation is that the $Nu = Gr^{1/3}$, where $Gr = \Delta T L^3/(T\nu^2)$ is the Grashof number and $Nu = h_s L/k$ is the Nusselt number. Again, if properties are presumed constant, and if it is assumed that Froude number constraints specify $[U_m/U_p] = [L_m/L_p]^{1/2}$, then substitution into Equation (4-8) yields:

(4-9)

$$\Delta T_m = [T_m/T_p]^{1/4}[L_m/L_p]^{3/8}\,\Delta T_p$$

Thus, if real LNG were spilled in the laboratory, similar density histories could only occur if $T_m = (L_p/L_m)^{3/2}\,T_p$, an unrealistic requirement for the length scale ratios of practical interest.

Indeed, the case where one spills LNG in a scaled situation, any heat transfer rate by free convection will be too large in the model plume compared to other advective and dispersive processes.

Accordingly, small releases of cold gases, subjected to free convection, that are intended to represent larger spills will always lose their negative buoyancy too quickly, and they will loft (or rise) more than the prototype release. This is true whether one is considering laboratory simulations or field releases. The thermal capacitance of a plume will vary as the volume (length scale cubed), whereas the surface area over which heat transfer occurs varies as the length scale squared; hence, one expects large-volume cold spills to respond to heat transfer more slowly than their scaled smaller counterpart. One may also find in the very large spill limit that releases of isothermal high-molecular-weight gases simulate very large LNG spills better than small LNG spills simulate large LNG spills.

Leovy (1969) correlated mixed-convection atmospheric data. He found that an empirical expression proportional to the square root of the temperature difference between the air and the boundary temperature correlated surface heat transfer coefficients over a wide range of convective conditions. In this case the equality required is:

$$\Delta T_m = [T_m/T_p]^{1/2}[L_m/L_p]^{5/6}\,\Delta T_p. \qquad (4\text{-}10)$$

Again thermal similitude is generally unlikely.

The example used above presumed that no mixing occurred across plume boundaries; hence, all density changes were due to thermal transport. In actuality, mixing is usually initially rapid, and the

thermal driving potential , $T_w - T_g$, drops to small values very quickly. Once this occurs, heat transfer rates drop considerably and may play only a minor role in the plume dynamics during very large spills.

4.1.7 Specific Heat Capacity Ratio

The effect of molar specific heat capacity differences between the air and the plume can be understood by considering the adiabatic mixing of two volumes of ideal, constant property gas. Let source gas be V_s and the ambient air be V_a. Consideration of the conservation of mass and energy for this system yields specific gravity variation (Skinner and Ludwig, 1978):

$$\frac{\rho_g}{\rho_a} = \frac{\frac{\rho_s}{\rho_a} V_s + V_a}{\left(\frac{T_a}{T_s} V_s + V_a\right)\left(\frac{(C_p^*)_s}{(C_p^*)_a} V_s + V_a\right)\left(\frac{(C_p^*)_s}{(C_p^*)_a}\frac{T_a}{T_s} V_s + V_a\right)^{-1}} \qquad (4\text{-}11)$$

If the temperature of the air equals the temperature of the source gas, $T_o = T_a$, or if the molar specific heat capacity is equal for both source gas and air, $Cp_g^* = Cp_a^*$, then the equation reduces to:

$$\frac{\rho_g}{\rho_a} = \frac{\left(\frac{\rho_s}{\rho_a}\right) V_s + V_a}{V_s + V_a}. \qquad (4\text{-}12)$$

Consider two prototype cases: 1) an isothermal plume and 2) a thermal plume which is mostly composed of air. It does not matter how one models the density ratio, thermally or isothermally, as long as the initial density ratio value is equal for both model and prototype. For the case of a thermal plume whose molar specific heat capacity is different from air, such as an LNG vapor plume, the modeling of the density history variation with the plume can only be approximate.

Section 4.2.4 discusses further situations when buoyancy is not conserved.

4.1.8 Humidity

The release of latent heat through the condensation of humid air can have a very significant effect on the density history of a thermal plume. When the plume temperatures are below the atmospheric dewpoint, moist air mixed with plume gases will condense water vapor, release heat, and result in loss of negative buoyancy. Subsequently as the moisture-saturated dense plume rises above dewpoint temperature, mixing with ambient air results in re-evaporation of condensed water vapor, decrease in dense plume temperature, and a possible recovery of negative buoyancy. These effects are discussed further in Section 4.2.4.

4.1.9 Terrain slope

Criteria were recommended in Section 3.5.3 to determine whether slope effects should be included in a model study of dense gas dispersion. These criteria presumed the release of a finite amount of fluid on very modest slopes. When dense gases are released suddenly on slopes exceeding 5^{o}, the cloud behaves more like a thermal than a gravity front (Beghin, Hopfinger, and Britter, 1981). In this case the plume initially accelerates, but then decelerates. The acceleration phase is more rapid on steeper slopes.

Alternatively, when the source is maintained (a starting plume) the frontal velocity, V_f, remains reasonably constant with β, and V_f does not vary with distance down the slope unless slopes are less than 0.5^{o} (Britter and Linden, 1980). In this case increased entrainment

as the slope steepens just balances the increase of momentum feeding into the gravity head by the following flow. Such clouds have much greater depths and markedly different shapes than zero slope plumes with the same initial conditions otherwise (see Britter and Linden, 1980).

The LNG field tests at China Lake (Koopman et al., 1979, 1981) and the associated isothermal wind tunnel tests (Neff and Meroney, 1979, 1982; Meroney, 1985) which model the China Lake terrain were run under conditions where the dense gas cloud was driven upward along a slope by the wind. An adverse ground slope ($\beta \simeq 0.29^{o}$) extends from the spill site to a distance of 150 m, beyond which the land is approximately level. Measurements made within this region of adverse slope satisfied the criterion proposed by Fay and Ranck (1983), $1/Ri_{*} << \beta$ (in radians), for adverse slope effects. Fay and Ranck (1981) concluded that the cloud drift distance for a given time was much less than would be the case for a level surface. The retarding effects of the sloping ground on the drifting motion of the cloud also led to greater dilution at a given distance from the source than would be experienced on level ground. During Burro Test Number 8, the part of the plume which impacted the hill behaved as described above, but the portion of the plume which was advected over the flatter region to the east of the primary terrain extended perceptibly further downwind (See Figures 4-14 and 4-15; also Section 4.2.2).

4.2 Partial Simulation of Plume Motions

Again rigorous similarity requires that, for a cold gas spill, the nondimensional parameters identified in Section 4.1 be matched in

both model and prototype. Unfortunately, strict equality results in model conditions either impossible or very difficult to maintain in a laboratory facility. It is important to examine each modeling situation and decide if an approximation to complete plume behavior may be employed without a significant loss in the quality of the results for design or safety evaluation purposes. Sections 4.2.1 to 4.2.4 discuss several approximation methodologies which might help formulate a fluid model, and they address the errors incurred in such approximations.

4.2.1 The relaxation of source density equality

The relaxation of source density equality, ie. $[\rho_g/\rho_a]_m \neq [\rho_g/\rho_a]_p$, during the modeling of plume dispersion has been frequently proposed to avoid low wind speeds that are operationally difficult to maintain in most wind-tunnel facilities. Low wind speeds also introduce questions concerning the Reynolds number invariance of the approach flow. All enhanced scaling schemes which use the relaxation of source density equality increase the velocities used in the model. The relaxation of source density equality prohibits simultaneous equality of the remaining plume parameters. One must now choose which of these parameters are dominant for the plume being studied.

When dense gases are emitted from stacks, chimneys, or flues with significant upward momentum, then equality of the Momentum Flux Ratio is required near the exhaust exit. Depending upon the Froude number chosen for specifying equality of the buoyancy forces this will result in some distortion in plume behavior farther downwind. As noted in Section 4.1.2, Elevated Source Releases, some authors prefer Flux

Froude Number equality, but care must be taken in all cases to adjust the concentration scaling as described in Section 4.3. Hoot et al. (1974) examined plume rise and fall from dense isothermal gases exhausted from model stacks. Since there are no field data available for elevated sources of dense gas, it is not possible to recommend with confidence any one technique for near-field simulation of dense gas behavior from stacks.

4.2.2 Similarity between plumes of negligible initial momentum

Many dense gas release scenarios result from boiloff from spills of cryogenic liquid spilled on the ground or water. In such cases the concern is not to match initial source momentum, but to correctly simulate the effect of density on plume buoyancy forces and inertia. Several alternative combinations of similarity variables are possible.

Alternative 1: Densimetric Froude Number and Volume Flux Ratio Equality

As noted in Section 4.1.2 if the density ratio is exaggerated, then a multitude of different recommendations for the priority of simulation of the various volume, mass and momentum ratios and Froude numbers exist. During the ground level release of a dense plume in which the release momentum is small, it has been argued that the dominant parameters are the Densimetric Froude Number with respect to the air, Fr_a, and the Volume Flux Ratio, V. Since plume momentum is negligible and the Flux Froude number is simply the ratio Fr_a/V, then the only neglected parameter of significance is the mass flux ratio, M.

A number of authors have found good agreement using model Alternative 1, comparing tests in which the source gas specific

gravities were large, ie. $SG_o > 2$. Hall (1979) claimed good agreement between two tests in which the source gas specific gravities were 2.37 and 4.74. Neff and Meroney (1982) examined cases where source specific gravities ranged between 1.22 and 4.18. They found similar decay rates and surface concentration profiles for specific gravities greater than 1.7; however, lower values for lower specific gravity deviated from one another as shown in Figures 4-10 and 4-11. It is likely that this deviation is caused by distortions due to microscopic diffusion effects, which occur when the Peclet/Richardson number ratio is too small (See discussion Section 4.1.5). It is not possible to determine whether additional deviations from the comparison cases occur because of density ratio distortion effects alone.

Schatzmann et al. (1985) and Meroney (1985) report simulations of Thorney Island and Burro series field tests, respectively, using Alternative 1 distorted density ratio scaling, for which microscopic diffusion effects are likely to be small. Both authors found concentration magnitudes were reasonably reproduced, but the time of arrival and departure of the model plumes were delayed. Figure 4-12 and 4-13 from Schatzmann et al. compares undistorted and distorted density model scaling of Thorney Island Test 15. Note that the maximum concentrations for model and prototype are similar in both cases, but density distortion appears to result in extended time durations of cloud passage. Simulation of the Burro 8 LNG spill by Neff and Meroney (1981) and Meroney (1985) also found the heavy gas clouds moving too slowly for the density distorted model (See Figures 4-14 and 4-15).

Contradictory evidence is reported by Duijm et al. (1985). Although they acknowledge that their concentrations are too low

because of sample dilutions due to non-isokinetic samples or Peclet/Richardson ratio effects; this may not invalidate their time of arrival or departure results. Their figures show no extended time durations of plume passage. It is worthwhile to note that nonsimilar velocity profiles near the ground surface will also produce distorted times of plume duration. Neff and Meroney (1981) performed replication tests of the Burro Test Numbers 4, 8, and 9 at scales of 1:85 and 1:240. Although the reference velocities were properly scaled, the velocity profiles near the ground during the 1:240 scale tests were significantly less than the field values, whereas during the 1:85 scale tests the velocity values were very close to the field values. Figures 4-16 and 4-17 compare model tests at the 1:85 and 1:240 scales.

Another explanation for the delayed arrival and departure of distorted density plumes may be the increased inertia of the source plume when ρ_g is exaggerated. Near the source, the Froude number referenced to source density, Fr_s, will be too small if Fr_a is used to specify model velocities. Any deviations caused by this effect are equivalent to presuming the Boussinesq approximation does not hold during dense plume dispersion. There are no measurements of gravity current speeds for large values of specific gravity, and, therefore, no direct method of resolving this uncertainty. Schatzmann and Policastro (1984) calculated that non-Boussinesq effects in strongly buoyant plumes can result in 20% greater plume rise, when fractional density, $\Delta \rho / \rho_a = 0.5$. Crapper and Baines (1977, 1978) suggested that when fractional density exceeded 0.05 the Boussinesq approximation is no longer valid. They also argued that a plume produced by a denser fluid falling through a lighter fluid will <u>not</u> be

a mirror image of a light plume having the same absolute magnitude of fractional density. Indeed their calculations seem to suggest a plume of light fluid spreads less and a plume of heavy fluid more per unit length than in the Boussinesq case. Resolution of these contradictory results will require new measurements of near-source behavior.

Given a large enough Reynolds number and Peclet/Richardson number ratio it appears that laboratory scale models can reproduce correct plume trajectories, plume widths, and maximum concentrations. It is not yet possible to conclude whether times of arrival, departure, or duration are distorted due to density ratio exaggeration alone.

Alternative 2: Flux Froude Number and Mass Flux Ratio Equality

An alternate enhanced scheme might be to maintain the equality of the Flux Froude Number, Fr_f, and the Mass Flux Ratio, M. This scheme might appear logical because it is the relationship between the momentum of the approach flow and the inertia of the plume which determines how rapidly the plume gases are accelerated to the approach wind speeds. Neff and Meroney (1982) examined Alternative 2 cases where source specific gravities ranged from 1.38 to 4.18. Again, those cases where specific gravities were greater than two showed fair correspondence, but lower specific gravities deviated from the others, as noted in Figure 4-10. It is likely that low Peclet/Richardson ratios caused these deviations. It is not possible to conclude whether density distortion will cause other variations during Alternative 2 scaling at lower source specific gravity ratios.

Alternative 3: Flux Froude Number Equality

In this technique it is assumed that the Flux Froude Number, Fr_f, is the only dominant parameter; however, the Volume Flux Ratio must not be grossly distorted. Indeed, whenever the Volume Flux Ratio is

distorted between model and field plumes, the model concentration field must be rescaled to field values as explained in Section 4.3.

Neff and Meroney (1982) grouped plume spread data by equality in the Flux Froude number, $Fr_f = L/l_b$ for continuous area source releases of dense gas. Comparing plume structure between tests of equal buoyancy length scale determined the similarity limits for volume ratio distortion. There was a definite tendency at a constant Flux Froude number (constant l_b) for increased plume growth with increasing Volume Flux Ratio, V (or, equivalently, decreasing Fr_a). The magnitude of this variation cannot be definitely stated because of the large experimental error associated with estimation of l_b ($\pm$45 %). This large error is primarily due to the cubic dependence of l_b on the mean velocity, which is accurate to only $\pm$15 %. If the trends in the data are assumed to be solely caused by variations in Volume Flux Ratio, V, then within a volume ratio distortion range of 1.5 there is no appreciable change in lateral or upwind plume extent.

Neff and Meroney (1982) also examined the decay of centerline concentrations versus downwind distance for the same set of area source data. It was hypothesized that plumes of equal Flux Froude number (equal l_b) are similar; hence, normalized concentration variations with downwind distance should be similar. There was definite similarity between centerline concentration decay curves for volume fraction distortions up to 1.5.

Figure 4-18 converts the variables associated with a field reference plume (u_p, Q_p, SG_p) to those used in a physical model, as constrained by the equality of the Densimetric Froude number, Fr_a, and the Volume Flux Ratio, V (and thus equality of Fr_f). The intersection of the dark line with the heavy dashed line representative of

wind-tunnel to field length scale ratio yields the unique point for rigid similarity. If distortion in source density is allowed (Alternative 1) the simulation variables may be any point along a dashed line characteristic of the chosen length scale.

Figure 4-19 presents an alternative enhanced situation where only equality of the Flux Froude Number F_f is specified. Instead of a unique similarity point for undistorted density scaling at a given length scale ratio, there is now a locus of points along a line where Q is proportional to u^3. If distortion of plume source density is permissible (Alternative 3), then there is a broad band over which similar wind tunnel conditions can be chosen.

4.2.3 Plume similarity when the velocity scale has been distorted

As discussed in Sections 3.1 and 3.2 a simulated atmospheric boundary layer may variously be scaled by its depth, δ, a roughness length, z_o, an integral scale, Lu_i, or the scale of the spectral peak, $(\lambda u_i)_m$. This is because these scaling lengths have large variations associated with their calculation. For example, the roughness length, z_o, can be estimated by different researchers to vary over a factor of two in describing the same velocity profile, and a flat-topped turbulent spectrum may allow choices of the spectral peak to vary by a factor of five. This wide latitude in geometric scale partially explains why model length scale ratios for similar atmospheric situations often vary by a factor of ten in the literature. Fortunately such variation in model length scale ratio is permissible because instantaneous plume dispersion will be dominated by the scales of motion of the same order as the plume dimensions.

Hence, it is not surprising that although the most judicious

evaluation of a boundary layer might recommend an optimum length scale ratio of 1:1000, other constraints, such as measurement resolution or Reynolds number invariance may suggest a scale ratio of 1:100 be imposed. Enhancing the wind-tunnel velocities in this manner is particularly viable if the plume being modeled only occupies a small portion of the boundary layer. Figure 4-20 displays the distortion in the mean shear flow for a length scale exaggeration of two. The deviation is quite small when one considers errors of this magnitude could be made in the estimation of the velocity profile in either boundary layer. The critical question is then: What amount of mismatch is permissible between the effective length scale ratio of a simulated boundary layer, and the length scale ratio desired for the dense gas cloud? Note that a similar distortion is involved when one attempts to scale the results from small scale LNG spills like the 40 m^3 Burro Series up to 25,000 m^3 spill conditions (a length scale ratio distortion of about nine).

The influence of scale mismatch may be determined by examining a series of experiments performed in the same boundary layer but at different imposed length scale ratios. Meroney and Neff (1982) examined their plume spread and concentration data with this thought in mind. A change of length scale between two tests usually results in a change in the Volume Flux Ratio. The data did not permit a decisive conclusion be drawn because a coupling between the distortion in length scale and distortion of Volume Flux Ratio existed. It did appear that a length scale distortion of 1.5 was acceptable.

Earlier, Neff and Meroney (1981) had performed simulations of the Burro Test Series at scales of 1:85 and 1:240 in a boundary layer for which the length scale relationship was found to be about 1:1000.

This ratio was determined by a comparison of the mean and turbulent characteristics of the model wind field to those cited for strong wind atmospheric situations. At the 1:85 scale very good reproduction of the field plume structure was obtained for Burro Test 9, and good replication of plume centerline concentration decay was found for the 1:240 scale tests of Burro 4, 5, 7, and 9, but plume duration was distorted during the 1:240 tests. These observations suggest that the following ill-understood factors are at play:

1. The scales of turbulent motion that are documented for strong wind atmospheric conditions may not be applicable to the low wind speed conditions of interest for heavy plume dispersion, and/or

2. Large distortions in the scales of the approach flow turbulent motion may have little effect on the near field dense plume dispersion. This suggests correct modeling of the mean wind shear over the height of the plume may be the most important approach flow characteristic.

It is not possible from such limited tests to determine permissible volume and length scale distortions before plume similarity is lost. Any additional influence caused by the presence of terrain or obstructions on the distortion constraints to similarity is also unknown.

4.2.4 Plume modeling when buoyancy is not conserved.

Most classical plume rise and entrainment theories assume that buoyancy is conserved during the rise and dispersion of typical fossil fuel generated chimney plumes. This is possible because the major constituent of such plumes is air, humidity plays a rather minor role, and the plumes do not contact the ground surface until diluted to near-ambient temperatures. Thus, fluid modelers can successfully model plume buoyancy using isothermal low molecular weight mixtures of equivalent buoyancy. Unfortunately, there are several thermal effects that can change the density history of a cold ground level plume as it

disperses. These are:

1. Release of latent heat during the entrainment of humid air,
2. Thermal expansion or contraction of the plume due to differences in the molar specific heat capacity of the plume source gas and air (ie. $Cp_a^* \neq Cp_g^*$), and
3. Heat transfer by conduction, convection, or radiation across plume boundaries.

Loss of negative buoyancy by latent heat release

The release of latent heat through the entrainment of humid air can have a very significant effect on the density history of a thermal plume. Assumption of adiabatic mixing of ideal constant-property gases permits the construction of simple formulae for the variation of mole fraction, χ, with plume temperature, T, and humidity, ϕ(Meroney, Cermak and Neff, 1976). Andriev, Meroney, and Neff (1983) prepared Figure 4-21 which demonstrates variations associated with entrainment of humid air into a cold methane plume. The dimensionless temperature is defined as $T_* = (T_a-T)/(T_a-T_o)$, where T_a is ambient temperature and T_o is initial source gas temperature. Density of an isothermal high-molecular-weight simulant mixture will vary linearly with concentration, but density of the real gas will vary inversely with temperature, T. The resultant variation of the specific gravity, SG, of an adiabatically mixed methane plume versus mole fraction is shown in Figure 4-22.

Dry air mixing with cold methane vapor will result in a gas mixture which will remain negatively buoyant over its entire lifetime. Latent heat release from condensation of entrained water vapor will diminish plume density. Indeed, when adiabatically mixed with air at 100% relative humidity, an LNG plume would become positively buoyant at mole fractions of 0.3. LNG vapor plumes will become marginally

buoyant for humidities slightly greater than 75% (See Figure 4-22). Of course for humidities less than 100%, the condensed water will evaporate as plume temperature rises, and eventually the plume (in the absence of heat transfer) will regain its negatively buoyant character as plume temperature rises above ambient dew point temperature.

An isothermal model plume can not replicate the density variations produced by latent heat release; however, inclusion of humidity effects in a simple numerical box model suggests that they are often minor compared with surface heat transfer perturbations (Andriev et al., 1983). In any event, an isothermal model gas will always provide an over-estimate of plume size and concentration magnitudes.

Loss or gain of negative buoyancy produced by specific heat capacity inequality

The effective specific gravity variation of a model LNG plume simulated by an isothermal source gas is not the deviation between the dry air curve in Figure 4-22 and a linear variation between 1.0 and 1.55. The model mole fraction must be corrected for the larger number of moles of gas actually released at cryogenic conditions in the field. Neff and Meroney (Appendix B, 1982) calculate the implications of not simulating thermal capacitance effects during isothermal modeling of an LNG vapor cloud. Correction for source effects has a compensating effect, such that the errors produced by not accounting for specific heat capacity effects are actually small. Figure 4-23 displays the deviation from the correct density history behavior for the isothermal simulation of an LNG vapor plume. Figure 4-24 displays the variation in the plume cross sectional area as the plume mixes with air for this same situation. Consideration of these two figures

suggests that, although an isothermal simulation of adiabatic mixing of an LNG vapor cloud as it entrains dry air is not exact, it is a very good approximation to actual behavior.

Andriev et al. (1983) performed experiments with cold dense gases where source gas mixtures were prepared to provide gases which were all initially heavy; but they were either isothermal, cold with $Cp_g^*/Cp_a^* = 1.00$ (cold nitrogen gas), or cold with $Cp_g^*/Cp_a^* > 1.00$ (cold carbon dioxide and cold methane). Thus one could evaluate whether dilution resulted from adiabatic entrainment, heat transfer effects, or unbalanced thermal contraction. Methane-equivalent concentrations for the carbon dioxide runs actually exceeded the isothermal concentrations, which could only be due to specific heat capacity effects. Nonetheless, these laboratory experiments tended to exaggerate all thermal effects, and normally heat capacity corrections will be small when applied to isothermal model plume measurements.

Loss of negative buoyancy due to surface heat transfer

Surface heating of the plume reduces the plume's negative buoyancy. The result is to decrease the local Richardson number thereby enhancing both dispersion by atmospheric turbulence and the subsequent downwind advection of the plume. As the buoyancy becomes positive and less stably stratified the plume may actually lift off the ground. Meroney (1980) found that the lift off will not occur immediately upon attaining positive buoyancy unless a lift off parameter $L_p = g'H/u_*^2$, is sufficiently large. For large spills of LNG under most wind conditions, it is not likely that significant lift off will occur before the lower flammability limit, LFL, is attained.

For small field spills or laboratory scale spills, surface heating effects will be exaggerated. When a large temperature

difference or a large depth spill exists it is hypothesized that heat transfer will go as $h_s L^3/U$, where L is the characteristic length scale of the plume, U is the characteristic velocity scale, and h_s is the convective heat transfer coefficient. The thermal capacity of a gas cloud will vary as $\rho_g Cp_g L^3$. The ratio of surface heat transport to thermal capacity will be a Stanton number, $h_s/(\rho_g Cp_g U)$. Since wind speed is normally scaled by a Froude number, $U^2/(g'L)$, smaller model scale plumes will see a temperature increase (or density decrease) which does not scale to the field equivalent. Cold model plumes will therefore entrain air faster and lift off before the comparable field situation.

Measurements on cold model plumes made by Andriev et al. (1983) verify the scenario projected in the previous paragraph. Although it is not possible to directly compare cold laboratory plumes with field scale plumes, it is possible to use the model measurements to validate heat transfer modules in numerical models. Box and slab models calibrated in this manner have been compared successfully to cryogenic spills at Maplin Sands and China Lake (Meroney, 1984 and 1985).

Colenbrander and Puttock (1984) described simulation of the cold propane spills at Maplin Sands in a wind tunnel using isothermal simulants. As long as Flux Froude number equality was maintained and the Peclet/Richardson number was sufficiently large, the isothermal model reproduced field concentration isopleths. Neff and Meroney (1981) and Meroney (1985) simulated the Burro Series 40 m^3 LNG spills with isothermal dense gases in the wind tunnel. Model concentrations, plume widths, and plume trajectories were closely predicted by the laboratory model. The model did not reproduce the lifting of the maximum concentration from the ground as observed during the Burro

4.2.5 Consequences of natural plume variability

Atmospheric motions cover a range of scales from small dissipative eddies on the order of 1 mm to the large synoptic weather features of the order of 10^6 m. Although there is some evidence of reduction in wind energy in the frequency range (gap) between 10 min and one hour as exhibited by van der Hoven (1957), there is seldom a complete absence of energy in this mesoscale range. But physical modeling and all available numerical models implicitly assume that transport by the mean wind can be clearly separated from diffusion by turbulence. The unresolved turbulent motions in the gap region can induce significant differences between field measurements of mean concentrations under seemingly identical weather conditions. In addition even properly modeled turbulence in a fluid facility can induce large concentration variations about the time-mean values (Fackrell and Robins, 1982a, 1982b; Meroney and Lohmeyer, 1984).

Consider afternoon conditions with light winds and relatively strong convection. Lewellen and Sykes (1985) conclude that a 10 m diameter plume released under such conditions will have significant regions where the concentration fluctuation intensity, σ_c/C, exceeds three. As shown in Figure 4-25, an instantaneous sample of the concentration in most of the plume region would have less than a 50% chance of being within an order of magnitude of its mean value. The sampling time must be greater than 20 times the turbulent time scale (to get $\sigma_c/C \simeq 1$) before there is a 50% probability of an instantaneous measurement in these same regions being within a factor of 2 of the mean concentration predicted by a perfect fluid model.

Fluid and numerical models are driven by input conditions which are themselves ensemble means; thus, it is not surprising that single realization field experiments may vary significantly from the mean values of model results. Fortunately measurements of concentration fluctuation standard deviations or ensemble measurements of multiple replications in the laboratory provide a means to evaluate such variability. Instantaneous concentration measurements in correctly scaled fluid model experiments may be expected to reproduce fluid variability caused by mechanically generated turbulence; however, dispersion and meandering caused by larger scale turbulence will not be modeled in either fluid models or in any current numerical models.

4.3 Concentration Scaling Theory

The local molar concentrations, measured in the model and the prototype will be directly proportional to the actual number of moles released at the source. Most plume studies measure the concentration magnitudes at distances far downwind from the source; hence, Snyder (pp. 148-150, 1981) encourages analysts to evaluate source volume flux rates at ambient (not stack) temperatures. Thus the conventional dimensionless concentration coefficient, K, may be expressed as:

(4-13)

$$K = \chi\ U\ L^2/Q_a = \chi\ U\ L^2/[(T_a/T_s)Q_s],$$

where T_a and T_s are the temperatures of the ambient air and the source gas respectively. Q_a and Q_s in this expression are the total source gas flow rate evaluated at ambient or source gas conditions, respectively. At long distances, the effects of Volume Flux Ratio distortion and source gas temperatures differences between a model and

prototype are corrected by this expression. This technique is completely satisfactory in the limit as concentration approaches zero, but in the case of modeling plume concentrations at modest dilution, such as is the case with flammable plumes, this relationship is not satisfactory. Neff and Meroney (1982) have recommended the alternative dimensionless concentration coefficient:

(4-14)

$$K = [T_s/T_a][\chi/(1 - \chi)][U L^2/ Q_s],$$

which relates the concentration distributions in plumes that are physically similar over their entire dilution range.

Alternatively, consider the definition of a mole fraction, $\chi = n_s/(n_s+n_a)$, where the n_s and n_a are (local) mole per unit volume of tracer gas and ambient air. The local molar concentration of source gas will be directly related to the molar flux from the source, ie.

(4-15)

$$n_s \simeq [(p\ A\ W)\ t]/(R\ T_s),$$

where p is pressure, A is source area, W is source exit velocity, R is the universal gas constant, T_s is the source temperature, and t is a characteristic time of release. Now Q = A W will be the source volume flow rate, and the characteristic time of release will be proportional to L/U. The relationship between the molar concentration measured in a model and in a prototype situation is then,

(4-16)

$$(n_s)_p = (n_s)_m\ [Q_p/Q_m][T_{sm}/T_{sp}][U_m/U_p][L_p/L_m],$$

and $(n_a)_p = (n_a)_m [T_{am}/T_{ap}][L_p/L_m]^3$.

Substitution of these expressions into the defining relation for mole fraction produces,

$$\chi^*_p = [\chi_m]/[\chi_m + (1 - \chi_m)[\dot{V}^\circ T_a/T_s]_m/[\dot{V}^\circ T_a/T_s]_p, \quad (4\text{-}17)$$

where $V = [Q/(U L^2)]$ is the Volume Flux Ratio. Thus, whenever the Volume Flux Ratio is not simulated, or there are different source temperatures used in the model and prototype, the model concentrations must be corrected to field values. Of course this relation presumes that plume kinematics and dynamics are correctly simulated in all other respects. Note that if $\dot{V}^\circ_m = \dot{V}^\circ_p$ and $(T_a/T_s)_m = (T_a/T_s)_p$, then $\chi^*_p = \chi_m$.

4.4 Summary and Recommendations

Similarity criteria for modeling dense gas plumes have been described in Section 4.1 and their constraints on plume modeling discussed in Sections 4.2 and 4.3. Rigorous similarity would require that the ten nondimensional parameters identified be matched in both model and prototype. In Sections 4.2.1 through 4.2.4 arguments for partial simulation were presented. The following constraints were identified:

a.) Exact simulation of ambient temperature high-molecular weight plume dispersion from ground or elevated sources requires matching (equal in model and prototype) the specific gravity ratio, SG, the Volume Flux Ratio, V, and a Froude Number, Fr_a. All other Froude Number and flux ratios are also held equivalent if this set is specified. In addition the source Reynolds numbers, Re_{Ds} and Re_{Da} should both preferably exceed 15,000, the gravity head Reynolds

number should exceed 1000, and the Peclet/Richardson number ratio, Pe_*/Ri_*, should exceed 0.5.

b.) In the event it is necessary to operate at low velocities, the source Reynolds number should exceed 2300 or, if one uses a trip to ensure a fully turbulent exhaust, one may operate as low as 300. The gravity head Reynolds number should not fall below 500, and the Peclet/Richardson number ratio should not fall below 0.15.

c.) In circumstances where exact scaling of the specific gravity ratio and Froude numbers result in model conditions where Reynolds number or Peclet/Richardson number ratio criteria are violated, it is appropriate to consider partial simulation through relaxation of the source density ratio equality or velocity scale distortion. If possible, the atmospheric shear layer scales should not differ from the dense plume scales by more than 1.5. There is some evidence the situation is forgiving up to scales mismatches of a factor of 10; there is no evidence greater distortions are permitted.

If it is felt necessary to utilize specific gravity distortion for an elevated finite-momentum source, it is preferable to insure:

i.) A fully turbulent effluent flow, and to match

ii.) Momentum Flux Ratio, M, and Flux Froude Number, Fr_f, (or the ratios of momentum and buoyancy length scales to the stack height), and arrange for Peclet/Richardson number to exceed 0.5.

In order of decreasing "correctness", if it is felt necessary to utilize specific gravity distortion for ground-level low-momentum sources, it is preferable to match:

i.) Densimetric Froude number, Fr_a, and Volume Flux Ratio, $\mathring{V}$, but arrange for Peclet/Richardson number to exceed 0.15, or

ii.) Flux Froude number, Fr_f, but arrange for Peclet/Richardson number to exceed 0.5, and Volume Flux Ratio, $\mathring{V}$, must not be distorted by more than a factor of 1.5, or

iii.) Flux Froude number, Fr_f, but arrange for Peclet/Richardson number to exceed 0.15.

d.) Exact simulation of cold gas clouds resulting from boil-off from cryogenic spills is not possible because of the unavoidable mismatch between prototype and model heat transfer rate similarity parameters.

e.) Errors caused by not adjusting for specific heat capacity effects when using an isothermal model gas to simulate cold prototype plumes are small. Thus an isothermal simulation of adiabatic mixing of an LNG vapor cloud as it entrains dry air is not exact, but it is a very good approximation to actual behavior ($\pm$5%).

f.) A cold gas model experiment will actually overpredict plume dilution due to exaggerated destruction of negative buoyancy caused by distortion of the thermal phenomena at small model scales. Model experiments with isothermal dense gases will conservatively predict mean concentration distributions for cold dense gas spills.

g.) The release of latent heat through the entrainment of humid air into a cold plume will diminish plume density. An isothermal model plume can not replicate the density variations produced by latent release. A cold gas model plume will reflect the influence of latent heat release, but it is not likely to be similar to a prototype plume because of surface heat transfer distortions discussed earlier. An isothermal model gas will normally provide a conservative estimate of cold plume size and concentration magnitudes.

h.) Many unresolved problems concerning the modeling of isothermal dense plume dispersion still exist. Basic, systematic studies should be supported, to examine dense plume behavior under the marginal conditions of low Reynolds number and low Peclet/Richardson number ratio.

i.) The exact entrainment roles played by the joint effects of a gravity head, the ambient turbulence, and the stratified shear layer over the top of the plume are not yet well defined. A limited number of laboratory studies have examined each of these mechanisms acting independently, but no data are available which examines their nonlinear interactions when combined in a dynamic dense gas cloud. Basic entrainment studies should be prepared to address this issue.

j.) Terrain slope is a critical factor in determining speed. Slopes of 1^{o} can dominate plume trajectories. Models must be accurately built. General "generic" tests will not be as useful for dense gases as they are for passive plumes. Many results will be highly site specific.

TABLE 4-1. TECHNIQUES USED FOR SIMULATION OF BUOYANT PLUMES AT VARIOUS FLUID MODELING FACILITIES

SCALING PARAMETER	"EXACT" SIMULATION	APPROXIMATE SIMULATIONS								
		UWO[1] (DMA)[11]	CSU[2]/MIT[3] (DVA)	CALSPAN[4] (BMA)	MONASH[5]	BRISTOL[6]	CERL[7] (BMS)	CERL[8] (DMS)	CERL[9] (DVS)	CERL[10] (BMD)
Density ratio $\Delta\rho/\rho_a$	yes	no	no	no	no	no	no	no	no	yes
Fr_a $W_s/(gD\Delta\rho/\rho_a)^{1/2}$	yes	no	yes	no	no	no	no	no	no	no
Fr_a^U $U/(gD\Delta\rho/\rho_a)^{1/2}$	yes	yes	yes	no	yes	yes	no	no	no	yes
Fr_s $W_s/(gD\Delta\rho/\rho_s)^{1/2}$	yes	yes	no	no	yes	yes	no	no	yes	no
Fr_s^U $U/(gD\Delta\rho/\rho_s)^{1/2}$	yes	no	no	no	no	no	no	yes	yes	yes
Velocity ratio W_s/U	yes	no	yes	no	no	no	no	no	yes	no
Momentum ratio for distorted stack $\rho_s D^2 W_s^2/(\rho_a H_s^2 U^2)$	yes	yes	no	yes	no	no	yes	yes	no	yes
Mass flow rate $\rho_s D^2 W_s/(\rho_a H_s^2 U)$	yes	no	no	no	yes	no	no	no	no	no
Volumetric flow rate $D^2 W_s/(H_s^2 U)$	yes	no	yes	no	no	yes	no	no	yes	no
Buoyancy length $\ell_B/H_s=gD\Delta\rho W_s D/(4U^3\rho_a H_s)$	yes	no	yes	yes	no	no	no	no	no	yes
Buoyancy length $\ell_B^s/H_s=gD\Delta\rho W_s D/(4U^3\rho_s H_s)$	yes	no	no	no	no	no	yes	no	yes	yes
Momentum length $\ell_m/H_s=\rho_s W_s^2 D/(4\rho_a U^2 H_s)$	yes	yes	no	yes	no	no	yes	yes	no	no
Geometric scale D/H_s	yes	yes	yes	yes	no	no	yes	yes	yes	no
Proven	x		x	xxx				x		
Disproven		xx	xx	x	x		x		x	x

1. University of Western Ontario, Isyumov et al., 1976. 2. Colorado State University, Cermak, 1971, 1975. 3. Massachusetts Institute of Technology, Hoult et al., 1977. 4. Calspan Corp., Skinner and Ludwig, 1978. 5. Monash University, Melbourne, 1968 (interpreted from Isyumov and Tanaka, 1980). 6. Bristol University, Barrett, 1973 (interpreted from Isyumov and Tanaka, 1980). 7-10. Central Electricity Research Laboratory, Robins, 1980. 11. Three-letter codes in parentheses are notations of Robins, 1980 (Snyder, 1981).

Table 4-2

MAPLIN SANDS TRIALS
Shell Research, Amsterdam 30 Nov 84

TRIAL NO.	GAS TYPE	SCALE	SPECIFIC GRAVITY	VELOCITY m/sec	LFL m	Pe/Ri
ACTUAL						
Maplin-46	LPG	1:1	1.9	8.1	210-280	-
W.TUNNEL						
MS46-1	Fr-Ar	1:110	1.9	0.77	230-290	2910
MS46-21	Fr	1:110	4.2	1.47	250-280	12120
MS46-22	Fr-AR	1:120	1.9	0.55	140-190	1340
ACTUAL						
Maplin-54	LPG	1:1	1.85	3.8	380-520	-
W.TUNNEL						
MS54-1	Fr-Ar	1:100	1.85	0.38	250-290	357
MS54-2	Fr	1:100	4.2	0.75	450-520	1560

$Pe/Ri = U^2 / (g'D)$

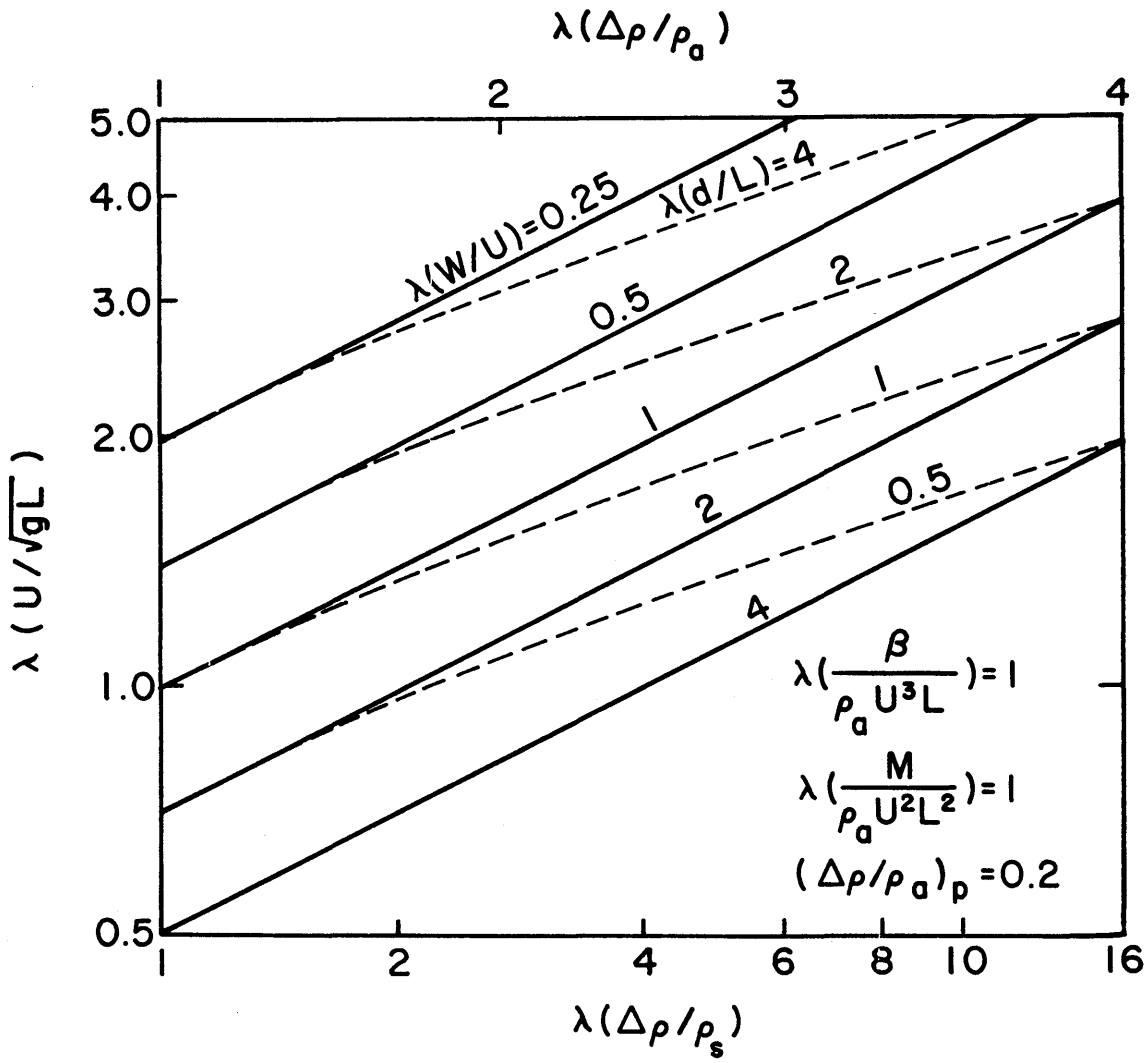

Figure 4-1. Distortion of density, diameter and velocity scales permitted when similarity of dimensionless buoyancy flux and momentum flux are considered sufficient to assure similarity for case $(\Delta\rho/\rho_a)_p = 0.2$. $\lambda(x) = x_m/x_p$. (Poreh, 1981).

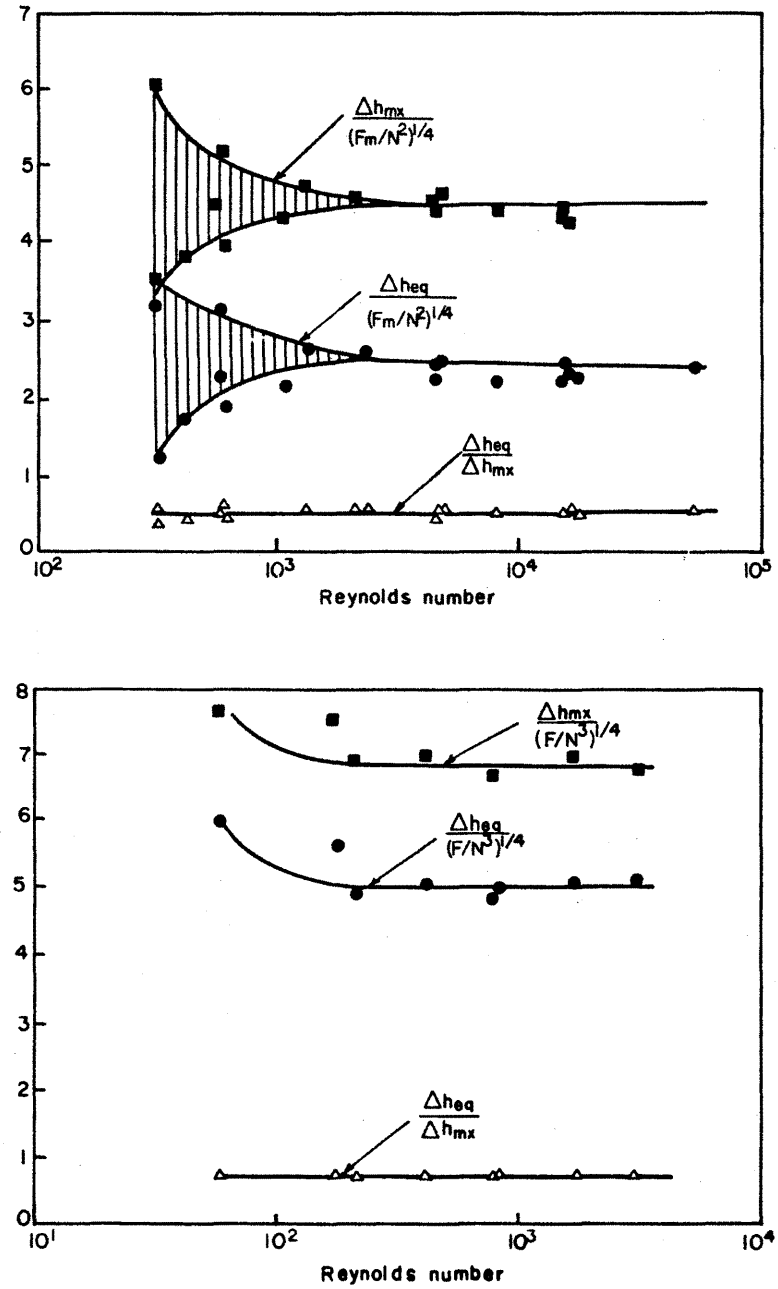

Figure 4-2. Variation of plum rise with Reynolds number (Δh_{mx} = maximum height reached by plume, Δh_{eq} = equilibrium plume hieght, F_m = source momentum flux, F = source buoyancy flux, N = Brunt-Vaisala frequency (Briggs and Snyder, 1980).

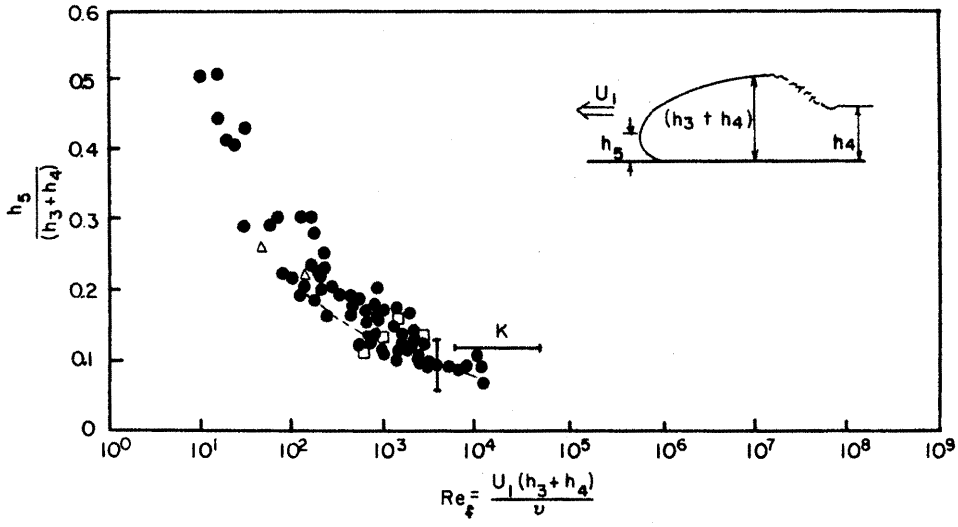

Figure 4-3. The variation of nose height, h_5, of a gravity current head with Reynolds number. The dashed line is from Simpson (1972), , Δ, and K are from works of Braucher (1950), Wood (1965), and Keulegan (1958). o is an atmospheric result from Lawson (1971). After Simpson and Britter, 1979.

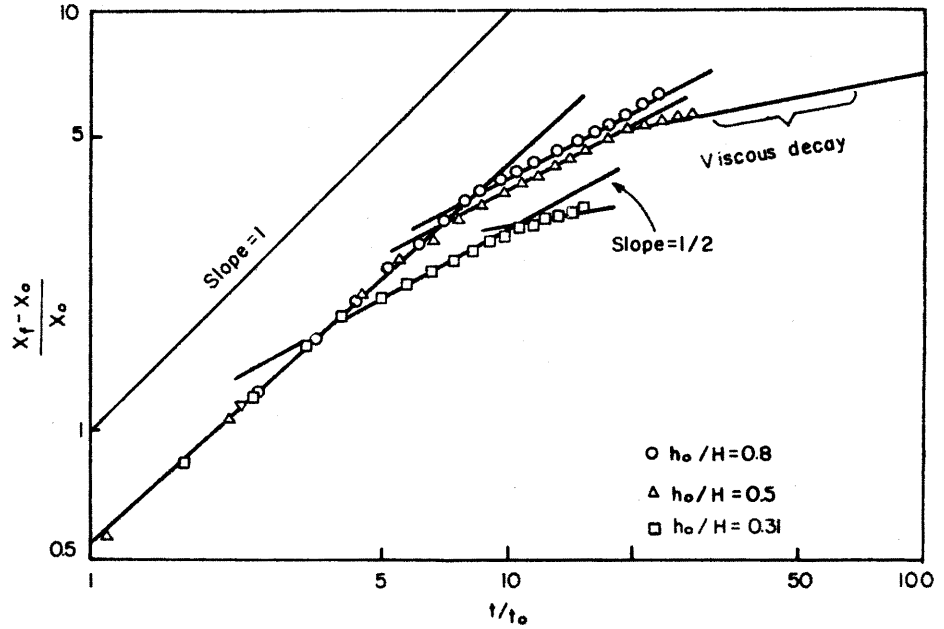

Figure 4-4. Frontal position, X_f, versus time, t/t_o, after release for axisymmetric gravity currents. Characteristic time $t_o = X_o/(g' h_o)^{\frac{1}{2}}$, where X_o is the initial length of the current. (Rottman, 1984).

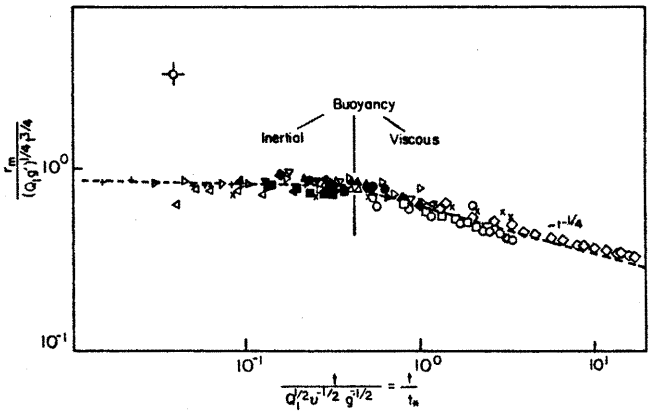

g' ms^{-2}	Q x 10^3 m^3s^{-1}	g' ms^{-2}	Q x 10^3 m^3s^{-1}	g' ms^{-2}	Q x 10^3 m^3s^{-1}	g' ms^{-2}	Q x 10^3 m^3s^{-1}
▲ 0.008	0.84	+ 0.353	0.63	◀ 0.781	1.70	▼ 0.971	1.56
■ 0.108	1.44	◁ 0.412	3.01	◆ 0.814	0.92	△ 1.069	1.56
● 0.128	0.63	▷ 0.441	2.62	▽ 0.844	0.79	□ 1.158	0.46
× 0.314	0.86	◇ 0.461	0.03	▶ 0.892	1.54	○ 1.236	0.45

Figure 4-5. The position of the leading edge of a dense plume, normalized with its expected temporal variation (Britter, 1979).

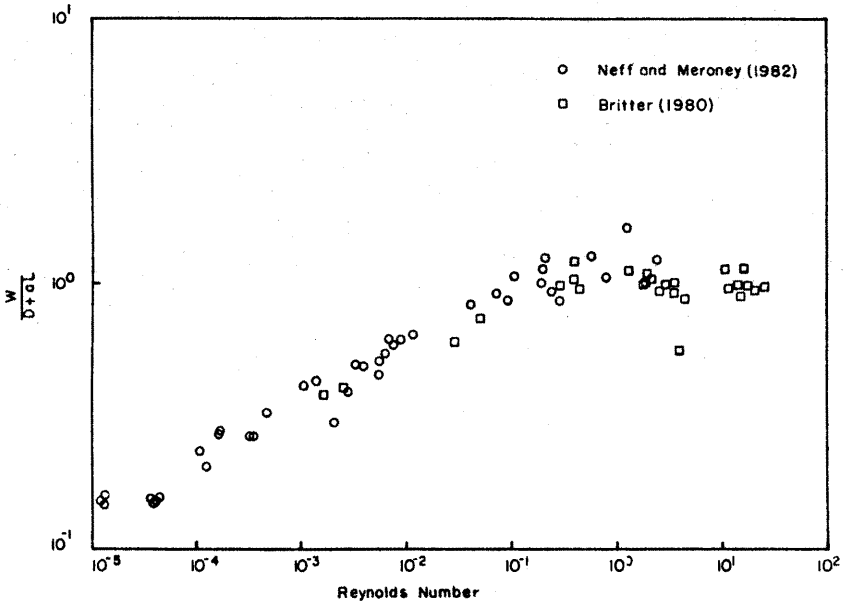

Figure 4-6. Dimensionless plume width versus Reynolds number (Fay and Zemba, 1985).

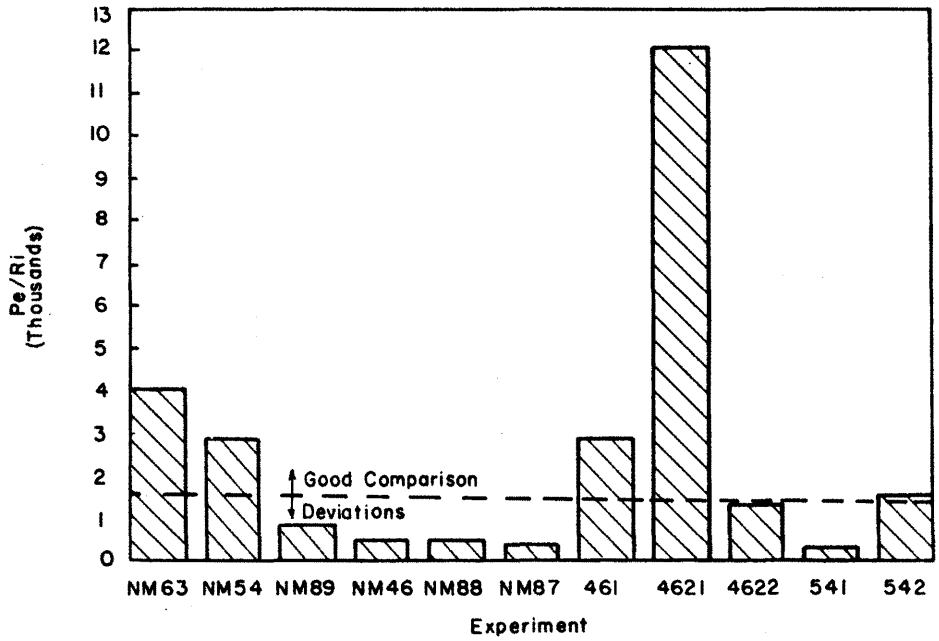

Figure 4-7. Peclet/Richardson parameter for Shell Maplin and Colorado State University model trials (Meroney, 1984).

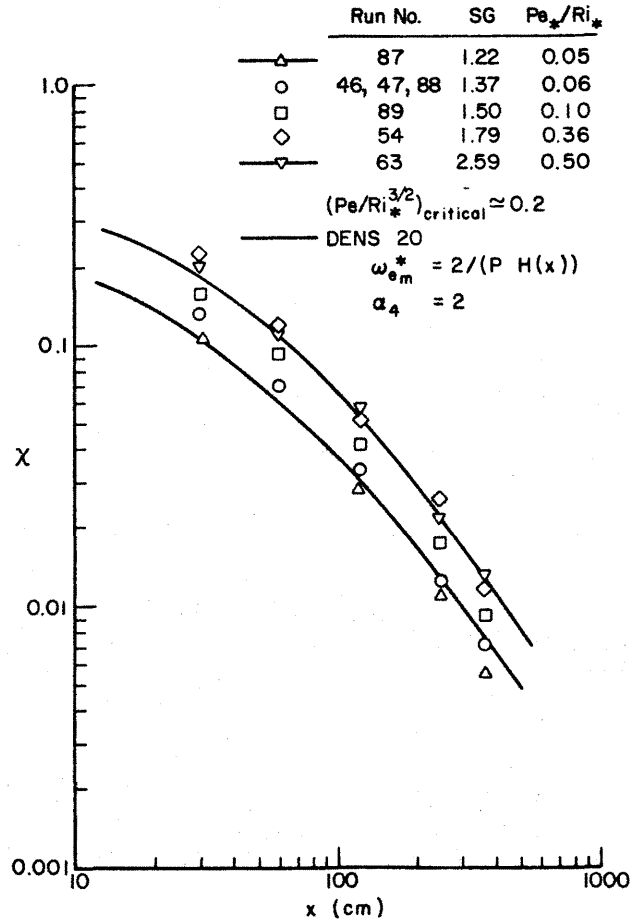

Figure 4-8. Microscopic diffusion effects during Model dense gas spills (Meroney, 1984).

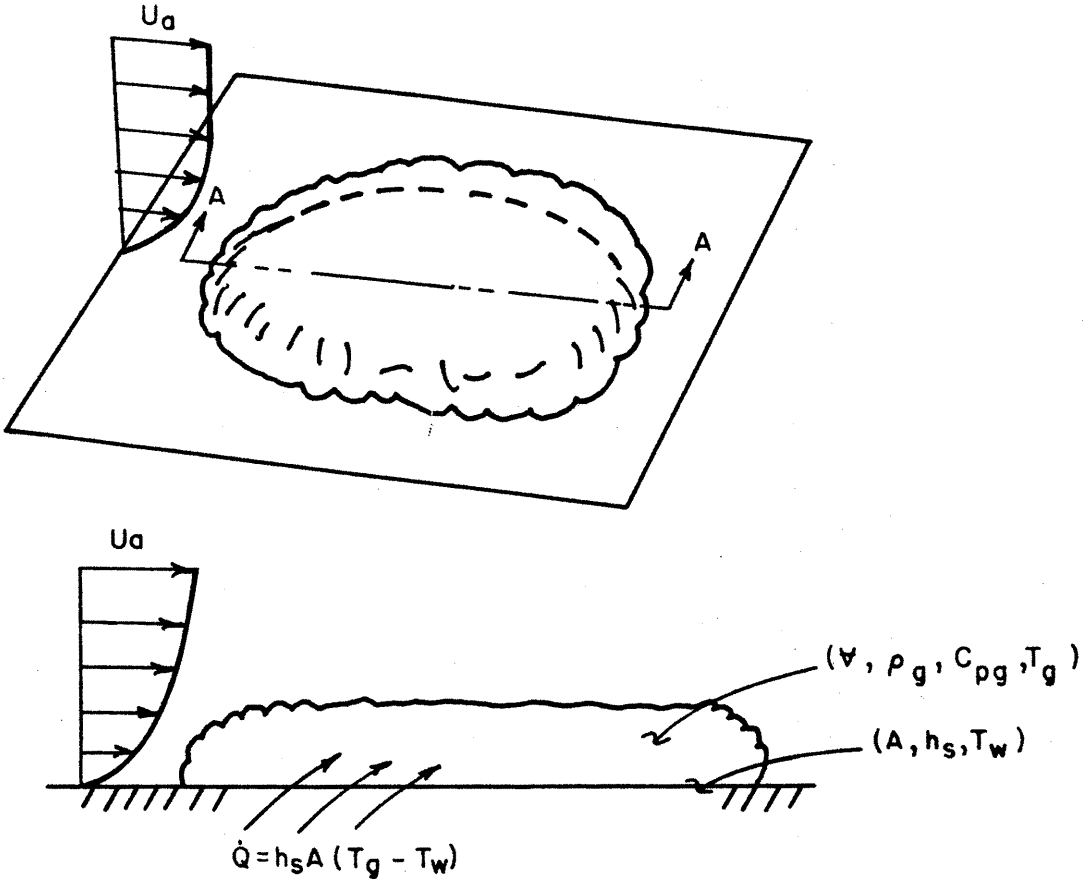

Figure 4-9. Schematic of well-mixed cold gas cloud advecting over hot surface.

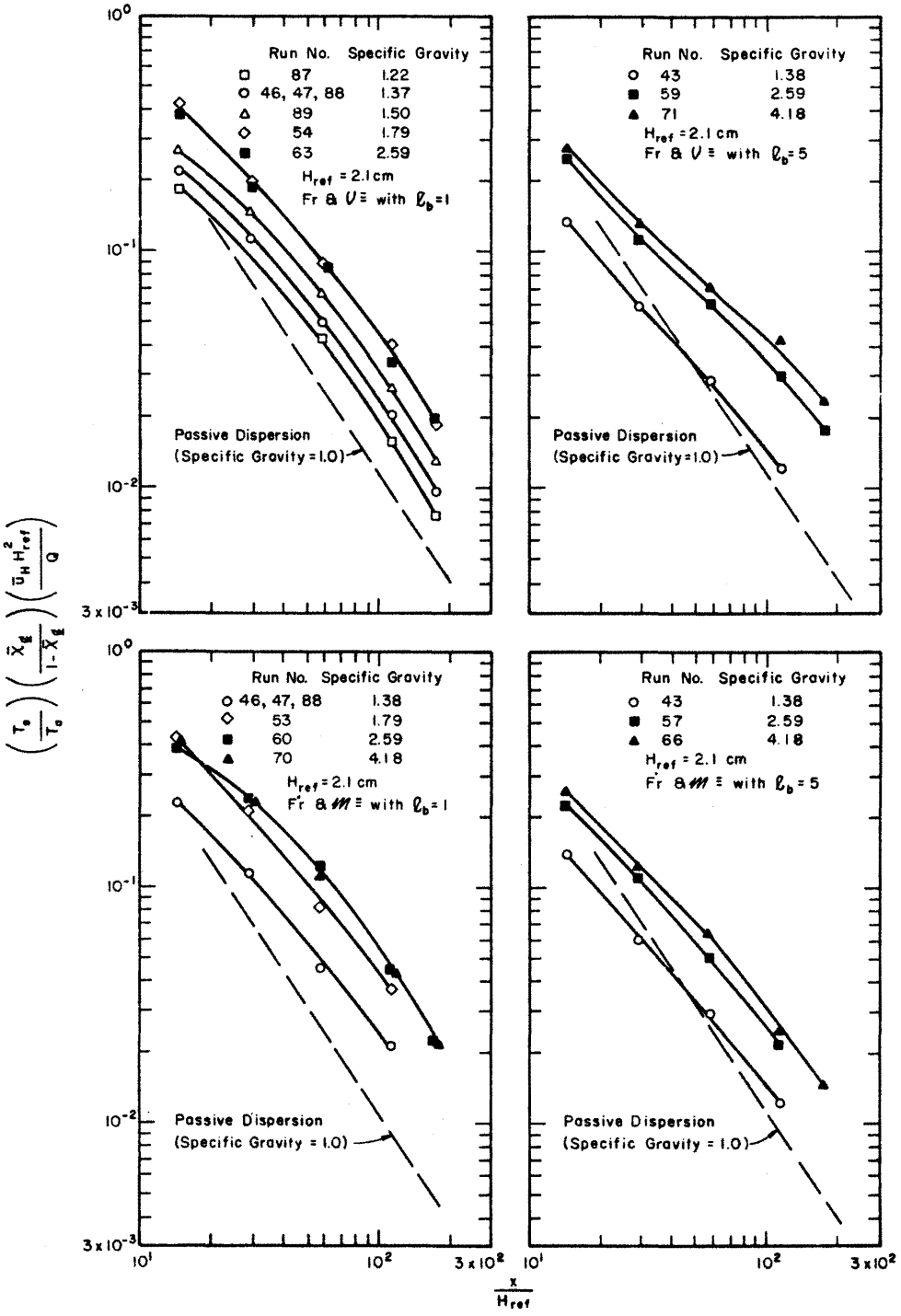

Figure 4-10. Normalized centerline concentration decay with downwind distance for source-specific gravity relaxation tests (Neff and Meroney, 1982).

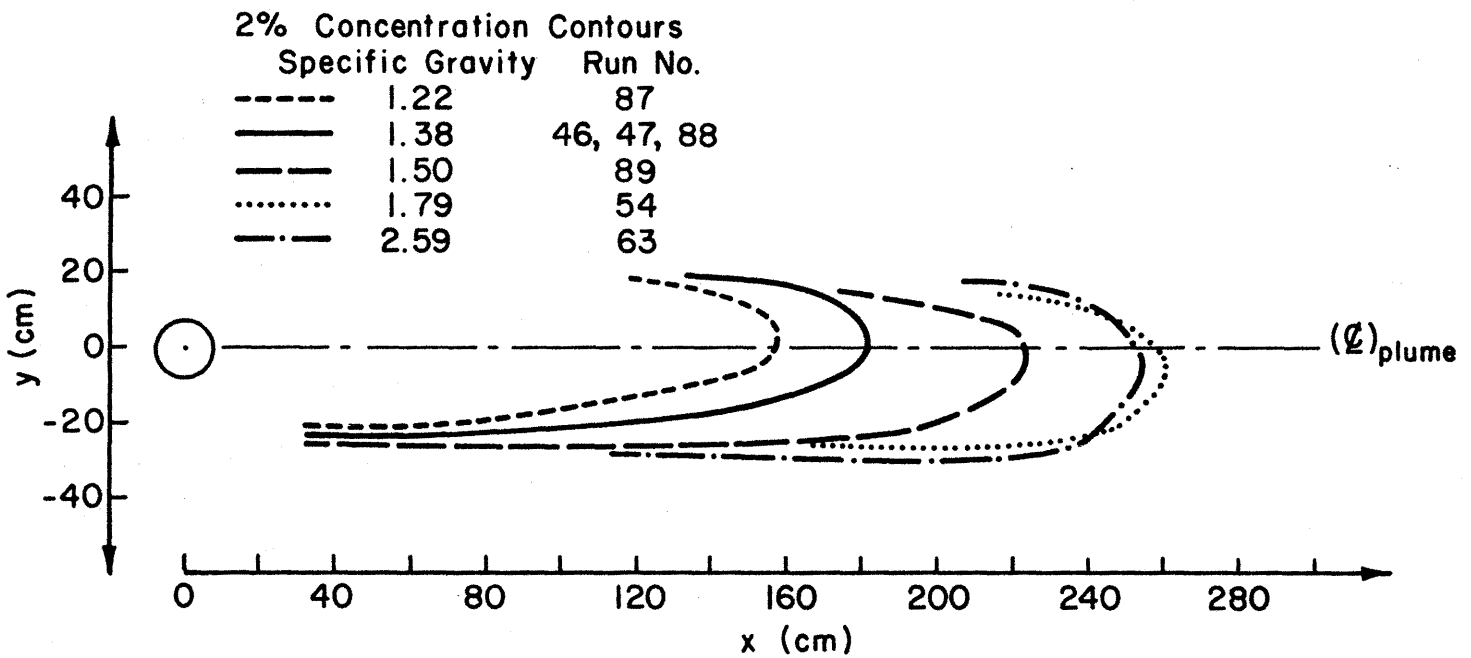

Figure 4-11 Ground-level two percent concentration contours for source-specific gravity relaxation tests (Neff and Meroney, 1982).

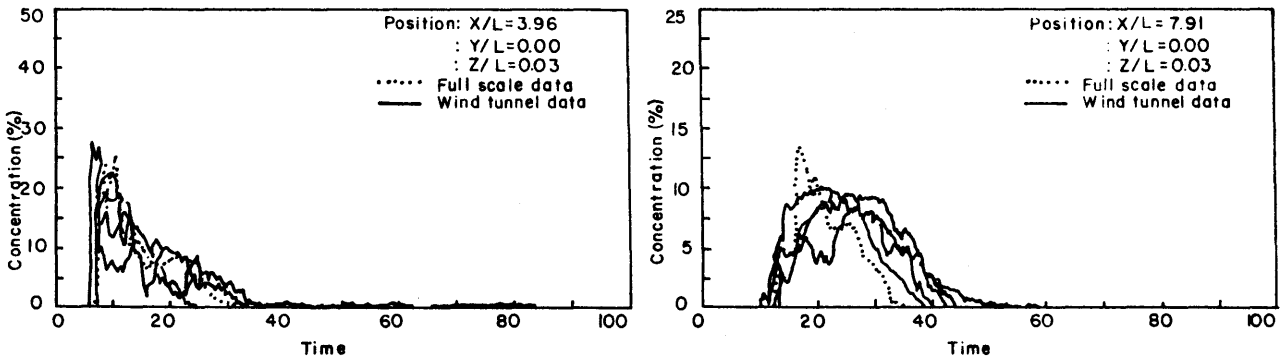

Figure 4-12. Comparison of continuous monitor measurements with model results for Thorney Island trial no. 15, at two subsequent downwind positions (Schatzmann et al., 1985), SG_p = 1.5, SG_m = 1.5.

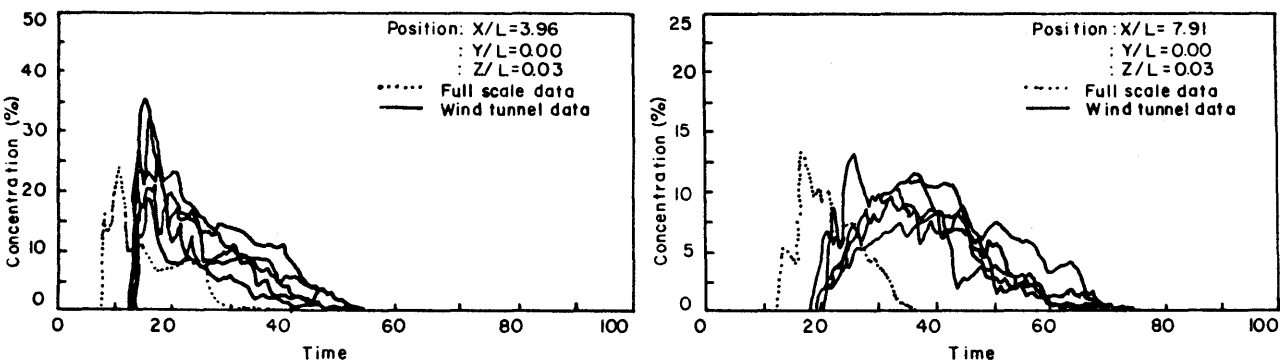

Figure 4-13. Comparison of continuous monitor measurements with model results for Thorney Island trial no. 15, at two subsequent downwind positions (Schatzmann et al., 1985), SG_p = 1.5, SG_m = 4.2.

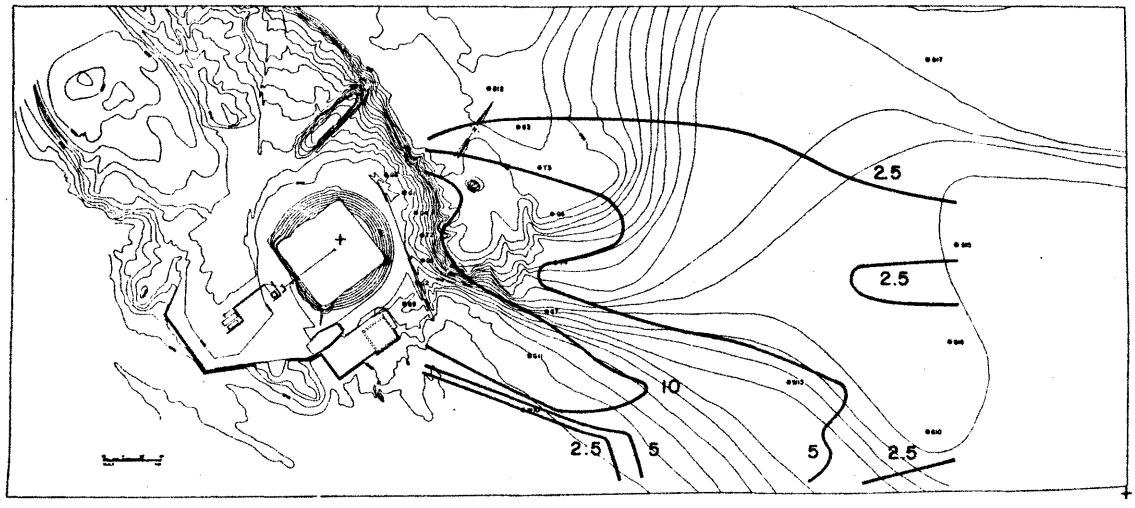

Figure 4-14. Average peak concentrations detected during Burro 8 model spill tests, using distorted density ratio scaling (Meroney, 1985).

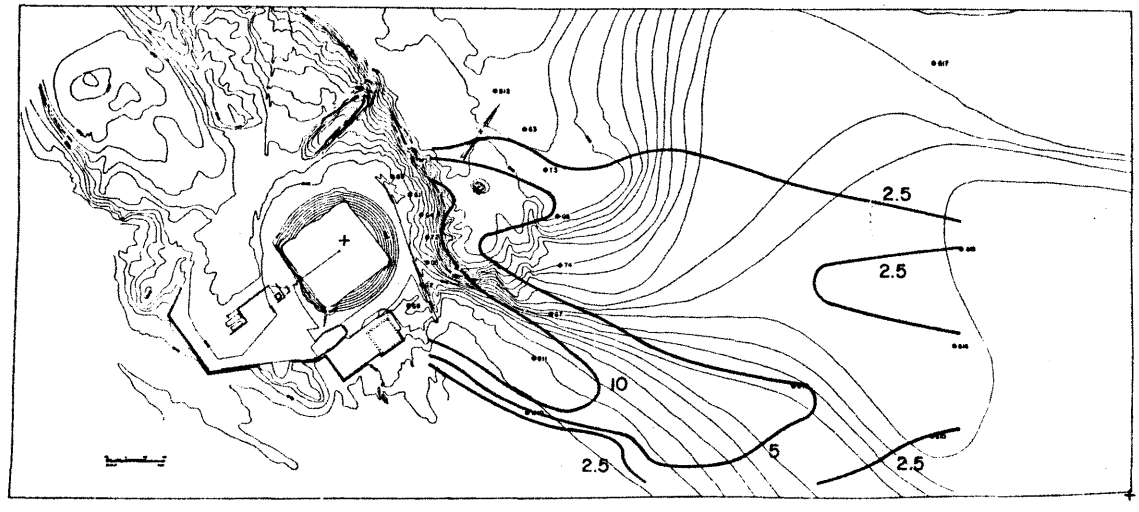

Figure 4-15. Maximum peak concentrations detected during Burro 8 model spill tests, using distorted density ratio scaling (Meroney, 1985).

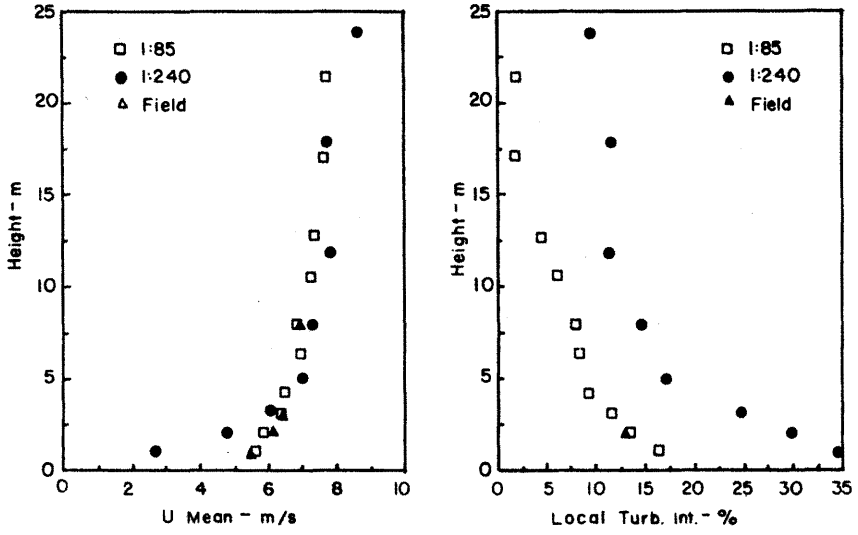

Figure 4-16. Velocity profile comparisons for different modeling scales, Burro test no. 9 (Neff and Meroney, 1981).

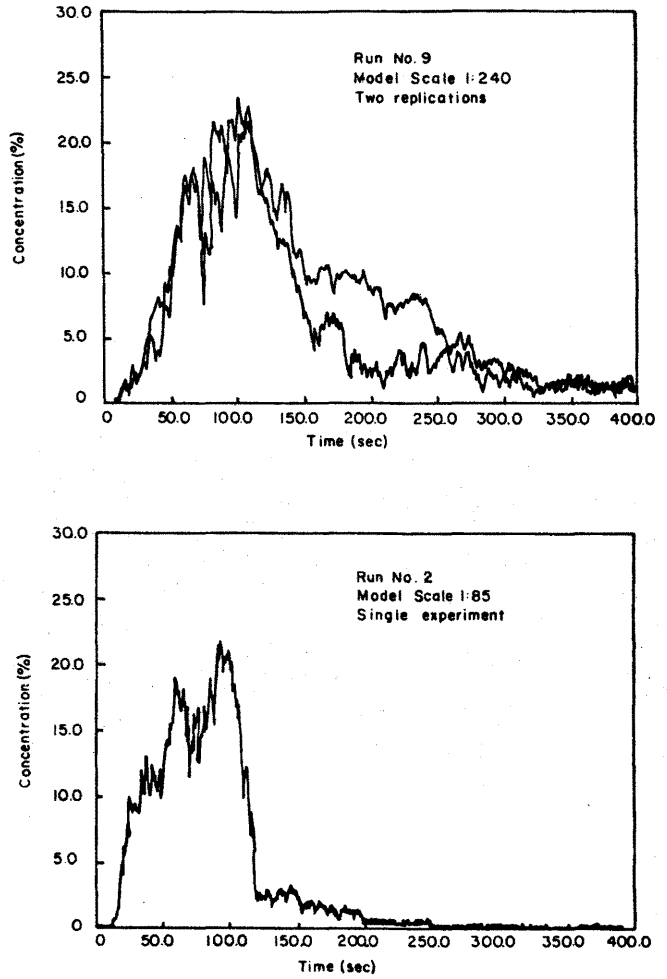

Figure 4-17. Concentration time history comparisons for different modeling scales, Burro test no. 9 (Neff and Meroney, 1981).

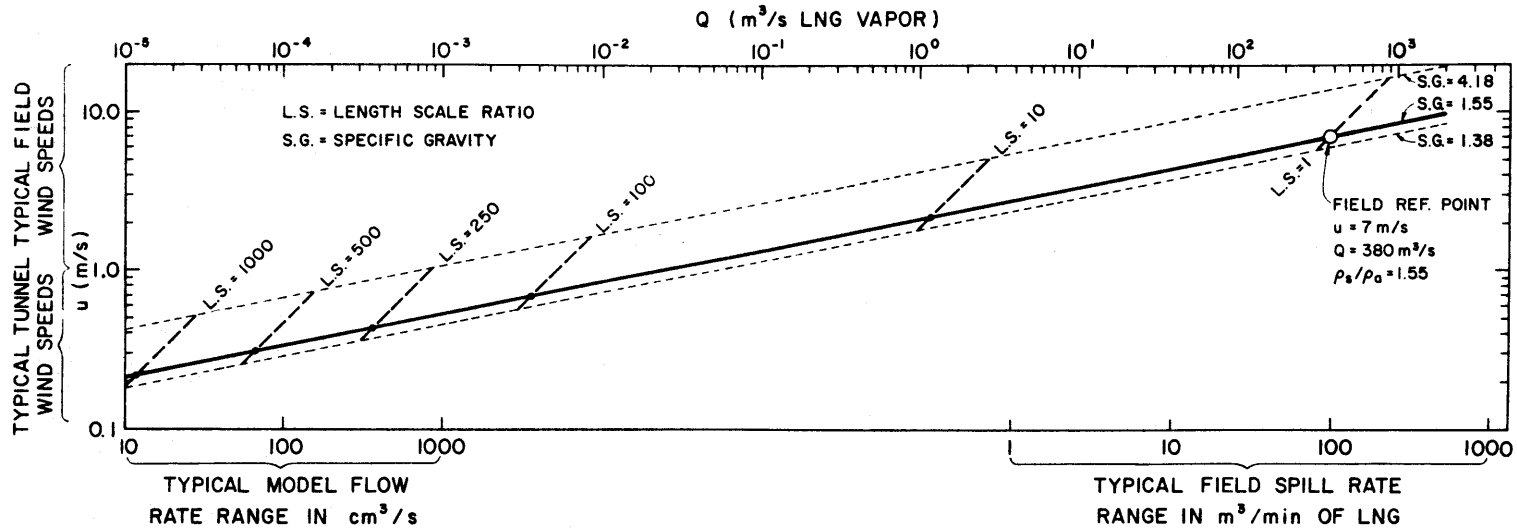

Figure 4-18. Field to model conversion diagram for densimetric Froude number and volume flux ratio equality (Neff and Meroney, 1982).

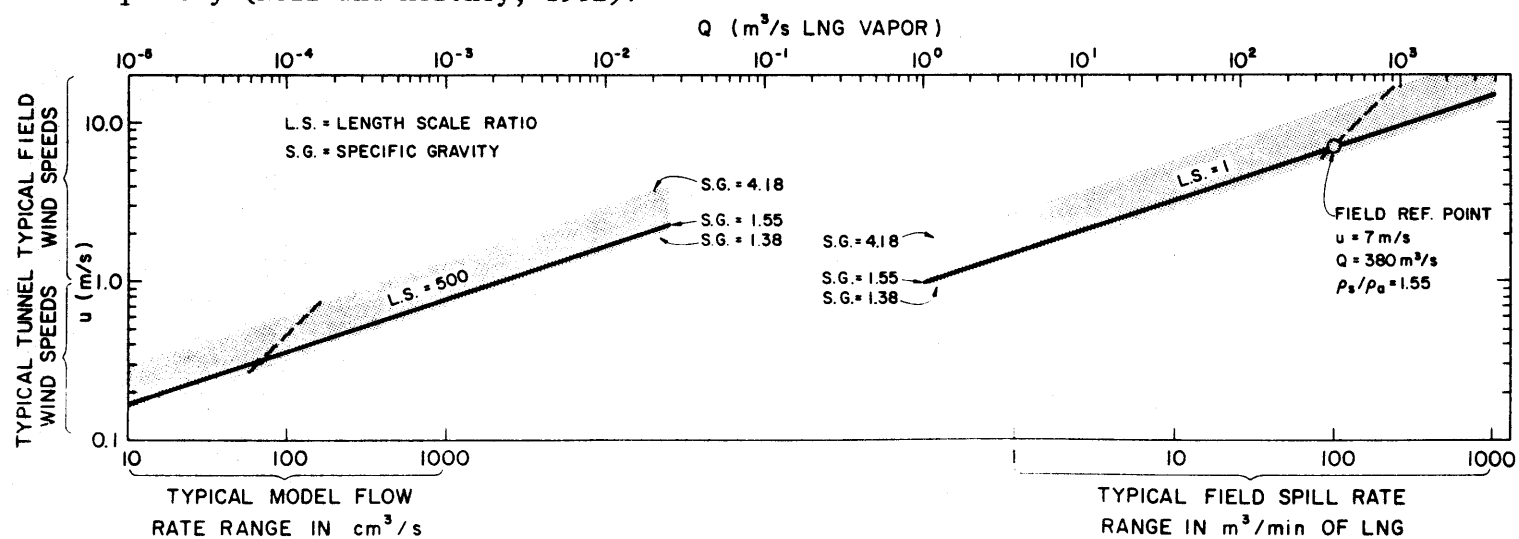

Figure 4-19. Field to model conversion diagram for flux Froude number equality (Neff and Meroney, 1982).

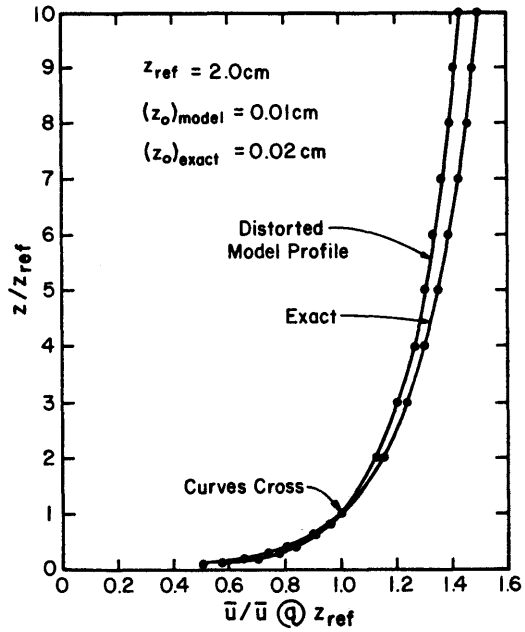

Figure 4-20. Mean wind shear variation, for a two-fold model length scale distortion (Neff and Meroney, 1982).

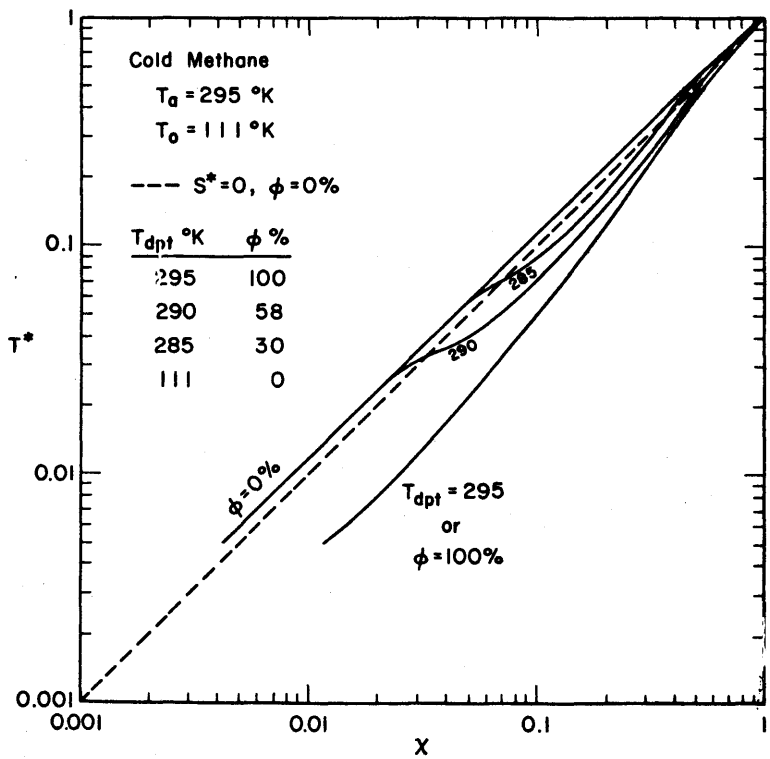

Figure 4-21. Dimensionless temperature versus concentration, adiabatic entrainment of humid air into a cold methand plume (Andriev et al., 1983).

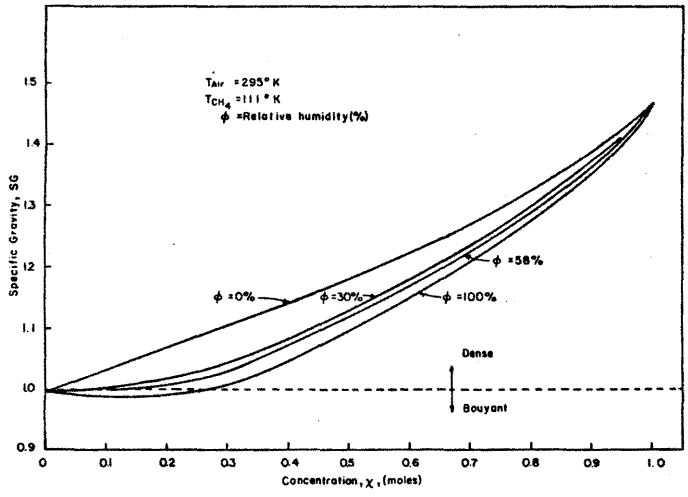

Figure 4-22. Specific gravity versus concentration, adiabatic entrainment of humid air into a cold methane plume.

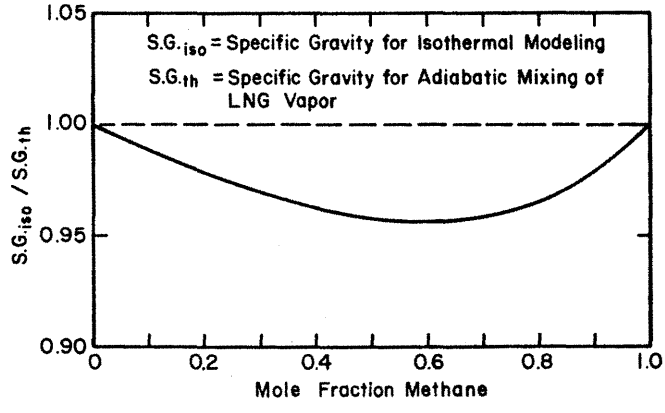

Figure 4-23. Specific gravity deviation, in an isothermal model of LNG vapor dispersion (Neff and Meroney, 1982).

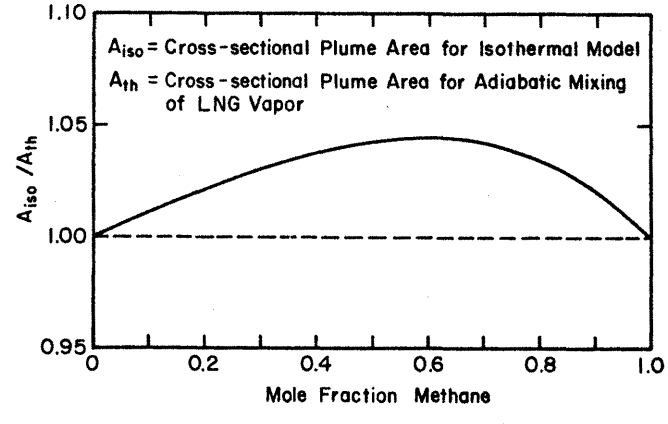

Figure 4-24. Plume cross-section area deviation, in an isothermal model of LNG vapor dispersion (Neff and Meroney, 1982).

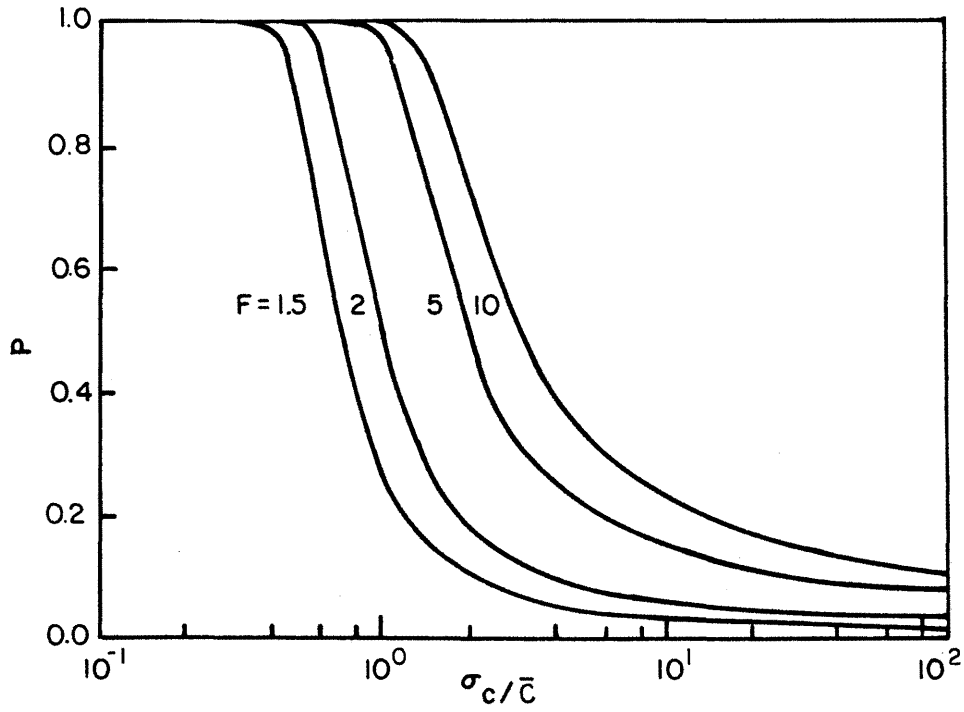

(a)

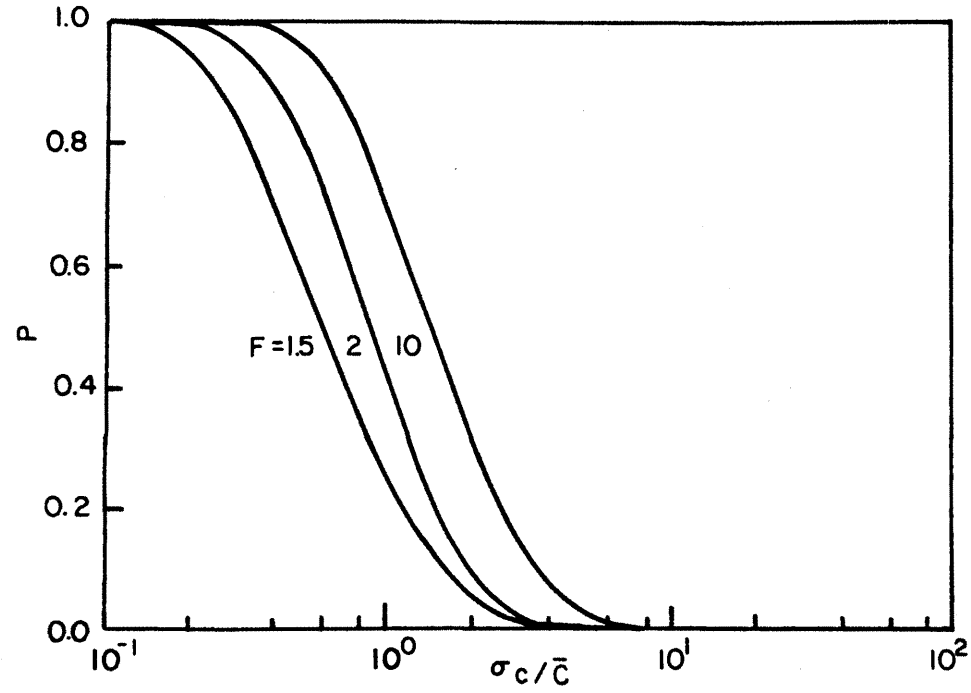

(b)

Figure 4-25. Probability P of finding a concentration sample within a factor F of its true mean value, as a function of e_c/C for (a) a lognormal probability distribution function and for (b) a clipped normal probability distribution function (Lewellen and Sykes, 1985).

5.0 VALIDATION OF PHYSICAL MODEL APPROACH

A single field event has a large number of uncontrolled or poorly specified variables, which have effects on the resultant concentration field that are not completely accounted for by either a physical or numerical modeling. The source conditions of an LNG spill situation must be approximated because it is difficult to predict or measure the time-dependent source size and boiloff characteristics accurately in the field. The wind field into which an LNG plume is released is typically nonstationary. The plume may experience a wind field that is undergoing a change of mean wind speed, mean wind direction, and turbulent characteristics with time. These nonstationary factors are not modeled in the wind tunnel and water channel simulations. The wind characteristics are assumed to be constant, ie., statistically stationary. These assumptions may lead to differences between the resultant concentration fields depending on the severity of the nonstationarities during the field tests.

As noted in Section 2.3 validation of a physical or numerical model is only possible within the natural limits to predictability permitted by the turbulent nature of the flow fields. Section 4.2.5 suggests that even if it were possible to introduce two separate field plumes into the same resolved wind field, there would be some variance in the dynamics of the two plumes due to the unresolved turbulence. This means that an effort to discriminate between models based on one data set is likely to be unjustified. The best safeguard against making large modeling errors will be an evaluation methodology which combines requirements that (a) the physical model approach be scientifically sound, and that (b) the modeling approach be tested

against a variety of observed data.

A top priority during evaluation is to determine how accurate physical modeling may be under realistic conditions. One desires to reasonably represent the spatial and temporal distribution of the plume concentration. For LNG hazard evaluation, the spatial distribution of plume concentrations appears to be more critical than the temporal distribution. A pattern comparability test is described in Section 5.1 that provides a quantitative measurement of how well the modeled spatial distribution of ground-level concentration agrees with real field observations. When possible this method is applied to the data in Section 5.2.

5.1 Surface Pattern Comparability Approach

Most model performance measures compare predicted versus observed values directly. Precise pairing in time and space imposes too strong a penalty on small misalignments, while pairing in time alone provides no information on spatial variability. Lewellen and Sykes (1985) have proposed a novel measure of the spatial comparison between observed and calculated patterns which compares over increments of decreasing spatial resolution. Essentially it estimates how much the predicted pattern must be shifted in space to cover all of the observed values.

Consider the segment of area $A(x_o, \delta\theta)$ sketched in Figure 5-1, which is defined by its position in polar coordinates, (r_i, θ_i), centered on the emission point and an angular displacement, $\delta\theta$. The area is bounded as shown by $\theta_i+\delta\theta$, $\theta_i-\delta\theta$, $r_i(1+\delta\theta)$, and $r_i(1-\delta\theta)$. The calculated concentration field within the area A is bounded by lower and upper values which we define as $C_c^l(A)$ and $C_c^u(A)$, respectively. Given observed concentrations $C_o(x_i)$ at a number of points i = 1, 2,

3,...M, one can assign calculated concentrations at these points as a function of $A(x_i, \delta\theta)$:

(5-1)

$$C_c(x_i, \delta\theta) = \begin{cases} C_c^l(A) & \text{if } C_o(x_i) < C_c^l(A) \\ C_o(x_i) & \text{if } C_c^l(A) < C_o(x_i) < C_c^u(A) \\ C_c^u(A) & \text{if } C_o(x_i) > C_c^u(A) \end{cases}$$

One can now calculate the fraction of the test points, f_N, which yield calculated concentrations within a specified ratio N of the observed values within the sector areas defined by ki.

(5-2)

$$f_N(\delta\theta, N) = \frac{1}{M} \sum_{i=1}^{M} H\{N - \exp[\, 31n\, (\frac{C_c(x_i, \delta\theta)3}{C_o(x_i)}\,]\}$$

with H {f} the Heavyside step function equal to 1 or 0, depending upon whether $f \geq 0$ or $f < 0$, respectively.

A plot of $f_N(\delta\theta, N)$ gives a direct measure of how well the laboratory-predicted spatial distribution compares with the observations. As an example, consider Figure 5-2, from a comparison of the mass consistent MATHEW/ADPIC numerical model with some field data. For N = 2, the figure shows that 90% of the observations are covered by a shift of 15° in the pattern, and that this rises to 100% for a 25° shift. Most emergency planners should be happy to expand a potentially affected area by only 15° to cover model uncertainty.

Ideally, the sum in Equation 5-2 should include all points where either the calculated or the observed concentrations are greater than background; however, it can only be applied at points where observed values are available. Lewellen and Sykes note that it is possible to create artificial patterns of high and low concentrations which would

yield high values of f_N; however, such patterns would not be created by any physically consistent modeling technique.

Additional comparisons considered include decay rate of peak concentrations with distance, distances to LFL, overlays of peak concentration isopleths, and overlays of concentration time histories at measurement locations.

5.2 Specific Laboratory/Field Comparison Studies

Puttock, Blackmore and Colenbrander (1982) identified over 22 field experiment programs on dense gas emissions. A number of these experiments have been simulated in fluid modeling facilities. This section will examine the evidence for model similarity between some of the more recent model/field comparison studies. Table 5-1 summarizes prototype, model, and similarity parameter characteristics for each test series. All pattern comparison figures are grouped together in Appendix A. Section 5.2.8 summarizes total model/field comparison performance.

5.2.1 AGA Capistrano tests

Field Measurement Program

The American Gas Association sponsored a series of more than 30 LNG releases into diked land areas from 1.8 m to 24.4 m in diameter in 1973 near San Clemente, California (AGA, 1974). One of these tests (AGA Test No. 44) was subsequently modeled by Meroney et al. (1977). LNG was pumped into 24.4 m diameter land areas surrounded by an insulated wall dike ≈0.5 m high. The test area was essentially flat, with vegetation and minor roughness removed by grading an area about 100 m wide and 300 m long. Thirty-six catalytic combustion sensors

(MSA) were distributed over the test area on short towers. Twenty-one sensors were mounted about 15 cm above the ground on five arcs ranging from 24 m to 293 m downwind. The MSA sensors are double-valued above about 10% methane concentration; hence, they are reliable only below 7% concentration, to an accuracy of about ±10% of the reading.

There appears to be a large uncertainty in source volume and boil-off rate. Some investigators have presumed a constant boil-off to about 80 seconds, followed by an exponential fall, others presume an exponential decaying source strength from zero time. Model experiments were performed to examine both scenarios. AGA Test 44 conditions are summarized in Table 5-1.

Model Measurement Program

The spill site was simulated at a 1:106 scale using a circular-source plenum with a porous punched plate upper surface, which emitted carbon dioxide at room temperature. Concentrations were measured with an aspirated hot-film anemometer system accurate for carbon dioxide to about ±10% of reading. Variable boil-off rates were produced by using a programmed cam to modulate a micrometer needle valve in the source supply line, to follow characteristic prototype vapor release rates calculated from liquid-level measurements. Two vapor release scenarios were studied: Case I, with a constant boil-off to about 80 seconds, followed by an exponential fall, and Case II, with an exponentially falling vapor production rate from an initial maximum. These two bracket the maximum values used by Havens and Spicer (1985) in their comparison of this case against the DEGADIS model. Case II boiloff is now considered more likely to be correct. The physical model source rates did not fall off as rapidly as their estimates. Measurements were made on and off plume centerline for

equivalent distances of 48 m to 293 m from source center. Data taken from Meroney et al. (1974) have been corrected for source strength effects as suggested in Section 4.3.

Model/Field Comparisons

Capistrano Model Case I yielded consistently higher concentrations than that of the Case II test, which is to be expected because it describes a higher boiloff rate. Peak concentrations measured for both cases were larger than peak values detected by the MSA sensors; however it is likely that the field sensors were limited by response time. The model did not predict the large and intermittent concentration peaks at late times that were observed in the field. These peaks may be due to gustiness and changes in wind direction and speed that are present in the atmosphere, but are not present in the wind tunnel. Figure 5-3 compares field measurements, physical model, and numerical model (DEGADIS) predictions for ground level centerline concentration decay with downwind distance.

Figure A-1 presents the results of the pattern test analysis for the Capistrano 44 test and Case II model measurements. For N = 1, a spatial shift of only 10^{o} would provide 100% agreement between model and test results. Considering the field test measurement errors and the large uncertainty in source strength, this must be considered a quite acceptable prediction.

5.2.2 DOE 5 m^3 LNG China Lake spills (Avocet Series)

Field Measurement Program

During a 3-month period in the early fall of 1978 a series of four liquefied natural gas experiments were performed at the Naval Weapons Center (NWC) at China Lake, California (Koopman, Bowman, and

Ermak, 1979). Each of the four experiments variously referred to as LNG Tests No. 18, 19, 20, and 21 (or Avocet 1, 2, 3, and 4) involved the release of about 5 m^3 of LNG through a 20 cm diameter pipe onto a pond of water at a rate of about 5 m^3/min. Field concentration measurements were made over two independent measurement grids. The NWC established a grid of ten MSA catalytic combustor sensors on a square grid, and the Lawrence Livermore National Laboratory (LLNL) provided eight towers distributed in a V-shaped array with a variety of concentration sensors, thermocouples, and grab samplers. Subsequent analysis suggested that the MSA sensors did not respond to the methane cloud, either because the peak concentration fluctuations were too rapid for the catalytic sensor, or the concentrations were above the sensor limit of 7%.

Model Measurement Program

A 1:85 scale model of the China Lake topography was examined in a meteorological wind tunnel by Neff and Meroney (1979). Argon was released from a circular plenum centered in the middle of the test site pond. The Model source gas was released from a 20 m equivalent diameter source area, over a step-function period of time, at a constant boil-off rate. Concentrations were measured isokineticly, with an aspirated hot-film anemometer, which had an effective circular sampling area of $\approx$ 1.6 m^2 and an accuracy of about $\pm$15% in the range of 5%-15% equivalent methane concentrations. A summary of the prototype and model test conditions for this spill series is presented in Table 5-1. Test conditions were specified on the basis of tower measurements provided by NWC at a 2 m height on an upwind tower. (Later post-test evaluations showed that measurements of wind speed and direction made by LLNL from anemometers downwind of the spill site

often varied markedly in magnitude and direction from the NWC values.)

Model/Field Comparisons

For such small spills, the wind speeds were too large (4.9 to 12.4 m/s) to exhibit strong density dominance. In addition, in every test there were large wind speed and wind direction fluctuations over the test periods (typically $\sigma_u \simeq 1$ m/s, and $\sigma_\theta \simeq 10^o$). In all field tests but the LNG-21 case, only the edge of the field plume touched the LLNL test grid. Although the background atmosphere was fairly dry (16%-29% relative humidity), Haselman (1980) compared plume temperatures and concentrations to the predictions of adiabatic mixing theory, and he concluded that condensed water initially evaporated from the pond may have increased plume temperatures during spills LNG 18, 19 and 21.

Model and field peak 1-m level concentrations are compared in Figures 5-4 to 5-7. For LNG-18, 19, and 20, it is likely that the mean wind directions provided by NWC were in error; hence, the model plumes do not overlay the field data. For these tests the decay of the concentrations with distance from the source appears to agree, but the direction of the plume is different. The most measurement locations were examined for the LNG-20 and 21 models (47 and 91 points respectively). Fortunately, during the LNG-21 test, the LLNL test grid and the model test grid fully overlapped.

Figures A-2 to A-5 present the results of the pattern test analysis. The poor showing for LNG-18, 19, and 20 are most likely due to the misalignment of the model, due to incorrect wind orientation information. The wind speed variations noted could also explain q50% variation in concentration magnitudes. The patterns for LNG-21 are quite good; for N = 1 a spatial shift of only 12.5^o would provide 100%

agreement between model and test results. (See Section 5.1 for discussion of pattern comparison nomenclature).

5.2.3 DOE 40 m^3 LNG China Lake spills (Burro Series)

Field Measurement Program

The Burro series of nine LNG spill experiments were performed at the Naval Weapons Center, China Lake, California during late summer 1980 over a pond area which had been resculptured with earth-moving equipment to reduce slopes along the pond banks (Koopman et al., 1982). The LNG volumes released on water ranged from 24 to 39 m^3, at rates from 11.6 to 18.4 m^3/min, with subsequent dispersion over land. Ninety gas sensors were distributed over an array of 30 measurement sites arranged in four arcs from 57 m to 800 m downwind from the center of the spill pond. Twenty wind-field stations were located at regular intervals from 800 m upwind to 900 m downwind, and 5 turbulence stations were located along the concentration sensor arcs. Thirty-three of the sensors were fast response (3 to 5 Hz) infra-red detectors capable of measuring even in dense fogs to within 1% methane, and forty-five were solid-state sensors which turned out to be less reliable, producing uncertainties of $\pm$20-30% below LFL and up to $\pm$50% errors at higher concentrations. The remaining sensors were MSA catalytic devices, reliable only below 10% concentrations to about 10% of reading. The reported concentrations are based on a 10 s averaging time; the lowest sensor position was 1 m above ground. Table 5-1 summarizes the relevant field conditions for Burro Tests 4, 5, 7, 8, and 9. The turbulent processes in the lower atmospheric boundary layer appeared to dominate the transport and dispersion of gas for all experiments except Burro 8. Burro 8 was conducted under

very low wind-speed conditions; hence, only during this test were density effects dominant. Energetic rapid phase transition (RPT) explosions occurred during the Burro 6 and 9 tests, influenced the plume dispersion, and damaged the facility.

Model Measurement Program

Five different field test, Burros 4, 5, 7, 8, and 9 were simulated in a meteorological wind tunnel (Neff and Meroney, 1981; Meroney, 1984, 1985). Burro 8 was simulated over two model scales (1:240 and 1:85) and with two different simulant gas specific gravities (1.38 and 4.18). Burro 9 was simulated over the two model scales but only with the 1.38 simulant gas specific gravity. Burro 4, 5, and 7 were simulated over one model scale (1:240) and with one simulant gas (1.38). Model conditions are summarized in Table 5-1. Since there was no data on the variable area and variable volume nature of the different LNG tests the source conditions were approximated by providing a steady source rate for the duration of the spill over a constant area. Concentration measurements were made in sets of eight with aspirated hot-wire anemometer probes. These probes were found to aspirate isokinetically over effective areas of 2.9 m^2 and 0.36 m^2 for the 1:240 and 1:85 scaled models respectively. Cumulative errors due to the combined effect of calibration uncertainties and nonlinear voltage drifting during the test time are estimated to be approximately $\pm$20% of the concentration value for the range of 5%-15% equivalent methane concentrations. Model tests provided an unique opportunity to examine plume variability; all tests were replicated between two to five times at each measurement location.

All model velocities were set to the average upwind speed

measured at a 2 m height. Wind shear profiles for the 1:240 scale model and source gas specific gravities of 1.38 are not in very good agreement with field results. The model winds were significantly lower near the ground than in the field. However, distorted density scaling for Burro 8 (SG = 4.18) over the 1:240 model did reproduce field wind shear. Wind speeds measured over the 1:85 scale model reproduced field results for Burro 8 and 9 very closely. Model longitudinal turbulence measurements appeared somewhat high for the Burro 8 case, but model measurements for Burro 9 were found to be very close to the field data.

Model/Field Comparisons

The model was oriented in the wind tunnel based on the average wind direction which occurred during the field tests. Drift in wind approach vector was sometimes substantial during the field tests. Burro 4 had significant wind direction changes, and Burro 8 experienced a steadily declining wind speed throughout the test. Unfortunately for the case of model Runs 1, 3, and 8, which were intended to model Burro 8, the topographic model was incorrectly turned to 215° from North rather than the 235° as specified by the field measured mean wind direction. Nonetheless, comparisons were made with the field data by rotating the measured model data 20° to coincide with the field wind direction. It is unfortunate that this mistake occurred because Burro 8 was the run most susceptible to the influences of topography. The comparisons of field and model data for Burro 8 and model Runs 1, 3, and 8 should therefore be viewed somewhat skeptically when drawing conclusions about model-field comparisons. Indeed, it may be better to interpret Runs 1, 3, and 8 as releases performed under equivalent source and wind conditions to Burro 8, but

with a different terrain orientation.

Peak centerline concentration decay with distance are considered in Figures 5-8 to 5-12. Typical concentration time histories are noted in Figures 5-13 and 5-14. Typical ground level concentration contours are provided as Figures 5-15 to 5-18.

Model Runs 4, 5, 7, 8, and 9, which correspond to Burro 4, 5, 7, 8, and 9, were all performed at a 1:240 scale and exact specific gravity equality. As noted in Table 5-1 and shown in Figure 5-17 for Burro 9, the 1:240 series did not correctly reproduce the field wind shear situation. In each case the model friction velocity was 50 to 100% too large, and model wind speeds below the 3 m reference height level were too small. This mis-scaling of the approach flow characteristics led to distorted concentration time history profiles and lower concentrations.

During Model Run 1 pure Freon was used to simulate Burro 8; hence, higher model wind speeds were possible. Some improvement in approach characteristics occurred; however, the terrain orientation was incorrect.

During Model Runs 2 and 3 a 1:85 scale model of the China Lake spill site was used to simulate Burro 9 and 8 respectively. This new model scale permitted higher tunnel velocities, larger $(Re_*)_m$ and larger $(Pe_*/Ri_*)m$. Concentration decay with downwind distance and the arrival and departure times of the simulated plumes now compared with field data much better than the earlier trials. (See Table 5-3).

During 1984-85, model tests were performed over a new 1:85 scale model of the China Lake terrain for the Burro 8 flow conditions. These new tests (Model Runs 8a and 8b) were correctly oriented to the wind, used improved instrumentation, and used argon and Freon as

simulant gases, respectively. As shown in Figure 5-11 and Figures 5-15 and 5-16 the model experiment reproduced the unique bifurcated lobed pattern seen during the field experiment. Maximum downwind concentrations for Run 8b agree very well with field measurements; although the model case did not reproduce the elevated plume behavior seen in the non-isothermal field plume.

Field-model comparisons for each of the five different Burro tests simulated are summarized below:

- o The 1:240 scale model of Burro 4 reproduced the peak centerline concentration decay with downwind distance. The arrival and departure concentration structure of the model plume was significantly different from the field because of poor modeling of the approaching wind profile at a 1:240 scale. Lateral plume extent comparisons indicate that deviations in the mean wind direction in the field caused the field plume to be wider than the model plume.

- o The 1:240 scale model of Burro 5 displayed all the same comparison characteristics as that of Burro 4 above. In addition, it was observed the concentrations in the interior of the field plume fluctuated much more than in the model plume. This difference is attributed to the highly turbulent atmosphere as a result of an unstable potential temperature gradient into which the plume was released. The model simulation was performed in a neutral wind field.

- o The 1:240 scale model of Burro 7 did not reproduce the centerline concentration decay with downwind distance. This disagreement is attributed to the Burro 7 plume being very narrow. It is likely the plume center missed the field concentration senors. The model plume arrived later and persisted longer than the field plume because of model wind speeds below the reference height were less than the scaled field values. Lateral plume extent comparisons indicate that deviations in the mean wind direction observed in the field caused the field plume to be wider than the model plume. This wind direction variation often caused the plume to leave the bounds of the field sensor array.

- o Five different model simulations were considered for Burro 8. Three of these (Model Runs 1, 3, and 8) were performed with a 20^{o} topographical model orientation error. Distortion of the plume initial density to obtain higher wind tunnel operating speeds resulted in significant improvement in approach wind characteristics and the avoidance of molecular diffusion effects; however, the distorted density did produce significantly different concentration histories. (See example Figures 5-13 and 5-14). The 1:85 scale model with an isothermal Freon simulant (Run 8b) reproduced maximum concentration decay rates, lateral plume

dimensions, and plume bifurcation. Field plume thermal effects definitely caused some plume lofting in Burro 8; this effect was not simulated by the isothermal physical model.

- o Two different types of model simulations were made on the Burro 9 plume. One was at the standard scale of 1:240, and the other was at a scale of 1:85 to better approximate the mean shear and total turbulent intensity reported in the Burro 9 wind field summary. Both simulations show good agreement with field data for the peak centerline concentration decay with downwind distance. The arrival and departure time structure of the model concentration time histories was improved for the 1:85 scale model. (See Figures 5-13 and 5-14). Overall, the 1:85 scale model simulation of Burro 9 had excellent agreement with field data.

Pattern comparison plots for the Burro Series model-field comparisons are provided as Figures A-6 to A-12. Pattern comparisons were not performed for Runs 1, 3, and 8 because of the orientation error. The patterns show improved model-field agreement as one changes from the 1:240 to 1:85 model, and from an argon to a Freon simulant. A pattern angle shift of from 15^{o} to 20^{o} produces 100% agreement with field data for N = 1. A shift from 10^{o} to 15^{o} produces agreement within a factor of N = 2 for all tests.

5.2.4 HSE Porton Downs experiment

Field Measurment Program

The field trials used a gas source in the form of a cubical box of about 3.5 m side containing 40 m^3 of gas (Picknett, 1981). The gas was released by allowing the sides of the box (made of thin pleated tarpaulin material) to collapse to the ground under gravitational forces in about 0.17 seconds, essentially leaving a cube of dense gas suddenly exposed to the wind. The top surface of the box remained fixed in place during the experiment. A total of forty-two individual trials were run, covering a range of wind speeds (<0.5 - 7.2 m/s), released gas density (specific gravity from 1.03 to 3.4), surface roughness (z_o = 2 to 150 mm), atmospheric stability (Pasquill stability

class from B to F) and ground slope ($\beta = 0^{o}$ to 4.4^{o}). Movement of the gas cloud was recorded by marking it with orange smoke and filming it, usually from the side and overhead. Measurements of the gas concentration were made with total integrated dosage monitors (bag samplers or absorptive charcoal) and continuously reading concentration monitors (Lovelock work-function detectors; maximum of ten in one test). Hall et al. (1982) reflect on the possibility that the dosage monitors were in error, since they typically provided integrated concentrations up to an order of magnitude smaller than the continuous monitors. Hall et al. also suggest that the time response of the continuous monitors may be between 0.5 to 5 seconds, as opposed to the 50 msec quoted by Picknett (1981).

Model Measurement Program

Six of the trials were picked for reproduction at a model scale of 1:25 by Hall et al. (1982). Table 5-1 summarizes the characteristics of the field and model tests selected. Trial 3 was carried out on a 1 in 13 upward slope, and yet was at similar conditions to Trial 37. Trial 8 was carried out in a very light wind, so for modeling purposes it was considered to have been carried out effectively in still air. Hall et al. adjusted test densities to account for the partial filling apparent in the field cinema films.

The experiments were carried out in the Warren Spring Laboratory's No. 1 wind tunnel. A model of the atmospheric boundary layer about 1 m deep was generated using a Counihan-type system followed by a fetch of rough surface. A model of the Porton collapsing tent source was constructed at a scale of 1:25 from square bellows material, which could collapse completely into a close fitting slot in the ground. The walls collapsed in a model time of 0.18 to 0.25 seconds which compares

well with the field equivalent collapse time of 0.17 seconds. Model simulant was the refrigerant BCF mixed with air. The gas concentration detector was an aspirated hot wire system into which air was drawn. Lower resolution was about 0.02% of BCF, accuracy was about ±10% of reading, and the upper frequency limit of the detector was about 20 Hz. Each experiment was replicated three times. Smoke-tagged gas clouds were photographed to compare with field pictures. Wind speed profiles were measured with a pulsed-wire anemometer.

Model/Field Comparisons

Hall et al. provided side-by-side comparison of photographic sequences of the Porton release series. These photographs exhibited truly remarkable model reproduction of the shape and appearance of the field releases. The wind-tunnel model reproduced the size, shape, spread rates and downwind travel distances as well as detailed reproduction of the characteristic cloud features. The model exhibited the rapid initial collapse to a low, even, height; the curved, sharply faced, upwind face including a rotating vortex; and the horseshoe-shaped downwind edge. Measurements of cloud width and downwind travel times are also generally very good (See Figures 5-19 and 5-20). Note that Run 33 is a strongly buoyancy-dominated plume, whereas Run 37 behaves like a passive gas cloud. Hall et al. concluded their model clouds were the same thickness as the full scale to within the "determinable level of accuracy."

Direct comparison between model and field concentration data present a much more confusing picture. In some cases the agreement is good, but sometimes is quite poor. Consider Figures 5-21 and 5-22. During Run 37 the field continuous monitors and the model results are quite close, whereas during Run 33 the field measurements are

significantly lower than the model values. During Runs 3 and 8, integrated doses from field bag samplers were generally of the same order as field and model continuous samplers when measurements were made at the same station. During the rest of the runs the Porton charcoal buttons generally produced dosimeter measurements up to an order of magnitude less than field or model continuous measurements. Post-facto analysis of the equipment showed the carbon buttons to be sensitive to temperature, humidity, gas concentration, wind speed, and even direction.

Differences also exist between the full-scale and model continuous measurements in both magnitude and variability. Realization-to-realization variations can explain up to an order of magnitude difference between the largest and smallest concentrations. Variation in arrival time of the experiments seemed to fall within the amount allowed by local cusp variations in the cloud shape. As quoted from Hall et al.: "With such large possible levels of variability in the concentration/time traces from both the model and the full-scale, almost any level of agreement levels within an order of magnitude for single realizations (sic) of the experiment might be classed as good agreement!"

Two qualitative differences between the appearance of the model and full-scale concentration/time traces are apparent: a) a sharp high initial peak in concentration appeared during the model experiments in locations near the source, and b) much higher levels of fluctuations occurred during the model experiments compared with the full scale. The high initial peak of the gas cloud is clearly associated with the gravity-driven head vortex. It was not detected by the field sensors; however, the location of the peak is very sensitive

to field detection location and field detection response time. The model sensor is believed to have excellent spatial and time resolution (20 Hz model scale, or about 4 Hz full scale), whereas aerodynamic characteristics of the field sensor alone suggest a full-scale frequency response of 1 Hz, and apparent smoothing of the concentration data suggest an actual response of 0.2 Hz (Hall et al., 1982).

The density of field and model data reported did not justify plotting pattern comparability.

Both the Porton Downs and the following Thorney Island experiments considered situations where an initially quiescent cloud collapses to the ground. The collapse itself produces enough kinetic energy and turbulence to dominate the mixing processes. Hence, parameters such as approach wind speed, thermal stratification, and surface roughness are unlikely to make significant changes in the dense cloud dilution rate over the distances monitored. Spills of LNG which result in generation of a vapor cloud over a finite period of time produce clouds which have small depth/width ratios.

5.2.5 NMI Thorney Islands experiments

Field Measurement Program

Between 1982 and 1984 a series of 29 experiments were performed at an airfield at Thorney Island, West Sussex, U.K., in which 2000 m^3 of gas of various densities were released in both unobstructed and obstructed configurations (Barrell and McQuaid, 1985). The data obtained were very comprehensive, including concentration, turbulence, visual records, and detailed meteorological information. Up to 100 gas sensor records were obtained in individual trials at distances up to 750 m from the release point. The fully developed field of 45

measurement stations carried a total of 215 transducers, 183 being gas sensing devices and 32 environmental sensors. The standard gas sensors used an oxygen depletion concept to cause variations in an electrochemical cell. These sensors had a frequency response of 1 Hz (McQuaid, 1985).

The field release volume was a twelve-sided polygon tent which was about 14 m diameter and 13 m high, containing a total volume of 2000 m^3. During a release a flexible top cover was withdrawn by raising it into a bundle above the gas tent cylinder. During some tests both permeable and impermeable vapor barriers of various heights were placed downwind of the dense gas releases. Only part of the Thorney Island data has been made available to the scientific community at this time (Roebuck, 1984); hence, only a few physical model comparison experiments have appeared.

Model Measurement Program

Three organizations have reported model simulation experiments of six of the Thorney Island trials (Hall and Waters, 1985; van Heugten and Duijm, 1984; Duijm et al., 1985; Schatzmann et al., 1985). The details of the trials selected and the model scales used are recorded in Table 5-1. Scale ratios used varied from 1:90 to 1:164. The collapsing tent source was simulated by a cubical volume with a collapsing bellows (Hall and Waters, 1985), or by a plastic truncated cylinder which was retracted downward by gravity beneath the tunnel floor at the time of release. All laboratory investigators used aspirated hot wire anemometer systems to detect continuous gas concentrations. Model experiments were replicated from 3 to 5 times each.

Hall and Waters (1985) compared three of the tests performed by

Hall et al. (1982) to Thorney Island trials 7, 11, 13, 15 and 18. The field tests selected for comparison were chosen because they had dimensionless bulk Richardson number parameters close to the model values examined by Hall et al. (ie. field to model variations of about $\pm$10%). Trials 13, 15 and 18 were at sufficiently close Richardson number conditions to be considered repeat runs of the same operating conditions. Since from earlier tests the Richardson number seemed to be the major dominant parameter during the Thorney Island trials, deviations in field/model surface roughness, slight deviations in release configuration, and the lower source aspect ratio during the model tests were considered insignificant. These tests thus provide an additional test of the sensitivity of the comparisons to such variables.

Van Heugten and Duijm (1984) and Duijm et al. (1985) simulated Thorney Island trials 8 and 13. Unfortunately the intake velocity of the aspirated probes they used was about 2.8 m/s. During post-analysis of their data Duijm noted that when a probe is mounted at 4 mm above a wind-tunnel floor, where the wind velocity is less than 0.8 m/s, the probe will smooth out the strong concentration gradients near the surface, and the concentration recorded would be systematically less than the actual concentration at probe position.

Schatzmann et al. (1985) reported results from model simulations of Thorney Island trial 15 in their open circuit meteorological wind tunnel. Details of their experiment were not described, but they did perform measurements with both equal and distorted specific gravity, while maintaining constant Richardson number.

Model/Field Comparisons

Considering that in the Hall and Water (1985) comparisons the model was not an exact representation of the trial either in source form or operating conditions, the general level of agreement was remarkably good. Dominance of the cloud dilution by turbulence produced during intial collapse may explain the tolerance of the comparison. Photographic comparisons between field and model displayed similar size, spread and travel rates. Figure 5-23 compares model results for travel times and spread rates to Trials 13, 15 and 18. Concentration measurements are also comparable, but not in all cases identical. Overall, nearly all the peak concentrations in the model are within a factor of two of the field trials. Figure 5-24 compares model and field concentration decay behavior for Trials 13, 15, and 18, while Fig 5-25 overlays concentration time histories for comparable model and trial samplers.

There is one comparison between model and full scale results where consistent differences occur. In Trial 7, the model concentrations within the cloud are lower and the model cloud persists over the samplers considerably longer than for the field case. Hall and Waters attribute this difference to the larger surface roughness in the model experiment, low plume Reynolds numbers, and deep boundary sublayers. The effect is very similar to that seen during modeling experiments performed by Neff and Meroney (1982) for the Burro series when a model scale of 1:240 produced high model shear rates and lower near surface wind speeds than during full scale conditions.

Since during the Duijm et al. (1985) experiments, ground level concentration measurements during model tests of Thorney Island trial 13 were systematically lower and elevated concentration measurements

were systematically higher than the full scale measurements, it would definitely appear that the model measurements are flawed by an excessively high aspiration rate (See Figure 5-26).

Schatzmann et al. (1985) provided time duration plots for only two locations during their model tests of Thorney Island trial 15. These plots were previously considered in Section 4.2.2 as Figures 4-12 and 4-13. The time of arrival, departure, peak concentrations, and fluctuations are all similar for undistorted density scaling. The peak concentrations are similar during the distorted density scaling (Alternative 1) situation, but the arrival and departure times are distorted.

5.2.6 Shell Maplin Sands experiments

Field Measurement Program

In 1980 Shell Research, Ltd. performed a series of controlled spills of LNG and refrigerated propane in quantities up to 20 m^3 on the sea at Maplin Sands in the South of England (Colenbrander and Puttock, 1983). Release of the liquid was either continuous or instantaneous. Continuous spills released liquid at a steady rate from the end of a pipe at or near the water surface. For instantaneous spills the liquid was poured into an open-topped insulated octagonal barge, 12.5 m across, which was then submerged, creating the spill as water flowed in to displace the liquefied gas. Model studies of only two of the continuous spills of propane (Runs 46 and 54) have been described by Puttock (1985). These cases used an open pipe release at water level for the source. Spill 54 was performed at a moderate wind speed (3.8 m/s) for the Maplin Sands site and displayed strong lateral and upwind buoyancy dominated spreading,

whereas spill 46 was released when the wind was 8.1 m/s, and was only marginally affected by the density of the gas.

Instruments were placed on 71 floating pontoons equipped with 4 m masts. There were about 360 instruments in the array. The gas sensor used was a device based on measurement of the heat loss from a filament under free convection. The sensor had a time constant of 3 seconds, and all data was smoothed by a three-second moving average to eliminate high frequency noise spikes. A fast response thermocouple was also placed close to the lowest gas sensor, and the spills were photographed from two land-based towers and a helicopter high overhead.

Model Measurement Program

Shell Laboratories in Amsterdam simulated spills 46 and 54 in their wind tunnel. These tests were selected because it was expected that heat transfer and latent heat release from condensed water vapor would have minimal effect during the field dispersion situations. The experiments were designed to emphasize the effect of molecular dispersion versus turbulent entrainment in the model mode. Specific concentration data was not available, but distances to LFL were reported. Projected model and field conditions are summarized in Table 5-1.

Model/Field Comparisons

These data were discussed earlier in Section 4.1.5, Table 4-2 and Figure 4-7. No tabulations of model data or comparison figures are available in the open literature.

5.2.7 HSE water spray curtain tests

Field Measurement Program

Full-scale dispersion experiments of dense gas dispersion in the presence of water curtains were performed by the Health and Safety Executive, U.K., in 1981 using CO_2 vapor (-79° C) at an estimated spill rate of 1.1 kg/s from a point source (Moodie, Taylor and Beckett, 1981). Two of these tests were selected for simulation in the wind tunnel at a scale ratio of 1:28.9. Trials HSE 41 and HSE 46 were chosen because of availability of model-size water-spray nozzles, practicality of scaling ratios, and apparent quality of the data.

The average field wind speed recorded for HSE 41 was about 3.2 m/s for the no-spray and spray intervals. Significant field concentrations were measured at large lateral distances; this was puzzling because the buoyancy length scale ratio, l_b/L, was very small, and projections from results by Britter (1979) and Neff and Meroney (1981) for continuous and finite time releases always produced narrow plumes under equivalent conditions. A mass balance performed over field measurement stations for HSE 41 failed to agree with the source strength provided by HSE. Further communications with HSE personnel revealed that during subsequent tests the recording anemometer was found to produce large errors. It was likely that the wind instrument used by HSE was in the wake of other test equipment during this test; thus, field and model data for this case are inconclusive.

The wind speeds at 1.25 m for HSE 46 were reported to range from 2.9 to 1.7 m/s over the test period. The wind field was variable, and wind directions varied from 293° to 340°. Shear measurements suggested that local surface roughness, z_o, was about 6.5 mm and $u_*/u_{10} = 0.06$. Ground level and elevated measurements were made of CO_2 concentration at six stations up and down-wind of the spray

curtain.

Model Measurement Program

The HSE tests were modeled at a scale of 1:28.9 by Meroney, Neff, and Heskestad (1984). Vortex generators and a wall trip at the wind tunnel entrance produced a boundary layer about 1 m deep over the test region, with z_o = 4.3 mm and u_*/u_{10} = 0.068. A miniature source was constructed to reproduce the radial exhaust characteristics of the source used by the HSE researchers. Sampling points were located at equivalent field locations, and an additional crosswind ground-level sampling array was placed just downwind of the HSE field sampler array. During HSE Trial 46, the model spray curtain consisted of 20 nozzles discharging at a 10.4 cm height, spaced 5.66 cm apart, and directed vertically downward. The source gas used in all runs to simulate the cold CO_2 was a mixture of 68% CO_2, 31% CCl_2F_2, and 1% C_2H_6. Concentrations were measured with a flame-ionization detector to values less than 0.1% with an accuracy of q5%. Measurements were made both with and without the water-spray curtain in operation.

Model/Field Comparisons

Ground-level concentration isopleths for the no-spray and spray configurations are shown in Figures 5-27 and 5-28 for HSE Trial 46. Vertical concentration profiles are displayed in Figures 5-29 and 5-30 respectively. Linear and logarithmic scatter diagrams of concentrations measured at equivalent points produce correlations of 0.87 and 0.97 respectively. Pattern comparisons are included as Figures A-13 and A-14.

5.2.8 Discussion of fluid modeling versus data comparisons

The twenty-four field experiments simulated include releases

exemplifying a wind range of heavy gas dispersion behavior. Continuous, instantaneous, and finite time release conditions are included, as well as cases which include topography, dikes, and water-spray curtains. Comparison of the model predictions with field observation is facilitated by the classification of the tests with a Release Richardson Number (Havens and Spicer, 1985). Richardson numbers are defined for continuous and instantaneous releases as follows:

Continuous Releases: $Ri_o^c = g'Q/(uu_*^2D)$

Instantaneous Releases: $Ri_o^I = g'V_i^{1/3}/u_*^2$

and characteristic frontal velocities are:

Continuous Releases: $V_f = \sqrt{g'H} = \sqrt{g'Q/(uD)}$

Instantaneous Releases: $V_f = \sqrt{g'H} = \sqrt{g'V_i^{1/3}}$

Table 5-2 shows release Richardson numbers calculated for the twenty-four cases modeled.

Britter (1980) suggested that the plume downwind of a release should be passive from the source for Ri_o^c less than about 1, and significant lateral and upwind spreading would occur for Ri_o^c greater than 10 and 40 respectively. Only one of the releases has a Richardson number near 1, nine have numbers between 10 and 40, and one has a Richardson number greater than 40.

Havens and Spicer (1985) propose that when Ri_o^I is greater than 1000 the flow and dilution processes which dominate down to average concentrations of about 5% are buoyancy dominated. Most of the Thorney Island tests and a few of the Porton Island tests exceed values of 1000.

Predicted and observed values of the upper flammability limit, UFL, lower flammability limit, LFL, and LFL/2 (15 / 5 / 2.5% for LNG,

10 / 2 / 1% for propane , and arbitrarily valves of 15 / 5 / 2.5% for the inert gas mixtures) are compared in Table 5-3. The observed values were determined from the reported experimental maximum concentrations on each radial arc by drawing a visual best-fit straight line on the respective log-maximum-concentration versus log-distance plot. The percentage deviation of the predicted from the observed distances for all of the experiments simulated are also shown in Table 5-3. These data permit the assignment of a 90% confidence interval for the predictions of distance to UFL, LFL, or LFL/2. For example, the Burro comparisons indicate a predicted maximum distance to the LFL gas concentration which would be from 25% below to about 6% above that observed. (Note, since Havens and Spicer (1985) provided the same format for their numerical verification exercise, examination of their report and this report provides a comparative perspective of the capabilities of physical and numerical model methods.)

Pattern Comparison Plots

Appendix A contains the individual Pattern Comparison plots prepared from the peak concentration contours at ground-level contours. Table 5-4 summarizes the values of Theta, Θ, at which there exists 100% agreement between field and model data at various magnitudes of N ratio. In no case is a Theta value greater than 15^{o} required to provide agreement within a factor of 2 between field and model results. Figure 5-31 provides the same information in a bar chart format. Figures 5-32 and 5-33 display the percent of measured data predicted exactly for each test in terms of Theta values varying from 0^{o} to 15^{o}.

To place these values in context of modeling alternatives one may consider pattern comparison plots for one of the more complicated

numerical models. The FEM3 model developed at LLNL which includes terrain, and heat transfer effects is among the most sophisticated primitive equation models. Chan and Ermak (1983) published ground level concentration contours for Burro series tests 8 and 9. Pattern comparison plots are provided as Figures A-15 and A-16. Theta shift values of 45^{o} and 12.5^{o} are required to produce 100% agreement with field data at N = 1 for tests 8 and 9, respectively. This compares with Theta values of 20^{o} and 15^{o} for the best comparable physical model effort. Hence, the most advanced calculations predict concentration isopleths of about the same order of spatial accuracy as physical simulation.

5.3 Indirect Evidence for Physical Modeling Similarity

Confidence in a physical modeling approach can also be obtained through secondary evidence that physical mechanisms have been appropriately simulated. Laboratory experiments can be performed which eliminate nonlinear interactions (examples are water vapor condensation, terrain effects, heat transfer, and meteorological and source nonstationarities) which confuse the understanding of the plume physics. Laboratory data can then be used to design and calibrate modules within numerical plume models. A short summary of such papers are included in Section 5.3.1. In addition many studies of neutral or buoyant plumes also substantiate the modeling approaches proposed herein. The reader is referred to this literature in Section 5.3.2.

5.3.1 Performance of calibrated numerical models

Laboratory experiments need not be designed to reproduce a

specific field experiment to have predictive value. It sometimes seems that the number of analytic and numeric models exceed the sets of quality data available to evaluate them. The latest models appear to be the most reliable, because they entail the least number of ad hoc assumptions, incorporate the latest understanding of plume physics, and are calibrated on the basis of more reliable experiments. Indeed, when a numerical model is calibrated on the basis of only laboratory experiments, and then the model is found to accurately replicate field experiments, one may justifiably infer that the plume physics was correctly simulated in the laboratory.

There are a number of models whose model constants have been completely specified based on laboratory experiments (Meroney, 1983; Meroney and Lohmeyer, 1984; Meroney, 1984; Meroney and Neff, 1984). Other predictors use laboratory models to specify particular sub-modules of their numeric codes (Havens and Spicer, 1985), and for many years entrainment algorithms used in most codes have been based on laboratory data (Germeles and Drake, 1975; Eidsvik, 1980). Only model comparisons completely based on development from laboratory data will be considered herein.

Meroney and Lohmeyer (1982) released suddenly small volumes of dense gas at ground level into a turbulent shear layer. During these tests, cloud Reynolds numbers based on approach wind speed, Re_{Da}, varied from 0 to 5133; the gravity head Reynolds number, Re_f, varied from 2226 to 7962; roughness Reynolds number, Re_*, varied from 0 to 0.08; Richardson number based on friction velocity, Ri_o^I, was infinity (for calm conditions) or varied from 26,000 to 445. These Richardson number conditions cover the entire range of available field data for instantaneous spills. They used this data to calibrate a box style

model (DENS4) which was compared favorably against the Porton data of Picknett (1981) Runs 3, 21, 28, 29, 33, 36, and 37. The model reproduced cloud travel times and spread rates, and the box model results differed from the field data in the same manner as the physical model experiments of Hall et al. (1982). Since post analysis of the field data suggested these differences were due to failures in field instrumentation, this is not serious. Meroney (1983) used the same model with improvements to allow for heat transfer and water vapor condensation to predict the decay of peak concentrations with distance for the Burro series measurements; agreement was within experimental scatter of the field data.

Neff and Meroney (1981) examined continuous and finite time releases of dense gas from small circular areas on the floor of an atmospheric wind tunnel. The continuous release Richardson number, Ri_o^C, ranged from less than one to 270, which includes cases of passive dispersion, buoyancy driven lateral spreading, and buoyancy driven upwind spreading. This range covers all field situations discussed except Burro 8. Later Andriev, Neff and Meroney (1983) examined continuous releases of dense cold gases in an environmental wind tunnel. They released methane, nitrogen, and carbon dioxide at cryogenic temperatures at continuous release Richardson numbers, Ri_o^C, varying from 27 to 245. These two sets of experiments were used to calibrate continuous- release versions of a box model (Neff and Meroney, 1983) and to select specifiable constants in a depth integrated model (Meroney, 1984).

The continuous release box model (DENS6) was used to calculate concentration isopleths, temperatures, cloud velocities, etc. for the Maplin Sands Spill series. Calculations were compared against LNG

Spills 15, 29, and 56 as well as Propane Spills 46 and 54. The field data were predicted within experimental scatter of the field data.

A depth integrated model (DENS20, DENS22) developed by Meroney (1983) from an earlier version reported by Meroney and Lohmeyer (1982) used the data discussed above to specify constants. The model has been compared to the Porton trials, the China Lake Burro series, and the Maplin Spill series. Table 5-5 compares predictions of LFL distance for the Maplin Spill series to predictions by HEGADAS, DENS6, and DENS22. The latter two numerical codes produce the highest correlation coefficients when compared against seven of the LNG spills and eight of the LPG spills ($\bar{r} = 0.83$ and $r = 0.89$ for DENS6 and DENS22 respectively).

Fay and Zemba (1985b) used the laboratory data of Hall (1979) and Neff and Meroney (1982) as well as the field experiments of propane plumes at Maplin Sands from Colenbrander and Puttock (1983) to specify constants in a quasi one-dimensional flow model of an isothermal dense gas plume. They observed that the laboratory data was taken prior to the Maplin Sands data and did not even cover the same regions of parameter space. Nonetheless, when the different sets of data were used to specify undefined constants, the resulting values were nearly equal. Thus it is not necessary to replicate a field experiment to define the coefficients in an analytic or emperical algorithm. In addition within the experimental scatter of the measurements, which is less for the laboratory than for the field experiments, there is no dependence upon physical scale or Reynolds number for any of the variables compared in their study. The Reynolds number at the source, $U_o H_o/\nu$, did not vary very much among the tests in each series, being 80-500 for the Neff and Meroney experiments, 400-1500 for the Hall

experiments and $4x10^4$-$2x10^5$ for the Maplin Sands field tests. Values of Reynolds number of the O(100) seem to be adequate to assure turbulent mixing in wind tunnel tests. The agreement found between the wind tunnel tests and the field tests confirms that a model properly posed physical model can relate data which scales over a factor of 100 in length scale and Reynolds number.

5.3.2 Laboratory/field comparisons for neutral density plumes

The very earliest analysis used for plume rise and dispersion were based on laboratory experiments performed by examining smoke behavior from model stacks in wind tunnels (Bosanquet & Pearson, 1936). Since that time almost every conceivable dispersion configuration has been considered in wind and water tunnel facilities--neutral, buoyant and negatively buoyant plumes; aerosols, heavy particles, and chemically reacting gases; stable and lapse conditions; building interactions or terrain perturbations; area, line, point, and volume sources; ground level sources, tall stacks, and cooling towers; and over smooth surfaces, urban models, forest canopies, and model agricultural crops. The data have been used to define physical models, plan field experiments, verify numerical models and mathematical analysis, etc.. A number of verification exercises have been completed. Laboratory data have been compared with the Prairie Grass field experiments by Davar (1961), Poreh (1961) and many others. Recently Li and Meroney (1984) compared plume spread rate in turbulent shear layers against the field data compiled by Draxler (1976). Poreh et al.(1984, 1985) have compared dispersion data from laboratory convective boundary layers against the field experiments of Briggs (1984). The list is so extensive that it is not

profitable to continue; rather one can positively assert that there is ample evidence that, under broad but still specific conditions, many atmospheric dispersion phenomena have been and can be adequately simulated in meteorological wind and water tunnel facilities. These constraints are described over a wide range of situations for neutral and passive plumes by Snyder (1981).

5.4 Summary and Recommendations

Seven field experiments which included 26 separate releases of dense gas have been compared with physical model simulations in Sections 5.2.1 to 5.2.7. In Section 5.2.8 the ability of fluid model methods to predict UFL, LFL, and LFL/2 levels is examined. Results of the Surface Pattern Comparability Approach described in Section 5.1 are also reported in Section 5.2.8. The following observations are appropriate:

a.) The level of agreement obtained between model and field experiments have been examined. The model clouds are very similar in appearance, they spread and travel at correct rates, measured concentrations compare very well, and peak concentrations are usually predicted to within a factor of two or better.

b.) Model simulations where specific gravity, volume flux ratio and Froude number equality have produced successful predictions of field concentrations are limited to situations where mean prototype wind speeds exceed 3 m/s, scale ratios do not exceed 250, and Pe_*/Ri_* ratio exceeds 0.15.

c.) During model simulations where Volume Flux ratio and Flux Froude number equality are stipulated, peak concentration isopleths are preserved if mean prototype wind speeds exceed 2 m/s, scale ratios do not exceed 100, and Pe_*/Ri_* ratio exceeds 0.15. However, in this case, the time of arrival and departure of the plumes are distorted.

d.) The recommendations with respect to scale ratio in parts b.) and c.) above are constrained by the range of field/model experiments actually performed. Other arguments are

advanced in Section 6.4 of the Volume I Report to specify the performance range permitted for scale ratio.

e.) Field/fluid model comparisons suggest that LFL distances for LNG spills are predicted within a standard deviation of 23% with a 90% confidence level.

f.) Field/fluid model comparisons suggest that ground level concentrations are predicted exactly (N = 1) for theta increments of less than 20^{o}, and within a factor of two (N = 2) for theta increments of less than 15^{o}.

g.) The most advanced fluid modeling effort and the most sophisticated numerical models appear to predict plume concentrations within comparable levels of spatial accuracy. It may be that this is associated with an inherent limit to the prediction of single realization field experiments.

h.) It does not appear that strict specification of Richardson number, Ri_{*}, is necessary to obtain adequate simulation of most aspects of a field trial. However, accurate specification of friction velocity, u_{*}, is so difficult for both field and model measurements that it is difficult to resolve this point decisively. It does appear necessary to roughly match velocity gradient over the plume depth.

i.) Strict observance of the roughness Reynolds number criterion ($Re_{*} > 2.5$) or the source Reynolds number criterion (Re ½ 3000), does not seem to be necessary when simulating flows dominated by gas release configuration. The roughness Reynolds number may be important during simulation experiments when one is concerned with decay of concentration to levels less than 0.1%.

j.) Very few field experiments have been performed which include the effects of obstacles, fences, water curtains, or other mitigation devices. Wind tunnel experiments are underway to model the Thorney Island obstacle trials; however, no published data are currently available. Since among the most appealing capabilities of fluid modeling is the possibility of examining many mitigation alternatives economically, it is important that these and other field/model experimental comparisons be made to validate the simulation process.

TABLE 5-1 a
PROTOTYPE AND MODEL CONDITIONS

CONTINUOUS RELEASES: PROTOTYPE:

TEST CONFIGURATION	NO. Field	Specific Gravity	Q(cu.m./s)	D(m)	u(m/s)	u*(m/s)	u*(m/s) +	Zo(cm)	P.G. Stab.	(Cpo/Cpa)*	Humidity %
AGA Capistrano (Meroney et al, 1977)	44	1.55	40.0 *	24.4	5.4	0.22		1*	C*	1.22	45
China Lake (Avocet)	18	1.55	14.9	20.0 *	6.7	0.28		0.02	C	1.22	16
5 cu. m. LNG	19	1.55	20.1	20.0 *	5.1	0.21		0.02	C-D	1.22	29
(Neff & Meroney, 1979)	20	1.55	13.3	20.0 *	12.4	0.51		0.02	D	1.22	15
	21	1.55	18.0	20.0 *	4.9	0.20		0.02	C	1.22	21
China Lake (Burro)	4	1.55	46.0	24.6	9.6	0.40	0.30	0.02	C	1.22	2
40 cu. m. LNG	5	1.55	44.1	24.0	7.8	0.33	0.37	0.02	C	1.22	6
(Neff & Meroney, 1981)	7	1.55	55.8	27.0	8.8	0.37	0.29	0.02	D	1.22	7
(Meroney, 1985)	8	1.55	60.8	28.2	2.0	0.07	0.14	0.02	E	1.22	5
		1.55	60.8	28.2	2.0	0.07	0.14	0.02	E	1.22	5
		1.55	60.8	28.2	2.0	0.07	0.14	0.02	E	1.22	5
		1.55	60.8	28.2	2.0	0.07	0.14	0.02	E	1.22	5
		1.55	60.8	28.2	2.0	0.07	0.14	0.02	E	1.22	5
	9	1.55	69.9	30.1	6.1	0.25	0.28	0.02	D	1.22	12
		1.55	69.9	30.1	6.1	0.25	0.28	0.02	D	1.22	12
Health & Safety Ex. Water spray tests (Meroney et al, 1984)	46 no spray	2.35	0.4	17.0 *	1.7	0.10		0.65	D*	1.28	--
	46 with spray	2.35	0.4	17.0 *	1.7	0.10		0.65	D*	1.28	--
Maplin Sands Tests	46	1.90	11.3	15.1 *	8.1	0.28		0.03	D	1.14	71
(Puttock et al, 1982)		1.90	11.3	15.1 *	8.1	0.28		0.03	D	1.14	71
		1.90	11.3	15.1 *	8.1	0.28		0.03	D	1.14	71
	54	1.85	9.3	13.8 *	3.8	0.13		0.03	D	1.14	85
		1.85	9.3	13.8 *	3.8	0.13		0.03	D	1.14	85

INSTANTANEOUS RELEASES: PROTOTYPE

TEST CONFIGURATION	NO.	Specific Gravity	V (cu.m.)	D (m)	u (m/s)	u* (m/s)	Zo(cm)	P.G. Stab.		Humidity %
Porton Downs, U.K.	3	2.30	40.0	3.9	5.5	0.25	0.2	D	--	--
40 cu. m.	8	2.00	40.0	3.9	0.5	0.02	0.2	F-G	--	--
(Picknett, 1981)	21	1.30	40.0	3.9	4.7	0.21	2	B-C	--	--
(Hall et al, 1982)	29	3.56	40.0	3.9	4.3	0.19	0.2	C	--	--
	33	2.08	40.0	3.9	2.0	0.09	1	B-C	--	--
	37	1.89	40.0	3.9	5.1	0.23	1	C-D	--	--
Thorney Is., U.K.	7	1.78	2000.0	14.0	3.2	0.13	1	E	--	81
1000 cu.m.	8	1.63	2000.0	14.0	2.4	0.12	0.3	D	--	88
(Hall & Waters, 1985)	11	2.03	2000.0	14.0	5.1	0.26	1	D	--	77
(Duijm et al, 1985)	13	1.96	2000.0	14.0	7.5	0.38	1	D	--	74
(Schatzman et al, 1985)		1.96	2000.0	14.0	7.5	0.38	1	D	--	74
		1.96	2000.0	14.0	7.5	0.38	1	D	--	74
	15	1.41	2000.0	14.0	5.4	0.27	1	C-D	--	88
		1.41	2000.0	14.0	5.4	0.27	1	C-D	--	88
		1.41	2000.0	14.0	5.4	0.27	1	C-D	--	88
	18	1.87	2000.0	14.0	7.4	0.30	1	C	--	

+ : Reanalysis of Burro velocity profiles (Neff and Meroney, 1981)

(Ri)c = g*(SG-1)*Q/[u^3*D]
(Ri)i = g*(SG-1)*V^.33/u^2

(Ri*)c = g*(SG-1)*Q/[u*(u*)^2*D]
(Ri*)i = g*(SG-1)*V^0.33/(u*)^2

(Vol. Ratio) = Q/(u*D^2)

(Re) = u*D/n
(Re*) = (u*)*Zo/n

Pe*/Ri* = (u*)^3/[g(SG-1)*D]

Table 5-1 b
PROTOTYPE AND MODEL CONDITIONS

TEST CONFIGURATION	NO. Field	NO. TEST	SCALE RATIO	SPECIFIC GRAVITY	Q(cc/s)	D(cm)	u(cm/s)	u*(cm/s)	u*(cm/s) +	Zo(cm)	P.G Stability	(cr
CONTINUOUS RELEASES: MODELS												
AGA Capistrano	44	II	106	1.4	340	23.0	52	2.13		0.02	D	
(Meroney et al, 1977)												
China Lake (Avocet)	18	18	85	1.38	186	23.5	60	2.70 *		0.02	D	
5 cu. m. LNG	19	19	85	1.38	251	23.5	46	2.07 *		0.02	D	
(Neff & Meroney, 1979)	20	20	85	1.38	166	23.5	112	5.04 *		0.02	D	
	21	21	85	1.38	225	23.5	44	1.98 *		0.02	D	
China Lake (Burro)	4	4	240	1.38	44	10.2	55	4.56	4.94	0.01	D	
40 cu. m. LNG	5	5	240	1.38	42	10.0	45	3.76	4.29	0.01	D	
(Neff & Meroney, 1981)	7	7	240	1.38	53	11.2	51	4.23	4.88	0.01	D	
(Meroney, 1985)	8	8	240	1.38	58	11.7	11	0.91	1.29	0.01	D	
		1	240	4.18	164	11.7	32	2.65	3.26	0.01	D	
		3	85	1.38	760	33.0	18	1.22	0.81	0.01	D	
		A	85	1.38	760	33.0	18	1.22	0.81	0.01	D	
		B	85	4.18	2195	33.0	52	3.47	3.47	0.01	D	
	9	9	240	1.38	66	12.6	34	2.82	3.27	0.01	D	
		2	85	1.38	874	35.6	57	3.87	2.52	0.01	D	
Health & Safety Ex.	46	--	28.9	2.35	87	59.0	32	2.18		0.01	D	
Water spray tests	no spray											
(Meroney et al, 1984)												
	46 with spray	--	28.9	2.35	87	59.0	32	2.18		0.01	D	
Maplin Sands Tests	46	M46-1	110	1.90	89	13.7	77	3.08 *		0.01 *	D	
(Puttock et al, 1982)		M46-21	110	4.18	167	13.7	147	5.88 *		0.01 *	D	
		M46-22	110	1.90	72	12.6	55	2.20 *		0.01 *	D	
	54	M54-1	120	1.85	93	13.8	38	1.52 *		0.01 *	D	
		M54-2	120	4.18	180	13.8	75	3.00 *		0.01 *	D	

TEST CONFIGURATION	NO.	NO. TEST	SCALE RATIO	SPECIFIC GRAVITY	V(cc)	D(cm)	u(cm/s)	u*(cm/s)	Zo(cm)	P.G Stability	(cm
INSTANTANEOUS RELEASES: MODEL											
Porton Downs, U.K.	3	T3	25	2.30	2744	16.0	110	6.00	0.02	D	
40 cu. m.	8	T8	25	2.00	2744	16.0	0	0.00	0.02	D	
(Picknett, 1981)	21	T21	25	1.30	2744	16.0	94	9.60	0.15	D	
(Hall et al, 1982)	29	T29	25	3.56	2744	16.0	86	4.50	0.02	D	
	33	T33	25	2.08	2744	16.0	40	3.00	0.40	D	
	37	T37	25	1.89	2744	16.0	102	6.70	0.40	D	
Thorney Is., U.K.	7	T33	90	2.08	2744	16.0	40	3.00	0.40	D	
1000 cu.m.	8	TN08	107	4.18	1633	13.0	53	2.80	0.02	D	
(Hall & Waters, 1985)	11	T29	90	3.56	2744	16.0	86	4.50	0.02	D	
(Duijm et al, 1985)	13	P3	90	2.00	2744	16.0	84	4.40	0.02	D	
(Schatzman et al, 1985)		TN013A	107	1.96	1633	13.0	73	3.90	0.01	D	
		TN013B	107	4.18	1633	13.0	132	7.20	0.01	D	
	15	P3	90	2.00	2744	16.0	84	4.40	0.02	D	
		UH15A	164	1.41	450	8.5	42	2.10 *	0.01	D	
		UH15B	164	4.18	450	8.5	117	5.87 *	0.01	D	
	18	P3	90	2.00	2744	16.0	84	4.40	0.02	D	

Table 5-1 c
PROTOTYPE AND MODEL CONDITIONS

CONTINUOUS RELEASES: DIMENSIONLESS PARAMETERS

TEST CONFIGURATION	NO. Field	(Ri)p	(Ri)m	(Ri*)p	(Ri*)p +	(Ri*)m	(Ri*)m +	(Vol. Ratio)p	(Vol. Ratio)m	(Re)m	(Re*)m	(Re*)m +	Pe*/Ri*	Pe*/Ri* +
AGA Capistrano (Meroney et al, 1977)	44	0.057	0.041	34.1		24.6		0.013	0.012	7973	0.28		0.16	
China Lake (Avocet)	18	0.013	0.014	7.7		6.7		0.006	0.006	9400	0.36		0.26	
5 cu. m. LNG	19	0.041	0.041	24.1		20.2		0.010	0.010	7207	0.28		0.12	
(Neff & Meroney, 1979)	20	0.002	0.002	1.1		0.9		0.003	0.003	17547	0.67		1.72	
	21	0.041	0.042	24.8		20.7		0.009	0.009	6893	0.26		0.10	
China Lake (Burro)	4	0.011	0.010	6.5	11.7	1.4	1.2	0.008	0.008	3740	0.30	0.33	1.27	1.62
40 cu. m. LNG	5	0.021	0.017	11.5	9.3	2.5	1.9	0.010	0.009	3000	0.25	0.29	0.71	1.06
(Neff & Meroney, 1981)	7	0.016	0.013	9.2	15.1	1.9	1.5	0.009	0.008	3808	0.28	0.33	1.01	1.56
(Meroney, 1985)	8	1.455	1.389	1062.8	296.9	203.0	101.0	0.038	0.039	858	0.06	0.09	0.01	0.03
		1.455	1.335	1062.8	296.9	194.7	128.7	0.038	0.037	2496	0.18	0.22	0.07	0.12
		1.455	1.473	1062.8	296.9	320.6	727.4	0.038	0.039	3960	0.08	0.05	0.02	0.01
		1.455	1.473	1062.8	296.9	320.6	727.4	0.038	0.039	3960	0.08	0.05	0.02	0.01
		1.455	1.477	1062.8	296.9	331.6	331.6	0.038	0.039	11440	0.23	0.23	0.15	0.15
	9	0.055	0.050	32.4	26.2	7.2	5.4	0.013	0.012	2856	0.19	0.22	0.30	0.47
		0.055	0.049	32.4	26.2	10.7	25.3	0.013	0.012	13528	0.26	0.17	0.78	0.21
Health & Safety Ex.	46	0.063	0.060	17.6		12.8		0.001	0.001	12587	0.22		0.05	
Water spray tests (Meroney et al, 1984)	no spray													
	46 with spray	0.063	0.060	17.6		12.8		0.001	0.001	12587	0.22		0.05	
Maplin Sands Tests	46	0.012	0.013	10.4		7.9		0.006	0.006	7033	0.10		0.22	
(Puttock et al, 1982)		0.012	0.012	10.4		7.5		0.006	0.006	13426	0.20		0.72	
		0.012	0.030	10.4		19.0		0.006	0.008	4620	0.07		0.08	
	54	0.102	0.102	87.6		64.0		0.013	0.013	3496	0.05		0.03	
		0.102	0.097	87.6		60.3		0.013	0.013	6900	0.10		0.10	

INSTANTANEOUS RELEASES: DIMENSIONLESS PARAMETERS:

TEST CONFIGURATION	NO.	(Ri)p	(Ri)m	(Ri*)p	(Ri*)m			(Re)m	(Re*)m	Pe*/Ri*
Porton Downs, U.K.	3	1.441	1.473	697.4	494.9	--	--	11733	0.80	1.88
40 cu. m.	8	134.116	--	83822.5	--	--	--	0	0.00	0.00
(Picknett, 1981)	21	0.455	0.465	228.1	44.6	--	--	10027	9.60	33.38
(Hall et al, 1982)	29	4.642	4.744	2377.7	1732.7	--	--	9173	0.60	0.40
	33	9.053	9.252	4470.5	1644.7	--	--	4267	8.00	0.28
	37	1.147	1.172	564.1	271.7	--	--	10880	17.87	3.83
Thorney Is., U.K.	7	9.397	9.252	5693.6	1644.7	--	--	4267	8.00	0.28
1000 cu.m.	8	13.493	13.054	5221.5	4677.0	--	--	4593	0.37	0.08
(Hall & Waters, 1985)	11	4.885	4.744	1879.6	1732.7	--	--	9173	0.60	0.40
(Duijm et al, 1985)	13	2.105	1.942	820.1	708.0	--	--	8960	0.59	0.96
(Schatzman et al, 1985)		2.105	2.077	820.1	727.8	--	--	6327	0.16	0.70
		2.105	2.104	820.1	707.3	--	--	11440	0.29	1.33
	15	1.734	1.942	693.8	708.0	--	--	8960	0.59	0.96
		1.734	1.745	693.8	697.9	--	--	2380	0.08	0.26
		1.734	1.744	693.8	692.8	--	--	6630	0.23	0.72
	18	1.960	1.942	1192.5	708.0	--	--	8960	0.59	0.96

TABLE 5-2 RICHARDSON NUMBER CLASSIFICATION OF FIELD EXPERIMENT RELEASES

CONTINUOUS RELEASES

TEST CONFIGURATION	NO.	g' (m/s/s)	Q (cu.m./s)	D (m)	u (m/s)	u* (m/s)	(Ri)o/c	NOTES:
AGA Capistrano (Meroney et al, 1977)	44	5.4	40.0 *	24.4 *	5.4	0.22 *	33.9	L
China Lake (Avocet)	18	5.4	14.9	20.0 *	6.7	0.28 *	7.7	
5 cu. m. LNG	19	5.4	20.1	20.0 *	5.1	0.21 *	24.1	L
(Neff & Meroney, 1979)	20	5.4	13.3	20.0 *	12.4	0.51 *	1.1	P
	21	5.4	18.0	20.0 *	4.9	0.20 *	24.8	L
China Lake (Burro)	4	5.4	46.0	24.6	9.6	0.40	6.5	
40 cu. m. LNG	5	5.4	44.1	24.0	7.8	0.33	11.5	L
(Neff & Meroney, 1981)	7	5.4	55.8	27.0	8.8	0.37	9.2	L
	8	5.4	60.8	28.2	2.0	0.07	1063.1	L & U
	9	5.4	69.9	30.1	6.1	0.25	32.4	L
Health & Safety Ex. Water spray tests (Meroney et al, 1984)	46 no spray	13.3	0.4	17.0 *	1.7	0.10 *	17.7	L
	46 with spray	13.3	0.4	17.0 *	1.7	0.10 *	17.7	L
Maplin Sands Tests	46	8.8	11.3	15.1 *	8.1	0.28	10.4	L
(Puttock et al, 1982)	54	8.3	9.3	13.8 *	3.8	0.13	87.1	L & U

INSTANTANEOUS RELEASES

TEST CONFIGURATION	NO.	g' (m/s/s)	V (cu.m.)	D (m)	u (m/s)	u* (m/s)	(Ri)o/c	
Porton Downs, U.K.	3	12.8	40.0	3.9	5.5	0.25 *	691.8	
40 cu. m.	8	9.8	40.0	3.9	0.5	0.02 *	*******	BD
(Hall et al, 1982)	21	2.9	40.0	3.9	4.7	0.21 *	222.1	
	29	25.1	40.0	3.9	4.3	0.19 *	2348.8	BD
	33	10.6	40.0	3.9	2.0	0.09 *	4420.8	BD
	37	8.7	40.0	3.9	5.1	0.23 *	555.6	
Thorney Is., U.K.	7	7.7	2000.0	14.0	3.2	0.13	5596.9	BD
1000 cu.m.	8	6.2	2000.0	14.0	2.4	0.12	5288.9	BD
(Hall & Waters, 1985)	11	10.1	2000.0	14.0	5.1	0.26	1835.3	BD
	13	9.4	2000.0	14.0	7.5	0.38	799.7	
	15	4	2000.0	14.0	5.4	0.27	674.0	
	18	8.5	2000.0	14.0	7.4	0.30	1160.2	BD

L: LATERAL SPREADING (Ri > 10), U: UPWIND SPREADING (Ri > 40), P: PASSIVE (Ri < 1), BD: BUOYANCY DOMINATED (Ri > 1000)
*: APPROXIMATED VALUES

TABLE 5-3

COMPARISON OF OBSERVED VS FLUID-MODEL PREDICTED MAXIUM DISTANCES TO GAS CONCENTRATIONS IN THE FLAMMABLE LIMIT RANGE

TEST CONFIGURATION	NO.	NO. TEST	OBSERVED UFL	OBSERVED LFL	OBSERVED LFL/2	PREDICTED UFL	PREDICTED LFL	PREDICTED LFL/2	[(PRE-OBS)/OBS](100) UFL	[(PRE-OBS)/OBS](100) LFL	[(PRE-OBS)/OBS](100) LFL/2	CONFIDENCE INTERVAL (90%)
AGA Capistrano (Meroney et al, 1977)	44	--	100	220	300	110	270	600	10	23	100	UFL : Mean % deviation from PRE -9.0 %
												% Standard deviation = +22.8 %
China Lake (Avocet)	18	18	--	--	--	65	130	--				
5 cu. m. LNG	19	19	65	--	--	85	--	--	31			
(Neff & Meroney, 1979)	20	20	45	70	100	27	75	125	-40	7	25	LFL : Mean % deviation from PRE +0.4 %
	21	21	70	100	--	85	--	--	21			% Standard deviation = +22.4 %
China Lake (Burro)	4	4	60	180	300	65	190	325	8	6	8	
40 cu. m. LNG	5	5	70	260	550	70	200	400	0	-23	-27	
(Neff & Meroney, 1981)	7	7	100	250	650	90	250	550	-10	0	-15	LFL/2: Mean % deviation from PRE +7.8 %
(Meroney, 1985)	8	a	150	400	700	100	300	660	-33	-25	-6	% Standard deviation = +32.5 %
		b	150	400	700	120	350	700	-20	-13	0	
	9	9	110	280	490	90	240	450	-18	-14	-8	
		2	110	280	490	100	290	550	-9	4	12	
Porton Downs, U.K.	3	T3	--	--	--	10	21	36				
40 cu. m.	8	T8	15	--	--	13	22	27	-13			
(Hall et al, 1982)	21	T21	--	--	--	8	28	50				
	29	T29	--	--	--	20	31	55				
	33	T33	--	--	--	14	25	36				
	37	T37	--	--	--	10	20	36				
Thorney Is., U.K.	7	T33	60	120	180	40	90	125	-33	-25	-31	
1000 cu.m.	11	T29	--	100	160	--	130	200		30	25	
(Hall & Waters, 1985)	13	P3	--	100	160	50	110	180		10	13	
	15	P3	80	160	250	50	110	180	-38	-31	-28	
	18	P3	--	100	140	50	110	180		10	29	
Maplin Sands, U.K.	46	M46-1	--	245	--	--	260	--		6		
Propane spills		M46-21	--	245	--	--	265	--		8		
(Puttock, 1985)		M46-22	--	245	--	--	165	--		-33		
	54	M54-1	--	452	--	--	270	--		-40		
		M54-2	--	452	--	--	485	--		7		
Health & Safety Ex.	46	--	--	15	25	--	22	30		47	20	
Water spray tests	no spray											
(Meroney et al, 1984)												
	46	--	--	< 6	--	--	< 6	--				
	with spray											

Table 5-4 : Pattern Comparison Plot Results

Configuration	Date	Run No.	Scale Ratio	Specific Gravity	Points Compared	Intercept of Theta, Degrees f-1	f-2	f-5	f-10
AGA Capistrano									
Field	(1974)			1.52					
Model	(1977)	44	106	1.55		10.0	7.5	0.0	0.0
China Lake (Avocet)									
Field	(1978)			1.5					
Model	(1979)	18	85	1.38	3	20.0	5.0	0.0	0.0
		19	85	1.38	5	15.0	5.0	5.0	0.0
		20	85	1.38	4	17.5	7.5	7.5	7.5
		21	85	1.38	6	12.5	0.0	0.0	0.0
China Lake (Burro)									
Field	(1980)			1.5					
Model	(1981)	4	240	1.38	8	20.0	15.0	12.5	7.5
	(1985)								
		5	240	1.38	6	15.0	12.5	7.5	7.5
		7	240	1.38	12	15.0	10.0	7.5	5.0
		8	85	1.38	17	45	15	7.5	5
		8	85	4.18	17	20.0	10.0	2.5	2.5
		9	240	1.38	13	17.5	15.0	12.5	10.0
		9	85	1.38	13	15.0	12.5	10.0	10.0
HSE Spray Tests									
Field	(1981)			2.35					
Model	(1983)	46 No Water Sprays							
			28.9	2.35	6	20.0	10.0	0.0	0.0
		46 With Water Sprays							
			28.9	1.35	6	12.5	5.0	0.0	0.0
FEM3 Numerical Prog.									
Heat transfer									
Terrain included									
Chan & Eraak	(1983)								
	Burro	8	1	--	13	45.0	2.5	0.0	0.0
	Burro	9	1	--	13	12.5	10.0	10.0	10.0

Table 5-5

Numerical Prediction of LFL Distances for Maplin Sands LNG and LPG Spill Trials Compared with Field Measurements

SPILL NO.	LFL (m)	** LFL HEGADAS (m)	** LFL dens6 (m)	** LFL dens22 (m)	*** LFL dens22 (m)
CONTINUOUS PROPANE					
42	220+-35	315	332	283	273
43	215+-20	245	270	270	216
46	245+-35	225	248	300	426
47	340+-80	320	370	378	414
49	285+-25	210	234	296	382
50	210+50-25	280	270	371	321
52	200+-30	315	315	385	315
54	450+-70	295	314	280	271
CONTINUOUS LNG					
9	135+-15	90	120	77	77
12	63+-4	45	70	52	52
15	165+-15	100	155	100	184
27	190+-20	235	245	110	110
29	140+-15	245	170	120	137
34	150+-20	185	190	106	133
35	175+-25	205	210	124	138
39	130+-20	290	215	110	112
56	110+-30	115	140	90	85
Correl. Coeff., r =		0.62	0.77	0.69	0.72
(no Run 54) r =		0.69	0.83	0.81	0.89

** Assume $u_*/u_{10} = 0.034$

*** Calculate u_* and Zo from logarithmic velocity profile fit to velocity data

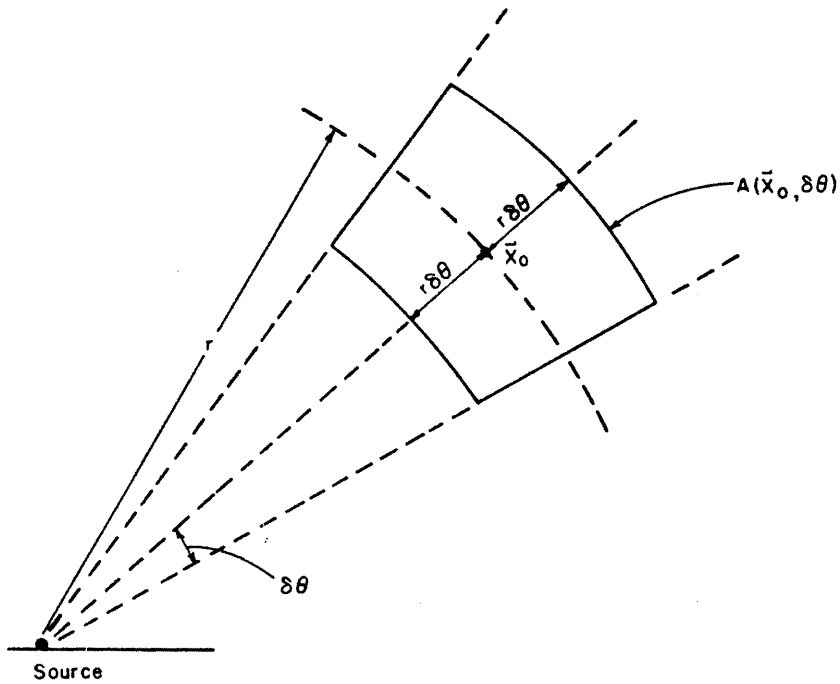

Figure 5-1. Schematic of the area segment, $A(x_i, \alpha\theta)$.

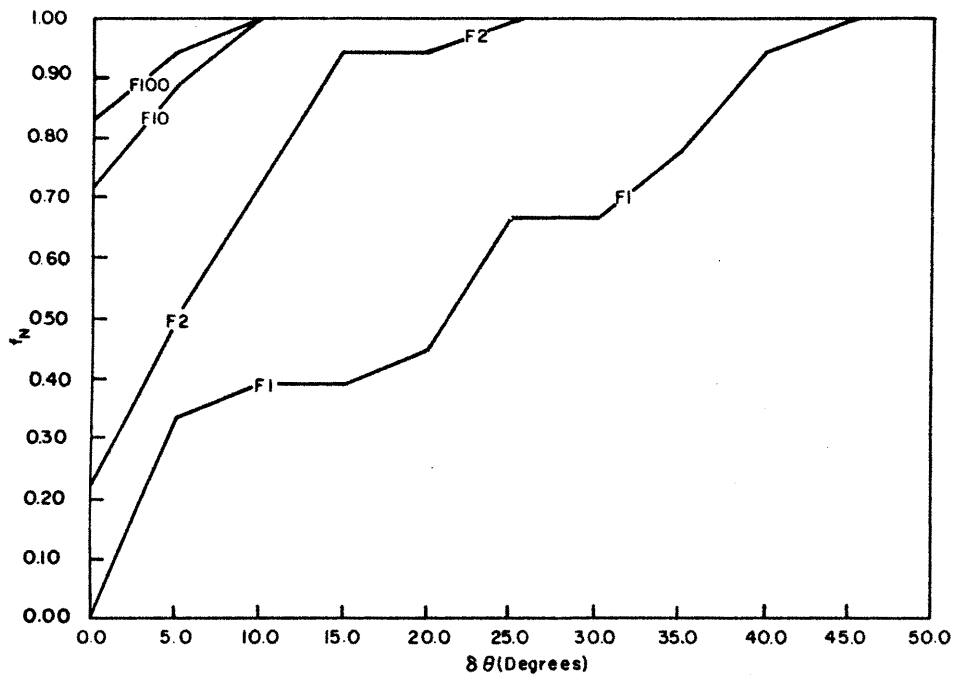

Figure 5-2. Pattern test result using the MATHEW/ADPIC numerical model against a typical set of field data. f_N equals the fraction of data points covered within a factor of N by the calculated pattern expanded through an angle so (Lewellen and Sykes, 1985).

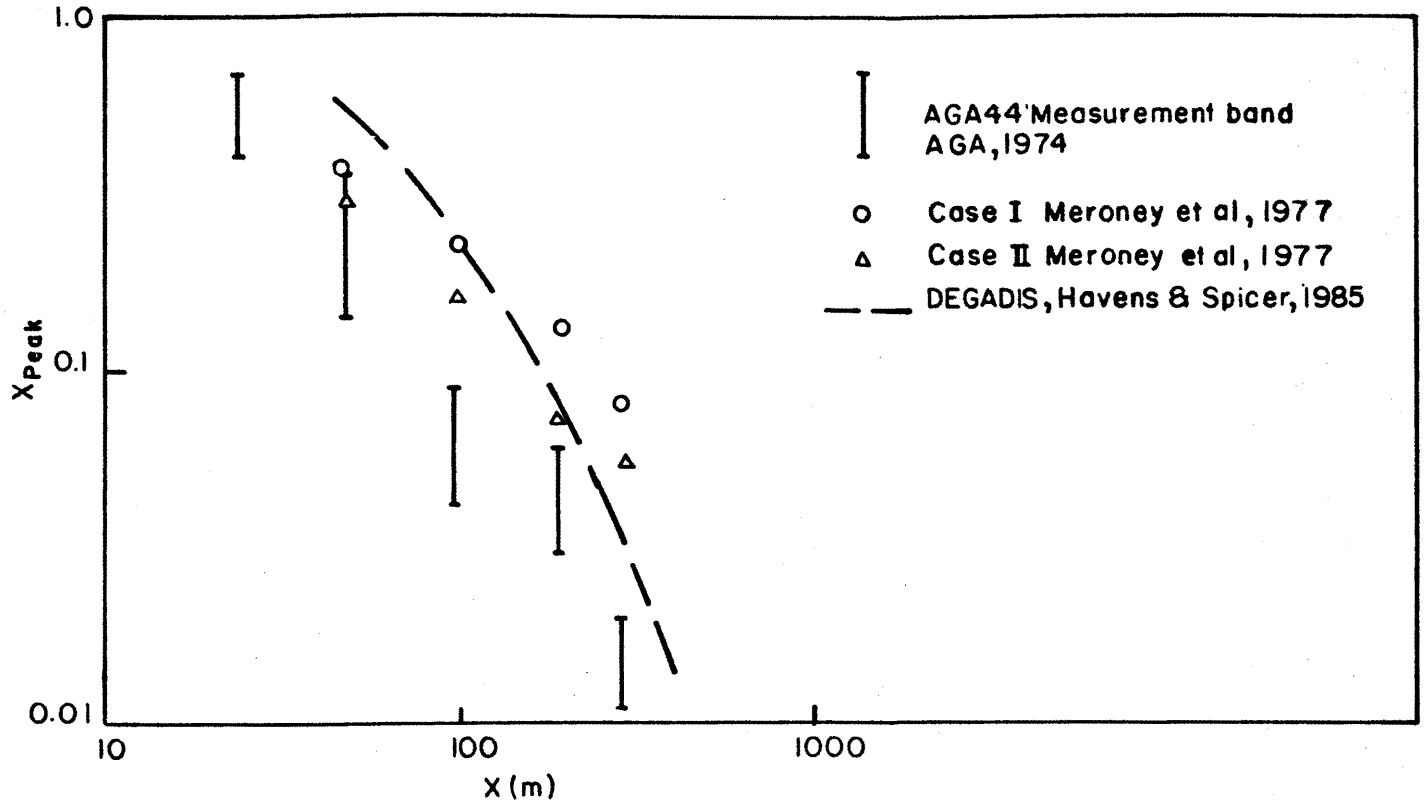

Figure 5-3. Centerline maximum concentrations versus downwind distance for AGA test no. 44, compared with DEGADIS numerical program.

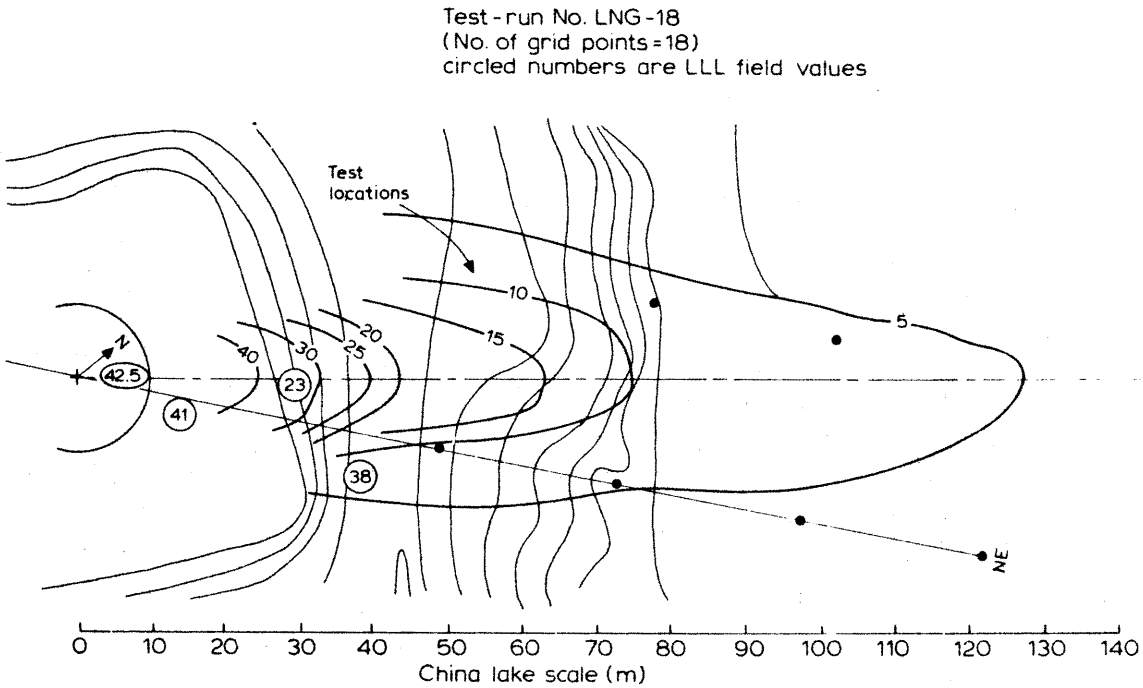

Figure 5-4. Concentration isopleth patterns for 5 m^3 China Lake test LNG - 18 (Avocet - 1)(Neff and Meroney, 1979).

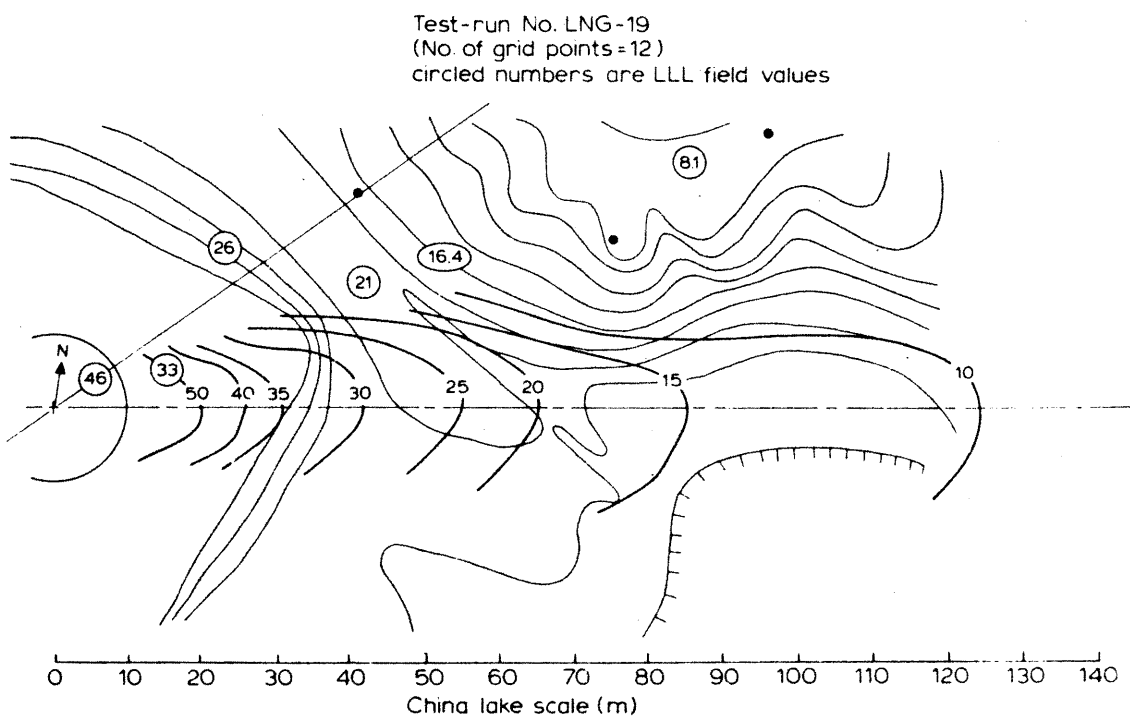

Figure 5-5. Concentration isopleth patterns for 5 m^3 China Lake test LNG - 19 (Avocet - 2)(Neff and Meroney, 1979).

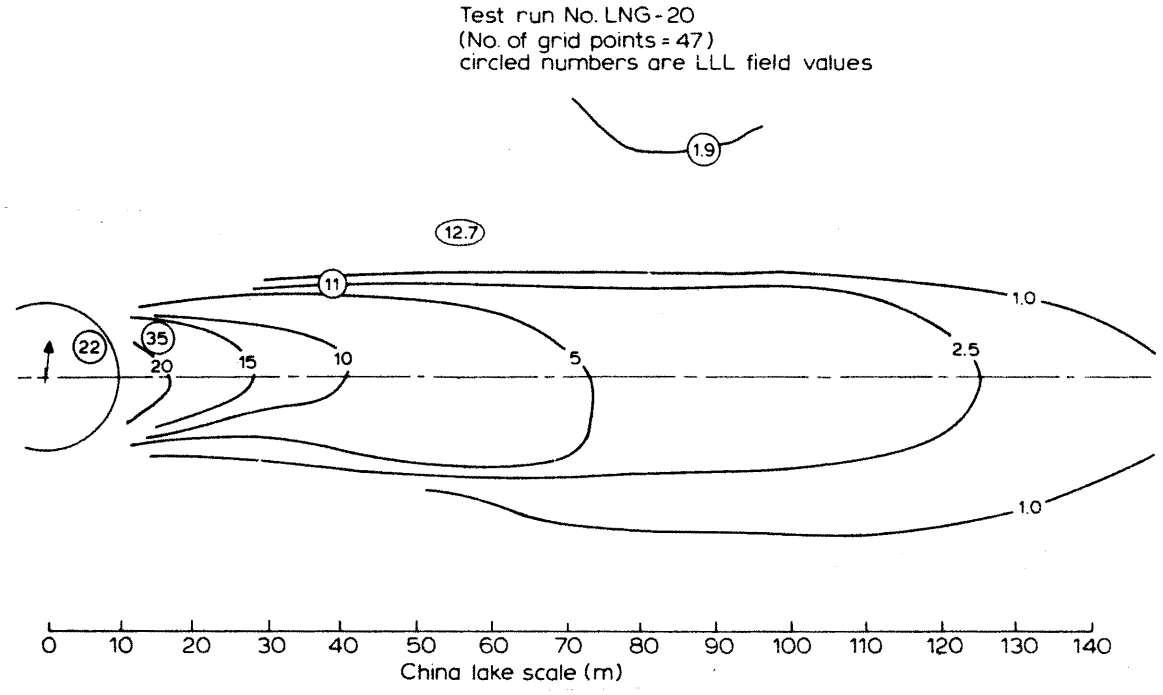

Figure 5-6. Concentration isopleth, patterns for 5 m^3 China Lake test LNG - 20 (Avocet - 3)(Neff and Meroney, 1979).

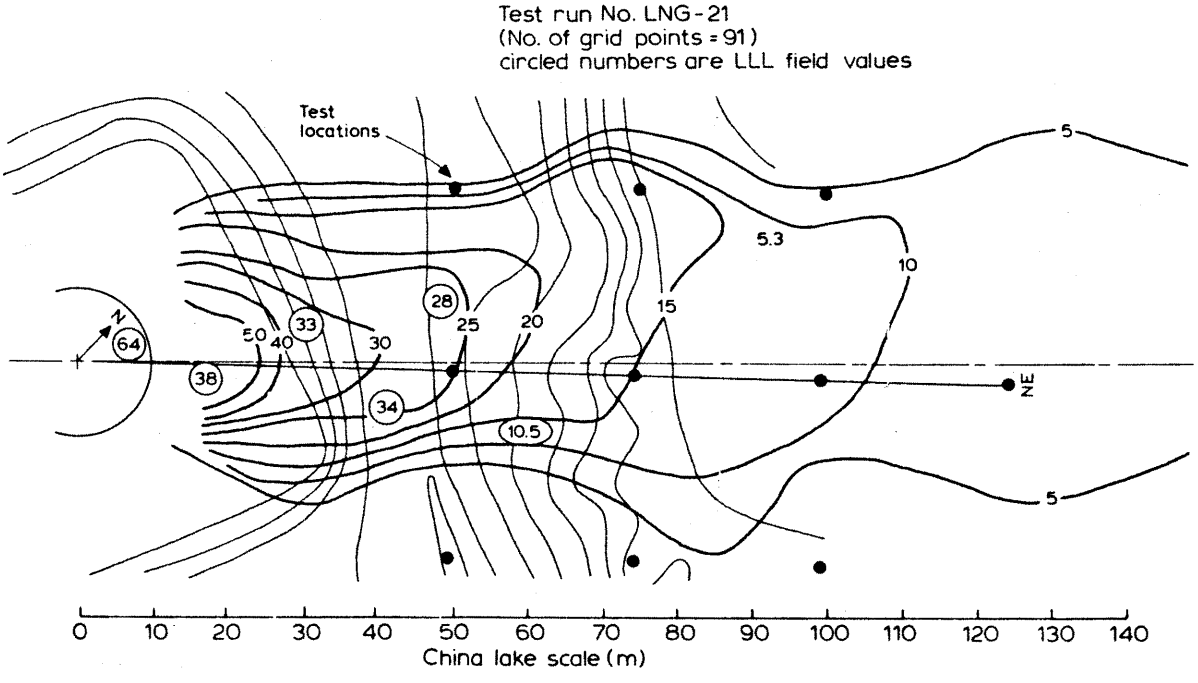

Figure 5-7. Concentration isopleth patterns for 5 m^3 China Lake test LNG - 21 (Avocet - 4)(Neff and Meroney, 1979).

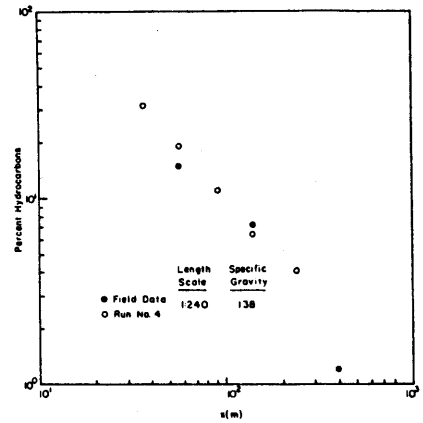

Figure 5-8. Peak plume centerline concentration decay with downwind distance at 1 m height for Burro 4 (Neff and Meroney, 1981).

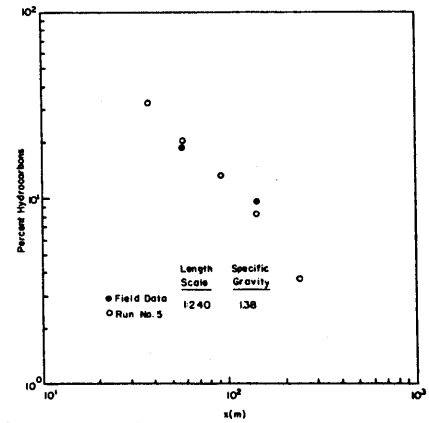

Figure 5-9. Peak plume centerline concentration decay with downwind distance at 1 m height for Burro 5 (Neff and Meroney, 1981).

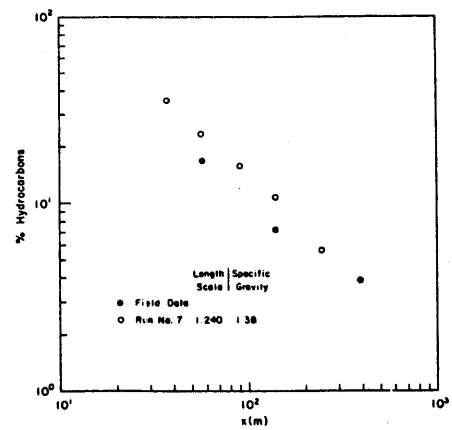

Figure 5-10. Peak plume centerline concentration decay with downwind distance at 1 m height for Burro 7 (Neff and Meroney, 1981).

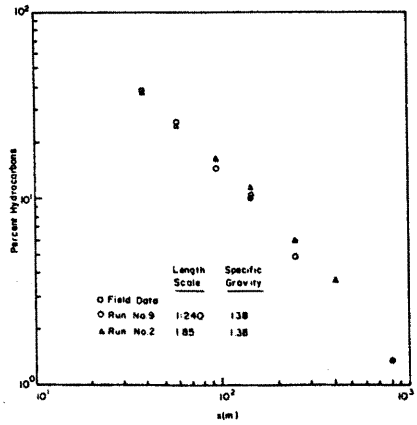

Figure 5-11. Peak plume centerline concentration decay with downwind distance at 1 m height for Burro 8 (Neff and Meroney, 1981).

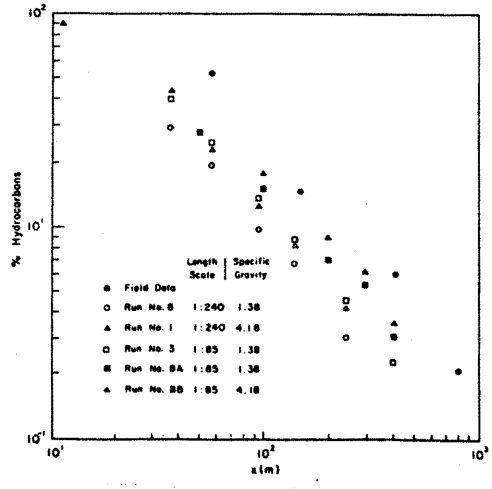

Figure 5-12. Peak plume centerline concentration decay with downwind distance at 1 m height for Burro 9 (Neff and Meroney, 1981).

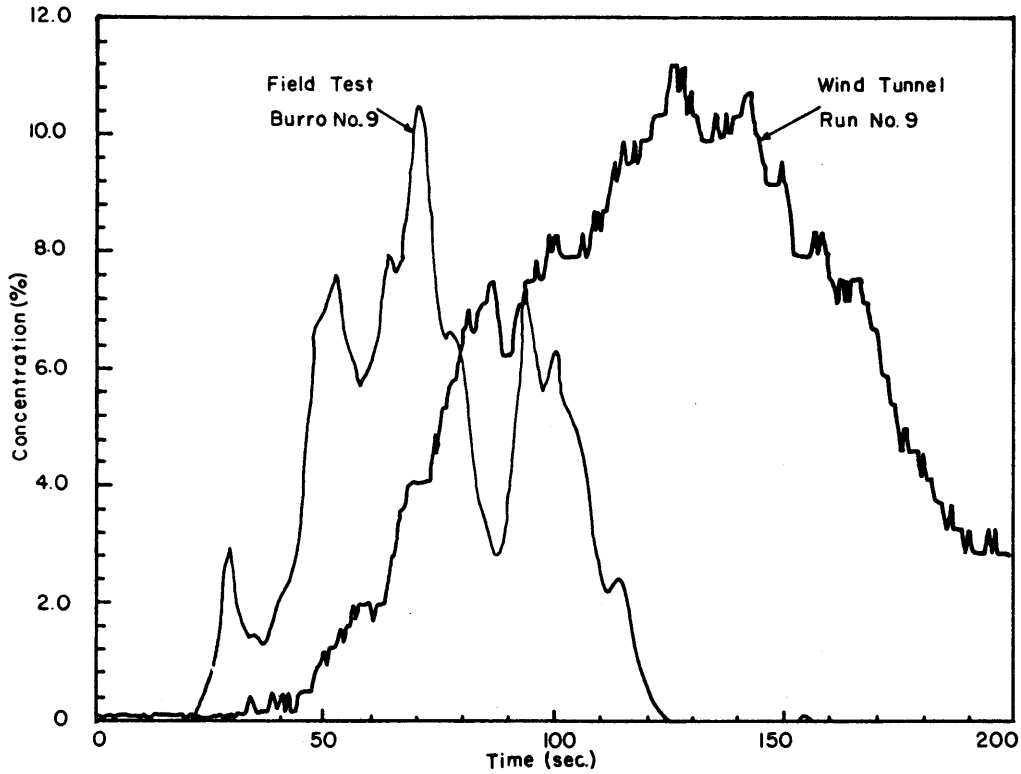

Figure 5-13. Concentration time history comparison between Burro 9 and Run 9, position T4 (Neff and Meroney, 1981).

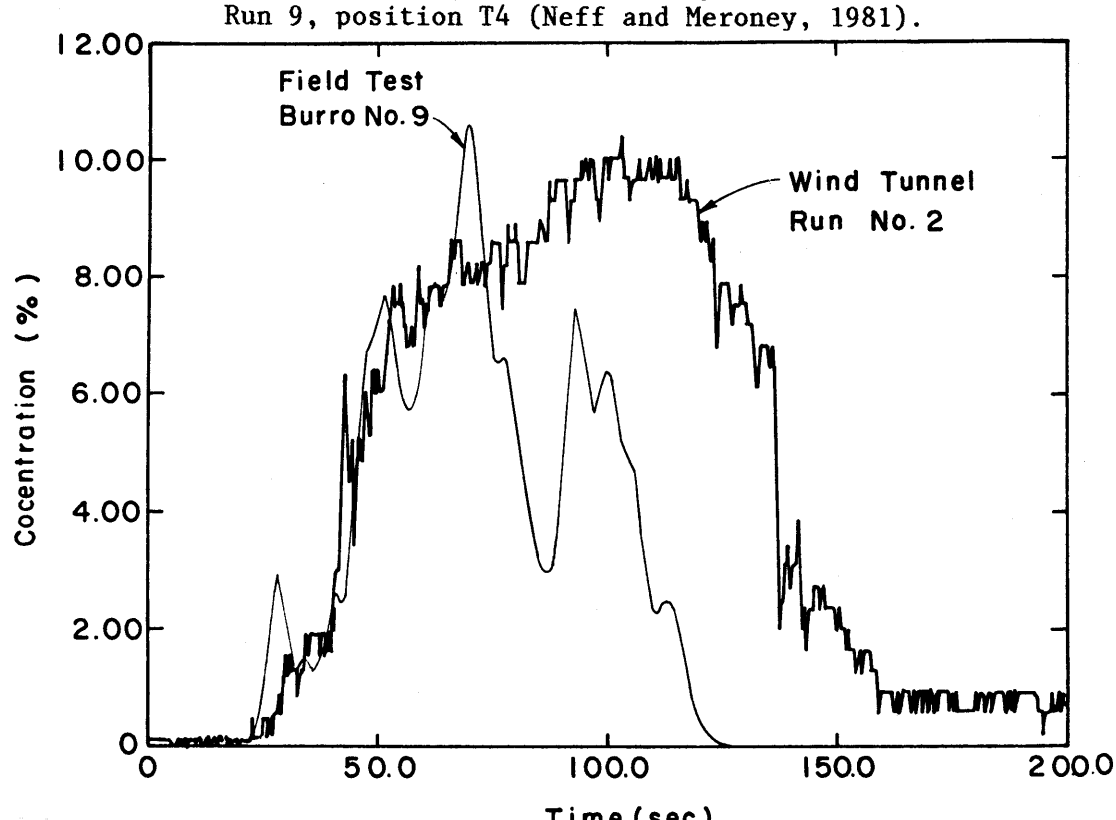

Figure 5-14. Concentration time history comparison between Burro 9 and Run 2, position T4 (Neff and Meroney, 1981).

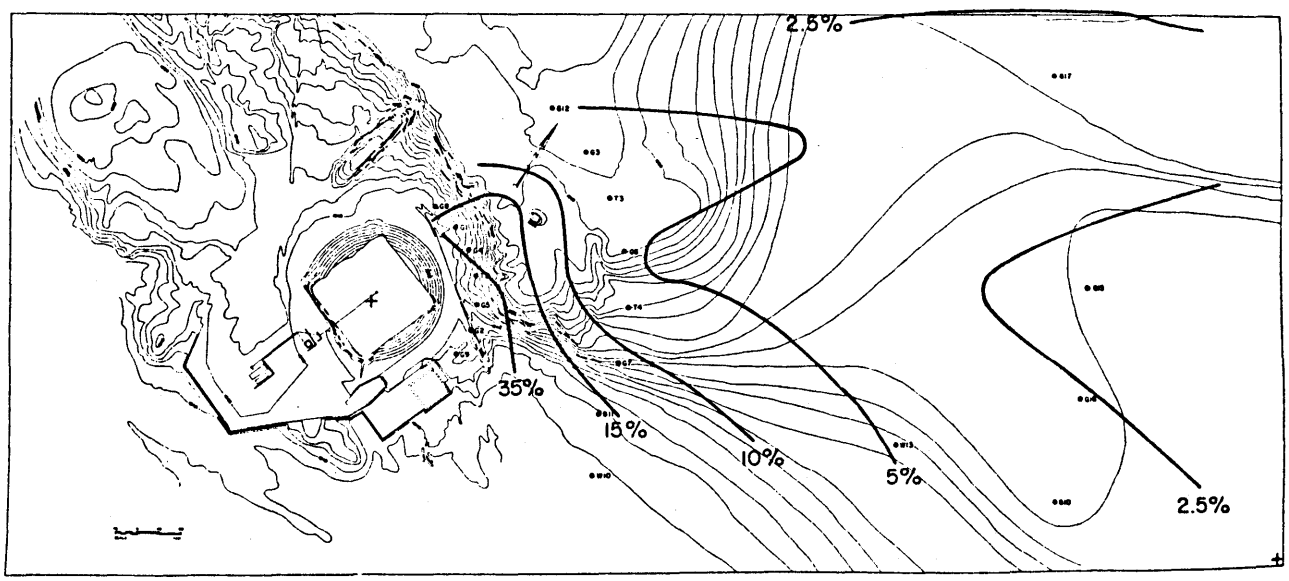

Field Results

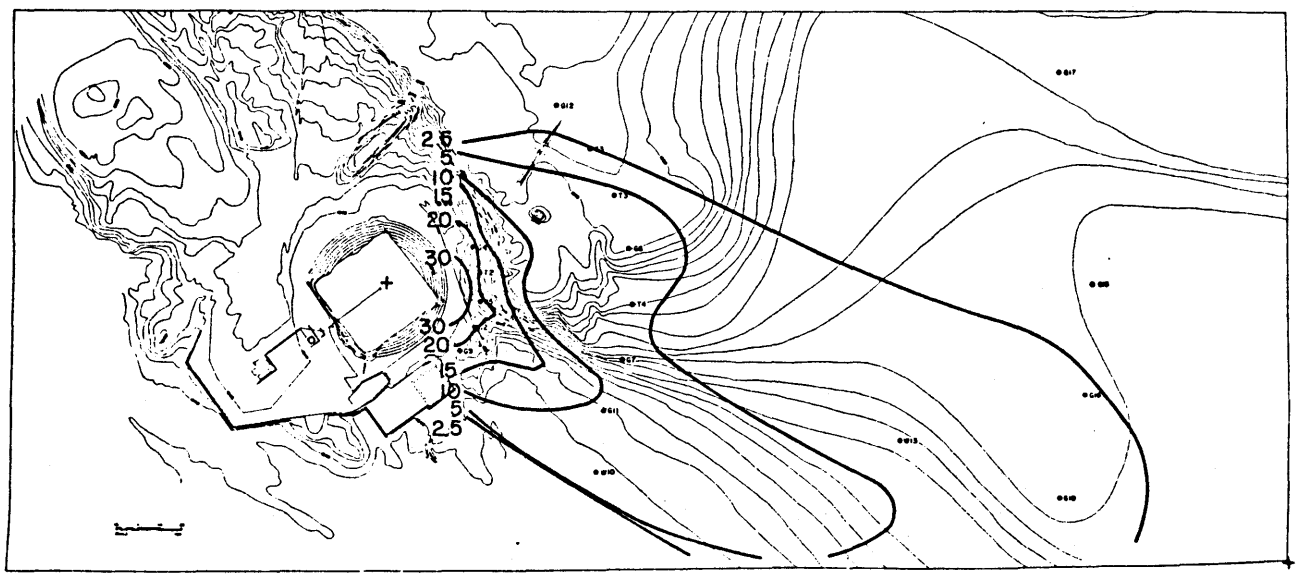

Model Results

Figure 5-15. Ground-level concentration extent comparison between Burro 8 and Run 8a, scale 1:85, $S.G._m$ = 1.38 (Meroney, 1985).

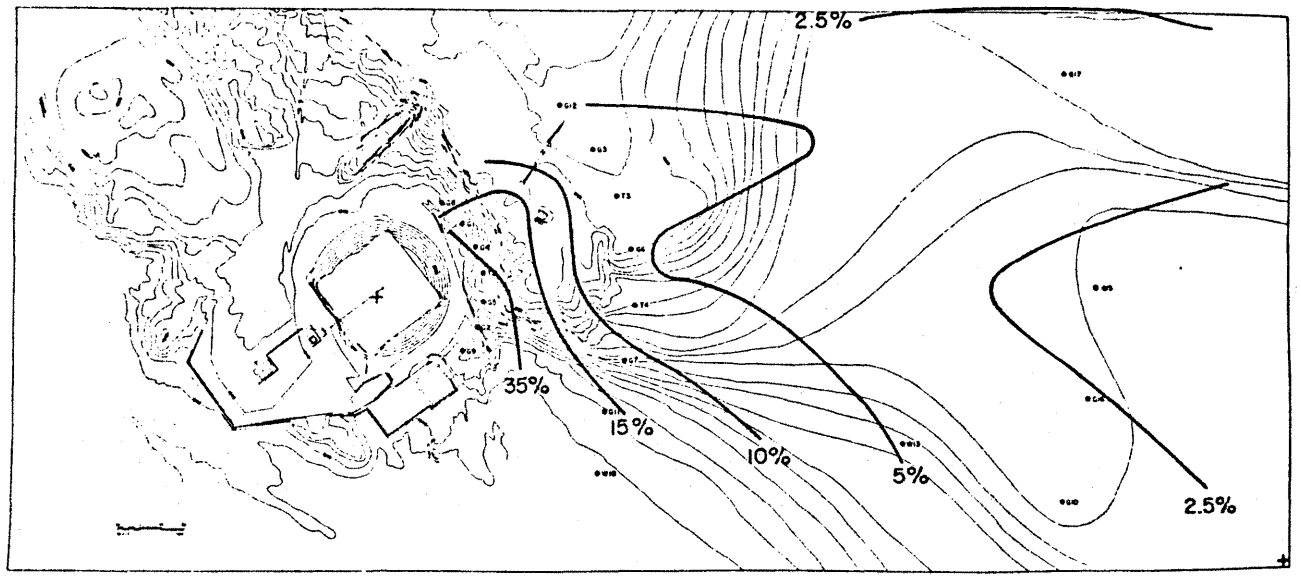

Field Results

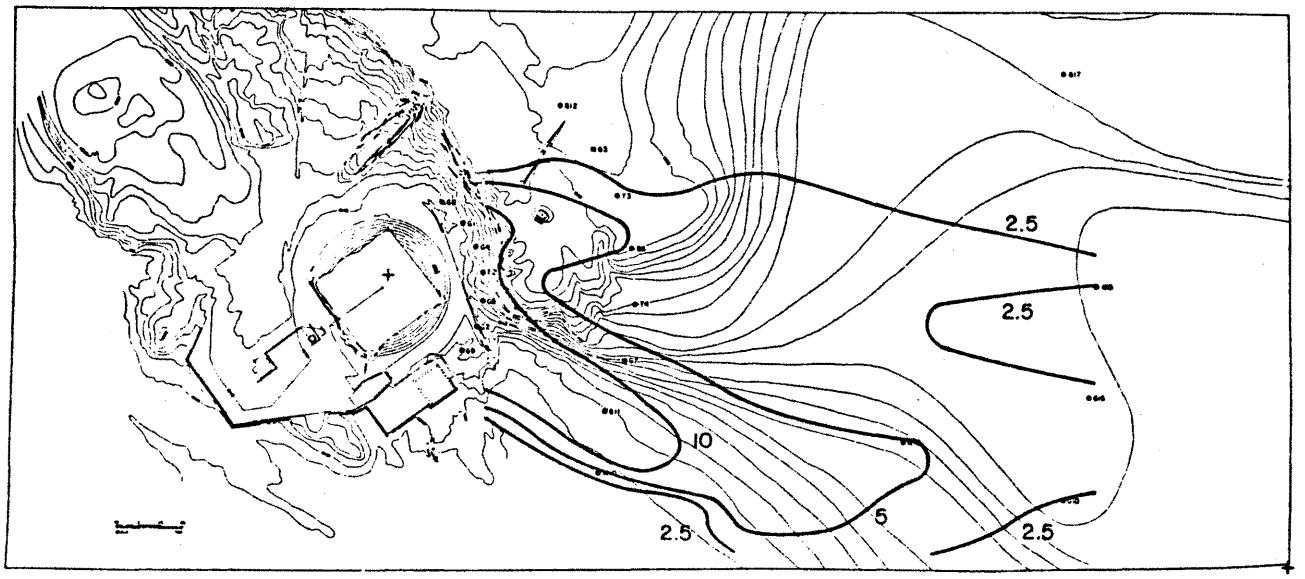

Model Results

Figure 5-16. Ground-level concentration extent comparison between Burro 8 and Run 8b, scale 1:85, $S.G._m$ = 4.18 (Meroney, 1985).

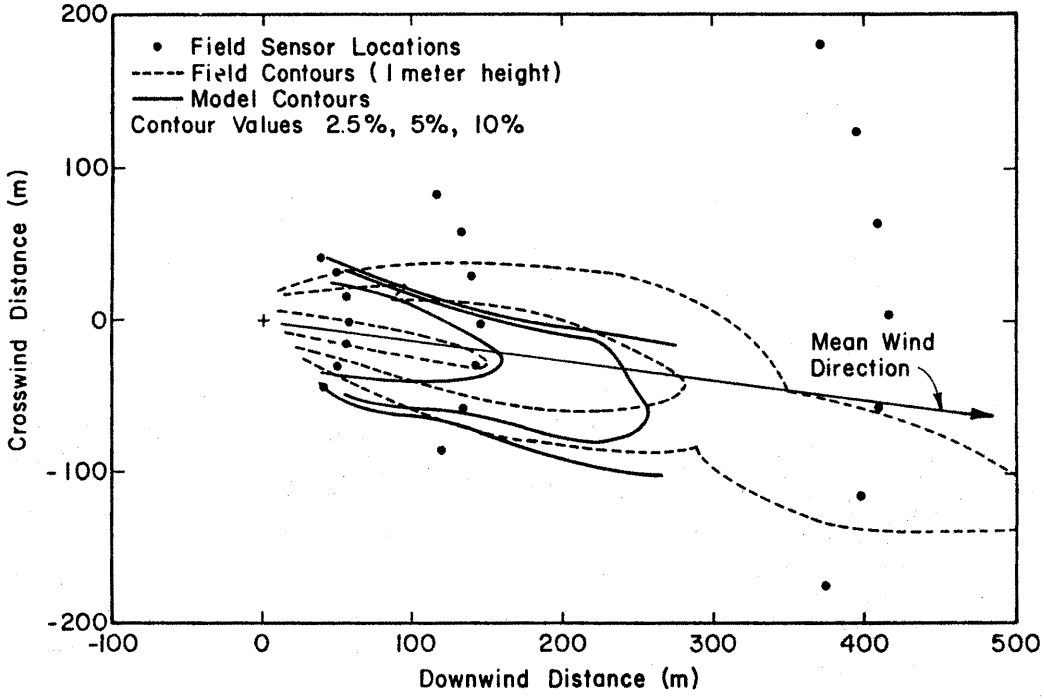

Figure 5-17. Ground-level concentration extent comparison between Burro 9 and Run 9, scale 1:240, $S.G._m$ = 1.38 (Neff and Meroney, 1981).

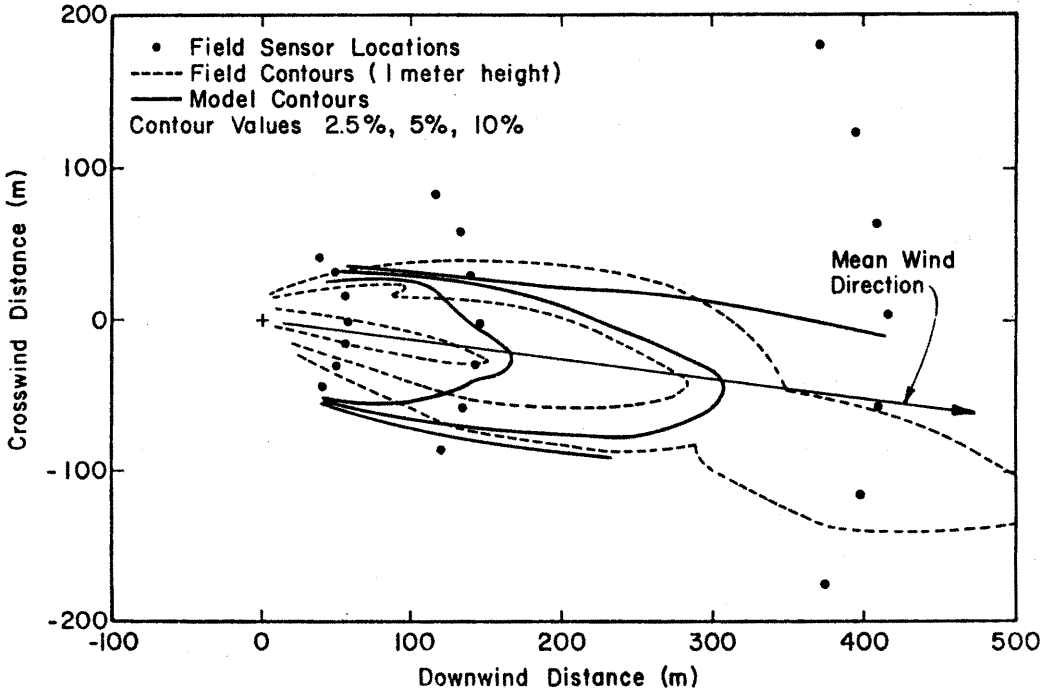

Figure 5-18. Ground-level concentration extent comparison between Burro 9 and Run 2, scale 1:85, $S.G._m$ = 1.38 (Neff and Meroney, 1981).

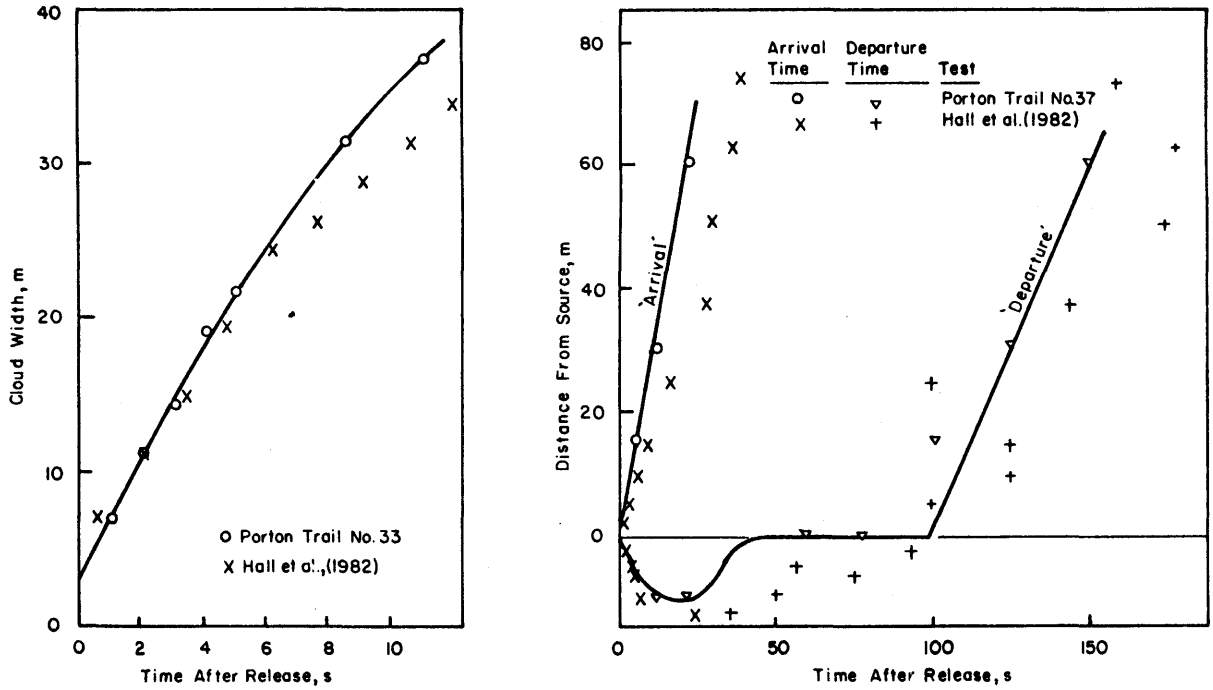

Figure 5-19. Porton trial no. 33, comparison of model/full scale cloud size and travel times (Hall et al., 1982).

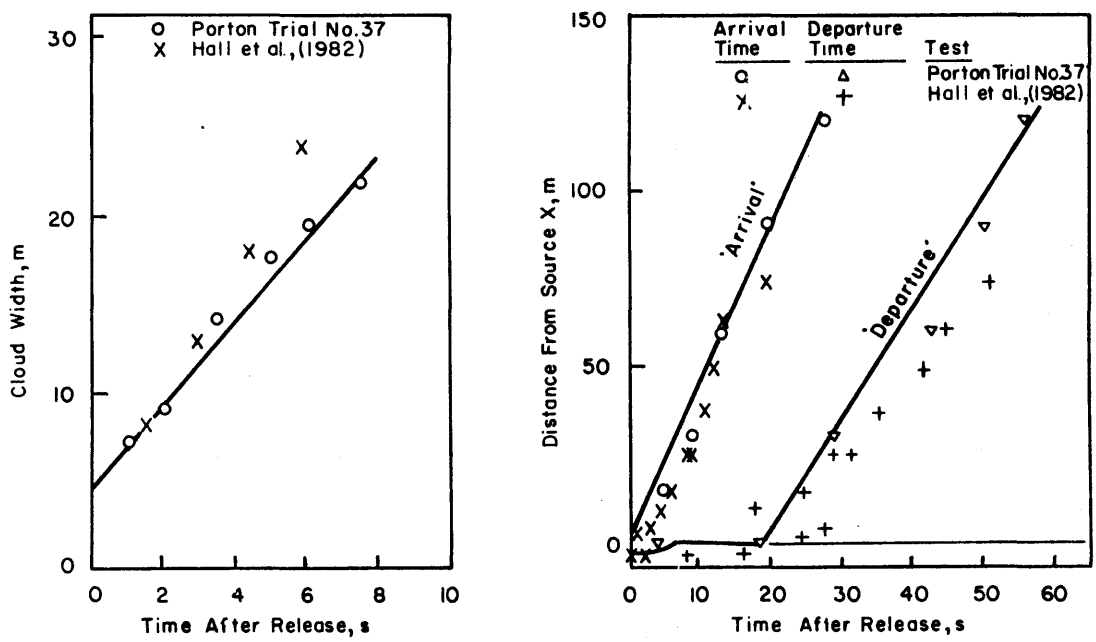

Figure 5-20. Porton trial no. 37, comparison of model/full scale cloud size and travel times (Hall et al., 1982).

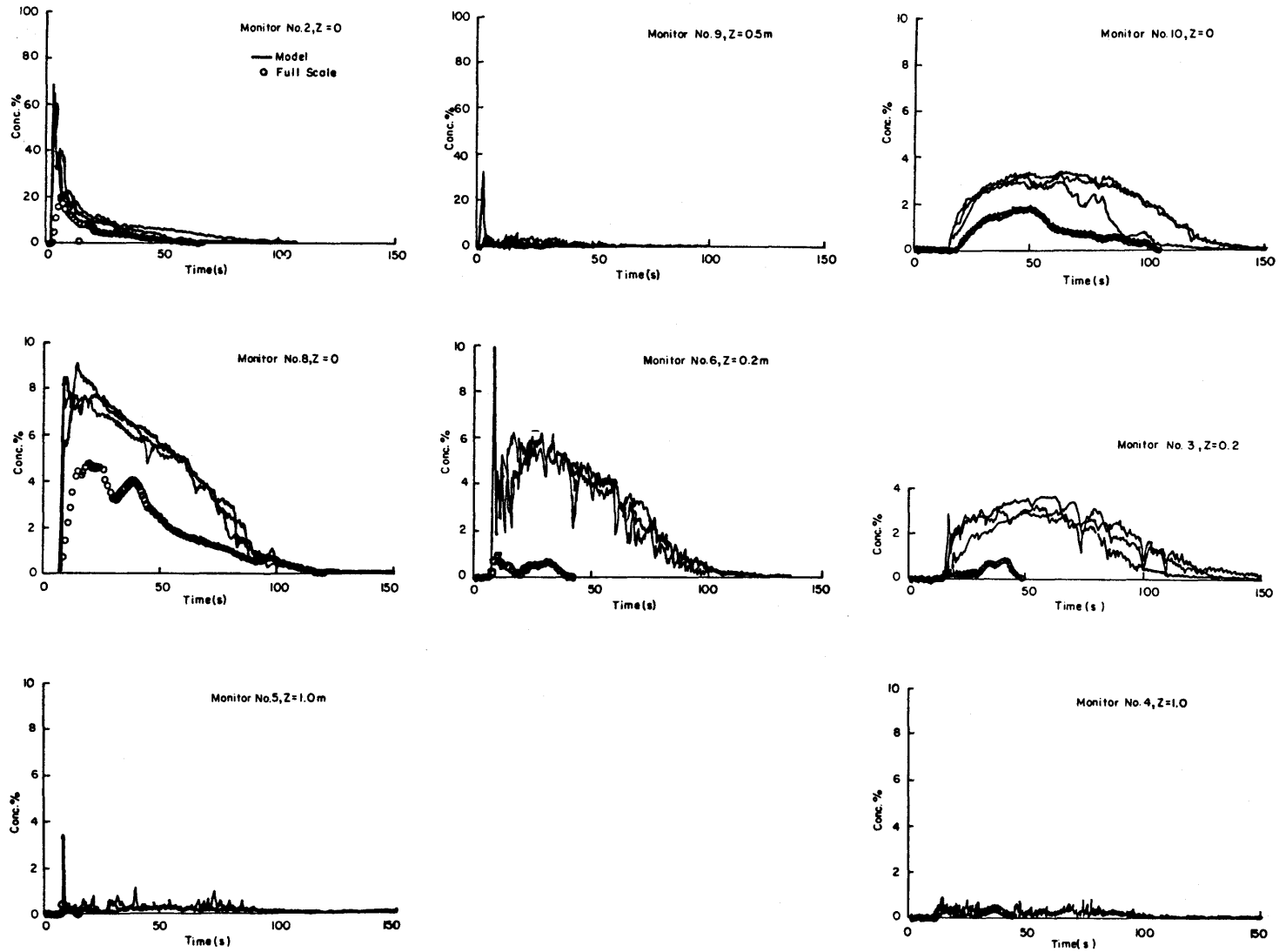

Figure 5-21. Porton trial no. 33, comparison of continuous monitor measurements with model results (Hall et al., 1982).

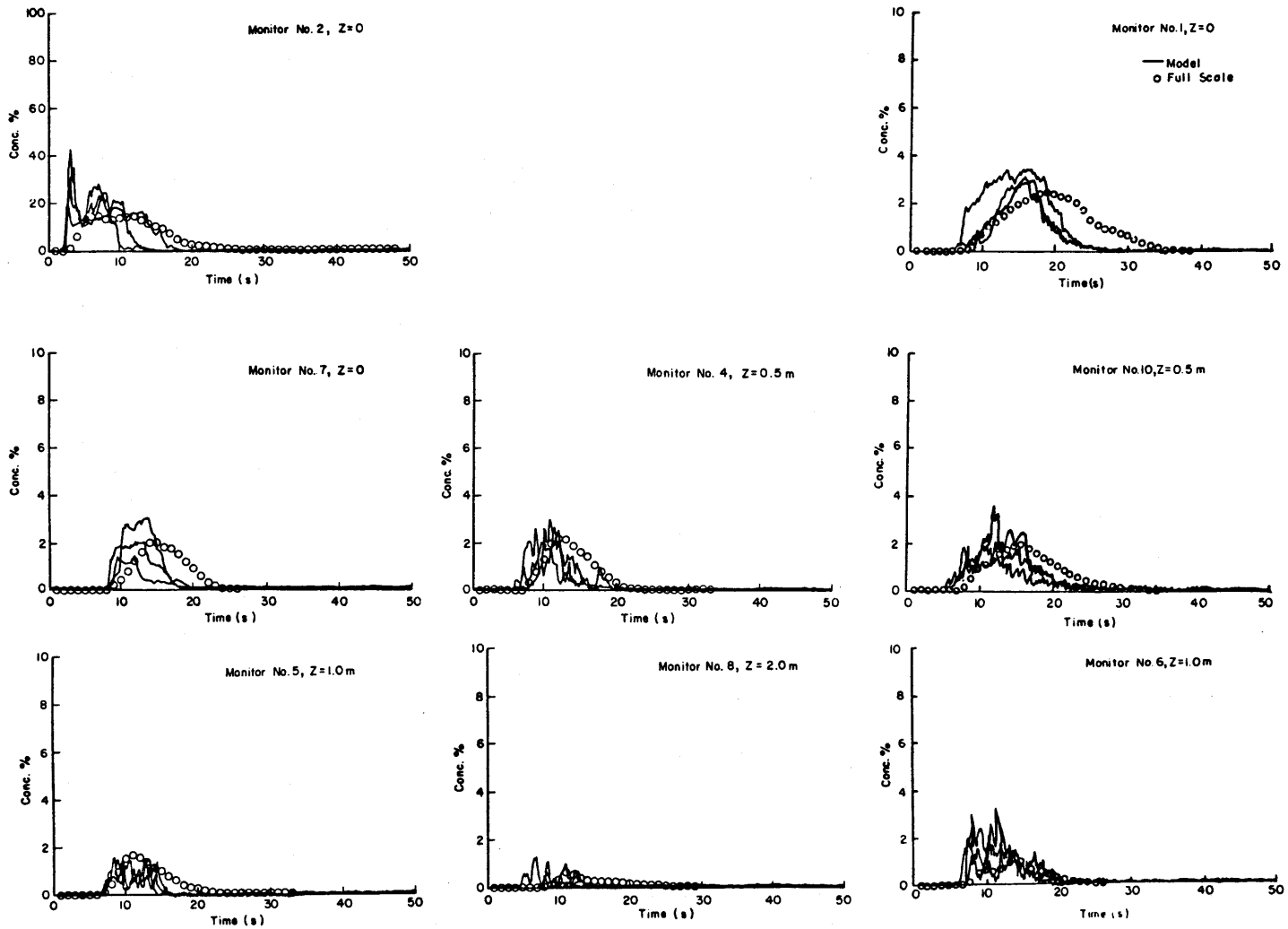

Figure 5-22. Porton trial no. 37, comparison of continuous monitor measurements with model results (Hall et al., 1982).

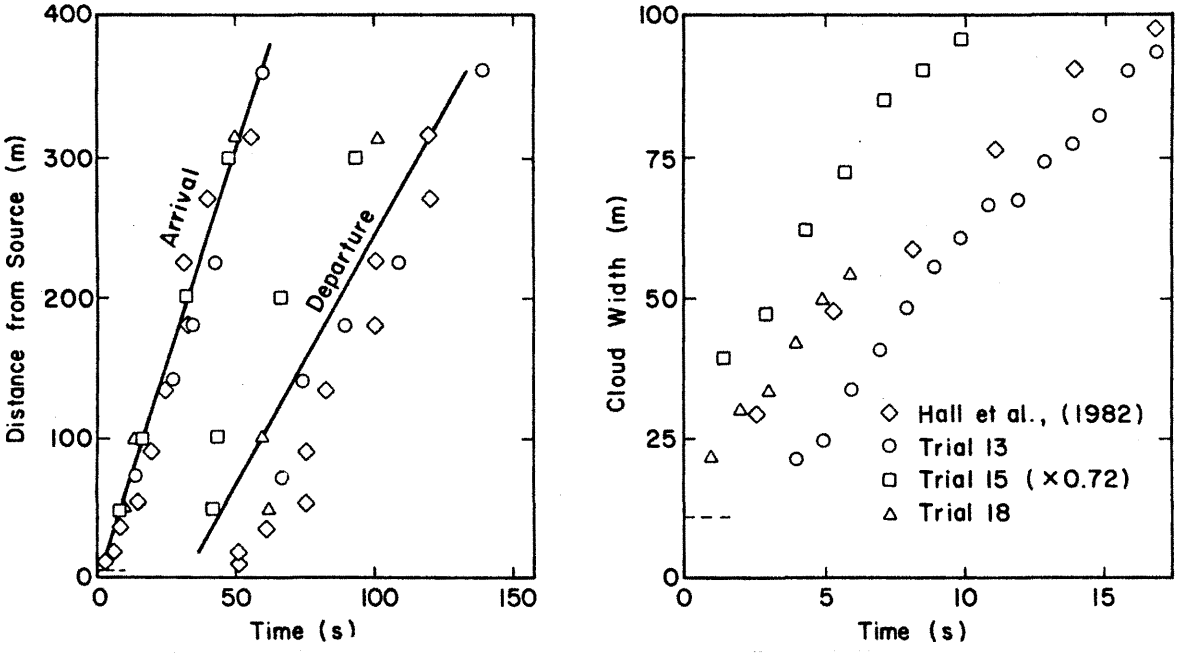

Figure 5-23. Thorney Island trial nos. 13, 15, 18. Comparison of model/full scale cloud size versus travel times (Hall and Waters, 1985).

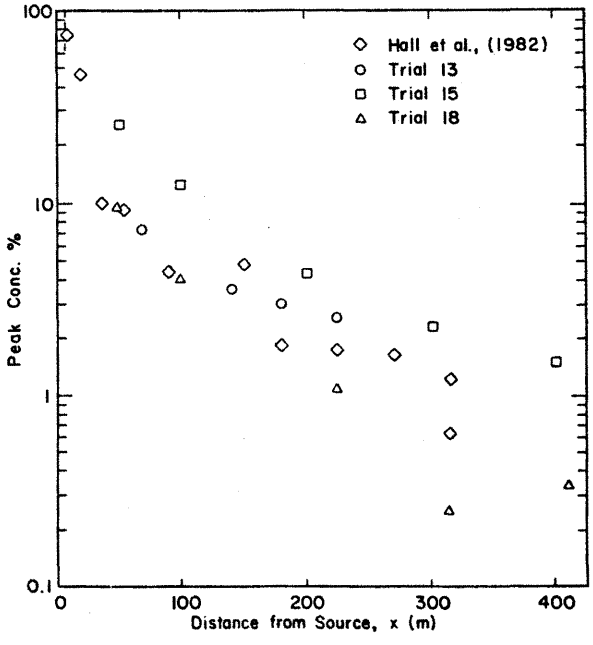

Figure 5-24. Thorney Island trial nos. 13, 15, 18. Comparison of peak ground-level concentrations along cloud centerline (Hall and Waters, 1985).

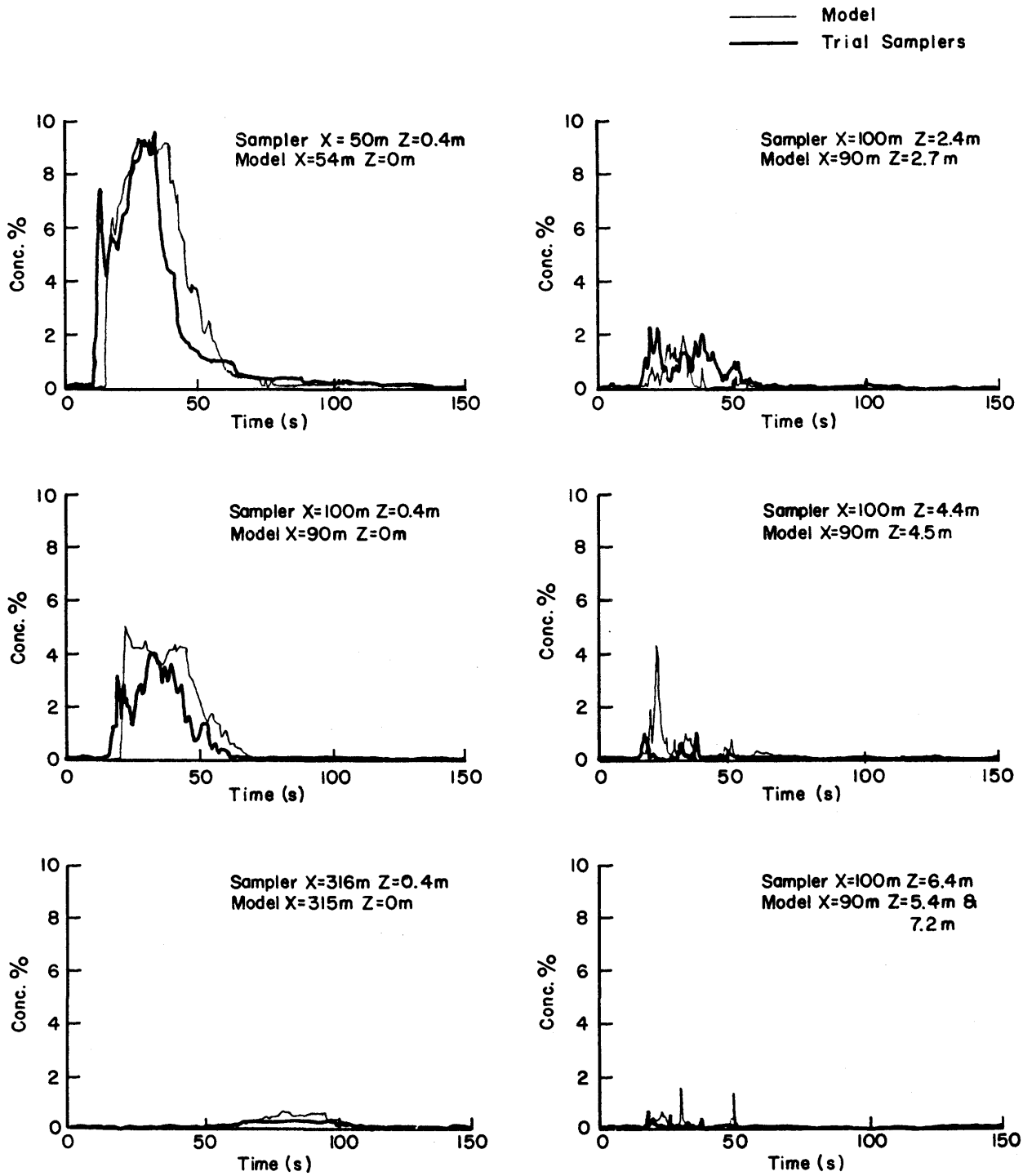

Figure 5-25. Thorney Island trial no. 18. Comparison of concentration samplers with model results (Hall and Waters, 1985).

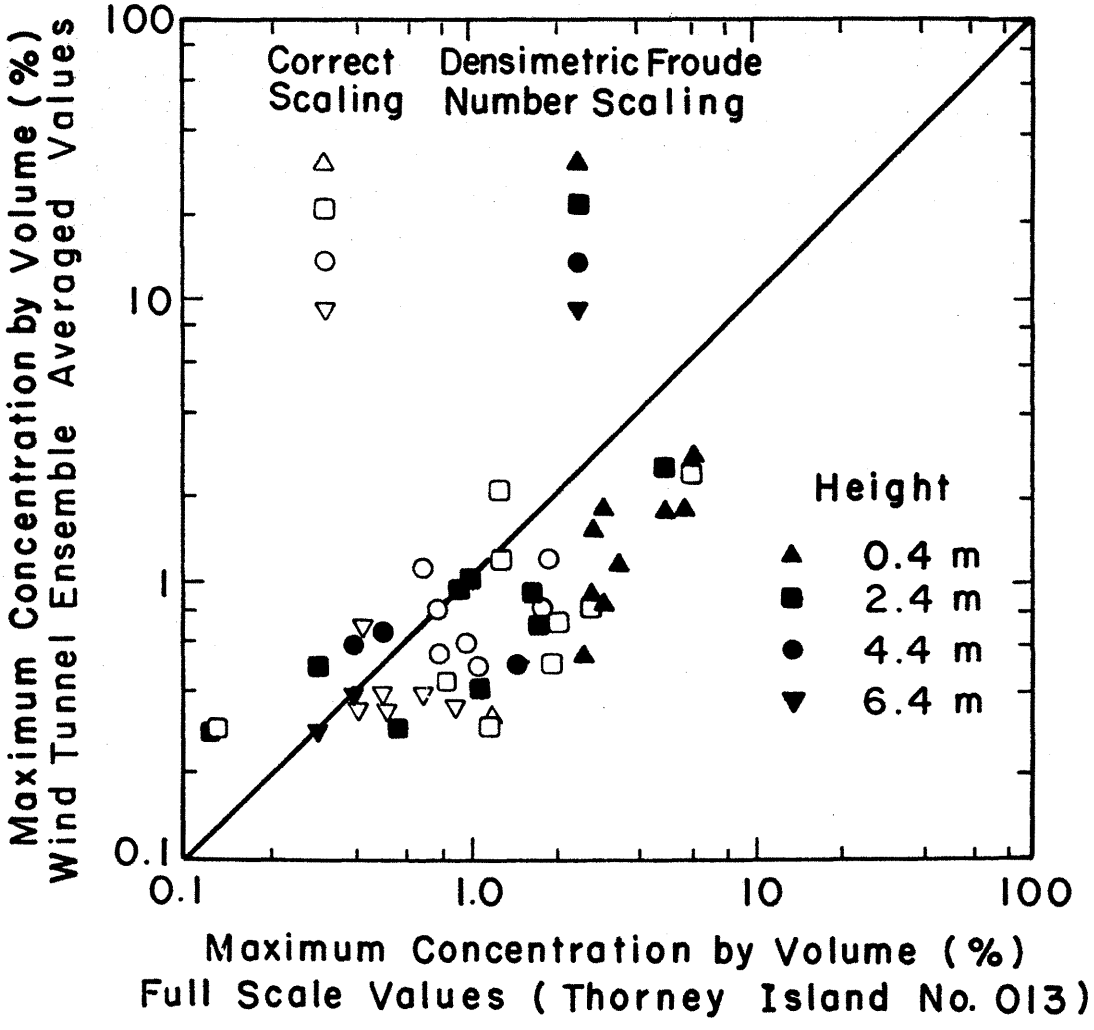

Figure 5-26. Scattergram of maximum detected concentrations obtained from full scale data (Thorney Island trial no. 13) and wind-tunnel experiments (ensemble-averaged values). (Duijm et al., 1985).

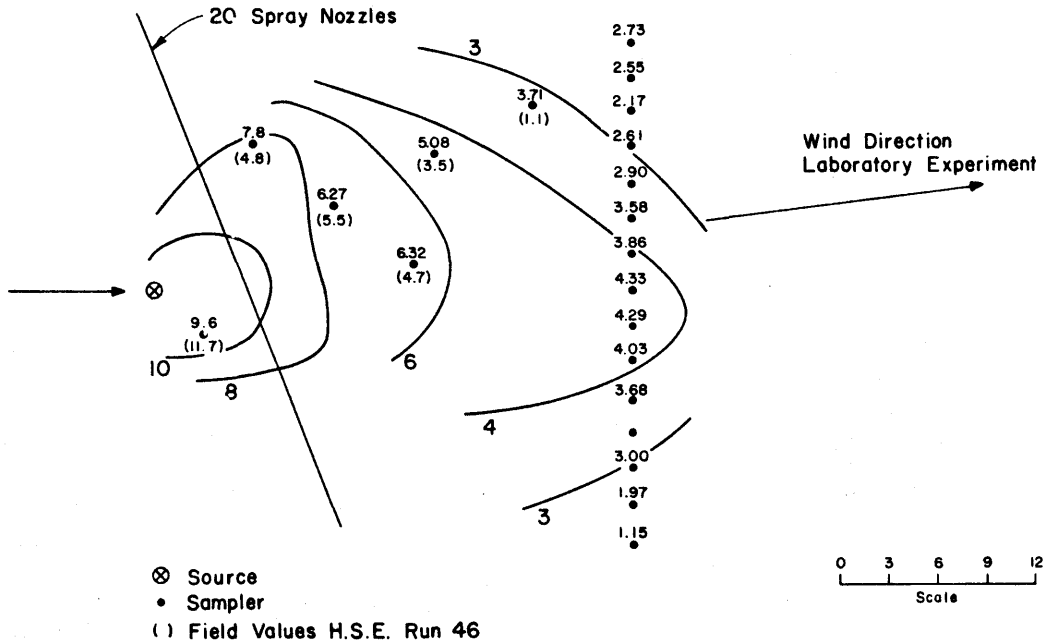

Figure 5-27. No-spray ground level concentration isopleths for HSE run no. 46 (Meroney et al., 1984).

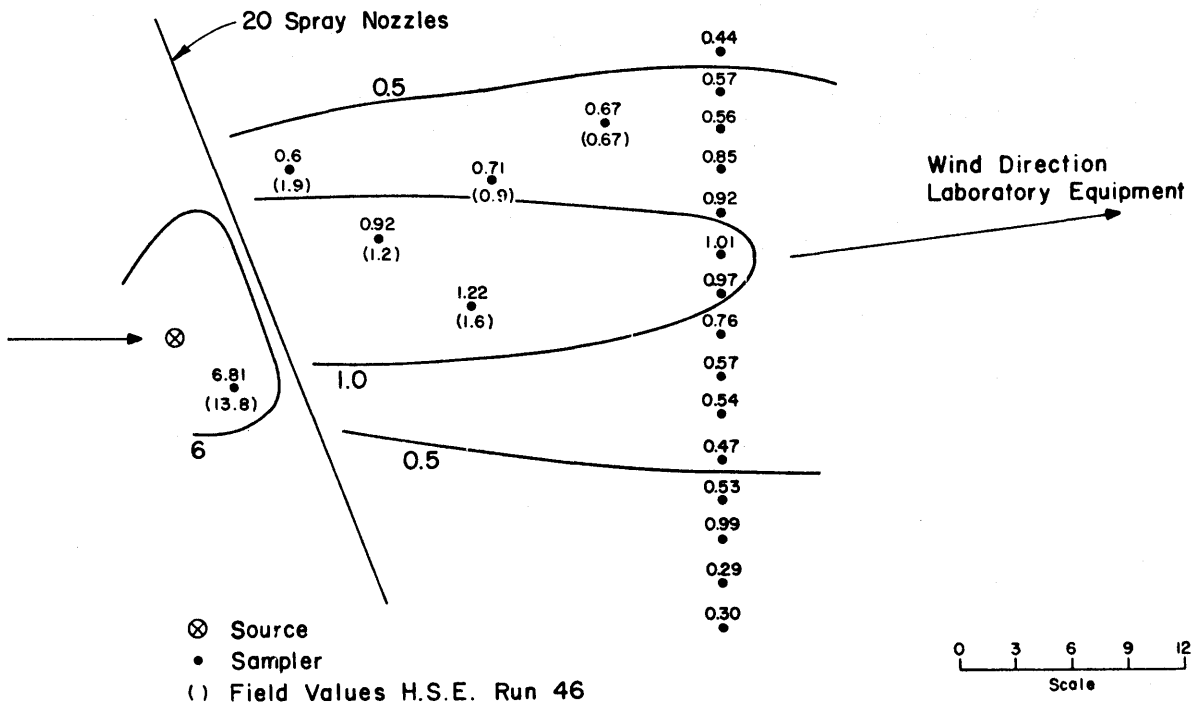

Figure 5-28. Active spray ground-level concentration isopleths for HSE run no. 46 (Meroney et al., 1984).

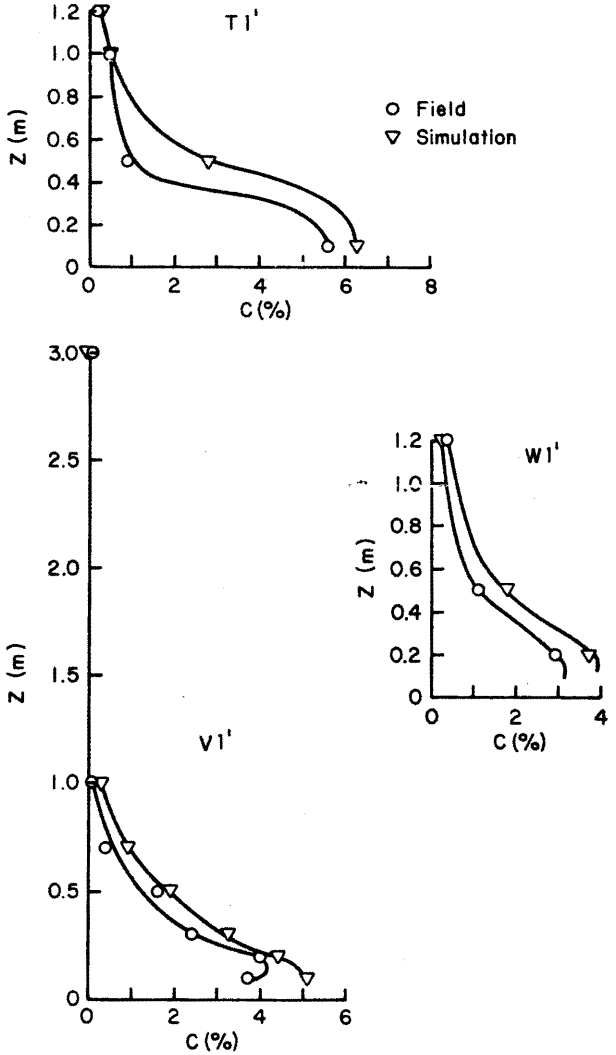

Figure 5-29. No spray vertical concentration profiles for HSE run no. 46 (Meroney et al., 1984).

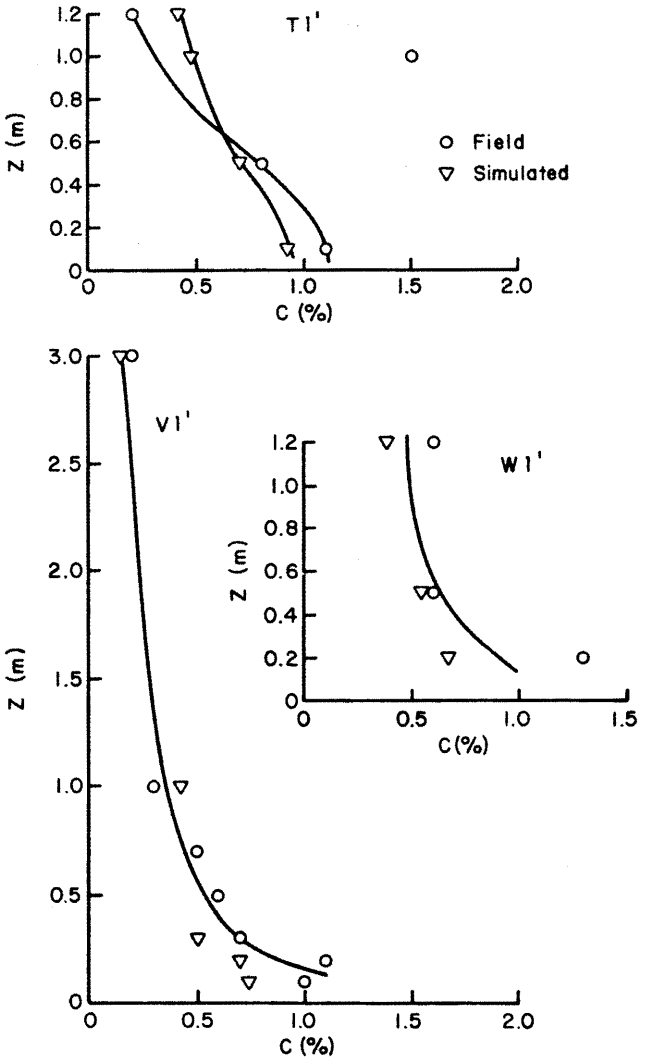

Figure 5-30. Active spray vertical concentration profiles for HSE run no. 46 (Meroney et al., 1984).

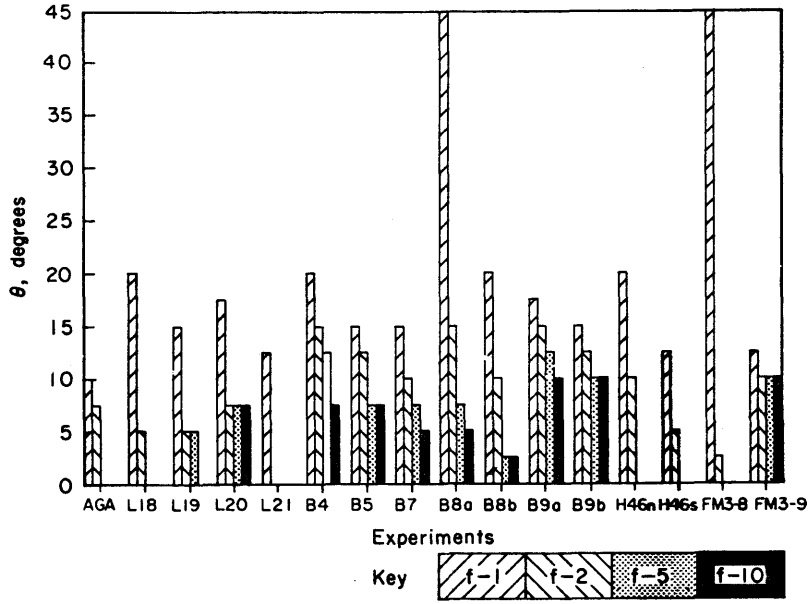

Figure 5-31.

Figure 5-31. Pattern comparison test summary bar chart for theta intercept (degrees).

Figure 5-32. Pattern comparison test summary bar chart for percent compatibility at theta angles between 0 and 7.5 degrees.

Figure 5-33. Pattern comparison test summary bar chart for percent compatibility at theta angles between 0 and 15 degrees.

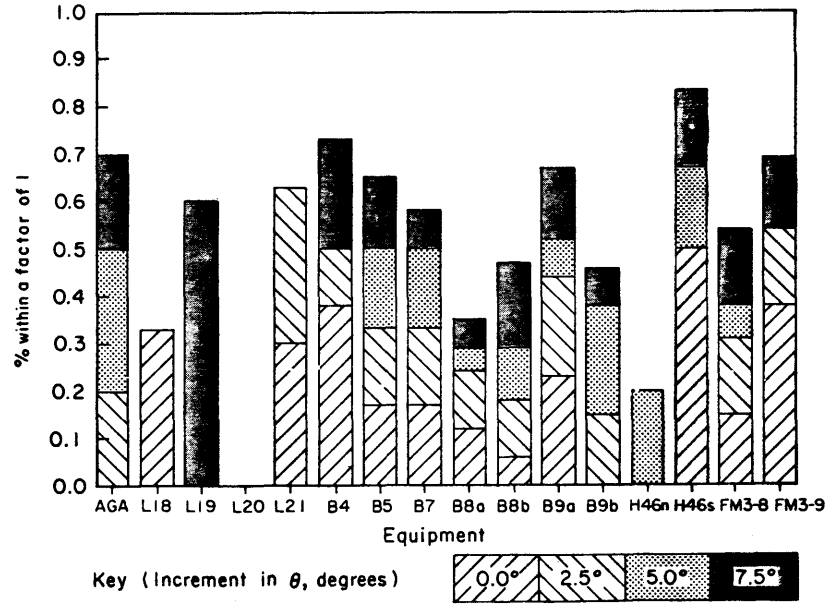

Figure 5-32.

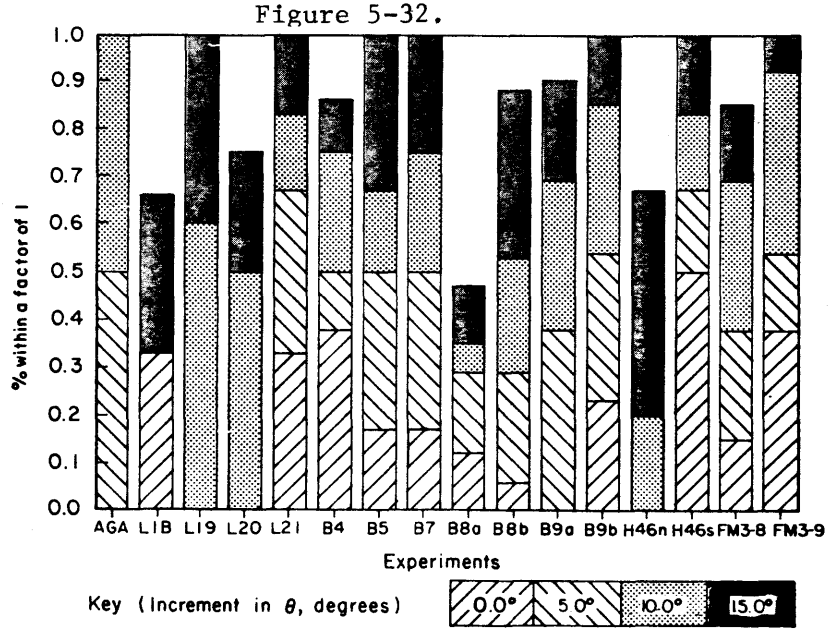

Figure 5-33.

6.0 CONCLUSIONS

There are three susinct reasons why fluid modeling retains its value in engineering analysis and health safety evaluation for LNG storage and transportaion. Duijm et al. (1985) prepared Table 6-1 comparing potential performance of mathematical and physical modeling based on the present state-of-the-art. First, note that fluid modeling does some things much better than the analytic and numerical alternatives examined. McQuaid (1985, p. 20) believes at the present time "that the physical model is much more reliable than the 3-D numerical codes." Wheatley and Webber (1984, p. II.149) observed that" the complexity and expense of the 3-D numerical models are not yet demonstrably justified by more accurate results."

Secondly, wind tunnels are, in effect, analog computers which have the advantage of "near-infinitesimal" resolution and "near-infinite" memory (Snyder, 1981). A fluid modeling study employs real fluids not models of fluids; hence, the fluid model is implicitly non-hydrostatic, non-Boussinesqu, compressible, includes variable fluid properties, non-slip boundary conditions, and dissipation. Real fluids permit flow separation and recirculation. All conservation equations are automatically included in their correct form in a laboratory model without truncation or differencing errors, and there are no missing terms or approximations.

Third, the fluid model bridges the gap between the fluid mechanician's analytic or numeric models of turbulence and dispersion, and their application in the field. Fluid modeling may be used to plan field experiments, provide conservative estimates of plume transport, and validate modules of numerical code. Wind-tunnel

simulation is likely to be most useful for near source dispersion estimates where mechanically induced turbulence is present from structures such as tanks, vapor detention systems, water sprays, etc., and where uncertainties in mathematical modeling of the complex dispersion process is greatest.

Table 6-1 POTENTIAL PERFORMANCE OF MATHEMATICAL AND PHYSICAL MODELLING (Modified from Duijm et al, 1985)

ASPECT	BOX MODEL	3D - MODEL ‡	PHYSICAL MODEL
Main model assumption	Rate of entrainment	Turbulence closure assumption	Similarity of full-scale and model-scale flow field
Model results	Averaged concentrations	Averaged concentrations	Visualization (film/video) Averaged and instantaneous concentrations
Spatial resolution	Low	Depends on grid size	Depends on measurement technique
Modelling Dispersion over flat terrain	Good	Good	Good
Modeling dispersion over obstacles	Impossible	Possible but difficult	Good
Modelling effects of atmospheric stratification	Fair to good	Fair to good	Possible but requires special facilities
Modelling effects of surface heat transfer	Good	Good	Difficult, requires special equipment. Limited conditions
Modelling effects of ambient humidity	Good	Good	Reasonable over limited conditions
Time needed, initialization of model included	Less than one day	Days to weeks, depends upon terrain complexity	Model making: weeks Separate experiment: minutes to day
Costs	Low	Medium to high	Reasonable in wind tunnel Higher in water tunnel

‡ Presumes problems with grid resolution, gradient transport assumptions, and numerical diffusivity are solved.

7.0 REFERENCES:

AGA (American Gas Association) (1974), "LNG Safety Program, Interim Report on Phase II Work," American Gas Association Project IS-3-1, Battelle Columbus Laboratories.

Alessio, S.; Briatore, L.; Elissi, G.; and Longletto, A (1981), "Hydraulic Modeling of Heavy-Gas Emission from Terrain," Il Nuovo Cimento, Vol. **4c**, N. 4, pp. 373-384.

American Meteorological Society (1983), "Synthesis of the Rural Model Reviews", prepared for Environmental Protection Agency, U.S.A., 41 pp.

Andriev, G., Neff, D.E., and Meroney, R.N. (1983), "Heat Transfer Effects During Cold Dense Gas Dispersion," Gas Research Institute Contract No. 5014-352-0203, Report GRI-83/0082, 224 pp.

Armitt, J. and Counihan, J. (1968), "The Simulation of the Atmospheric Boundary Layer in a Wind Tunnel," Atmos. Envir., Vol. 2, pp. 49-71.

Arya, S.P.S., and Plate, E.J. (1969), "Modeling of the Stably Stratified Atmospheric Boundary Layer," J. Atmos. Sci., Vol. 26, No. 4, pp. 656-665.

Arya, S.P.S., (1968), "Structure of Stably Stratified Turbulent Boundary Layer," Ph.D. Thesis, Civil Engineering Department, Colorado State University, 157 pp.

Arya, S.P.S. (1975), "Buoyancy Effects in a Horizontal Flat-Plate Boundary Layer," J. Fluid Mech., Vol. 68, Pt. 2, pp. 321-343.

Arya, S.P.S. (1977), "Suggested Revisions to Certain Boundary Layer Parameterization Schemes Used in Atmospheric Circulation Models, Mon. Wea. Review, Vol. 105, No. 2, pp. 215-226.

Barad, M.L., Ed. (1958), Project Prairie Grass: A Field Program in Diffusion, Geophysical Research Papers, No. 59, Vols. I and II, Report AFCRC-TR-58-235, Air Force Cambridge Research Center.

Barnett, K.M. (1964), "The Investigation of Atmospheric Phenomena by Use of Wind Tunnels," U.S. Army, Electronics Research and Development Activity, Fort Huachuca, Arizona, Meteorological Research Note 7, Report USAERDAA MET-2-64, 63 pp.

Barrell, A.C. and McQuaid, J. (1985), "The HSE Program of Research and Model Development on Heavy Gas Dispersion," I. Chemical Eng. Symposium on the Assessment and Control of Major Hazards, Manchester, U.K., 22-24 April, 17 pp.

Batchelor, G.K. (1953), "The Conditions for Dynamical Similarity of Motions of a Frictionless Perfect-Gas Atmosphere," Quart. J. Roy. Meteorol. Soc., Vol. 79, pp. 229-235.

Beghin, P., Hopfinger, E.J., and Britter, R.E. (1981), "Gravitational Convection From Instantaneous Sources on Inclined Boundaries," J. Fluid Mech., Vol. **107**, pp. 407-422.

Binkowski, F.S. (1979), "A Simple Semi-Empirical Theory for Turbulence in the Atmospheric Surface Layer," Atmos. Envir., Vol. 13, No. 2, pp. 247-253.

Bosanquet, C.H. and Pearson, J.L. (1936), "The Spread of Smoke and Gases from Chimneys," Trans. Faraday Society, Vol. **32**, p. 1249.

Bowne, N.E., and Londergan, R.J. (1983), "Overview, Results and Conclusions for the EPRI Plume Model Validation and Development Project: Plains Site," EPRI Report EA-3074, 234 pp.

Bowne, N.E., and Londergan, R.J. (1985), "Summary of Results and Conclusions for the EPRI Plume Model Validation and Development Project: Moderately Complex Terrain Site," EPRI Report EA-3755, 188 pp.

Bowne, N.E., Londergan, R.J., Minott, D.H. and Murray, D.R. (1981), "Preliminary Results from the EPRI Plume Model Validation Project - Plains Site," EPRI Report EA-1788.

Bowne, N.E., Londergan, R.J., Murray, D.R. and Borenstein, H.S. (1983), "Overview, Results, and Conclusions for the EPRI Plume Model Validation and Development Project: Plains Site," EPRI Report EA-3074.

Bradley, C.I. and Carpenter, R.J. (1983), "The Simulation of Dense Vapour Cloud Dispersion Using Wind Tunnels and Water Flumes," 4th International Symposium on Loss Prevention and Safety Promotion in the Process Industries, The Institution of Chemical Engineers Symposium Series No. 80, EFCE Publication Series No. 33, Vol. 1, pp. F56-F65.

Briggs, G.A. (1969), "Plume Rise", U.S. Atomic Energy Commission, AEC Critical Review Series, 81 pp.

Briggs, G.A. (1984), "Diffusion Modeling with Convective Scaling and Effects of Surface Inhomogeneities", AMS Specialty Conference on Air Quality Modeling of the Urban Boundary Layer, 29 November - 2 December, Baltimore, MD, 43 pp.

Briggs, G.A. and Snyder, W.H. (1980), "Laboratory Measurements of Plume Rise in Calm, Stable Surroundings," Envir. Prot. Agcy. Rpt. to be published.

Britter, R.E. (1979), "The Spread of a Negatively Buoyant Plume in a Calm Environment," Atmos. Envir., Vol. **13**, pp. 1241-1247.

Britter, R.E. (1980), "The Ground Level Extent of a Negatively Buoyant Plume in a Turbulent Boundary Layer," Atmos. Envir., Vol. **9**, pp. 779-785.

Britter, R.E. and Linden, P.F. (1980), "The Motion of the Front of a Gravity Current Traveling Down an Incline," J. Fluid Mech., Vol. **99**, pp. 531-543.

Carn, K.K. and Chatwin, P.C. (1984), "Variability and Heavy Gas Dispersion," Special issue of J. Hazardous Materials, Sheffield Symposium on Thorney Island Trials, 32 pp.

Castro, I.P., Jackson, N.A., and Robins, A.G. (1975), "The Structure and Development of a 2 m Simulated Suburban Boundary Layer," Central Electric Generating Board Research Report R/M/N800,Marchwood Engrg. Lab., Southampton, U.K.

Cermak, J.E. (1958), "Wind Tunnel for the Study of Turbulence in the Atmospheric Surface Layer," Dept. of Civil Engineering, Colorado State University, Fort Collins, Report CER58-JEC-42, 40 pp.

Cermak, J.E. (1975), "Applications of Fluid Mechanics to Wind Engineering--A Freeman Scholar Lecture," J. of Fluids Engineering, Vol. 97, pp. 9-38.

Cermak, J.E. (1982), "Physical Modeling of the Atmospheric Boundary Layer (ABL) in Long Boundary-layer Wind Tunnels (BLWT)," Proceedings of the Wind Tunnel Modeling in Civil Engineering Conference, Gaithersburg, MD., pp. II.2-1 to II.2-41.

Cermak, J.E., Shrivastava, P.K., and Poreh, M. (1983), "Wind-tunnel Research on the Mechanics of Plumes in the Atmospheric Surface Layer," Civil Engineering Department Report CER83-84JEC-PKS-MP12, Colorado State University, Fort Collins, CO, Annual Progress Report to U.S. Dept. of Army Contract DAAK11-82-K-0004, 140 pp.

Chan, S.T. and Ermak, D.L. (1983), "Recent Progress in Modeling the Atmospheric Dispersion of Heavy Gases Over Variable Terrain Using the Three-Dimensional Conservation Equations," IUTAM Symposium on Atmospheric Dispersion of Heavy Gases and Small Particles, Delft University of Technology, The Netherlands, 29 August to 2 September, 1983, 32 pp.

Chaudhry , F.H. and Meroney, R.N. (1973), "A Laboratory Study of Diffusion in Stably Stratified Flow," Atmos. Envir., Vol. 7, pp. 443-454.

Cheah, S.C. Cleaver, J.W. and Millward A. (1983), ""The Physical Modelling of Heavy Gas Plumes in a Water Channel," 4th International Symposium on Loss Prevention and Safety Promotion in the Process Industries, The Institution of Chemical Engineers Symposium Series No. 80, EFCE Publication Series No. 33, Vol. 1, pp. F35-F44

Cheah, S.C., Chua, S.K., Cleaver, J.W. and Millward, A. (198), "Modelling of Heavy Gas Plumes in a Water Channel," 2nd Battelle Symposium on Heavy Gases and Risk Analysis, pp. 199-210.

Chuang, H., and Cermak, J.E. (1967), "Similarity of Thermally Stratified Shear Flows in the Laboratory and Atmosphere," The Physics of Fluids Supplement, Vol. 10, Part II, No. 9, Proceedings of an International Symposium on Boundary Layers and Turbulence With Geophysical Applications, Kyoto, Japan, Sept. 1966,1967, pp. S255-S258.

Colenbrander, G.W. and Puttock, J.S. (1983), "Maplin Sands Experiments 1980: Interpretation and Modeling of Liquefied Gas Spills onto the Sea," Atmospheric Dispersion of Heavy Gases and Small Particles, IUTAM Symposium Delft 1983, ed. G. Ooms and H. Tennekes, Springer-Verlag, Berlin, 1984, pp 277-295.

Colenbrander, G.W. and Puttock, J.S. (1984) Personal communication.

Corrsin, S. (1961), "Theories of Turbulent Dispersion," Mechanique de la Turbulence, Marseille, France, pp. 27-52.

Counihan, J. (1969), "An Improved Method of Simulating an Atmospheric Boundary Layer in a Wind Tunnel," Atmos. Envir., Vol. 3, pp. 197-214.

Counihan, J. (1975), "Adiabatic Atmospheric Boundary Layers: A Review and Analysis of Data from the Period 1880-1972,", Atmos. Envir., Vol. 9, pp. 871-905.

Crapper, P.F. and Baines, W.D. (1977), "Non-Boussinesq Forced Plumes," Atmos. Envir., Vol. **11**, pp. 415-420.

Crapper, P.F. and Baines, W.D. (1978), "Some Remarks on Non-Boussinesq Forced Plumes," Atmos. Envir., Vol. **12**, pp. 1939-1941.

Dagliesh, W.A. (1975), "Comparison of model/full-scale wind pressures on a high-rise building," J. Industrial Aerodynamics, Vol. **1**, pp. 55-66.

Deardorff, J.W. (1972), "Numerical Investigation of Neutral and Unstable Planetary Boundary Layers," J.- Atmos. Sci., Vol. 29, pp. 91-115.

de Nevers, Noel (1984), "Spread and Down-Slope Flow of Negatively Buoyant Clouds," Atmospheric Environment, Vol. 18, No. 10, pp. 2023-2027.

Draxler, R.R. (1976), "Determination of atmospheric diffusion parameters," Atmos. Envir., Vol. **10**, pp. 99-105.

Duijm, N.J., van Ulden, A.P., and van Heugten, W.H.H. (1985), "Physical and Mathematical Modeling of Heavy Gas Dispersion - Accuracy and Reliability," 15th International Technical Meeting on Air Pollution Modelling and Its Applications, Washington University, St. Louis, 16-19 April 1985, 17 pp.

Dutton, J.A., Panofsky, H.A., Larko, D., Shirer, H.N., Stone, G., and Vilardo, M. (1980), "Statistics of wind fluctuations over complex terrain," Final Report, DOE ET-28-S-06-1110.

Eidsvik, Karl J. (1980), "A Model for Heavy Gas Dispersion in the Atmosphere," Atmospheric Environment, Vol. 14, pp. 769-777.

Egan, B.A.; Fox, D.G.; Hanna, S.R.; Randerson, D.; and White, F. (1981), "Air Quality Modeling and the Clean Air Act: Recommendations to EPA on Dispersion Modeling for Regulatory Applications," American Meteorological Society, Boston, Massachusetts, 1981, 288 pp.

ESDU (1974), "Characteristics of Atmospheric Turbulence Near the Ground," Engineering Science Data Unit Reports 74030 and 74031.

Fackrell, J.E. and Pearce, J.E. (1981), "Parameters Affecting Dispersion in the Near Wake of Buildings," Central Electricity Generating Board, Report RD/M/1179N81, Marchwood Engineering Laboratories, U.K., 41 pp.

Fackrell, J.E. and Robins, A.G. (1982a), "The Effects of Source Size on Concentration Fluctuations in Plumes," Boundary Layer Meteorology, Vol. **22**, pp 335-350.

Fackrell, J.E. and Robins, A.G. (1982b), "Concentration Fluctuations and Fluxes in Plumes from Point Sources in a Turbulent Boundary Layer," J. Fluid Mech., Vol. **117**, pp. 1-26.

Fage, A. and Warsap, J.H. (1929), "Effects of Turbulence and Surface Roughness on Drag of Circular Cylinders," U.K., ARC R&M 1283.

Farell, C., Carrasquel, S., Guven, O., and Patel, V.C. (1977), "Effect of Wind-Tunnel Walls on the Flow Past Circular Cylinders and Cooling Tower Models," J. of Fluids Engineering, Vol. **99**, pp. 470-479.

Fay, J.F. and Ranck, D.A. (1983), "Comparison of Experiments on Dense Gas Cloud Dispersion," Atmos. Envir., Vol. **17**, No. 2, pp. 239-248.

Fay, J.A. and Zemba, S. (1985a), "The Lateral Extent of a Dense Gas Plume Near the Source," ASME Intl. Symposium on Modeling Environmental Flows, New York, 1985, pp 1-4.

Fay, J.A. and Zemba, S. (1985b), "Dispersion of Initially Compact Dense Gas Clouds," Atmos. Envir., July 1985, Vol. 19, No. 8, 25 pp.

Fox, D.G. (1981), "Judging Air Quality Model Performance (A Summary of the AMS Workshop on Dispersion Model Performance Woods Hole, Massachusetts, 8-11 September 1980)," Bull. Amer. Meteorol. Soc., **62**,599-609.

Germeles, A.E. and Drake, E.M. (1975), "Gravity Spreading and Atmospheric Dispersion on LNG Vapor Clouds," Proceedings of the 4th International Symposium on Transport of Hazardous Cargoes by Sea and Inland Waterways, Jacksonville, Florida, pp. 519-539.

Golden, J. (1961), "Scale Model Techniques," M.S. Thesis, Dept. of Met. and Ocean., New York University, 42 pp.

Golder, D.G. (1972), "Relations among Stability Parameters in the Surface Layer," Boundary Layer Meteorol., Vol. 3, No. 1, pp. 47-58.

Halitsky, J., Golden, J., Halpern, P., and Wu, P. (1963), "Wind Tunnel Tests of Gas Diffusion from a Leak in the Shell of a Nuclear Power Reactor and from a Nearby Stack," N.Y.U. Meteorol. and Oceanog. Geophys. Sciences Lab. Report 63-2 (New York Univ., College of Engineering, New York).

Halitsky, J. (1968), "Gas Diffusion Near Buildings," Meteorology and Atomic Energy, 1968, editor D.H. Slade, Atomic Energy Commission, Ch. 5-5, pp. 221-256.

Halitsky, J. (1969), "Validation of Scaling Procedures for Wind Tunnel Model Testing of Diffusion Near Buildings," Report No. TR-69-8, Geophysical Science Laboratory, Dept. of Meteor. and Oceanog., New York University, 200 pp.

Hall, D.J., Barrett, C.F., and Ralph, M.O. (1974), "Experiments on a Model of an Escape of Heavy Gas. Stevenage: Warren Spring Laboratory, Report LR 217 (AP).

Hall, D.J. (1979), "Further Experiments on a Model of an Escape of Heavy Gas, Warren Springs Laboratory Report LR(312)AP, Dept. of Trade and Industry, Stevenage, Hertfordshire, U.K., 47 pp.

Hall, D.J. (1982), "Wind Tunnel Modelling of Heavy Gas Spills", Warren Springs Laboratory, Department of Industry, Stevenage, Hertfordshire, U.K., 15 pp.

Hall, D.J., Hollis, E.J., and Ishaq, H. (1982), " A Wind-tunnel Model of the Porton Dense Gas Spill Field Trials," Warren Springs Laboratory Report No. LR 394 (AP), Dept. of Trade and Industry, Stevenage, Hertfordshire, U.K., 103 pp.

Hall, D.J. and Waters, R.A. (1985), "Wind-Tunnel Model Comparisons with the Thorney Island Dense Gas Release Field Trials," Warren Springs Laboratory Report LR 489 (AP)M, Dept. of Trade and Industry, Stevenage, Hertfordshire, U.K., 39 pp.

Hartwig, S. and Flothmann, D. (1980), "Open and Controversial Problems in the Development of Models for the Dispersion of Heavy-Gas", Heavy Gas and Risk Assessment, ed. S. Hartwig, Battelle-Institut, Frankfurt am Main, B.R.D., pp. 1-14.

Haselman, L.C. (1980), "Effect of Humidity on the Energy Budget of a Liquefied Natural Gas (LNG) Vapor Cloud," Liquefied Gaseous Fuels Safety and Environmental Control Assessment Program: Second Status Report, Dept. of Energy, DOE/EV-0085, Vol. 2 of 3, Appendix C, pp. C-1 to C-13.

Hatcher, R.V. and Meroney, R.N. (1977), "Dispersion in the wake of a model industrial complex," Joint Conf. on Applications of Air Pollution Meteorology, Proceedings, Am. Meteorol. Soc., Salt Lake City, Utah, 29 November-2 December, 1977, pp. 343-346.

Haugen, D.A., Kaimal, J.C., and Bradley, E.F. (1971), "An Experimental Study of Reynolds Stress and Heat Flux in the Atmospheric Surface Layer," Quart. J. Roy. Meteorol. Soc., Vol. 97, pp. 168-180.

Haugen, D.A., ed. (1973), Workshop on Micrometeorology, American Meteorology Society, Boston, MA, 392 pp.

Havens, J.A. and Spicer, T.O. (1985), "Development of an Atmospheric Dispersion Model for Heavier-than-Air Gas Mixtures", Vol. 1, Final Report, Dept. of Transportation Contract DT-CG-23-80-C-20029, 191 pp.

Hilst, G.R. (1978), "Plume Model Validation," EPRI EA-917-SY, Workshop WS-78-99, EPRI, Palo Alto, California, October 1978.

Hinze, J.O. (1975), Turbulence, McGraw Hill, New York, 2nd. edition, 790 pp.

Hadjitofi, A. and Wilson, M.J.G. (1979), "Fast Response Measurements of Air Pollution," Atmos. Envir., Vol. **13**, pp. 755 ff.

Hoerner, S.F., (1965), Fluid-Dynamic Drag, Pub. by Author, Midland Park, New Jersey, U.S.A.

Hoot, T.G., Meroney, R.N., and Peterka, J.A. (1973), "Wind-Tunnel Tests of Negatively Buoyant Plumes," Envir. Prot. Agcy. Rpt. No. EPA-650/3-74-003, Research Triangle Park, NC, 94 pp.

Holjstrup, J. (1981), "A Simple Model for the Adjustment of Velocity Spectra in Unstable Conditions Downstream of an Abrupt Change in Roughness and Heat Flux," Boundary Layer Meteorol., Vol. 21, pp. 341-356.

Horst, T.W. (1979), "Lagrangian Similarity Modeling of Vertical Diffusion from a Ground Level Source," J. Appl. Meteorol., Vol. 18, pp. 733-740.

Hosker, R.P., Jr. (1984), "Flow and Diffusion Near Obstacles", Atmospheric Science and Power Production, DOE/TIC-27601, pp. 241-326.

Huang, C.H. (1979), "A Theory of Dispersion in Turbulent Shear Flow," Atmos.Envir., Vol. **13**, pp. 453-463.

Humphries, W., and Vincent, J.H. (1976), "Experiments to Investigate Transport Processes in the Near Wakes of Disks in Turbulent Air Flow," J. Fluid Mech., Vol. **75**, Part 4, pp. 737-749.

Hunt, J.C.R. (1974), "Wakes Behind Buildings," presented at the Aeronautical Research Council's Atmospheric Environment Committee Meeting, Oct. 23, ARC Report 35601, Atmos. 229, Aeronautical Research Council of Great Britain, Her Majesty's Stationery Office, London.

Hunt, A. (1981), "Scale Effects on Wind Tunnel Measurements of Surface Pressures on Model Buildings," Proceedings Colloque Construie avec le Vent (Designing with the Wind), 15-19 June, 1981, Nantes, France, pp. VIII-8-1 to VIII-8-15.

Hunt, J.C.R., Rottman, James W., and Britter, R.E. (1984), "Some Physical Processes Involved in the Dispersion of Dense Gases," Atmospheric Dispersion of Heavy Gases and Small Particles, Ed. G. Ooms and H. Tennekes, Springer-Verlag, 35 pp.

Hunt, J.C.R., Snyder, W.H., and Lawson, R.E. Jr. (1978), "Flow Structure and Turbulent Diffusion around a Three-Dimensional Hill: Fluid Modeling Study on Effects of Stratification: Part I: Flow Structure," Envir. Prot. Agcy. Report No. EPA 600/4-78-041, Research Triangle Park, NC, 84 pp.

Islitzer, N.F. and Dumbauld, R.K. (1963), "Atmospheric Diffusion-Deposition Studies over Flat Terrain," Int. J. Air Water Pollut., Vol. 7 (11-12), pp. 999-1022.

Irwin, J.S. (1979), "A Theoretical Variation of the Wind Profile Power-Law Exponent as a Function of Surface Roughness and Stability," Atmos. Envir., Vol. 13, No. 1, pp. 191-194

Jensen, M. (1958), "The Model-Law for Phenomena in a Natural Wind, Ingenioren, Int. Ed., Vol. 2, No. 4, pp 121-128.

Jensen, M. and Franck, N. (1963), Model-Scale Tests in Turbulent Wind, Part 1: Phenomena Dependent on the Wind Speed, Danish Technical Press, Copenhagen, 97 pp.

Jones, C.D. (1983), "On the Structure of Instantaneous Plumes in the Atmosphere," J. Hazardous Materials, Vol. 7, pp. 87-112.

Kaimal, J.C., Wyngaard, J.C., Izumi, Y. and Cote, O.R. (1972), "Spectral Characteristics of Surface Layer Turbulence," Quart. J. Roy. Meteor. Soc., Vol. 98, No. 417, pp. 563-589.

Kaimal, J.C. (1973), "Turbulence Spectra, Length Scales, and Structure Parameters in the Stable Boundary Layer," Boundary Layer Meteorol., Vol. 4, pp. 289-309.

Kline, S.J. (1965), Similitude and Approximation Theory, McGraw-Hill Book Company, New York, 229 pp.

Knox, J.B. (1984), "Model Validation: Purpose and Expectations," DOE Model Validation Workshop, October 23-26, 1984, Charleston, SC, Lawrence Livermore National Laboratory Preprint UCRL-91664, 13 pp.

Kothari, K.M. and Meroney, R.N. (1981), "LNG Plume Interaction with Surface Obstacles," for Gas Research Institute, Contract No. 5014-352-0203, Report GRI 80/0095, 156 pp.

Kothari, K.M. and Meroney, R.N. (1982), "Accelerated Dilution of Liquified Natural Gas Plumes with Fences and Vortex Generators," for Gas Research Institute, Contract No. 5014-352-0203, Report GRI 81/0074, 222 pp.

Koopman, R.P., Bowman, B.R., and Ermak, D.L. (1979), "Data and Calculations of dispersion on 5 m^3 LNG spill tests," Lawrence Livermore Laboratory Report UCRL-52876, 31 pp.

Koopman, R.P., Cederwall, R.T., Ermak, D.L., Godwire, H.C. Jr., Hogan, W.J., McClure, J.W., McRae, T.G., Morgan, D.L. Rodean, H.C. and Shinn, J.H. (1982), "Analysis of Burro Series 40-m^3 LNG Spill Experiments," J. Hazardous Materials, Vol. 6, pp. 43-83.

Lamb, R.G. (1982), "Diffusion in the Convective Boundary Layer", Chapter 5, Atmospheric Turbulence and Air Pollution Modeling, Nieuwstadt and van Dop, editors, D. Reidel Publishing Company, Dordrecht, Holland, pp. 159-230.

Lee, B.E. (1977), "Wind Flow Around Bluff Bodies", Proceedings of the Sixth Course Airflow and Building Design, 5-6 January 1977. 25 pp.

Lewellen, W.S. and Sykes, R.I. (1985), "A Scientific Critique of Available Models for Real-Time Simulations of Dispersion," Nuclear Regulatory Commission Report NUREG/CR-4157, 170 pp.

Leovy, C.B. (1969), "Bulk Transfer Coefficient for Heat Transfer," J. of Geophysical Research, Vol. 74, No. 13, pp. 3313-3321.

Li, W.W. and Meroney, R.N. (1984), "The Estimation of Atmospheric Dispersion at Nuclear Reactor Plants Utilizing Real Time Anemometer Statistics," U.S. Nuclear Regulatory Commission, Final Report, NRC Contract No. 04-81-202, Mod. 1, Colorado State University, CER84-85RNM-WWL2, 244 pp.

Londergan, R.J.; Minott, D.H.; Wockter, D.J.; Kincaid, T.M.; and Bonita, D.M. (1982), "Evaluation of Rural Air Quality Simulation Models," TRC Environmental Consultants, Inc., East Hartford, Connecticut, April 1982.

Lumley, J.L. and Panofsky, H.A. (1964), The Structure of Atmospheric Turbulence, Interscience, New York, 239 pp.

McQuaid, J. (1982), "Observations on the Current Status of Field Experimentation on Heavy Gas Dispersion," Proceedings of Symposium on Atmospheric Dispersion of Heavy Gases and Small Particles, Delft University of Technology, 29 August-2 September 1982, Springer-Verlag, Berlin, 25 pp.

McQuaid, J. (1985), "Overview of Current State of Knowledge on Heavy Gas Dispersion and Outstanding Problems/Issues", Proceedings of the Heavy Gas (LNG/LPG) Workshop, editor R.V. Portelli, Toronto, Ontario, 29-30 January 1985, pp. 5-28.

Meroney, R.N. (1979) "Lift Off of Buoyant Gas Initially on the Ground," J. of Industrial Aerodynamics, Vol. 5, pp. 1-11.

Meroney, R.N. (1980), "Wind-Tunnel Simulation of the Flow Over Hills and Complex Terrain," J .of Industrial Aerodynamics, Vol. 5 pp. 297-321.

Meroney, R.N. (1981), "Physical Simulation of Dispersion in Complex Terrain and Valley Drainage Flow Situations," in Air Pollution Modelling and Its Application, C. De Wispelaere, Ed., Plenum Publishing Co., 21 pp.

Meroney, R.N. (1982a), "Wind-tunnel Experiments on Dense Gas Dispersion," J. of Hazardous Materials, Vol. 6, pp. 85-106.

Meroney, R.N. (1982b), "Turbulent Diffusion Near Buildings," Engineering Meterology Chapter 11, pp. 481-521.

Meroney, R.N. (1983), "Unsteady Behavior of a Simulated LNG Vapor Cloud Suddenly Released into a Wind-tunnel Boundary Layer," Proceedings American Gas Association Transmission Conference, Seattle, Washington, 2-4 May, 1983, 21 pp.

Meroney, R.N. (1984), "Quarterly Report: Test and Design Guidelines for Fluid Modeling of LNG Vapor Clouds", September-November, 1984, Gas Research Institute Contract No. 5083-252-0962, 14 pp.

Meroney, R.N. (1984), "Transient Characteristics of Dense Gas Dispersion. Part I: A Depth-averaged Numerical Model," J. Hazardous Materials, Vol. 9, pp. 139-157.

Meroney, R.N. (1985), "Quarterly Report: Test and Design Guidelines for Fluid Modeling of LNG Vapor Clouds", December-February, 1985, Gas Research Institute Contract No. 5083-252-0962, 10 pp.

Meroney, R.N. (1985), "A Time Dependent, Quasi-Three Dimensional Depth-Integrated Numerical Model to Calculate Surface Heat Transfer and Entrainment to Cold Fluid Intrusions", Proceedings of the International Symposium on Refined Flow Modeling and Turbulence Measurements, 16-18 September 1985. The University of Iowa, Iowa City, Iowa. pp. E14-1-E14-10

Meroney, R.N., Cermak, J.E., and Neff, D.E. (1976), "Dispersion of Vapor from LNG Spills - Simulation in a Meteorological Wind Tunnel," Proceedings of Third AMS Symposium on Atmospheric Turbulence, Diffusion and Air Quality, 19-22 October, 1976, Raleigh, NC, pp. 243-246. (also errata sheet).

Meroney, R.N., Cermak, J.E., Neff, D.E., and Megahed, M. (1977), "Dispersion of Vapor from LNG Spills - Simulation in a Meteorological Wind Tunnel," Colorado State University, Civil Engineering Report CER76-77RNM-JEC-DEN-MM57, 152 pp. (also errata sheet).

Meroney, R.N., Chien, H.C. and Sandborn, V.A. (1980), " Sites for Wind-Power Installations: Physical Modeling of the Wind Field over Kahuku Point, Oahu, Hawaii," Proceedings of the Third International Symposium on Wind Energy Systems, August 26-29, 1980, Copenhagen, Denmark, pp. 75-90.

Meroney, R.N. and Lohmeyer, A. (1983), "Statistical Characteristics of Instantaneous Dense Gas Clouds Released in an Atmospheric Boundary Layer Wind Tunnel, Boundary-Layer Meteorol., Vol. 28, 22 pp.

Meroney, R.N. and Lohmeyer, A. (1984), "Prediction of Propane Cloud Dispersion by a Wind-Tunnel-Data Calibrated Box Model," J. Hazardous Materials, Vol. 8, pp. 205-221.

Meroney, R.N. and Neff, D.E. (1979), "Laboratory Simulation of Liquid Natural Gas Vapor Dispersion Over Land Or Water," Proceedings of 5th Intl. Conf. on Wind Engineering, Colorado State University, Fort Collins, 8-13 July, 1979, pp. 1139-1150.

Meroney, R.N., Neff, D.E., and Heskestad, G. (1984), "Wind-tunnel Simulation of Field Dispersion Tests (By the U.K. Health and Safety Executive) of water-spray curtains," Boundary-Layer Meteorol., Vol. 28, pp. 107-119.

Meroney, R.N.; Sandborn, V.A.; Bouwmeester, R.J.B.; Chien, H.C.; and Rider, M. (1978), "Sites for Wind-power Installations: Physical Modeling of the Influence of Hills, Ridges and Complex Terrain - Part II: Executive Summary", Dept. of Energy Report RLO/2438-77/3, 90 pp.

Mery, P., Schon, J.P., and Solal, J. (1974), "Comparison of Thermally Neutral and Unstable Shear Flows in the Wind Tunnel and the Atmosphere," Adv. Geophys., Vol. 18B, pp. 273-287.

Moodie, K., Taylor, G., and Beckett, H. (1981), "Water Spray Barrier Trials: 181, Test Parameters and Concentration Data for Trials 35-48", Health and Safety Executive Report FM/15/82/3, U.K., 60 pp.

Mueller, T.J. and Batill, S.M. (1982), "Experimental Studies of Separation on a Two Dimensional Airfoil at Low Reynolds Numbers," AIAA Journal, Vol. 20, pp. 457-463.

Neff, D.E. and Meroney R.N. (1979), "Dispersion of vapor from LNG spills--Simulation in a Meteorological Wind Tunnel of spills at China Lake Naval Weapons Center, California," Final Report, Dept. of Transportation Contract No. DOT CG-75279-A, Colorado State University, Civil Engineering Dept. Rept. CER78-79DEN-RNM41, 77 pp.

Neff, D.E. and Meroney, R.N. (1981), "THE BEHAVIOR OF LNG VAPOR CLOUDS: Wind-Tunnel Simulation of 40 M^3 LNG Spill Tests at China Lake Naval Weapons Center, California," Gas Research Institute Report No. GRI 80/0094, Chicago, IL, 155 pp.

Neff, D.E. and Meroney, R.N. (1982), "THE BEHAVIOR OF LNG VAPOR CLOUDS: Wind-Tunnel Tests on the Modeling of Heavy Plume Dispersion," Gas Research Institute Report No. GRI 80/0145, Chicago, IL, 120 pp.

Niemann, H.J. and Ruhwedel, J. (1980), "Full-scale and Model Tests on Wind-induced, Static and Dynamic Stresses in Cooling Tower Shells," Eng. Struct, Vol. 2, pp. 81-89.

Nieuwdtadt, F.T.M. and van Dop, H., ed. (1982), Atmospheric Turbulence and Air Pollution Modelling, D. Reidel Publishing Company, Dordrecht: Holland, 357 pp.

Ogawa,Y., Diosey, P.G., Uehara, K., and Ueda, H. (1981), "A Wind Tunnel for Studying the Effects of Thermal Stratification in the Atmosphere," Atmos. Envir., Vol. **15**, pp. 807-821.

Ogawa, Y., Diosey, P.G., Uehara, K., and Ueda, H. (1985), "Wind Tunnel Observation of Flow and Diffusion Under Stable Stratification," Atmos. Envir., Vol. **19**, pp. 65-74.

Panofsky, H.A. (1974), "The Atmospheric Boundary Layer Below 150 Meters," Annual Review of Fluid Mech., Vol.**6**, pp. 147-178.

Panofsky, H.A. (1984), Atmospheric Turbulence: Models and Methods for Engineering Applications, John Wiley and Sons, Inc., New York, 397 pp.

Panofsky, H.A. and Dutton, J. A. (1984), Atmospheric Turbulence: Models and Methods for Engineering Application, John Wiley and Sons, New York, 397 pp.

Panofsky, H.A., Blackdar, A.K. and McVehil, G.E. (1960), "The Diabatic Wind Profile," Quart. J. Roy. Meter. Soc., Vol. 86, pp. 390-398.

Pasquill, F. (1962) Atmospheric Diffusion, D. van Nostrand Company, Ltd., New York, 297 pp.

Peterka, J.A., Meroney, R.N. and Kothari, K. (1985) "Wind Flow Patterns About Buildings," J. of Wind Engineering and Industrial Aerodynamics, accepted for publication, March 1985.

Petty, D.G. (1979), "The Effect of Turbulence Intensity and Scale on the Flow Past Square Prisms," J. of Industrial Aerodynamics, Vol. **4**, pp. 247-252.

Picknett, R.G. (1981), "Dispersion of Dense Gas Puffs Released in the Atmosphere at Ground Level," Atmos. Envir. Vol. **15**, pp. 509-525.

Plate, E.J. and Cermak, J.E. (1963), "Micro-meteorological Wind-tunnel Facility," Fluid Dynamics and Diffusion Laboratory Report CER63EJP-JEC9, Colorado State University, Fort Collins, CO, 65 pp.

Plate, E.J. ed. (1982) Engineering Meterology.

Poreh, M. and Kacherginsky, Alexander (1981), "Simulation of Plume Rise Using Small Wind-Tunnel Models", Journal of Wind Engineering and Industrial Aerodynamics, (7)1-14.

Poreh, M. and Cermak, J.E. (1984), "Wind Tunnel Simulation of Diffusion in a Convective Boundary Layer," Boundary-Layer Meteorol., Vol. **30**, pp. 431-455.

Poreh, M. and Cermak, J.E. (1985), "Wind-tunnel Research on the Mechanics of Plumes in the Atmospheric Surface Layer, Part II," Annual Report to U.S. Dept of Army, Chemical Systems Laboratory, Aberdeen Proving Ground, Maryland, CSU Civil Engineering Department Report CER84-85MP-JEC47, 45 pp.

Poreh, M. and Kacherginsky, A. (1981), "Simulations of Plume Rise Using Small Wind-tunnel Models," J. of Wind Engineering and Industrial Aero., Vol. 7, pp. 1-14.

Puttock, J.S. (1985), "Summary of Heavy Gas Spills Experimental Research," Paper presented at Heavy gas (LNG/LPG) workshop, January 19-30, 1985, Toronto , Ontario, Canada.

Puttock, J.S., Blackmore, D.R., and Colenbrander, G.W. (1982), "Field Experiments on Dense Gas Dispersion," J. Hazardous Materials, Vol. 6, pp. 13-41.

Puttock, J.S. and Colenbrander, G.W. (1985), "Dense Gas Dispersion - Experimental Research", Proceedings of the Heavy Gas (LNG/LPG) Workshop, ed. R.V. Portelli, Toronto, Ontario, 29-30 January 1985, pp. 32-50.

Raj, P.K.P. and Kalelkar, A.S. (1973), "Fire-Hazard Presented by a Spreading, Burning Pool of LNG on Water," 1973 Fall Meeting, Western States Section, Combustion Institute.

Ranga Raju, K.G. and Singh, V. (1976), "Blockage Effects on Drag of Sharp Edged Bodies," J. of Industrial Aerodynamics, Vol. 1, pp. 301-309.

Rao, S.T. and Visalli, J.R. (1981), "On the Comparative Assessment of the Performance of Air Quality Models," Journal Air Pollution Control Association, Vol. 31, No. 8, August 1981, pp 851-860.

Ricou, F.P. and Spalding, D.B. (1961), "Measurements of Entrainment of Axisymmetrical Turbulent Jets," J. Fluid Mech., Vol. 12, No. 5, pp. 1033-1044.

Roebuck, B. (1984), "The Presentation and Availability of the Data and Plans for Future Analysis," HSE Symposium on Heavy Gas Dispersion Trials at Thorney Island, Sheffield, UK, 3-5 April, 15 pp.

Roper, A.T. (1967), "Cylinder in a turbulent shear layer," Ph. D. Dissertation, Civil Engineering, Colorado State University, Fort Collins, CO, 215 pp.

Rottman, J.W. (1984), "The Spreading of Dense Gas Clouds," Report to Health and Safety Executive under contract No. 1918/01.01, Dept. of Applied Math. and Theor. Physics, Univ. of Cambridge, 52 pp.

Rottman, J.W., Simpson, J.E. and Stansby, P.K. (1984), "The motion of a two-dimensional cloud released instantaneously in a uniform cross flow," in preparation.

Sawford, B.L. and Hunt, J.C.R. (1984), "Effects of Turbulence Structure, Molecular Diffusion and Source Size on Fluctuations of Concentration in Homogeneous Turbulence," Dept. of Applied Math. and Theor. Physics, U. of Cambridge, U.K., 62 pp.

Schatzmann, M. and Policastro, A.J. (1984), "Effects of the Boussinesq Approximation on the Results of Strongly-Buoyant Plume Calculations," J. of Climate and Applied Meteorology, Vol. 23, pp. 117-123.

Schatzmann, M., Konig, G., and Lohmeyer, A. (1985), "Dispersion Modeling of Hazardous Materials in the Wind Tunnel," 15th Int. Meeting on Air Pollution Modeling and Its Applications, 15-18 April, St. Louis, MO., 12 pp.

Schlichting, H. (1968), Boundary Layer Theory, McGraw Hill Book Co., New York, 774 pp.

Schon, J.P. and Mery, P. (1971), "A Preliminary Study of the Simulation of Neutral Atmospheric Boundary Layer Using Air Injection in a Wind Tunnel," Atmos. Enviro., Vol. 5, No. 5, pp. 299-312.

Simiu, E. and Scanlan, R.H. (1978), Wind Effects on Structures, John Wiley and Sons, Inc., New York, 458 pp.

Simpson, J. and Britter, R. (1979), "The Dynamics of the Head of a Gravity Current Advancing Over a Horizontal Surface," J. Fluid Mech., Vol. 94, No. 3, pp. 477-496.

Skinner, G.T. and Ludwig, G.R. (1978), "Physical Modeling of Dispersion in the Atmospheric Boundary Layer," Calspan Technical Report No. 201, 31 pp.

Snyder, W.H. (1972), "Similarity Criteria for the Application of Fluid Models to the Study of Air Pollution Meteorology," Boundary-Layer Meteorol., Vol. 3, pp. 113-134.

Snyder, W.H., Britter, R.E., and Hunt, J.C.R. (1979), "A Fluid Modeling Study of the Flow Structure and Plume Impingement on a Three-Dimensional Hill in Stably Stratified Flow," Proc. Fifth Int. Conf. on Wind Engr., Pergamon Press, NY, Vol. 1, pp. 319-329.

Snyder, W.H. (1981), "Guidelines for Fluid Modeling of Atmospheric Diffusion", EPA Report EPA-600/8-81-009, 185 pp.

Strom, G.H., Hackman, M. and Kaplin, E.J. (1957), "Atmospheric Dispersal of Industrial Stack Gases Determined by Concentration Measurements in Scale Model Wind Tunnel Experiments," Journal of APCA, Vol. 7, No. 3, pp. 198-204

Symes, C.R. and Meroney, R.N. (1970), "Cone Frustrums in a Shear Layer," Atomic Energy Commission Report No. COO-2053-4, Colorado State University, CER70-71CRS-RNM-11, 142 pp.

Szechenyi, E. (1975), "Supercritical Reynolds Number Simulation for Two-dimensional Flow over Circular Cylinders," J. Fluid Mech., Vol. 70, pp. 529-542.

Teunissen, H.W. (1975), "Simulation of the Planetary Boundary Layer in a Multiple Jet Wind Tunnel," Atmos. Envir., Vol. 9, pp. 145-174.

Townsend, A.A. (1956), The Structure of Turbulent Shear Flow, Cambridge Univ. Press, Cambridge, U.K., 315 pp.

Van der Hoven, I. (1957), "Power Spectrum of Horizontal Wind Speed in the Frequency Range from 0.0007 to 900 Cycles per Hour," J. Meteorol., Vol. **14**, pp. 160-164.

Van Heugten, W.H.H. and Duijm, N.J. (1984), "Some Findings Based on Wind Tunnel Simulation and Model Calculations of Thorney Island Trial No. 008," HSE Symposium on Heavy Gas Dispersion Trials at Thorney Island, Sheffield, UK, 3-5 April 1984, 9 pp.

Van Ulden, A.P. (1974), "On the Spreading of a Heavy Gas Released Near the Ground," Loss Prevention and Safety Promotion Seminar, Delft, Netherlands, 8 pp.

Vincent, J.H. (1977), "Model Experiments on the Nature of Air Pollution Transport Near Buildings," Atmos. Envir., Vol. **11**, No. 8, pp. 765-774.

Vincent, J.H. (1978), "Scalar Transport in the Near Aerodynamic Wakes of Surface Mounted Cubes," Atmos. Envir., Vol. **12**, No. 6/7, pp. 1319-1322.

Warhaft, Z. and Lumley, J.L. (1978), "An Experimental Study of the Decay of Temperature Fluctuations in Grid-generated Turbulence," J. Fluid Mech., Vol. **88**, Part 4, pp. 659-684.

Wheatley, C.J. and Webber, D.M. (1984), "Aspects of the Dispersion of Denser-than-air Vapours Relevant to Gas Cloud Explosions," Safety and Reliability Directorate, United Kingdom Atomic Energy Authority, Final Report of Contract SR/007/80/UK/H, 450 pp.

Wheatley, C.J., Brighton, P.W.M., and Prince, A.J. (1985), "Comparison Between Data from the Heavy Gas Dispersion Experiments at Thorney Island and Predictions of Simple Models," 15th Int. Meeting on Air Pollution Modeling and Applications, NATO, 15-18 April, St. Louis, MO., 15 pp.

Wiersma, S.J. (1983), "Recommendations for Research to Assess LNG Safety Hazards", Proceedings of AGA Transmission Conference, Seattle, Washington, 3 May 1983, 23 pp.

Willis, G.E. and Deardorff, J.W. (1974), "A Laboratory Model of the Unstable Planetary Boundary Layer," J. Atmos. Sci., Vol. **31**, pp. 1297-1307.

Willis, G.E. and Deardorff, J.W. (1976), "A Laboratory Model of Diffusion into the Convective Planetary Boundary Layer," Quart. J. Roy. Meteorol. Soc., Vol. **102**, pp. 427-445.

Willis, G.E. and Deardorff, J.W. (1978), "A Laboratory Study of Dispersion From an Elevated Source Within a Modeled Convective Planetary Boundary Layer," Atmos. Envir., Vol. **12**, pp. 1305-1311.

Wilson, D.A.; Cox, W.M.; and Mackay, K.P. (1982), "Suggested Procedures for Evaluating Air Quality Models," 3rd Joint Conf. on Applications of Air Pollution Meteorology, January 12-15, 1982, San Antonio, Texas, pp 280-283.

Wolfe, D.E. (1985), "Early Morning Evolution of the Convective Boundary Layer at the Boulder Atmospheric Observatory," M.S. Thesis, Dept. of Atm. Science, Colorado State University, Fort Collins, 173 pp.

Yang, B.T. and Meroney, R.N. (1973), "On Diffusion from an Instantaneous Point Source in a Neutrally Stratified Turbulent Boundary Layer with a Laser Light Scattering Probe," Project THEMIS Technical Report No. 20, Office of Naval Research Contract No. N00014-68-A-0493-0001, Colorado State University, Fort Collins, CO, 219 pp.

Appendix A: Figures A-1 to A-16

Pattern Comparison Plots: Field Measurements Versus Laboratory Simulation of Ground Level Concentration Isopleths. Figures A-1 to A-14.

Pattern Comparison Plots: Field Measurements Versus Numerical Simulation of Ground Level Concentration Isopleths. Figures A-15 to A-16.

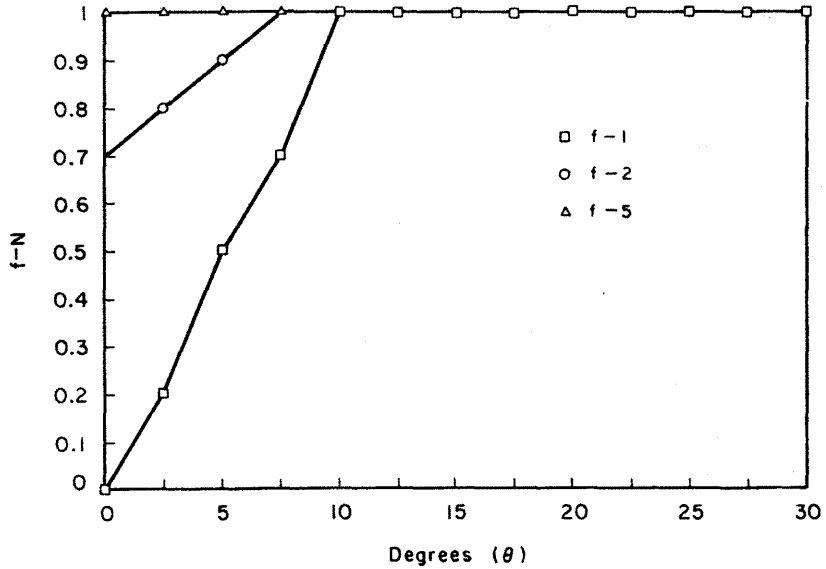

Figure A-1. Capistrano Test 44 - Case 11.

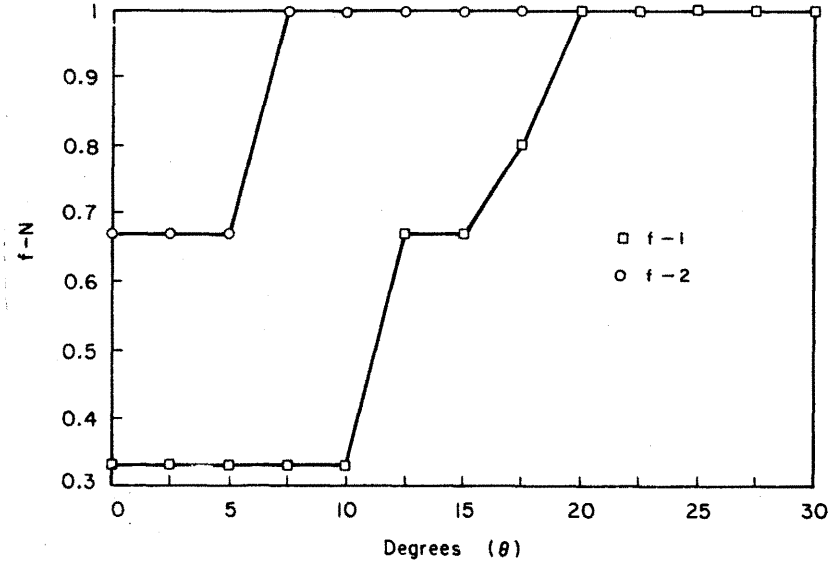

Figure A-2. China Lake 5 cubic M Spills, LNG-18.

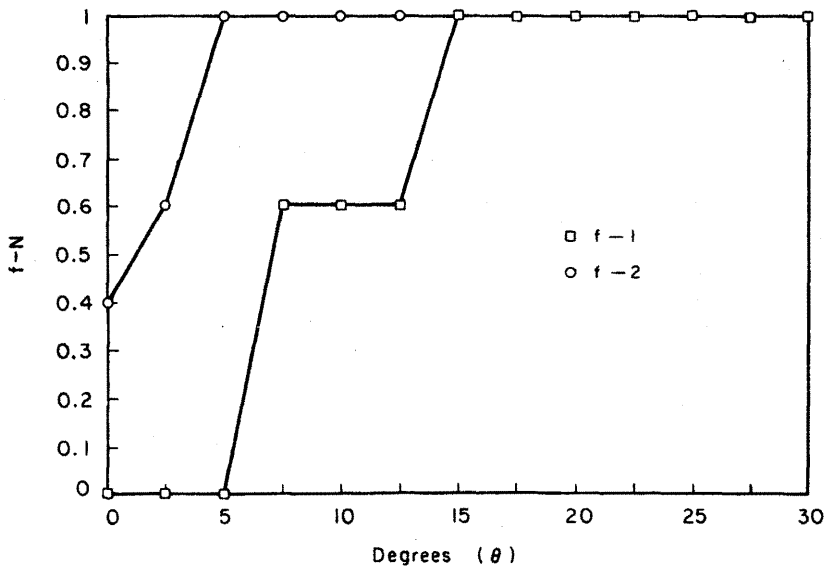

Figure A-3. China Lake 5 cubic M spills, LNG-19.

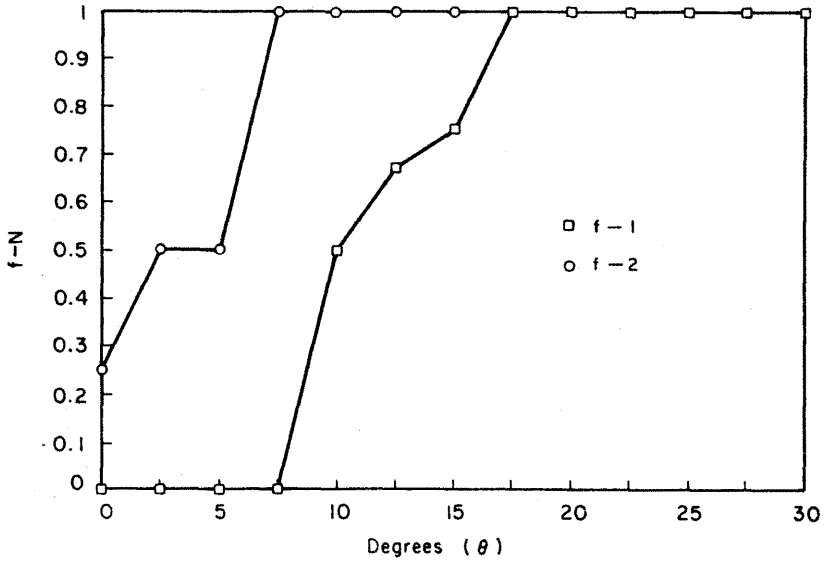

Figure A-4. China Lake 5 cubic M Spills, LNG-20.

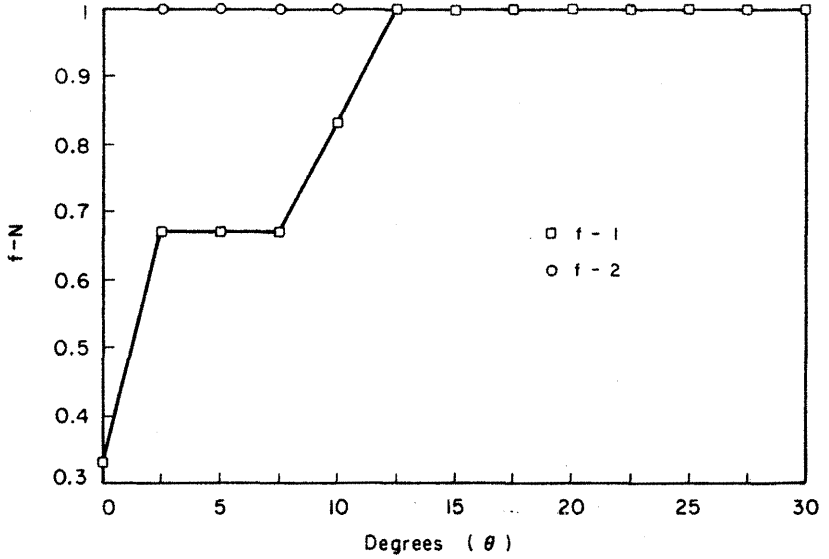

Figure A-5. China Lake 5 cubic M Spills, LNG-21.

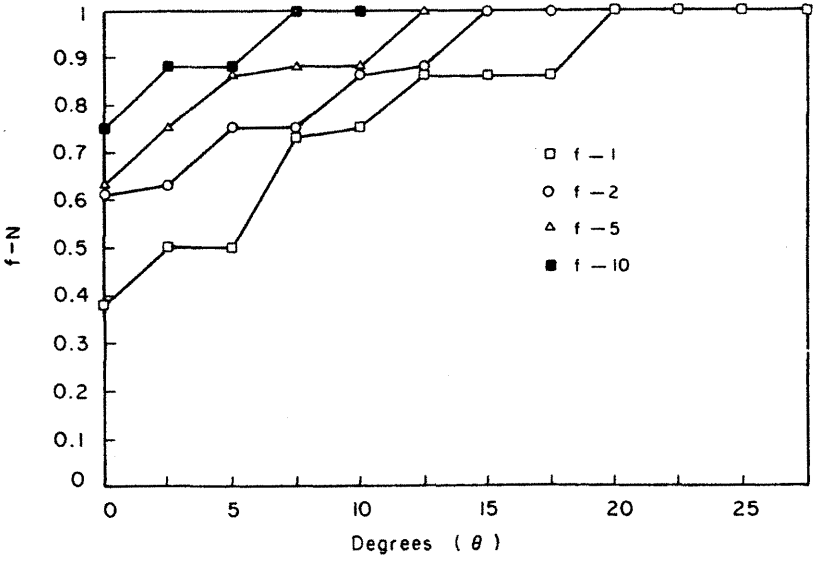

Figure A-6. Burro No. 4.

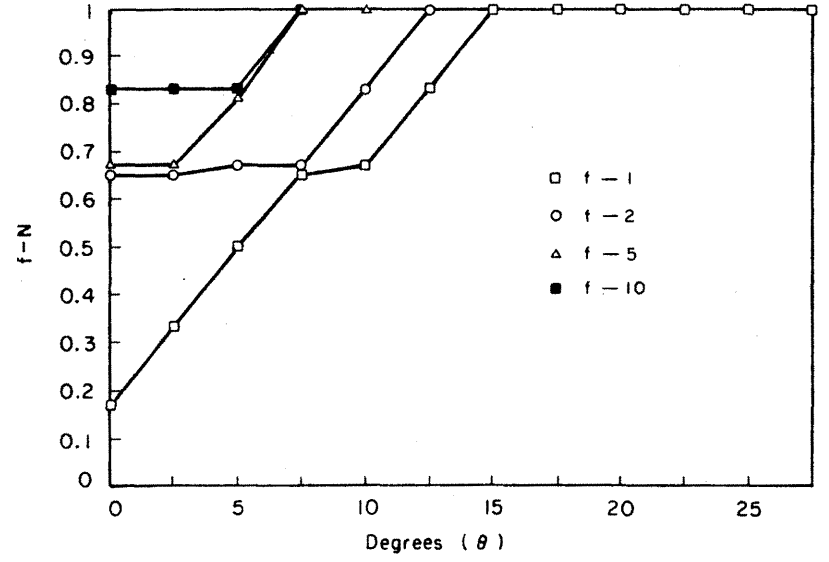

Figure A-7. Burro No. 5.

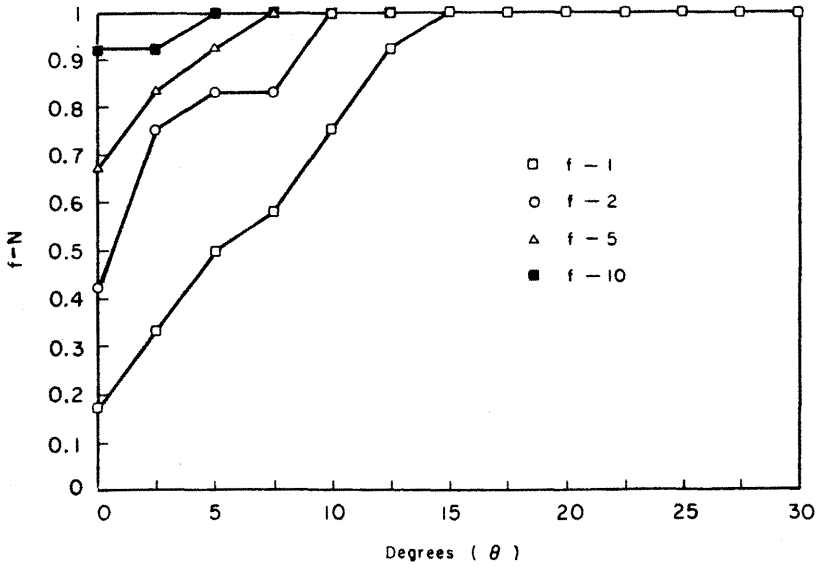

Figure A-8. Burro No. 7.

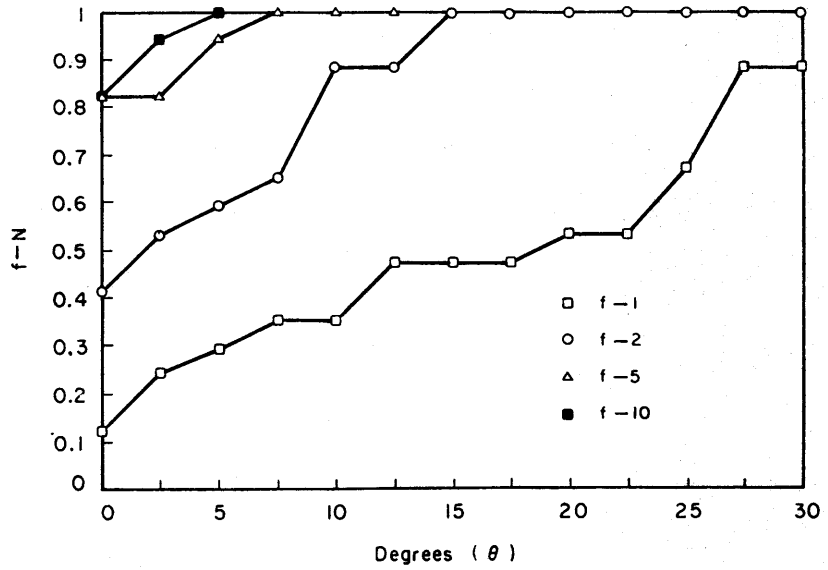

Figure A-9. Burro No. 8 (1:85 scale, SG = 1.38).

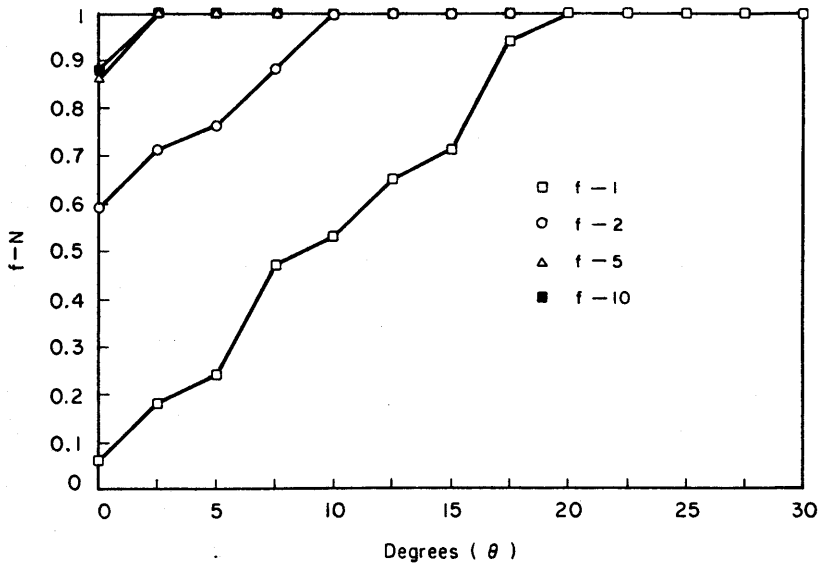

Figure A-10. Burro No. 9 (1:240 model).

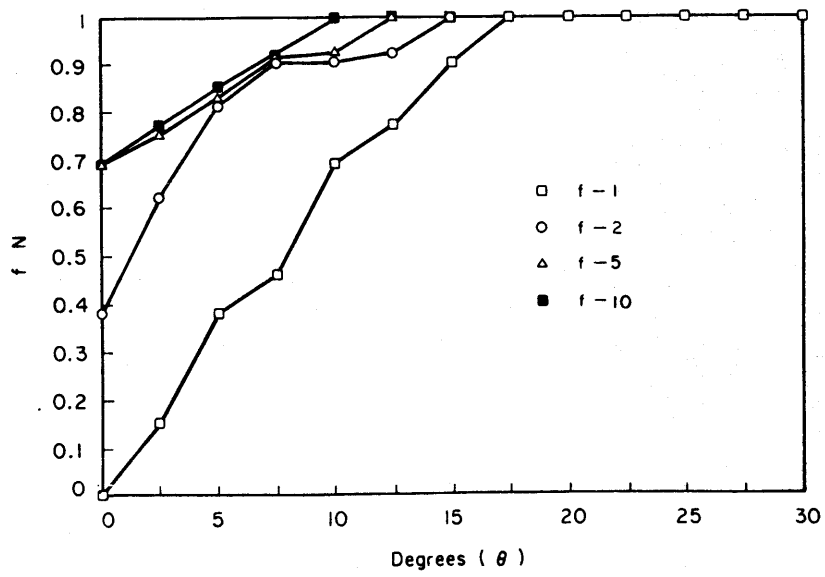

Figure A-11. Burro No. 8 (1:85 scale, SG = 4.18).

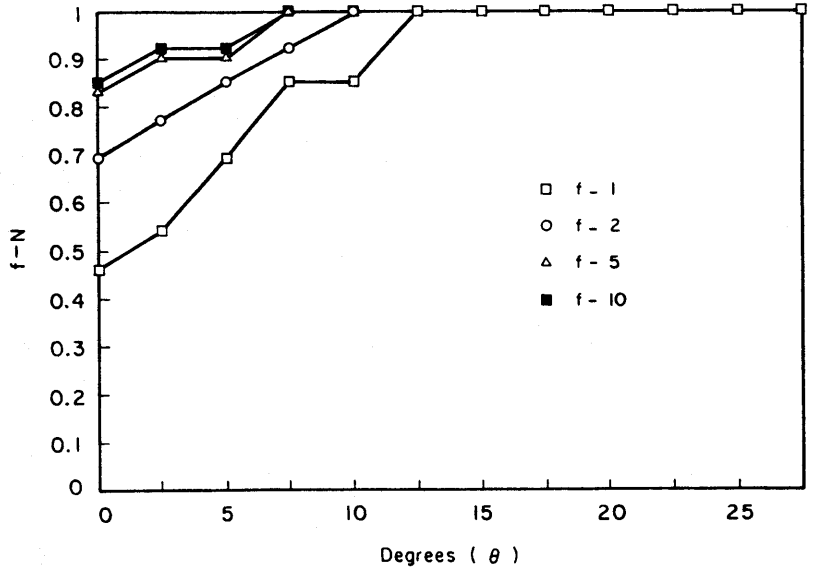

Figure A-12. Burro No. 9 (1:85 model).

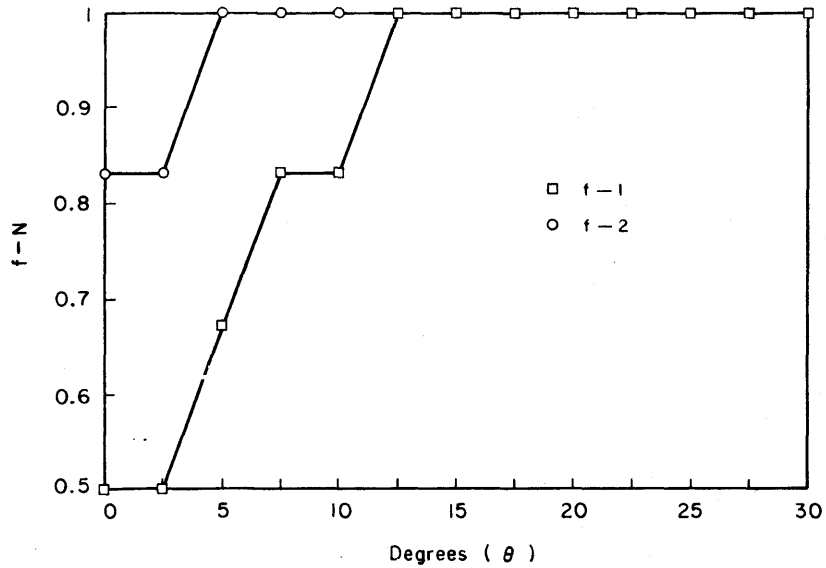

Figure A-13. HSE run 46, Spray.

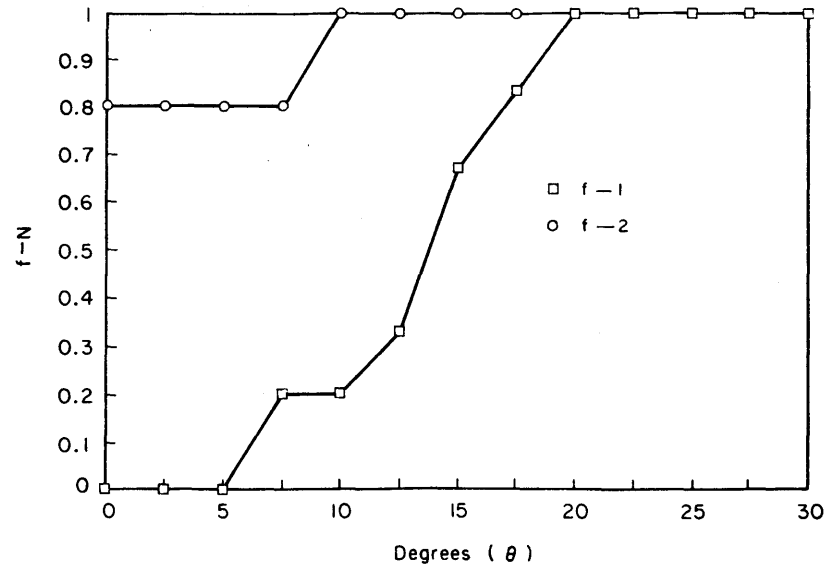

Figure A-14. HSE run 46, No spray.

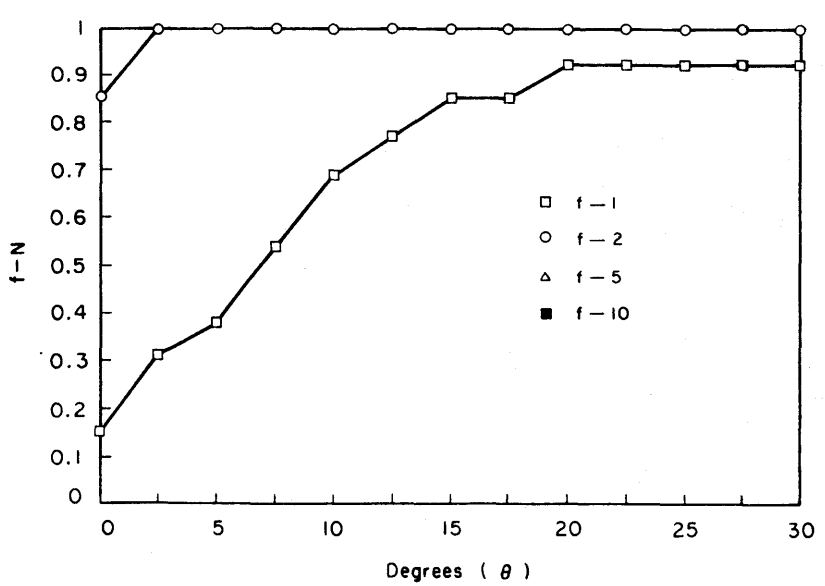

Figure A-15. Burro No. 8 - FEMS (Chan & Ermak, 1983).

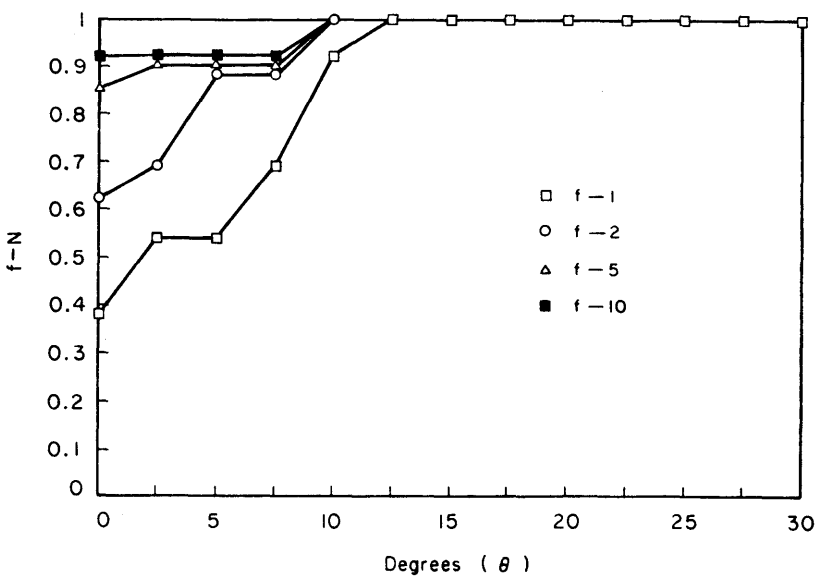

Figure A-16. Burro No. 9, FEM3 (Chan & Ermak, 1983).